



HAL
open science

Surfactants in atmospheric aerosols and their role on cloud formation

Violaine Gérard

► **To cite this version:**

Violaine Gérard. Surfactants in atmospheric aerosols and their role on cloud formation. Other. Université de Lyon, 2016. English. NNT : 2016LYSE1216 . tel-01486860

HAL Id: tel-01486860

<https://theses.hal.science/tel-01486860>

Submitted on 10 Mar 2017

HAL is a multi-disciplinary open access archive for the deposit and dissemination of scientific research documents, whether they are published or not. The documents may come from teaching and research institutions in France or abroad, or from public or private research centers.

L'archive ouverte pluridisciplinaire **HAL**, est destinée au dépôt et à la diffusion de documents scientifiques de niveau recherche, publiés ou non, émanant des établissements d'enseignement et de recherche français ou étrangers, des laboratoires publics ou privés.



N°d'ordre NNT: 2016LYSE1216

THESE de DOCTORAT DE L'UNIVERSITE DE LYON

opérée au sein de

l'Université Claude Bernard Lyon 1

Ecole Doctorale de Chimie de l'Université de Lyon

ED 206

Spécialité de doctorat : Chimie

Soutenue publiquement le 16/11/2016, par :

Violaine Myriam Francine Gérard

Surfactants in atmospheric aerosols and their role on cloud formation

**Surfactants dans les aérosols atmosphériques
et leur rôle dans la formation des nuages**

Devant le jury composé de :

Prof. Didier Léonard	ISA, UCBL1, Lyon, France	Président
Prof. Ronald Carl Cohen	University of California, Berkeley, USA	Rapporteur
Dr. Anne-Marie Delort (DR)	ICCF, CNRS, Clermont-Ferrand, France	Rapporteuse
Dr. Corinne Ferronato (MCF)	IRCELYON, CNRS, Lyon, France	Examinatrice
Dr. Barbara Nozière (CR)	IRCELYON, CNRS, Lyon, France	Directrice de thèse

Violaine Myriam Francine Gérard

**Surfactants in atmospheric aerosols
and their role on cloud formation**

**Surfactants dans les aérosols atmosphériques
et leur rôle dans la formation des nuages**

© Copyright
Violaine Gérard, 2016
All rights reserved.

UNIVERSITE CLAUDE BERNARD - LYON 1

Président de l'Université

Président du Conseil Académique

Vice-président du Conseil d'Administration

Vice-président du Conseil Formation et Vie
Universitaire

Vice-président de la Commission Recherche

Directeur Général des Services

M. le Professeur Frédéric FLEURY

M. le Professeur Hamda BEN HADID

M. le Professeur Didier REVEL

M. le Professeur Philippe CHEVALIER

M. Fabrice VALLÉE

M. Alain HELLEU

COMPOSANTES SANTE

Faculté de Médecine Lyon Est – Claude Bernard

Directeur : M. le Professeur J. ETIENNE

Faculté de Médecine et de Maïeutique Lyon Sud
– Charles Mérieux

Directeur : Mme la Professeure C. BURILLON

Faculté d'Odontologie

Directeur : M. le Professeur D. BOURGEOIS

Institut des Sciences Pharmaceutiques et
Biologiques

Directeur : Mme la Professeure C. VINCIGUERRA

Institut des Sciences et Techniques de la
Réadaptation

Directeur : M. X. PERROT

Département de formation et Centre de
Recherche en Biologie Humaine

Directeur : Mme la Professeure A-M. SCHOTT

COMPOSANTES ET DEPARTEMENTS DE SCIENCES ET TECHNOLOGIE

Faculté des Sciences et Technologies

Directeur : M. F. DE MARCHI

Département Biologie

Directeur : M. le Professeur F. THEVENARD

Département Chimie Biochimie

Directeur : Mme C. FELIX

Département GEP

Directeur : M. Hassan HAMMOURI

Département Informatique

Directeur : M. le Professeur S. AKKOUCHE

Département Mathématiques

Directeur : M. le Professeur G. TOMANOV

Département Mécanique

Directeur : M. le Professeur H. BEN HADID

Département Physique

Directeur : M. le Professeur J-C PLENET

UFR Sciences et Techniques des Activités
Physiques et Sportives

Directeur : M. Y.VANPOULLE

Observatoire des Sciences de l'Univers de Lyon
Polytech Lyon

Directeur : M. B. GUIDERDONI

Ecole Supérieure de Chimie Physique
Electronique

Directeur : M. le Professeur E.PERRIN

Directeur : M. G. PIGNAULT

Institut Universitaire de Technologie de Lyon 1

Directeur : M. le Professeur C. VITON

Ecole Supérieure du Professorat et de
l'Education

Directeur : M. le Professeur A. MOUGNIOTTE

Institut de Science Financière et d'Assurances

Directeur : M. N. LEBOISNE

„L'union fait la force. Toute puissance est faible à moins que d'être unie.”

„Il faut s'entraider, c'est la loi de la nature.”

Jean de la Fontaine (1621 - 1695)

„What we know is a drop, what we don't know is an ocean.”

Isaac Newton (1643 - 1727)

„I have not failed. I've just found 10,000 ways that don't work.”

Thomas Edison (1847 - 1931)

„Si je diffère de toi loin de te léser je t'augmente.”

Antoine de Saint-Exupéry (1900 - 1944)

„The most exciting phrase to hear in science, the one that heralds new discoveries, is not 'Eureka!' but 'That's funny...’”

Isaac Asimov (1920 - 1992)

To my family and Joffrey

Abstract

Clouds are essential components of the Earth's hydrological system and climate but some aspects of their formation are still not completely understood. In particular, although Köhler theory predicts that surfactants should enhance cloud droplet activation, current models consider this role negligible. At the time of this PhD work, a few studies had started to demonstrate the contrary but atmospheric evidence for the role of these compounds was still missing and very little was known about their atmospheric concentrations, sources, and mechanism of action.

The objective of this PhD work was to investigate these aspects to improve the understanding of atmospheric surfactants and their role in cloud formation. Several milestones were achieved. First, a method was developed to quantify surfactant concentrations in aerosols, which was applied to samples from different regions. This method led to the first absolute surface tension curves for atmospheric surfactants, in PM_{2.5} aerosols from a coastal region in Sweden, and to the identification of the key parameter controlling the cloud-forming efficiency of aerosols, the C/CMC ratio. A second study revealed strong correlations between cloud occurrence and intrinsic surfactant properties in PM₁ aerosols in a boreal region in Finland, thus demonstrating for the first time the role of surfactants in cloud formation from direct atmospheric observations. The results predicted Cloud Condensation Nuclei numbers four times larger on average than when neglecting surfactant effects, showing the quantitative importance of including surfactant effects in cloud predictions. The importance of surfactants inferred from macroscopic measurements was confirmed by laboratory experiments on individual micron-sized droplets showing an increase of droplet growth in the presence of surfactants. Finally, observations from the different field studies (correlations with biological markers, chemical structure ...) concurred to indicate a biological origin for the surfactants present in atmospheric aerosols.

This work thus accomplished some important steps in the understanding of atmospheric surfactants and their role in cloud formation.

Key words: Surfactants – atmospheric aerosols – cloud droplet – surface tension – CMC – micron-sized droplet – optical trap – origin of surfactants in atmosphere

Résumé (en français)

Les nuages sont essentiels dans le cycle de l'eau et dans le budget climatique, mais certains aspects de leur formation sont encore incompris. En particulier, bien que la théorie de Köhler prédise que les surfactants devraient favoriser l'activation des particules en goutte de nuage, les modèles actuels les considèrent comme négligeables. Au moment de ce travail de thèse, quelques études avaient commencé à démontrer le contraire mais des preuves du rôle de ces composés dans l'atmosphère étaient encore manquantes et peu d'études traitaient de leur concentration dans l'atmosphère, leur source et leur mécanisme d'action.

L'objectif de ce travail de thèse était d'étudier ces aspects pour améliorer la compréhension des surfactants dans l'atmosphère et de leur rôle dans la formation des nuages. Plusieurs étapes ont été franchies. Premièrement, une méthode a été développée pour déterminer la concentration en surfactants dans les aérosols et a été appliquée à des échantillons de différentes régions. Cette méthode a conduit aux premières courbes de tension de surface pour des surfactants atmosphériques, dans des aérosols PM_{2.5} d'une région côtière en Suède, et à l'identification du paramètre clé contrôlant l'efficacité des aérosols à former des nuages, le ratio C/CMC. Une seconde étude a révélé des corrélations fortes entre la présence de nuages et les propriétés intrinsèques des surfactants dans des aérosols PM₁ d'une région boréale en Finlande. Cela a démonstré pour la première fois le rôle des surfactants dans la formation des gouttes de nuage à partir d'observations directes dans l'atmosphère. Les résultats ont prédit un nombre de noyaux de condensation quatre fois plus important en moyenne que lorsque les effets des surfactants étaient négligés, montrant l'importance quantitative d'inclure les effets des surfactants dans la prédiction des nuages. L'importance des surfactants déduite des expériences à l'échelle macroscopique a été confirmée en laboratoire par des expériences sur des gouttes individuelles microniques, montrant une augmentation du grossissement des gouttes en présence de surfactants. Enfin, des observations à partir des différentes études (corrélations avec des marqueurs biologiques, étude structurale...) indiquent une origine biologique des surfactants dans les aérosols atmosphériques.

Ainsi ce travail a permis de franchir d'importantes étapes dans la compréhension des surfactants atmosphériques et de leur rôle dans la formation des nuages.

List of contributions

Most of the results presented in this work (including experimental procedures) were (or will be) published in articles or were presented during conferences (see list below).

PUBLICATIONS

Renard, P.; Delort, A.-M.; Canet, I.; Sancelme, M.; **Gérard, V.**; Nozière, B., *Biosurfactants from fine atmospheric aerosols*, **2017 (in preparation)**.

Nozière, B.; **Gérard, V.**; Baduel, C.; Ferronato, C., *Extraction and characterization of surfactants from atmospheric aerosols*, *Journal of Visualized Experiments*, **2016 (under review)**.

Frossard, A. A.; Li, W.; **Gérard, V.**; Nozière, B.; Cohen, R. C., *Surfactants Enhance Growth of Individual Water Droplets*, *Geophysical Research Letters*, **2016 (under review)**.

Gérard, V.; Nozière, B.; Fine, L.; Ferronato, C.; Frossard, A. A.; Cohen, R. C.; Asmi, E.; Lihavainen, H.; Kivekäs, N.; Aurela, M.; Brus, D., *Atmospheric evidence for the role of aerosol surfactants in cloud formation*, *Nature Geoscience*, **2016 (under review)**.

Gérard, V.; Nozière, B.; Baduel, C.; Fine, L.; Frossard, A. A.; Cohen, R. C., *Anionic, Cationic, and Nonionic Surfactants in Atmospheric Aerosols from the Baltic Coast at Askö, Sweden: Implications for Cloud Droplet Activation*, *Environmental Science & Technology*, **2016**, 50 (6), 2974-2982.

CONFERENCES

❖ Presented by the author

International

22nd European Aerosol Conference **EAC 2016**, Tours, France, 4 - 9 September 2016

Gérard, V.; Nozière, B.; Asmi, E.; Lihavainen, H.; Kivekäs, N.; Aurela, M.; Brus, D.; Fine, L.; Frossard A. A.; Cohen R. C., *Surfactants in PM1 aerosols from boreal Northern Finland: importance for cloud droplet formation?*, **2016**, P1-AAS-AAP-085, EAC2016

(Poster presentation, Best Poster Award)

European Geoscience Union General Assembly **EGU 2015**, Vienna, Austria, 12 - 17 April 2015

Gérard, V.; Nozière, B.; Baduel, C., *Seasonal evolution of anionic, cationic and non-ionic surfactant concentrations in coastal aerosols from Askö, Sweden*, Geophysical Research Abstracts, Vol. 17, EGU2015-851, **2015**, EGU General Assembly 2015

(Oral presentation)

National

Annual Meeting 2015 Ecole doctorale de Chimie, Lyon, France, 7 May 2015

Gérard, V.; Nozière, B.; Frossard, A.; Cohen, R. C.; Delort, A.-M. *Surfactants in atmospheric aerosols: SONATA project.*

(Poster presentation, Best Poster Award)

XXXIV^{ème} édition du Colloque Annuel du Groupe Français de Cinétique et Photochimie **GFCP 2014**, Villeurbanne, France, 23 - 24 June 2014

Gérard, V.; Nozière, B.; *Surfactants in atmospheric aerosols: the physical-chemistry of cloud formation*, 2014, GFCP

(Poster presentation)

❖ Author contribution

International

AGU Fall meeting 2015, San Francisco, 14 - 18 December 2015

Frossard, A. A., **Gérard, V.**, Nozière, B., Cohen, R. C., *Effects of Atmospheric Surfactants on the Microphysics of Individual Cloud Droplets*, **2015**, A52E-02, AGU 2015

(Oral presentation)

Table of contents

Dedication	i
Abstract	ii
Résumé (en français)	iii
List of contributions	iv
Table of contents	vi
List of Figures	ix
List of Tables	xvii
Abbreviations and symbols	xviii
1. Scientific context	1
1.1. Atmosphere	1
1.2. Clouds	2
1.2.1. General information on clouds	2
1.2.2. Importance of clouds in atmosphere	4
1.3. Formation of liquid clouds	7
1.3.1. Köhler equation	7
1.3.2. Role of chemistry	10
1.3.3. Atmospheric aerosol composition and implication for cloud formation	11
1.4. Measurement of cloud droplet formation and comparison with theory	12
1.5. Recent developments	15
1.6. Surfactants	17
1.6.1. Definition	17
1.6.2. Surface tension and CMC	19
1.7. Surfactants in aerosols: State of the Science	21
1.8. Objectives of the study	23
1.9. Thesis overview	23
2. Experimental techniques	25
2.1. Aerosol sampling	25
2.1.1. Aerosol sampler	25
2.1.2. Sampling sites and experimental sampling procedure	26
2.1.2.1. Askö, Sweden: coastal station	26
2.1.2.2. Villeurbanne, France: urban station	28
2.1.2.3. Pallas-Sammaltunturi, Finland: boreal station	29
2.2. Surfactant extraction from aerosols	33
2.2.1. Reference surfactants	33
2.2.2. Surfactant extraction	35
2.2.2.1. Principle	35
2.2.2.2. Improvement of the extraction	37
2.2.2.3. Experimental procedure	38

2.3.	Surface tension by pendant drop tensiometry	41
2.3.1.	Principle	41
2.3.2.	Experimental procedure	43
2.4.	Surfactant concentration by colorimetric methods	46
2.4.1.	Principle	47
2.4.2.	Experimental procedure: adaptation to extracts	49
2.4.2.1.	Determination of anionic surfactants concentration	49
2.4.2.2.	Determination of cationic surfactants concentration	50
2.4.2.3.	Determination of non-ionic surfactants concentration	50
2.4.2.4.	Quantification, uncertainties and detection limits	51
2.4.2.5.	Determination of total surfactant concentrations	54
2.4.2.6.	Interferences from other species	55
2.5.	Fluorescence spectroscopy	57
2.5.1.	Principle	57
2.5.2.	Experimental procedure	59
2.6.	Chemical characterization of surfactants by LC-MS/MS	60
2.6.1.	Principle	60
2.6.2.	Experimental procedure	62
2.7.	Study of micron-sized droplets using an optical trap	64
2.7.1.	Principle	64
2.7.2.	Experimental procedure	66
2.8.	Other atmospheric and geophysical data	70
2.8.1.	Chlorophyll data from MODIS aqua satellite	70
2.8.2.	Air mass sources by HYSPLIT model trajectories	71
2.8.3.	Presence of clouds by visibility data	72
2.8.4.	Volume of PM ₁ aerosol particles by DMPS and APS	73
2.8.4.1.	Principle	74
2.8.4.2.	Experimental procedure	78
2.8.5.	Calculation of theoretical number of activated particles	79
3.	<i>First study: Absolute concentrations and surface tension curves of surfactants in aerosols at a coastal site in Sweden</i>	<i>83</i>
3.1.	Objectives and method	83
3.2.	Results and discussion	84
3.2.1.	Development of a method for the extraction and analysis of surfactants in aerosols	84
3.2.2.	Atmospheric surfactant concentrations	85
3.2.3.	Absolute surface tension curves and CMC values	87
3.2.4.	Implications for particle activation	88
3.3.	Conclusion	90
4.	<i>Second study: Atmospheric evidence for the role of aerosol surfactants in cloud formation at a boreal site in northern Finland</i>	<i>91</i>
4.1.	Objectives and method	91
4.2.	Results and discussion	93
4.2.1.	Correlation between cloud occurrence and surfactant concentrations	93

4.2.2.	Real-time evolution of surfactant concentration and visibility.....	95
4.2.3.	Correlation between cloud occurrence and surfactant properties.....	96
4.2.4.	CCN efficiency calculation	100
4.3.	Conclusion	102
5.	<i>Third study: Effect of surfactants on the growth of individual micron-sized droplets using an optical trap.....</i>	103
5.1.	Objectives and method	103
5.2.	Results and discussion.....	104
5.2.1.	Effect of surfactants on the change of droplet size	104
5.2.2.	Implication for droplet size distribution.....	108
5.3.	Conclusion	110
6.	<i>Fourth study: Investigation of the origin of surfactants in aerosols</i>	111
6.1.	Objectives and method	111
6.2.	Results and discussion.....	112
6.2.1.	Surfactant properties (CMC)	112
6.2.2.	Fluorescence.....	114
6.2.3.	Comparison with a marine biological marker: chlorophyll- <i>a</i>	116
6.2.4.	Comparison with vegetation and seas	118
6.2.5.	Chemical structure	120
6.3.	Conclusion	122
7.	<i>Summary and outlook</i>	123
8.	<i>Appendix.....</i>	127
8.1.	Reference surfactants	127
8.2.	Chemicals used in the study	128
8.3.	Surface tension curves and surfactant properties (σ_{\min}, CMC) of reference surfactants	129
8.4.	Average and range of CMC values of surfactants in atmospheric aerosols and of reference surfactants	131
8.5.	Real-time evolution of visibility and surfactant concentration in aerosols at Pallas-Sammaltunturi	132
8.6.	Back trajectories at Pallas-Sammaltunturi	136
9.	<i>Résumé étendu de la thèse en français.....</i>	137
10.	<i>Acknowledgments.....</i>	141
10.1.	Funding.....	141
10.2.	People	142
11.	<i>References.....</i>	145

List of Figures

Figure 1.1:	Layers of the Earth’s atmosphere and temperature profile along these layers (reproduced from [Russell, 2015] © Copyright 2015). The Exosphere, uppermost atmospheric layer and considered as space-like layer (starting from altitude of 500 - 1000 km and extended to about 100 000 km), is not represented here. ... 1
Figure 1.2:	Types of clouds and heights of formation (reproduced from [Encyclopædia-Britannica, 2016] © Copyright 2016)..... 3
Figure 1.3:	Typical diameters D of liquid hydrometeors (cloud droplets and raindrop) and of a Cloud Condensation Nuclei (CCN) aerosol particles in atmosphere (redrawn from [Houze, 2014] © Copyright 2014, with permission from Elsevier). 4
Figure 1.4:	Water cycle in the climatic system in its liquid, solid and vapor state and exchanges between the different reservoirs: the ocean, the atmosphere, the continental surfaces and the cryosphere (adapted from [Boucher, 2012] © Copyright 2012 Springer). 5
Figure 1.5:	Earth’s annual and global mean energy budget (reproduced from [Trenberth, 2009] © Copyright 2009 American Meteorological Society)..... 5
Figure 1.6:	Radiative forcing of climate change during the industrial era with associated uncertainty ranges (with black and green horizontal bars corresponding to IPCC 2013 report and IPCC 2007, respectively). The cooling contributions, such as clouds, are situated on the left ($< 0 \text{ W m}^{-2}$) and the warming contributions on the right ($> 0 \text{ W m}^{-2}$). (reproduced from [Stocker, 2013] © Intergovernmental Panel on Climate Change 2013) 6
Figure 1.7:	(up) Schematic of cloud droplet activation and (bottom) Köhler curves (supersaturation SS as a function of droplet diameter D_p) for $(\text{NH}_4)_2\text{SO}_4$ particles with dry diameters 0.05, 0.1 and 0.5 μm at 293 K, assuming spherical dry particles and $\sigma = \sigma_{\text{water}}$ (adapted from [Andreae, 2008] © Copyright 2008, with permission from Elsevier). 9
Figure 1.8:	Schematic representation of the effect of chemicals in cloud droplet formation, with water molecules in blue, chemicals in red and droplet surface in dashed line. The presence of chemicals reduces the surface tension of the droplet (red arrow) and lowers the water vapor pressure (green arrow)..... 10
Figure 1.9:	Illustration of the effect on Köhler curves of (A) the dry particle diameter (for ammonium sulfate particles) and of (B) the chemical composition (for particles with dry diameter of 80 nm) (OA: organic aerosol). The gray-filled region indicates a supersaturation $SS < 1.0 \%$ and the yellow-filled region $SS < 0.3 \%$, generally representative of stratocumulus and cumulus cloud systems, respectively. (reproduced with permission from [Farmer, 2015] © Copyright 2015 American Chemical Society)..... 11
Figure 1.10:	Schematic overview of on-line instruments studying the activation of particles into cloud droplets: HTDMA (Hygroscopic Tandem Differential Mobility Analyzer) and CCNC (Cloud Condensation Nuclei Counters)..... 12

Figure 1.11: Schematic representation of the determination of predicted and measured CCN efficiency, defined by the ratio CCN/CN (Cloud Condensation Nuclei / Condensation Nuclei), corresponding to the number of activated particles into cloud droplets over the number of initial dry particles.....	13
Figure 1.12: Number of published items in each year relative to the κ parameter introduced by [Petters, 2007] (replotted from [Web-of-Science, 2016]).....	14
Figure 1.13: Intercomparison of HTDMAs with different residence times showing the underestimation of the cloud-forming efficiency (growth factor GF) of aerosols at short residence times ([Duplissy, 2009] © Copyright 2009).	15
Figure 1.14: Comparison between predicted and experimental data (from instruments with a residence time of 15 s) using a model which neglects the effect of surfactants by considering the surface tension as the one of water ([Good, 2010b] © Copyright 2010). A systematic underestimation of the number of predicted activated particles ($X\ CCN = CCN_{predicted}/CCN_{measured}$) is observed ($X\ CCN < 1$).	15
Figure 1.15: (A) Köhler curve observations for the system “ammonium sulfate + α -pinene secondary organic aerosol particles” ($D_{p,dry} = 175\text{ nm}$) and (B) corresponding surface tension σ ([Ruehl, 2016] © Copyright 2016). For the signification of the symbols and curves, see the corresponding article.....	16
Figure 1.16: Structural feature of a typical surfactant, with the example of Sodium Dodecyl Sulfate (SDS) adsorbed at the air/water interface.....	17
Figure 1.17: Examples of biological and man-made surfactants.....	19
Figure 1.18: Schematic of (A) a surface tension curve showing the surface tension σ as a function of surfactant concentration $C_{surf,w}$ and (B) the corresponding organization of surfactants for a system air/water (hydrophobic part of the surfactant in orange and hydrophilic part in blue) (redrawn from [Biolin-Scientific, 2016] © 2016 Biolin Scientific Holding AB).	20
Figure 1.19: Comparison of recent surface tension curves as a function of relative surfactant concentration in aerosol particles $C_{surf,p}$ (<i>i.e.</i> the position of the surface tension curves on the x-axis is estimated) for aerosol extracts obtained with a simple water extraction (red curve) and by a double extraction method (blue and grey curves) (adapted from [Mircea, 2005] © Copyright 2005; [Ekström, 2010] © Copyright 2010; [Badel, 2012] © Copyright 2012, with permission from Elsevier)	22
Figure 2.1: Schematic view of aerosol sampling (redrawn and adapted from [Digitel, 2014] © Copyright 2014 DIGITEL Elektronik AG).....	25
Figure 2.2: (A) Location (red oval) and (B) sampling site at the marine research station of Askö, Sweden.	27
Figure 2.3: (A) Location (red arrow) and (B) sampling site at Villeurbanne, France.	28
Figure 2.4: Location of Pallas-Sammaltunturi station (red arrow) in Pallastunturi-Yllästunturi National Park (from [Hatakka, 2003] © Copyright 2003 Boreal Environment Research, reproduced with permission from the publisher).....	29

Figure 2.5:	Pallas-Sammaltunturi station in October 2015 with the aerosol particles sampler (Digitel DA80).	30
Figure 2.6:	Schematic representation of source regions for air parcels arriving to Pallas-Sammaltunturi (red arrow): I Local (North Scandinavia), II Arctic, III East, IV South, V North Atlantic (reproduced from [Aalto, 2002] © Copyright 2002).	31
Figure 2.7:	Example of orographic cloud (Pallastunturi-Yllästunturi National Park, Finland, October 2015). Orographic lift occurs when an air mass is forced from a low elevation to a higher elevation in response to the earth topography (mountains for example).	31
Figure 2.8:	Reference surfactants used in this study (details available in Appendix 8.1 and 8.2).	34
Figure 2.9:	Schematic SPE (Solid-Phase Extraction) procedure used for this work (redrawn and adapted from [Macherey-Nagel-GmbH-&Co, 2015] © Copyright 2015 MACHEREY-NAGEL GmbH & Co. KG).	36
Figure 2.10:	Schematic of the developed extraction method: 1. water extraction of aerosols from the sampled filter; 2. filtration of the solution through syringe filter; 3. SPE procedure; 4. Evaporation of SPE extraction solvent under N ₂ flux; 5. adding of water on the dry surfactant extract; 6. sample ready for further analysis.	39
Figure 2.11:	Schematic of (A) pendant drop and (B) parameters of droplet shape.	41
Figure 2.12:	Comparison of the surface tension curve (surface tension as a function of surfactant concentration) of the glutaric acid between bulk tensiometry and measurements on micron-sized droplets (atomic force microscopy [Morris, 2015] and optical tweezer). The lines are the surface tension parametrizations performed by [Shulman, 1996; Gaman, 2004; Aumann, 2010; Lee, 2014]. The upper axis gives the water activity a_w (Raoult's term). ([Bzdek, 2016] - Published by The Royal Society of Chemistry).....	42
Figure 2.13:	(A) Dataphysics OCA 15EC tensiometer and (B) drop formation. The shape of the droplet before it falls is correlated to the surface tension.....	43
Figure 2.14:	Example of determination, from a surface tension curve, of the CMC value for a surfactant extract sample from aerosols. The red dot represents the initial extract, the black dots at lower concentrations are those obtained from successive dilutions, and the black dot at the largest concentration, corresponding to the concentration in the aerosol, is obtained from the volume ratio between the extract and the aerosol. The blue dashed line represents the value for pure water, and red dashed lines illustrate the graphical determination of the CMC. (reproduced with permission from [Gérard, 2016] © Copyright 2016 American Chemical Society).....	44
Figure 2.15:	Principle of colorimetric method by formation of a surfactant-dye complex followed by a liquid-liquid extraction.	47
Figure 2.16:	Schematic of a UV-visible spectrometer.	48
Figure 2.17:	UV-visible spectra obtained from the reaction of ethyl violet with various concentrations of SDS. Upper right corner: calibration curve for anionic surfactants obtained from the absorbance at 612 nm for SDS (blue points) and	

AOT (orange points). Gray points: blanks. (adapted with permission from [Gérard, 2016] © Copyright 2016 American Chemical Society)	51
Figure 2.18: UV–visible spectra obtained from the reaction of disulfine blue with various concentrations of zephiramine. Upper right corner: calibration curve for cationic surfactants obtained from the absorbance at 628 nm for zephiramine (blue points) and CTAC (orange points). Gray points: blanks.	52
Figure 2.19: UV–visible spectra obtained from the reaction of cobalt thiocyanate with various concentrations of Brij35. Upper right corner: calibration curve for non-ionic surfactants obtained from the absorbance at 317 nm. Gray points: blanks.....	53
Figure 2.20: Effects of interferences on the measured absorbance for the different types of surfactants relative to the calibration curve (horizontal full lines) and the uncertainty range (horizontal dashed lines): NaCl (blue squares), ammonium sulfate (green circles), and oxalic acid (red triangles). The color dashed curves are the best fits through the experimental points. (A) corresponds to the colorimetric method for anionic surfactants (SDS, 2 μM), (B) for cationic surfactants (zephiramine, 2 μM) and (C) for non-ionic surfactants (Brij35, 20 μM).....	56
Figure 2.21: Simplified representation of fluorescence principle. After absorption of a photon of high energy by the electrons of the molecule, the system is excited into one of the many higher energy vibrational states. Some energy is transferred into vibrational energy and then the excited electron relaxes into the ground state, releasing a photon of lower energy than the photon initially absorbed. (adapted from Jablonski diagram).....	57
Figure 2.22: (A) Absorbance (dark blue line) and fluorescence spectra of methylene blue solution CAS 61-73-4 (emission spectrum at a fixed excited wavelength of 292 nm in light blue line and excitation spectrum at a fixed emission wavelength of 700 nm in dashed blue-green line) and (B) methylene blue chemical structure (spectra determined in this work, consistent with [Chu, 2009]).	58
Figure 2.23: Schematic of a fluorescence spectrometer.	58
Figure 2.24: (A) Perkin Elmer LS 45 fluorescence spectrometer and (B) quartz cell containing the sample.....	59
Figure 2.25: Schematic of Liquid Chromatography-Tandem Mass Spectrometry (LC-MS/MS).	60
Figure 2.26: Schematic of a Mass Spectrometer (MS) (redrawn from [Premier-Biosoft, 2016] © Copyright 2016 Premier Biosoft).	61
Figure 2.27: Schematic of tandem mass spectrometry (MS/MS) for product or daughter ion scanning (adapted from [ThermoFisher-Scientific, 2015] © 2015 Copyright ThermoFisher Scientific).	62
Figure 2.28: LC-MS/MS used for this study: Dionex UltiMate 3000 UHPLC coupled with a Q Exactive Hybrid Quadrupole-Orbitrap mass spectrometer, Thermo Scientific, USA.	63
Figure 2.29: Schematic of the optical trap (adapted from [Frossard, 2016 under review])...	65

Figure 2.30: Example of measured Raman spectrum from a single droplet (611 mM NaCl in water, droplet diameter 3722 nm) of overlaid on the matching Mie theory spectrum, which is a function of the droplet radius and refractive index.	66
Figure 2.31: (A) Optical trap set-up built by Amanda A. Frossard from Ronald C. Cohen research group, University of California, Berkeley, USA, with (B) zoom on the elements to manipulate for each experiment.	67
Figure 2.32: Droplet radius as a function of relative humidity and time (with example of a droplet composed of 611 mM NaCl and 0.35 mM Igepal in water). The decrease of the radius corresponds to the evaporation of water at the surface of the droplet and the increase corresponds to the condensation of water onto the droplet.	68
Figure 2.33: (A) Comparison of droplet radii initially and finally at 80 % RH for all of the droplets in the evaporation and condensation experiment. (B) Comparison of droplet radii of aqueous NaCl at 80 % and 70 % RH calculated using Köhler theory (grey squares) and measured in the experiment (circles). The black line represents the r_{70}/r_{80} ratio (0.91 [Tang, 1997; Lewis, 2004]) for similar droplets (reproduced from [Frossard, 2016 under review]).	69
Figure 2.34: Example of data given by the MODIS Aqua satellite (Level 3 Global Monthly): Chlorophyll- <i>a</i> in July 2010 [OceanColor-NASA, 2015].	70
Figure 2.35: Example of 24 h - back trajectories (with a new trajectories starting every hour) at Askö station, Sweden, obtained from HYSPLIT model [Draxler, 2015; Rolph, 2015].	71
Figure 2.36: (A) Simplified schematic of visibility measurement ([Vaisala, 2002] © Copyright 2002 Vaisala) operated by (B) the Vaisala FD12P weather sensor.	72
Figure 2.37: Example of visibility data (blue line) at Pallas-Sammaltunturi in July 2015. Cloud events were considered when a sudden drop in the visibility below 1000 m (red dashed line) appeared.	73
Figure 2.38: Simplified principle of the operating of the Differential Mobility Particle Sizer (DMPS) constituted of a Differential Mobility Analyzer (DMA) and a Condensation Particle Counter (CPC).	74
Figure 2.39: Schematic of the two main parts composing the DMPS: (A) Differential Mobility Analyzer (DMA) and (B) Condensation Particle Counter (CPC) ([TSI, 2002, 2014] © Copyright 2002, 2014, TSI Incorporated).	75
Figure 2.40: Example of size distribution graphs obtained from the DMPS instruments, at Pallas-Sammaltunturi in 2015: (A) time resolved PM _{0.5} size distribution for days 187-189 (year 2015) and (B) average number of particles (blue line) and calculated particles volume (red line) as a function of particle diameter for day 187.	76
Figure 2.41: Schematic of an aerosol flow through an Aerodynamic Particle Sizer Spectrometer (APS) ([TSI, 2012] © Copyright 2012 TSI Incorporated).	77
Figure 2.42: DMPS and APS instruments with the total inlet at Pallas-Sammaltunturi station.	78

Figure 2.43:	Example of determination of critical saturation S_c from Köhler curve calculated as explained in Section 2.8.5, for a dry particle with a diameter $D_{p,dry} = 43$ nm and with $\sigma = \sigma_w = 72.8$ mN m ⁻¹ . The critical saturation S_c corresponds to the maximum of the Köhler curve. For this example, at $S = S_c = 100.8$ % and for a same composition, all particles with a diameter $D_{p,dry} \geq 43$ nm are activated.....	81
Figure 2.44:	Average size distribution of PM1 determined from DMPS and APS data at Pallas-Sammaltunturi station (Section 2.8.4.2) over the 7-months campaign (Avril-November 2015).	82
Figure 3.1:	Concentration of anionic (blue and vertical lines), cationic (red), and non-ionic (green and diagonal lines) surfactants in the aerosols sampled at Askö, Sweden, from July to October 2010: (A) in the aerosol particles volume and (B) in sampled air. Concentrations not shown (in particular for cationic surfactants) are under the detection limit. (reproduced with permission from [Gérard, 2016] © Copyright 2016 American Chemical Society)	86
Figure 3.2:	Absolute surface tension curves for the surfactant fractions of the 11 aerosol samples collected in Askö, Sweden. See the sample list in Table 3.1. (reproduced with permission from [Gérard, 2016] © Copyright 2016 American Chemical Society).....	87
Figure 3.3:	Schematic representation of the importance of $C_{surf,p}/CMC$ in particle activation, based on the absolute surface tension curves determined at Askö station. The average $C_{surf,p}/CMC$ being at 27 - 1000 means that the CCN particle can take water and grow by about a factor of 3 - 10 in radius, while keeping a low surface tension (< 50 mN m ⁻¹).	89
Figure 4.1:	Overview of the period of sampling at Pallas-Sammaltunturi (April - November 2015): cloud events determined from visibility < 1000 m (grey lines) and measured concentration of surfactants in air $C_{surf,a}$ (blue line) over 24-h sampling in the 150 analyzed samples.	92
Figure 4.2:	Correlations between surfactant concentrations in PM1 aerosols with % cloud time for all the aerosol samples analyzed in this work over the 7-months campaign: (A) $C_{surf,p}$ in aerosol particles volume (mM) and (B) $C_{surf,a}$ in air (pmol m ⁻³). The grey points are the original data, and the red and blue ones are the averaged data over 10 % - increments in % cloud time [Gérard, 2016 under review].....	93
Figure 4.3:	Example of real-time evolution of the visibility (m) (blue line), the surfactant concentration in aerosol particles volume $C_{surf,p}$, (mM) (orange line) and the PM1 volume on filters V_{PM1} (10 ⁻² nm ³) (grey line) during the cloud event of days 246 - 252 [Gérard, 2016 under review].	95
Figure 4.4:	Absolute surface tension curves for the surfactants extracted from the 35 PM1 samples (including on average 5 to 6 samples per month of campaign and covering the entire range of % cloud time). Each color represents a range of % cloud time: black = 0 %; brown = 0 - 20 %; blue = 20 - 40 %; green = 40 - 60 %; orange = 60 - 90 %; red = 100 %. The blue dashed line represents the surface tension of pure water, and black dashed lines illustrate the graphical determination of the CMC. [Gérard, 2016 under review].	96

Figure 4.5:	Correlations between (A) CMC values and (B) ratios $C_{surf,p}/CMC$ with % cloud time. Grey points are the original data and red ones are the averaged data over 10 % - increments in % cloud time [Gérard, 2016 under review].....	98
Figure 4.6:	Results of the CCN calculations as a function of saturation S (%): (A) CCN efficiency ("CCN/CN") for the PM1 population for $\sigma = \sigma_w$ (grey dashed line), $C_{surf}/CMC = 100$ (blue line) and 3000 (red line) and (B) corresponding ratios $CCN_{3000}/CCN_{\sigma_w}$ (grey dashed curve) and CCN_{3000}/CCN_{100} (red line) between the different scenarios [Gérard, 2016 under review].	101
Figure 5.1:	Ratio of the equilibrium radius at 70 % RH ($r = r_{70}$) to the equilibrium radius at 80 % RH (r_{80}) for droplets containing NaCl only and NaCl with 0.4 and 4 times the CMC concentration of Igepal ($r = r_{70}$). For droplets with NaCl and 22 and 48 times the CMC concentration of Igepal, the equilibrium radius at the point the droplet was lost (higher than 70 % RH) is used in the ratio ($r = r_{lost}$). The black markers represent individual values. The solid line is the median, boxes represent the 25 to 75 percentiles, and the whiskers are the 10 and 90 percentiles. The dashed horizontal lines are at $r_{70}/r_{80} = 0.87$ (Köhler theory) and 0.91 [Tang, 1997] for droplets containing NaCl only (adapted from [Frossard, 2016 under review])	105
Figure 5.2:	Illustration of comparison between different r_{70}/r_{80} ratios (blue: higher ratio; orange: lower ratio) with (A) schematic Köhler curves representing RH (%) as a function of the droplet radius r (blue line: droplet with NaCl only; orange line: droplet with surfactant Igepal + NaCl) and (B) corresponding droplet growth for RH varying from 70 to 80 % RH. (Note: schematics not at scale).....	107
Figure 5.3:	Number size distributions at an initial RH of 70 % (green) and final RH of 80 %. For NaCl at 80 % RH (dark blue), the number size distribution was calculated using Köhler theory growth from 70 % to 80 % RH. For the NaCl and Igepal mixtures, the number size distribution at 80 % RH (light blue) was calculated using the average ratio of r_{70}/r_{80} (0.82) measured in the experiment for low Igepal concentrations of 0.4 or 4 times the CMC value (reproduced from [Frossard, 2016 under review]).....	109
Figure 6.1:	Comparison of average surface tension curves of aerosols extracts with reference surfactants: coastal aerosols PM2.5 from Askö, Sweden (green line); boreal aerosols PM1 from Pallas-Sammaltunturi, Finland (pink line); urban aerosols PM1 from Villeurbanne, France (red line); HULIS (Humic-like substances) (dashed orange line) [Salma, 2006]; salt and small organic molecules found in atmospheric aerosols (dashed grey line) [Ekström, 2010]; typical ranges of CMC of man-made surfactants (orange area) [Mukerjee, 1971] and biological surfactants (green area) [Desai, 1997].	112
Figure 6.2:	Fluorescence spectra at the different steps of extraction of PM1 collected on quartz filters at Villeurbanne, France: (A) blank method, (B) after water extraction, (C) remaining solution after SPE (matrix containing the interferents) and (D) surfactant fraction extracted after SPE. The diagonal lines appearing in the blank are interferences (Rayleigh scattering and Raman scattering) but do not prevent (here) the observation of the fluorescence spectra of the samples. .	114

- Figure 6.3: Fluorescence spectra at the different extraction steps of PM1 collected on quartz filters at Pallas-Sammaltunturi, Finland: (A) blank method, (B) after water extraction, (C) remaining solution after SPE (matrix containing the interferences) and (D) surfactant fraction extracted after SPE. The diagonal lines appearing in the blank are interferences (Rayleigh scattering and Raman scattering) but do not prevent (here) the observation of the fluorescence spectra of the samples. 115
- Figure 6.4: Correlations between anionic (blue circles), cationic (red triangles), non-ionic (green squares), and total surfactant (black diamonds) concentrations in the atmospheric samples and seawater chlorophyll-*a* concentrations, provided by aqua MODIS satellite (adapted with permission from [Gérard, 2016] © Copyright 2016 American Chemical Society)..... 117
- Figure 6.5: (A) Vegetation map of Europe (adapted from [Adams, 1997]) and (B) Example of back trajectories (30/08/15 22:00 UTC) arriving at the station Pallas-Sammaltunturi (red arrows). The trajectories were obtained from HYSPLIT back trajectories ([Draxler, 2015; Rolph, 2015]): source at 67.97N 24.12E, 72 h - back trajectories (with a new trajectories starting every three hours during the 72 h), model vertical velocity, height 10 m AGL (above ground level). 118
- Figure 6.6: Comparison of the surfactant concentrations ((A) concentration in aerosol particle $C_{surf,p}$ and (B) concentration in air volume $C_{surf,a}$) and properties ((C) CMC and (D) $C_{surf,p}/CMC$) in aerosols from Pallas-Sammaltunturi with the air mass sources. The solid line is the median, boxes represent the 25 to 75 percentiles, and the whiskers are the minimum and maximum values (note: preliminary results)..... 119
- Figure 6.7: Example of LC-MS (ESI+, full MS) spectra of a surfactant aerosol extract from Pallas-Sammaltunturi: (A) LC-chromatogram and corresponding (B) MS-spectra for the retention time range 5 - 11 min and $m/z > 1000$ 121
- Figure 8.1: Surface tension curves of reference surfactants (listed in Sections 8.1 and 8.2) plotted as explained in Experimental Section 2.3.2. 129
- Figure 8.2: Real-time evolution of the visibility (m) (grey lines), the 24 h - averaged surfactant concentrations in aerosol particles volume, $C_{surf,p}$ (mM) (orange lines) and the PM1 volumes on filters, V_{PM1} (10^{-2} nm^3) (blue lines), for the 72 cloud events observed during the campaign at Pallas-Sammaltunturi [Gérard, 2016 under review]..... 135
- Figure 8.3: Example of 72 h - back trajectories arriving at the station Pallas-Sammaltunturi classified by vegetation and seas: (A) Arctic sea (05/07/15 22:00 UTC), (B) North Atlantic sea (13/08/15 22:00 UTC), (C) Baltic sea (22/08/15 22:00 UTC), (D) boreal vegetation (26/07/15 22:00 UTC), (E) temperate vegetation (18/11/16 UTC+2) and (F) Tundra (03/07/15 22:00 UTC). The trajectories were obtained from HYSPLIT back trajectories [Draxler, 2015; Rolph, 2015]: source at 67.97N 24.12E, 72 h -back trajectories (with a new trajectories starting every three hours during the 72h), model vertical velocity, height 10 m AGL (above ground level). 136

List of Tables

Table 1.1:	Examples of surfactants classified according to their chemical structure (adapted from [Myers, 2005; Tadros, 2006; Olkowska, 2011]).	18
Table 1.2:	Examples of biological and synthesized surfactants with their surface tension and CMC values (adapted from [Christofi, 2002] © Copyright 2002 John Wiley & Sons, Inc.).....	21
Table 2.1:	Concentrations of Igepal and NaCl in the micron-sized droplets studied by the optical trap method (modified from [Frossard, 2016 under review])	67
Table 3.1:	List of aerosol samples, CMC (μM) values determined in this work from Askö field campaign and ratios to the aerosol surfactant concentration ($C_{\text{surf,p}}$ in μM) (adapted with permission from [Gérard, 2016] © Copyright 2016 American Chemical Society).....	88
Table 8.1:	Name, formula, CAS and molecular mass of reference surfactants used for the development of the extraction and analysis methods of surfactants in aerosols.	127
Table 8.2:	Comparison between experimental values of σ_{min} and CMC of reference surfactants (listed in Sections 8.1 and 8.2) determined from experimental procedure described in Section 2.3.2 and values from literature, at room temperature. The differences can be attributed to differences of purity.....	130
Table 8.3:	Comparison of CMC between aerosol samples determined in this work and known microbial and artificial surfactants.....	131

Abbreviations and symbols

ACN	Acetonitrile
APS	Aerodynamic Particle Sizer
CN	Condensation Nuclei
CCN	Cloud Condensation Nuclei
CCNC	Cloud Condensation Nuclei Counter
CMC	Critical Micelle Concentration (M)
$C_{\text{surf,p}}$	Surfactant concentration in aerosol particles volume (M = mol L ⁻¹)
$C_{\text{surf,a}}$	Surfactant concentration in air volume (mol m ⁻³)
$C_{\text{surf,w}}$	Surfactant concentration in water (M)
DMPS	Differential Mobility Particle Sizer
HTDMA	Hygroscopicity Tandem Differential Mobility Analyzer
LC-MS/MS	Liquid Chromatography - tandem Mass Spectrometry
PM1	Particulate Matter (=aerosol particles) with diameter $\leq 1 \mu\text{m}$
PM2.5	Particulate Matter (=aerosol particles) with diameter $\leq 2.5 \mu\text{m}$
SPE	Solid-Phase Extraction
A	Absorbance
ϵ	Absorption coefficient (M ⁻¹ cm ⁻¹)
λ	Wavelength (nm)
σ	Surface tension (mN m ⁻¹)
σ_{min}	Minimum surface tension value (mN m ⁻¹) (plateau of surface tension curve)
σ_{dry}	Surface tension value (mN m ⁻¹) in the “dry” aerosol particles volume
m	Mass (kg)
T	Temperature (K in equations, °C in experimental procedures)
V	Volume (m ³)
ρ	Mass density (kg m ⁻³)
C	Concentration (M)
M	Molecular mass (kg mol ⁻¹)
r	Radius of particle (m)
D_p	Diameter of particle (wet or dry) (m)
$D_{p,\text{dry}}$	Diameter of dry particle (m)
RH	Relative humidity (%)
S	Saturation (%)
SS	Supersaturation (%)
S_c	Critical saturation (%)

1. Scientific context

1.1. Atmosphere

The subject of this PhD work was the investigation of the role of some chemical compounds in cloud formation in the Earth's atmosphere. The atmosphere is the gas layer surrounding the Earth and extending from the surface out to thousands of kilometers. It is held in place by gravitation and becomes less dense as altitude increases. The atmosphere protects all life on Earth from meteors and harmful solar radiation and warms the Earth's surface by heat retention (greenhouse effect). The Earth's atmosphere is characterized by layers that are defined by changes in the vertical temperature profile: troposphere, stratosphere, mesosphere, thermosphere and exosphere (Figure 1.1).

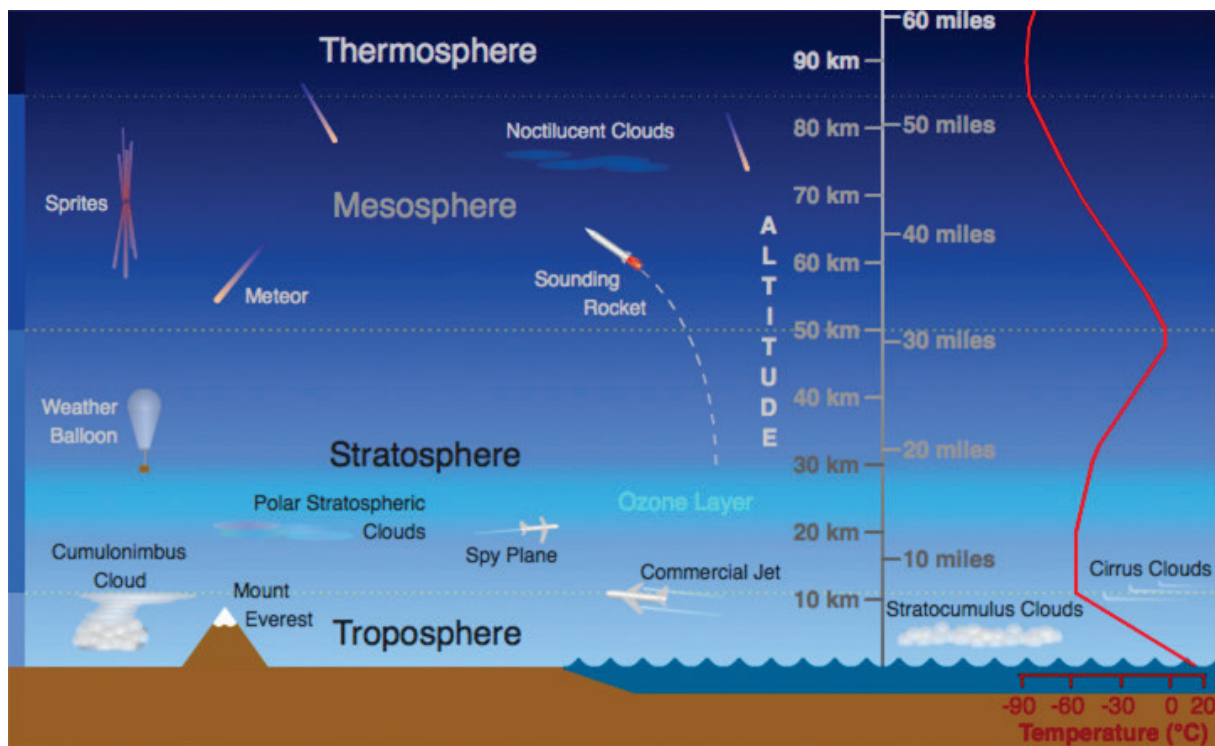


Figure 1.1: Layers of the Earth's atmosphere and temperature profile along these layers (reproduced from [Russell, 2015] © Copyright 2015). The Exosphere, uppermost atmospheric layer and considered as space-like layer (starting from altitude of 500 - 1000 km and extended to about 100 000 km), is not represented here.

The atmosphere contains both gases and suspended particles. Dry air is made by volume of about 78 % of nitrogen (N₂) and 21 % of oxygen (O₂), the remaining 1 % consisting of argon, carbon dioxide and trace amounts of other gases. Water vapor is one of these trace gases and is present in concentrations varying widely with the meteorological conditions, the altitude and the latitude. The atmosphere interacts with other elements of the Earth's system, such as the oceans, the lithosphere, the pedosphere, the biosphere and the cryosphere.

The present study focuses on the formation of clouds, thus on the lowest layer, the troposphere, which extends from the Earth's surface up to 10 - 15 km altitude (the tropopause), depending on latitude and time of year. The troposphere is characterized by a decreasing temperature with altitude and a rapid vertical mixing. This is the densest part of the atmosphere and where emissions (anthropogenic or biogenic) have the most influence.

1.2. Clouds

1.2.1. General information on clouds

The World Meteorological Organization [WMO, 1975] defines a *cloud* as “a hydrometeor consisting of minute particles of liquid water or ice, or of both, suspended in the free air and usually not touching the ground. It may also include larger particles of liquid water or ice and non-aqueous liquid or solid particles such as those present in fumes, smoke and dust”. Clouds cover roughly two thirds of the globe. They are constantly forming and evaporating and only 10 % precipitate [Boucher, 2013].

Several types of clouds, of different shapes and heights, are present in the atmosphere (Figure 1.2). Their variability depends on their formation processes, the vertical and horizontal air velocity, the liquid water content of the air mass in which they are present, etc.

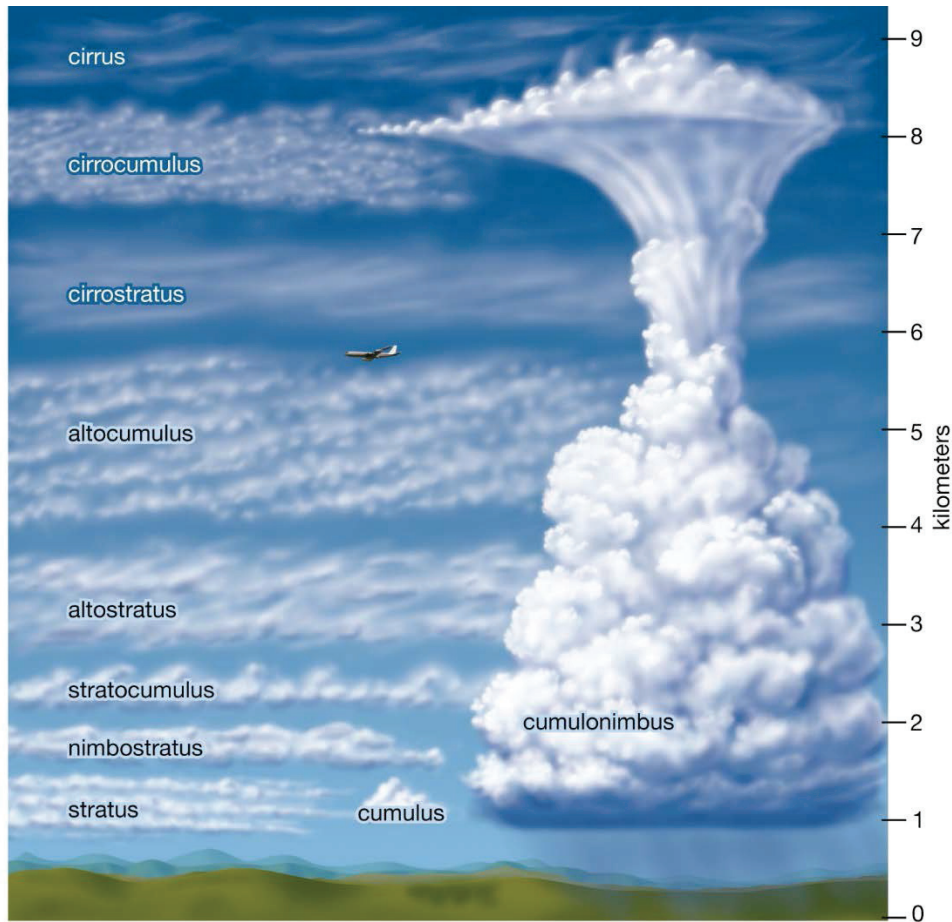


Figure 1.2: Types of clouds and heights of formation (reproduced from [Encyclopædia-Britannica, 2016] © Copyright 2016).

Clouds can also be distinguished in three main groups according to their particulate composition. The American Meteorology Society [AMS, 2016] distinguishes warm clouds (also called water clouds), ice-crystal clouds and mixed clouds. A cloud composed entirely of liquid water droplets is called a water cloud. Analogously, a cloud consisting entirely of ice crystals is called an ice-crystal cloud and a mixed-phase cloud contains both water droplets (supercooled at temperature below 0°C) and ice crystals.

In liquid clouds, the size of the droplets varies with the cloud type. Figure 1.3 shows the typical sizes for liquid cloud droplets. Liquid droplets are formed by condensation of water onto a pre-existing atmospheric aerosol particle (*i.e.* a small solid or liquid particle in suspension in the atmosphere) called “Cloud Condensation Nuclei” (CCN). Fully grown cloud droplets range generally from 1 to 100 μm in diameter. If they grow until $> 200 \mu\text{m}$, they can become raindrops.

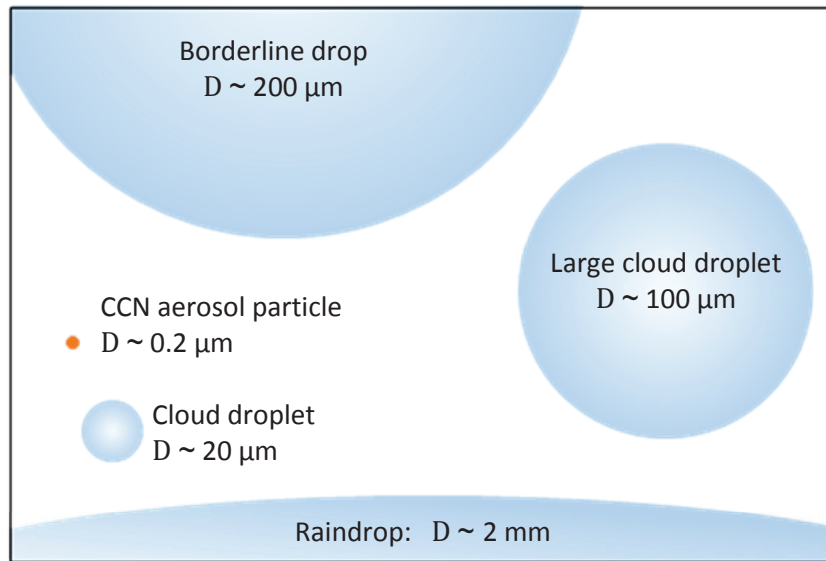


Figure 1.3: Typical diameters D of liquid hydrometeors (cloud droplets and raindrop) and of a Cloud Condensation Nuclei (CCN) aerosol particles in atmosphere (redrawn from [Houze, 2014] © Copyright 2014, with permission from Elsevier).

The present study focuses on liquid cloud droplets only, thus will not address ice clouds.

1.2.2. Importance of clouds in atmosphere

Clouds cover about two thirds of the globe and are one of the most important elements of the atmospheric system, playing many key roles in hydrology and in the climate budget [Seinfeld, 2006; Boucher, 2013]. Clouds are central in the hydrological cycle (Figure 1.4) as they are the main source of fresh water to the continents, as rain or snow. And, by warming or cooling the lower atmosphere, clouds are a major factor in the Earth's radiation budget; clouds warm the lower atmosphere by trapping infrared radiation emitted by the Earth's surface and cool the atmosphere by reflecting solar radiation back to the space. Clouds are thus the main cooling component of the climate budget (Figure 1.5 and Figure 1.6) [Stocker, 2013].

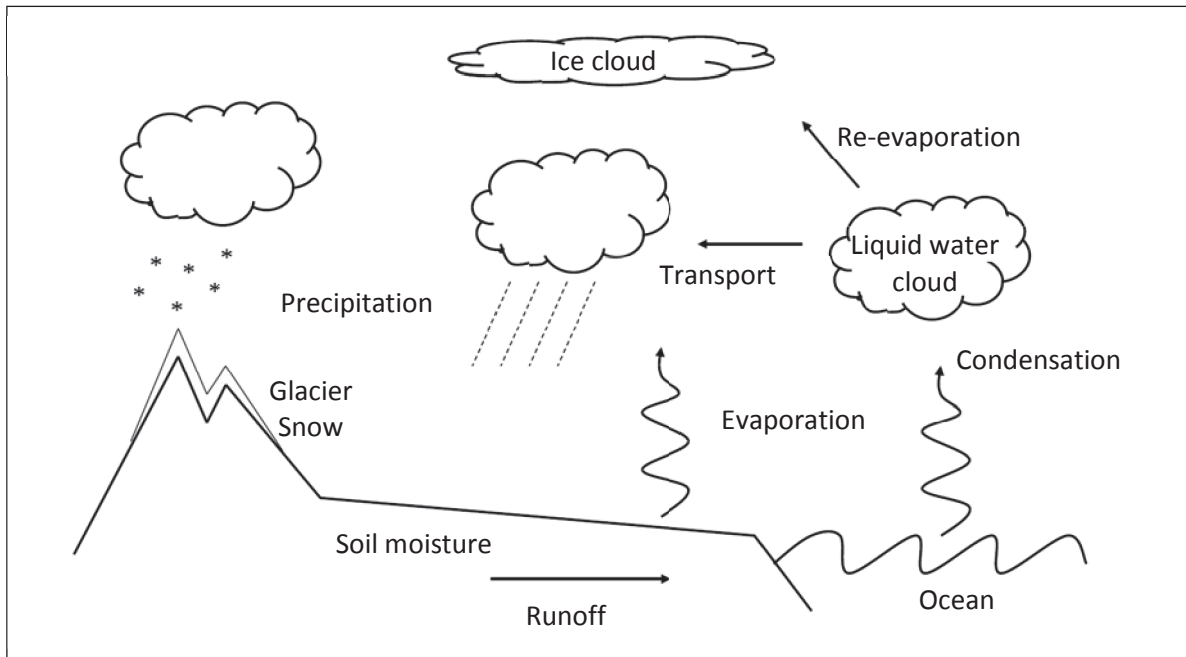


Figure 1.4: Water cycle in the climatic system in its liquid, solid and vapor state and exchanges between the different reservoirs: the ocean, the atmosphere, the continental surfaces and the cryosphere (adapted from [Boucher, 2012] © Copyright 2012 Springer).

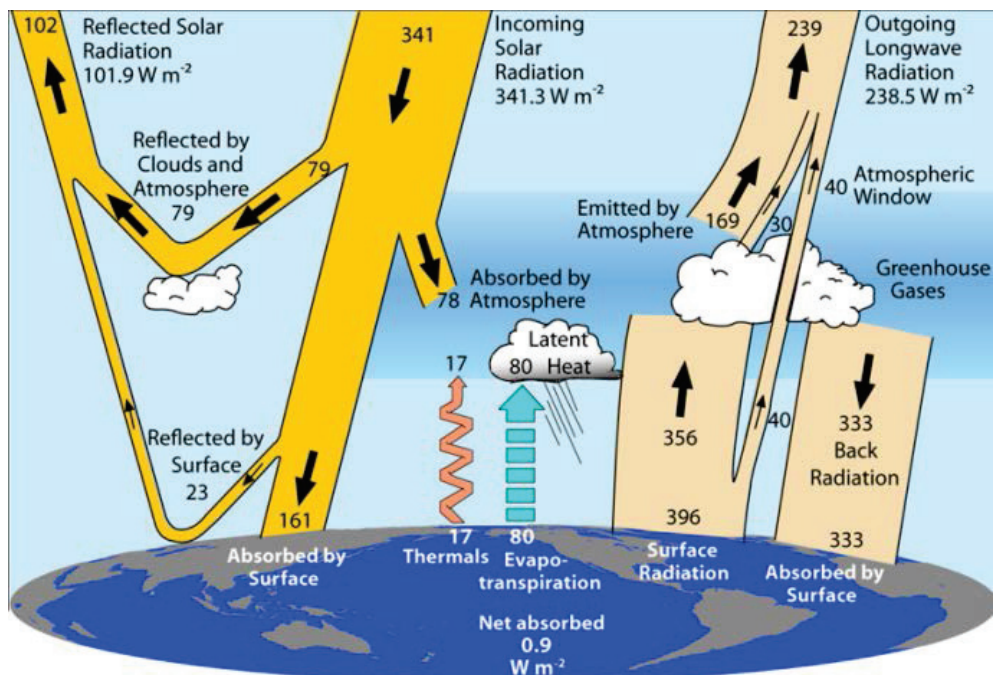


Figure 1.5: Earth's annual and global mean energy budget (reproduced from [Trenberth, 2009] © Copyright 2009 American Meteorological Society).

Clouds also scavenge gaseous and particulate materials and return them to the surface (wet deposition) and provide a medium for aqueous-phase chemical reactions and production of secondary species. Finally, clouds affect the vertical redistribution of particles or gases in the atmosphere [Seinfeld, 2006].

Despite their central importance, predicting cloud formation is still beyond model capacities and is not expected to improve in the near future [Boucher, 2013]. Many of the challenges are due to computational limitations, and in the representation of cloud microphysical processes in climate models. In particular, the latest IPCC (Intergovernmental Panel on Climate Change) report points out the need for more investigation of the role of surfactants (in mixed organic/inorganic aerosols) in cloud droplet activation [Boucher, 2013]. Due to the low confidence in all these aspects of cloud formation processes, clouds contribute to the largest uncertainties in the climate radiative budget [Stocker, 2013] (Figure 1.6).

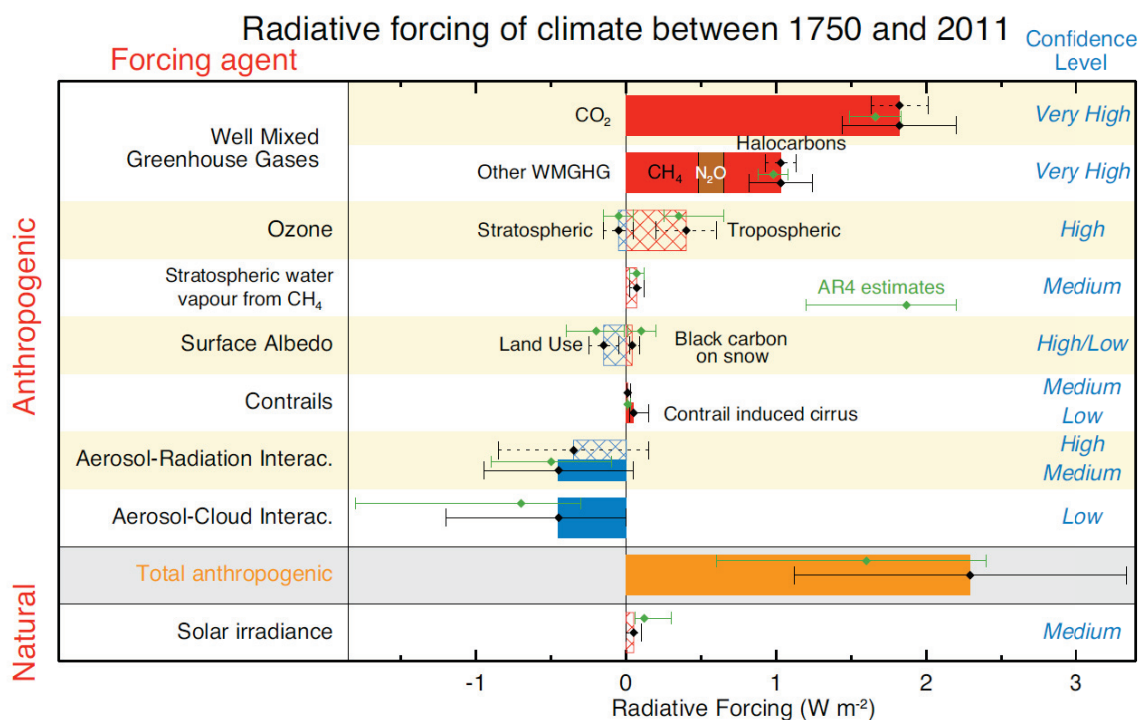


Figure 1.6: Radiative forcing of climate change during the industrial era with associated uncertainty ranges (with black and green horizontal bars corresponding to IPCC 2013 report and IPCC 2007, respectively). The cooling contributions, such as clouds, are situated on the left ($< 0 \text{ W m}^{-2}$) and the warming contributions on the right ($> 0 \text{ W m}^{-2}$). (reproduced from [Stocker, 2013] © Intergovernmental Panel on Climate Change 2013)

1.3. Formation of liquid clouds

Liquid clouds are formed when an air mass ascends and cools down enough so that the water vapor it contains, $p_{\text{H}_2\text{O}}$, reaches saturation, $p_{\text{H}_2\text{O}}^{\text{sat}}$, thus triggering the formation of liquid droplets. In the atmosphere, water vapor is often expressed in term of relative humidity RH defined as:

$$\text{RH} = 100 \% \frac{p_{\text{H}_2\text{O}}}{p_{\text{H}_2\text{O}}^{\text{sat}}} . \quad (1.1)$$

The ratio $S = \frac{p_{\text{H}_2\text{O}}}{p_{\text{H}_2\text{O}}^{\text{sat}}}$ corresponds to the saturation. The supersaturation SS is defined by $\text{SS} = S - 1$ and corresponds to the excess of water vapor over the saturation water vapor, *i.e.* when $S > 1$. For example a relative humidity of 101 % corresponds to a supersaturation of 1 %.

1.3.1. Köhler equation

At the microscopic scale, the processes are more complex and are described in this section. The phase change from water vapor to liquid water implies the formation of droplets. Thus, the Gibbs energy budget for this transition involves the vapor pressure difference between the two states, the vapor pressure around the droplets, $p_{\text{H}_2\text{O}}^{\text{sat,drop}}$, being higher than in the initial gas, $p_{\text{H}_2\text{O}}$, and the formation energy of the new surface. At equilibrium, the difference in Gibbs energy is null, which leads to a relationship between the ratio of the vapor pressures, $p_{\text{H}_2\text{O}}^{\text{sat,drop}} / p_{\text{H}_2\text{O}}^{\text{sat}}$, and the surface energy term, called Kelvin equation:

$$\frac{p_{\text{H}_2\text{O}}^{\text{sat,drop}}}{p_{\text{H}_2\text{O}}^{\text{sat}}} = \exp\left(\frac{4 \sigma M_w}{\rho_w R T D_p}\right) \quad (1.2)$$

where D_p is the diameter of the droplet, M_w is the molecular weight of water, ρ_w is the water volumetric mass density, R is the gas constant, T is the temperature of the system and σ is the surface tension between the droplet and the air surrounding the droplet. The surface tension σ results from the imbalance of intermolecular forces (cohesive and repulsive forces). It corresponds to an energy per unit area (J m^{-2} , usually expressed in mN m^{-1}) and is a measure

of the energy needed to enlarge the surface area by 1 m². For a liquid in suspension in air, the system tends to minimize the interfacial free energy. At the interfacial area, the dispersed phase tends to form spherical droplets, because a sphere is the shape with the smallest surface-to-volume ratio.

In Earth's atmosphere, the supersaturation rarely exceeds 1 % [Seinfeld, 2006; Boucher, 2012], which, according to the above equation (1.2), would require water molecular clusters to have a diameter of $D_p > 0.2 \mu\text{m}$ to be able to grow into a cloud droplet. As this is unrealistic (the majority, in number, of aerosol particles having generally diameters $< 0.2 \mu\text{m}$), cloud formation cannot occur by homogenous nucleation of water in the Earth's atmosphere. **In the atmosphere, cloud droplets can only form by heterogeneous nucleation of water onto pre-existing aerosol particles** [Aitken, 1880].

Heterogeneous nucleation on pre-existing particles makes possible cloud droplet formation in the atmosphere because "impurities" brought into the water by the particle lower the water vapor pressure above the liquid ("Raoult's effect") (Figure 1.8). In that case, the vapor pressure above the solution, $p_{\text{H}_2\text{O}}^{\text{sat}}$, is given by the Raoult's law:

$$p_{\text{H}_2\text{O}}^{\text{sat}} = \gamma_w x_w p_{\text{H}_2\text{O}}^{\text{sat,solution}} = a_w p_{\text{H}_2\text{O}}^{\text{sat,solution}} \quad (1.3)$$

where γ_w is the water activity coefficient, x_w is the mole fraction of water in the solution, and a_w the "Raoult's term" ($a_w = 1$ for pure water and $a_w < 1$ for soluble solutes diluted in solution). Replacing (1.3) in equation (1.2) gives the following equation called Köhler equation [Köhler, 1936]:

$$p_{\text{H}_2\text{O}}^{\text{sat,drop}} = a_w \exp\left(\frac{4 \sigma M_w}{p_w R T D_p}\right) p_{\text{H}_2\text{O}}^{\text{sat,solution}} \quad (1.4)$$

where $p_{\text{H}_2\text{O}}^{\text{sat,drop}}$ is the vapor pressure around the droplet.

Equation (1.4) can also be written:

$$S = a_w \exp\left(\frac{4 \sigma M_w}{p_w R T D_p}\right) \cdot \quad (1.5)$$

The Köhler equation, $S(D_p)$, thus describes the evolution of forming droplets as a function of saturation S (or as function of supersaturation $SS = S - 1$).

Figure 1.7 shows examples of Köhler curves for droplets formed from particles made of $(\text{NH}_4)_2\text{SO}_4$ with different initial (dry) diameters. Because of the opposition of the surface tension and the Kelvin effect, all Köhler curves display a maximum, corresponding to the critical supersaturation and critical diameter. To grow spontaneously into a cloud droplet, the forming droplet must pass this maximum (equivalent to an energy barrier). As it can be seen in the Köhler equation, cloud droplets are much easier to form when starting from large particles than from smaller ones, because the Kelvin effect is smaller in that case.

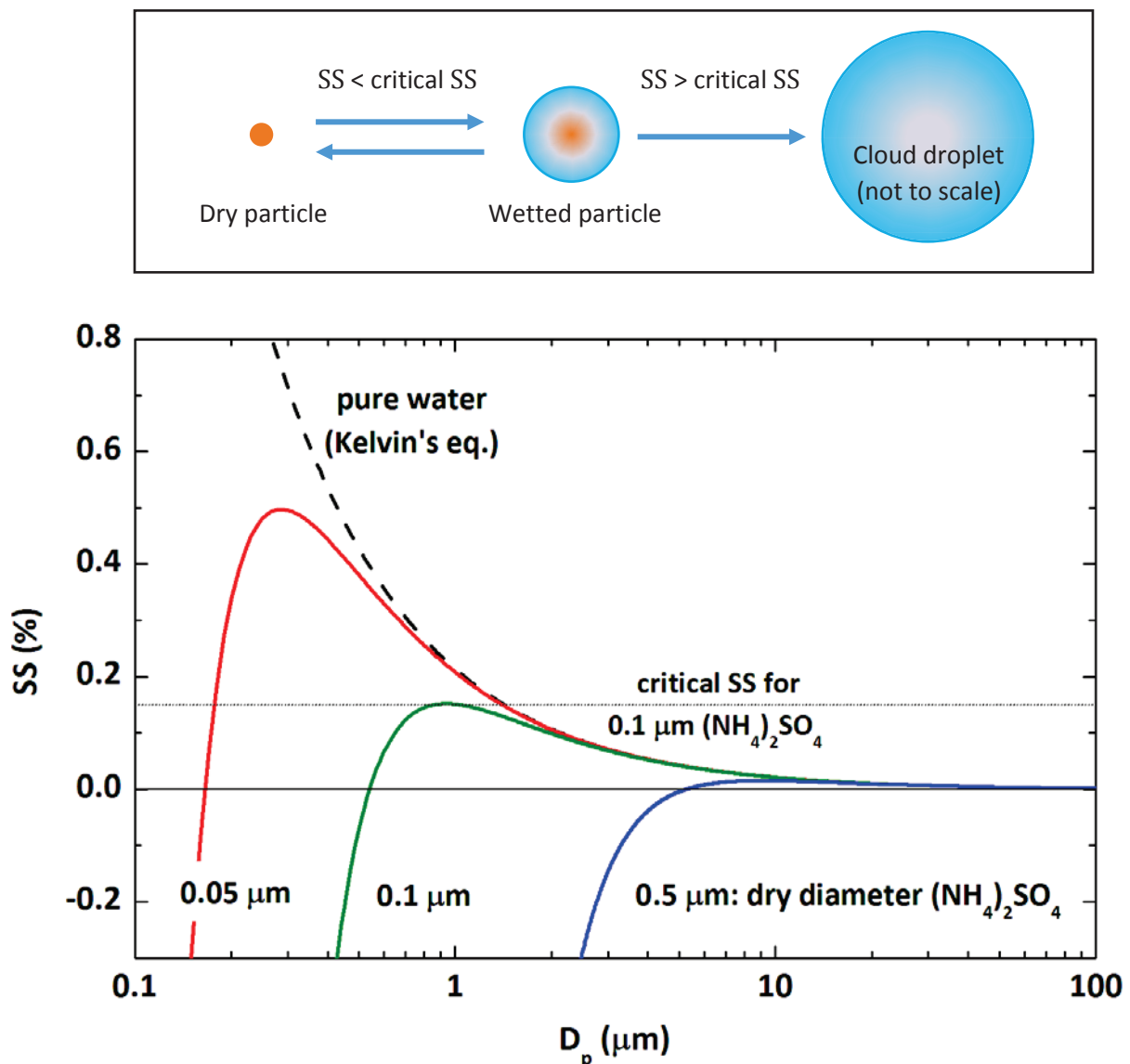


Figure 1.7: (up) Schematic of cloud droplet activation and (bottom) Köhler curves (supersaturation SS as a function of droplet diameter D_p) for $(\text{NH}_4)_2\text{SO}_4$ particles with dry diameters 0.05, 0.1 and 0.5 μm at 293 K, assuming spherical dry particles and $\sigma = \sigma_{\text{water}}$ (adapted from [Andreae, 2008] © Copyright 2008, with permission from Elsevier).

1.3.2. Role of chemistry

In the above Köhler equation (1.5), chemical compounds brought by the initial particles can affect droplet growth on only two parameters: the Raoult's term a_w and the surface tension σ (Figure 1.8).

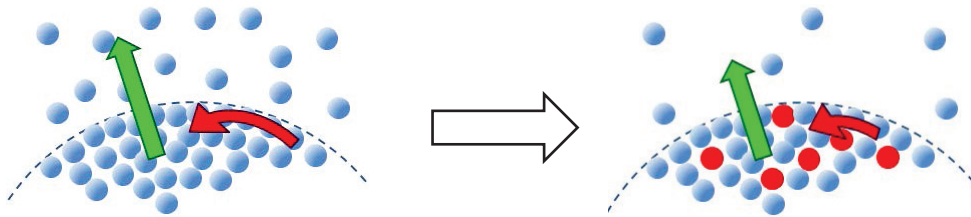


Figure 1.8: Schematic representation of the effect of chemicals in cloud droplet formation, with water molecules in blue, chemicals in red and droplet surface in dashed line. The presence of chemicals reduces the surface tension of the droplet (red arrow) and lowers the water vapor pressure (green arrow).

The Raoult's effect increases (*i.e.* a_w decreases) with the number of dissolved molecules, since the molecules of water are replaced by less volatile molecules in the droplet. As inorganic salts dissociate entirely, while organic compounds dissolve only partly in water, inorganic compounds generally have a larger Raoult's effect than organic compounds, thus are more efficient cloud nuclei.

The surface tension, on the other hand, can be decreased by the presence of compounds called surfactants (see Section 1.6), which will favor droplet formation.

Thus, according to the Köhler equation (1.5), the ability of an aerosol particle to activate into cloud droplet will depend both on its size and its chemical composition (Figure 1.9). For a same value of supersaturation, larger particles ($> 1 \mu\text{m}$) will nucleate easier than small ones. Thus, the effect of chemical composition on the cloud-forming properties of particles will be mostly significant on small particles.

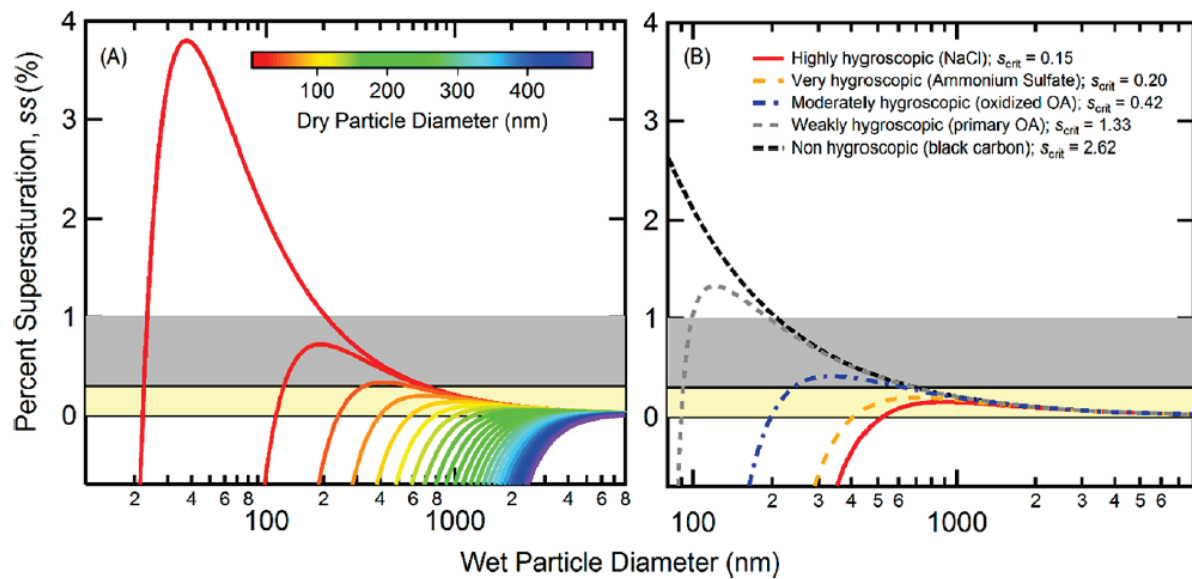


Figure 1.9: Illustration of the effect on Köhler curves of (A) the dry particle diameter (for ammonium sulfate particles) and of (B) the chemical composition (for particles with dry diameter of 80 nm) (OA: organic aerosol). The gray-filled region indicates a supersaturation $SS < 1.0\%$ and the yellow-filled region $SS < 0.3\%$, generally representative of stratocumulus and cumulus cloud systems, respectively. (reproduced with permission from [Farmer, 2015] © Copyright 2015 American Chemical Society)

1.3.3. Atmospheric aerosol composition and implication for cloud formation

In addition to the presence of gases, the atmosphere contains a wide range of aerosols, which are defined as a suspension of fine solid or liquid particles in suspension in the air. The sources of these aerosol particles can be natural or anthropogenic. Natural emissions include soil and rock debris (windborne dust), volcanic action, sea spray, biomass burning, biogenic aerosols (pollens, fungal spores, bacteria cells...) and reactions between natural gaseous emissions. Emissions of particulate matter due to the activities of humans arise from fuel combustion, industrial processes, non-industrial fugitive sources (roadway dust from paved and unpaved roads, wind erosion of cropland, construction, etc.), and transportation sources (automobiles, etc.) [Colbeck, 1998; Seinfeld, 2006]. The atmospheric aerosols can have different compositions, shapes and sizes, depending of their sources and processes of formation.

Aerosol particle concentrations are typically in the range $10^2 - 10^6$ particles cm^{-3} air. But only a very small fraction of these particles are expected to become Cloud Condensation Nuclei (less than $1 / 1000$), and even less cloud droplets. The particles that do not participate in the cloud formation are referred as “interstitial” particles.

1.4. Measurement of cloud droplet formation and comparison with theory

The only techniques used until now to investigate the growth of cloud droplets are so called “on-line” instruments, which consist in measuring the growth in particle size (*Hygroscopicity Tandem Differential Mobility Analyzers, HTDMAs*) or number (*Cloud Condensation Nuclei Counters, CCNCs*) of a known aerosol population subjected to a controlled relative humidity [Good, 2010a]. Thus none of these instruments measures directly the parameters needed in the Köhler equation (Figure 1.10).

	HTDMA	CCNC
Aerosol inlet	selected particle size	total inlet
Conditions in chamber	constant relative humidity RH (< 95 %)	specific supersaturation SS (%)
Data	hygroscopicity (growth factor $GF = D_{\text{droplet}} / D_{\text{dry}}$) at a fixed dry particle size and RH	number of activated particles (CCN) as a function of SS

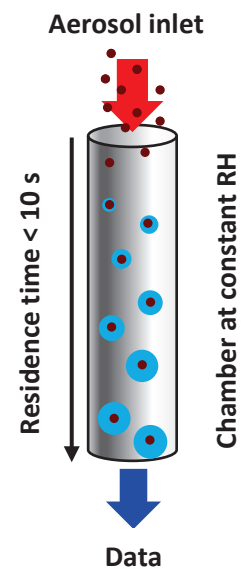


Figure 1.10: Schematic overview of on-line instruments studying the activation of particles into cloud droplets: HTDMA (Hygroscopic Tandem Differential Mobility Analyzer) and CCNC (Cloud Condensation Nuclei Counters).

Comparisons between the CCN numbers predicted by Köhler theory and measured by CCNCs in a given region of the atmosphere (or “closure experiments”) have been the main criterion so far to assess the understanding of cloud formation processes in the atmospheric community. For this, the Growth Factor (GF) values measured by HTDMA are used to determine the value of a_w to be used in the Köhler equation. (Figure 1.11).

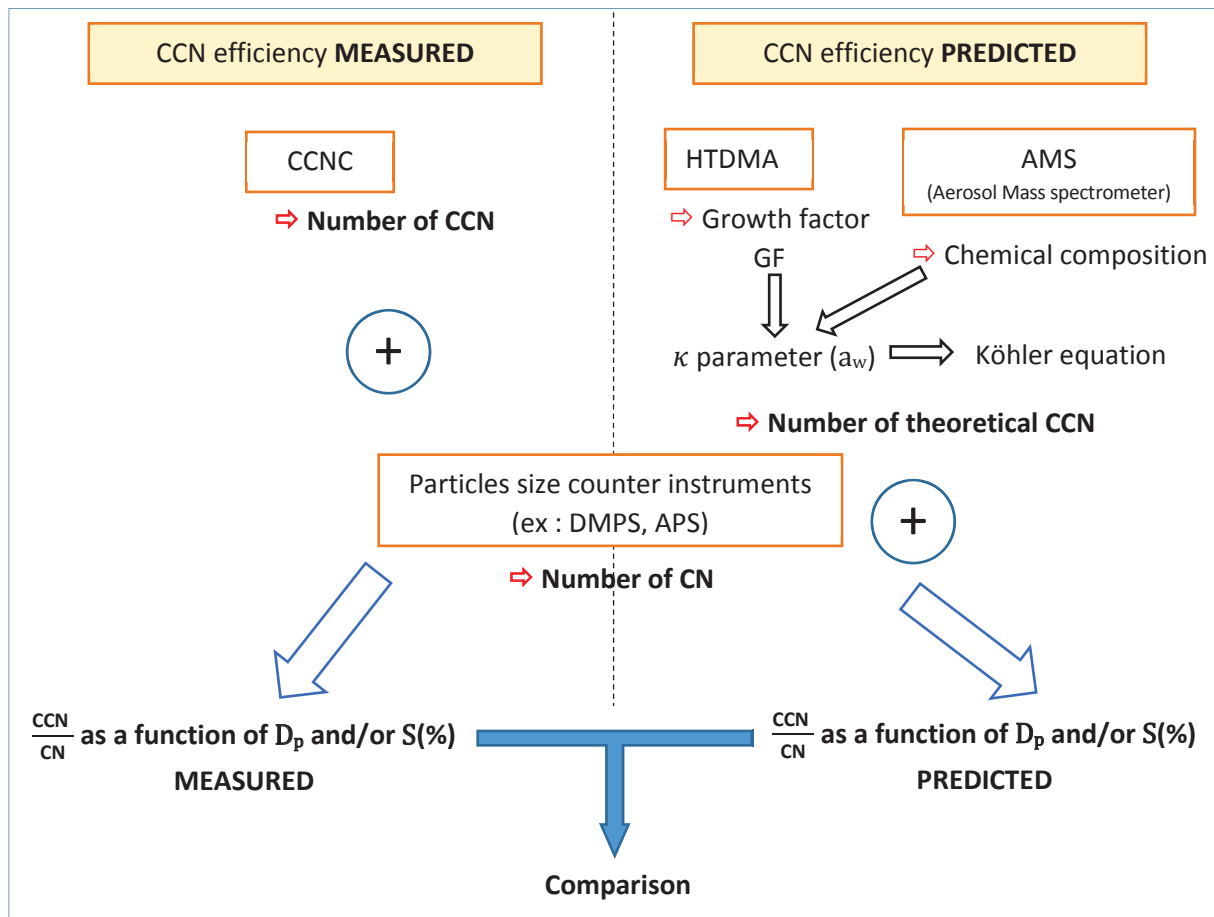


Figure 1.11: Schematic representation of the determination of predicted and measured CCN efficiency, defined by the ratio $\frac{\text{CCN}}{\text{CN}}$ (Cloud Condensation Nuclei / Condensation Nuclei), corresponding to the number of activated particles into cloud droplets over the number of initial dry particles.

Note that, in the recent literature the parameter a_w is expressed by the hygroscopic parameter κ , [Petters, 2007], defined by:

$$\frac{1}{a_w} = 1 + \kappa \frac{V_s}{V_w} \quad (1.7)$$

where V_s is the volume of the solute (the dry particulate matter) and V_w is the volume of the water. The volume of the whole droplet is defined by the sum of V_s and V_w .

The parameters a_w or κ represent the hygroscopicity, *i.e.* the ability of the particle bulk to absorb moisture from the air [Petters, 2007].

Numerous efforts have been dedicated in studies of the role of aerosol chemistry on the κ parameter, as shown by the more than 600 articles published on this subject (Figure 1.12). This includes recent efforts in predicting the value of κ based on the simplified aerosol chemical composition measured by Aerosol Mass spectrometer (AMS).

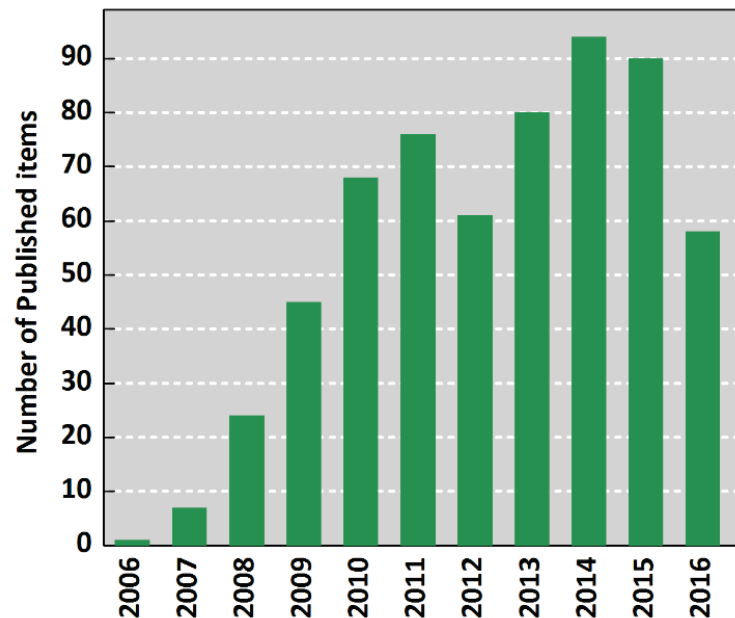


Figure 1.12: Number of published items in each year relative to the κ parameter introduced by [Petters, 2007] (replotted from [Web-of-Science, 2016]).

However, in all these determinations, the surface tension σ of the forming droplets is always assumed to be the one of pure water, σ_w , because the effect of surfactants on droplet growth could never be observed by CCNCs and HTDMAs (to a few exceptions, see next section). Thus, the good agreement (or “closure”) between measured and predicted CCN numbers reported in numerous studies is, in reality, based on one side by the lack of detection of surfactants by the instruments and, on the other side, by neglecting their role in the calculations.

The lack of detection of surfactant effects by these classical techniques also explains why these compounds have hardly been studied, in spite of the predictions of Köhler theory.

1.5. Recent developments

Over the last decades, several studies have started to evidence a role of surfactants in cloud droplet formation and to show that the classical investigation techniques, HDTMAs and CCNCs, might be instrumentally biased against surfactants.

Studies suggesting instrumental limitations in the classical techniques operating include intercomparisons of 6 HTDMAs providing, for the same aerosol, growth factors (GF) that were proportional to the instrument residence time [Duplissy, 2009] (Figure 1.13).

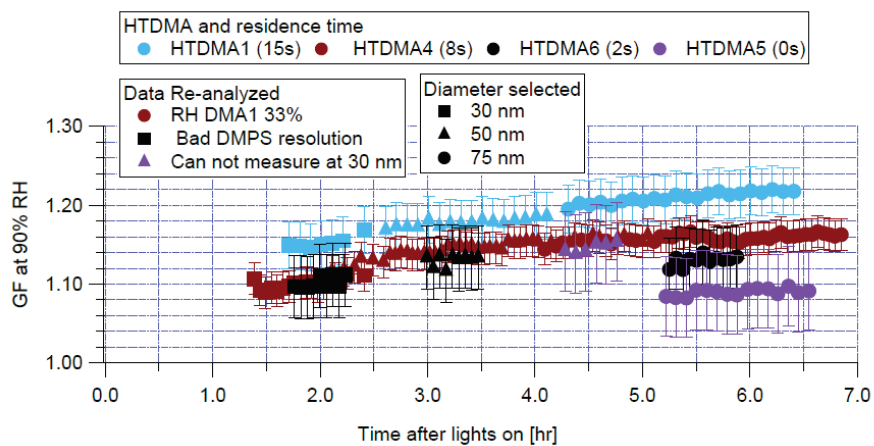


Figure 1.13: Intercomparison of HTDMAs with different residence times showing the underestimation of the cloud-forming efficiency (growth factor GF) of aerosols at short residence times ([Duplissy, 2009] © Copyright 2009).

Other studies have extended the residence time of their instrument (15 s - 60 s) and reported twice as many CCNs as with the classical techniques, which could only be accounted for with a surface tension of less than 50 mN m^{-1} [Good, 2010b; Irwin, 2010] (e.g. Figure 1.14).

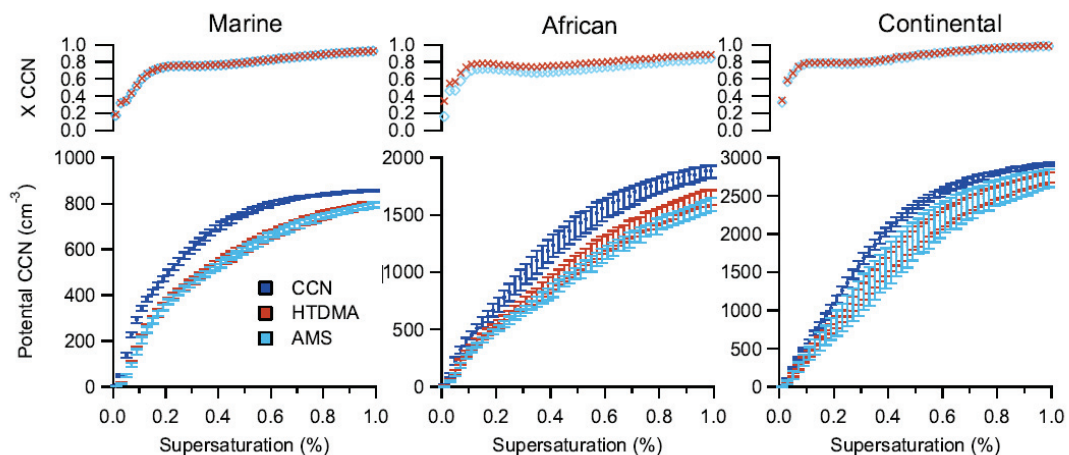


Figure 1.14: Comparison between predicted and experimental data (from instruments with a residence time of 15 s) using a model which neglects the effect of surfactants by considering the surface tension as the one of water ([Good, 2010b] © Copyright 2010). A systematic underestimation of the number of predicted activated particles ($X \text{ CCN} = \text{CCN}_{\text{predicted}}/\text{CCN}_{\text{measured}} < 1$) is observed ($X \text{ CCN} < 1$).

This was explained by the long delay to equilibrium of strong surfactants, predicted to require more than 30 s to reach their full effect, thus not detectable by classical on-line instruments [Nozière, 2014]. This prediction has now been confirmed by direct measurements on micron-sized particles with an optical tweezer, reporting delays to equilibration for strong surfactants over a minute [Reid, 2017 in preparation].

Other studies than [Good, 2010b] and [Irwin, 2010] have also evidenced the role of surfactants in cloud droplet formation. And they also involved the use of non-classical approaches. In laboratory, CCNC measurements on biomass burning aerosols combined with surface tension measurements showed the importance of surface properties on CCN activity [Asa-Awuku, 2008; Giordano, 2013]. Variations with proportion of organics in particles (organics found in atmospheric aerosol particles such as malonic acid, succinic acid, α -pinene secondary organic aerosol particles, etc.) indicated reduced surface tension in measurements of water uptake in gradient chamber [Ruehl, 2012; Ruehl, 2014; Ruehl, 2016] (Figure 1.15).

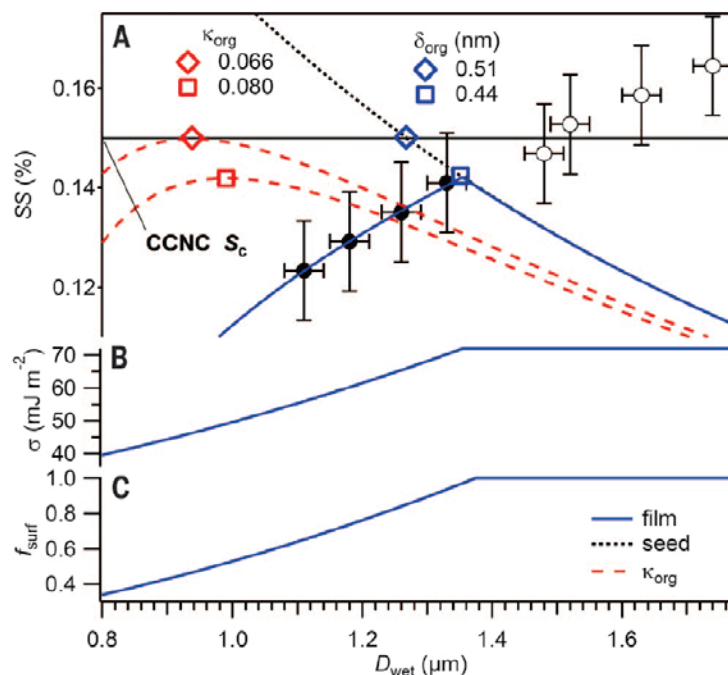


Figure 1.15: (A) Köhler curve observations for the system “ammonium sulfate + α -pinene secondary organic aerosol particles” ($D_{p,dry} = 175$ nm) and (B) corresponding surface tension σ ([Ruehl, 2016] © Copyright 2016). For the signification of the symbols and curves, see the corresponding article.

Consequently, because **some studies started to show that surfactants are more important as previously thought**, it is **essential to go further** and to study them, hence this work.

1.6. Surfactants

1.6.1. Definition

According to the International Union of Pure and Applied Chemistry (IUPAC), a *surfactant* (contraction of surface - active agent) is “a substance which lowers the surface tension of the medium in which it is dissolved, and/or the interfacial tension with other phases, and, accordingly, is positively adsorbed at the liquid/vapour and/or at other interfaces.”

Many surfactants are amphiphilic molecules, having a water insoluble (hydrophobic) part and a water soluble (hydrophilic) one. Surfactants place themselves at the interface of two phases (liquid/gas or two immiscible liquids). In aqueous systems, the hydrophobic group is generally a long-chain hydrocarbon group and the hydrophilic head is an ionic or highly polar group (example in Figure 1.16).

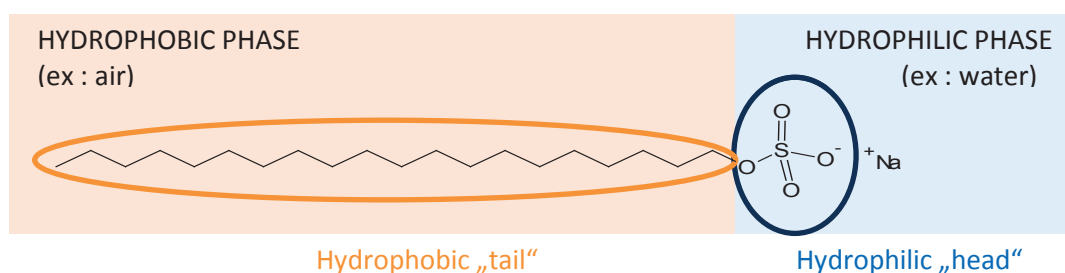


Figure 1.16: Structural feature of a typical surfactant, with the example of Sodium Dodecyl Sulfate (SDS) adsorbed at the air/water interface.

Surfactants are often distinguished by their ionic properties: anionic, cationic, non-ionic, or amphoteric. Anionic (respectively cationic) surfactants are surfactants that carry a negative (respectively positive) charge on the surface-active portion of the molecule. Amphoteric surfactants can be either cationic or anionic depending on the pH or other solution conditions, including those that are zwitterionic, possessing permanent charge of each type. The non-ionic surfactants have no charge. Examples of surfactant structures are given in Table 1.1.

Table 1.1: Examples of surfactants classified according to their chemical structure (adapted from [Myers, 2005; Tadros, 2006; Olkowska, 2011]).

Charge of head group	Type of charge	Chemical structure
Non ionic		Nonylphenols $C_6H_4(OH)C_9H_{19}$
		Alkylphenoethoxylates $RO(CH_2CH_2O)_nH$ R=alkylphenol group
		Alcohol ethoxylates $C_nH_{2n+1}(OCH_2CH_2)_nOH$
Ionic	anionic	Soaps (carboxylates) $C_nH_{2n+1}COO^-X^+$
		Linear alkylbenzene sulfonates Secondary alkyl sulfonates $C_nH_{2n+1}SO_3^-X^+$
		Alkylether sulfates $C_nH_{2n+1}-(OCH_2CH_2)_n-OSO_3^-X^+$
		Alcoholic sulfates $R-O-SO_3^-X^+$
		Phosphates $C_nH_{2n+1}OPO(OH)O^-X^+$
	cationic	Quaternary ammonium compounds $R_1R_2R_3R_4N^+Y^-$
Esters of quaternary ammonium compounds $RCO-O-CH_2CH_2-N(CH_3)_2^+Y^-$		
Derivatives of pyridine and imidazolines $[NC_5H_5]^+$, $R_1-C=N-(CH_2)_2-N-R_2^+Y^-$		
amphoteric	Aminocarboxylic $N^+H_2(CH_2)_nCOO^-$	
	Betaine derivatives $N^+(CH_2)_nCOO^-$	
	Sulfobetaine derivatives $N^+(CH_2)_nCH_2SO_2^-$	

Because of their interest in industrial processes, many surfactants have been synthesized (man-made). But many others are known to be produced by microorganisms (biosurfactants) such as bacteria (*e.g.* [Renard, 2016]). Basically there are six major classes of biosurfactants: glycolipids (rhamnolipid, trehalolipid, sophorolipids,...), lipopeptides/lipoproteins (serrawettin, viscosin, surfactin, subtilisin,...), phospholipids, neutral lipids, fatty acids and lipopolysaccharides [Kosaric, 1993; Desai, 1997]. Some examples of synthesized and biological surfactants are given in Figure 1.17.

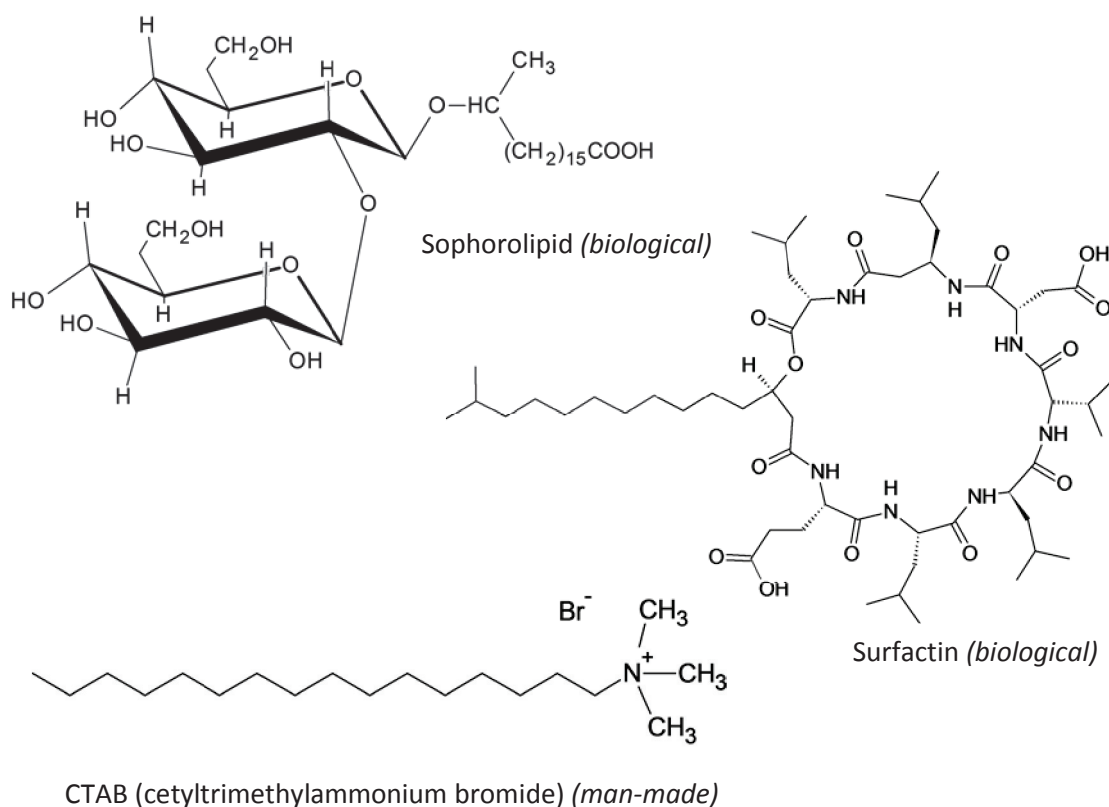


Figure 1.17: Examples of biological and man-made surfactants.

Microorganisms extracted from cloud water and snow have been shown to be able to produce biosurfactants and to be metabolically active in cloud water [Ahern, 2007; Amato, 2007b; Amato, 2007a; Delort, 2010; Vaïtilingom, 2012; Vaïtilingom, 2013].

1.6.2. Surface tension and CMC

In this work, the interfacial tension of the surfactants in the aerosols, between the droplet and the air surrounding the droplet, was investigated.

The air-water interfaces studied in this work are characterized by surface tension curves, reflecting the effect of each surfactant. These curves give the surface tension of the interface as a function of the surfactant concentration (Figure 1.18).

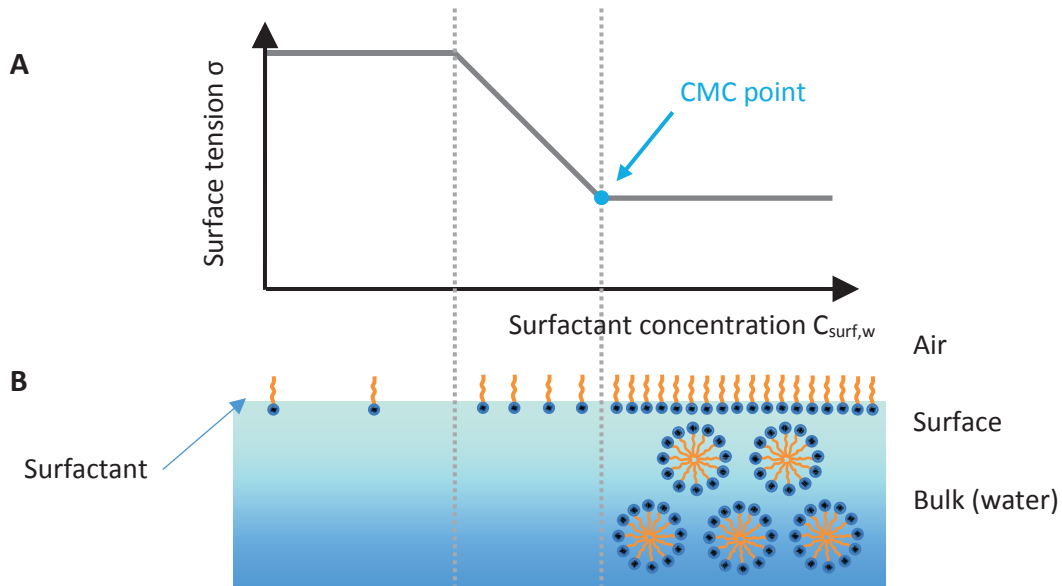


Figure 1.18: Schematic of (A) a surface tension curve showing the surface tension σ as a function of surfactant concentration $C_{surf,w}$ and (B) the corresponding organization of surfactants for a system air/water (hydrophobic part of the surfactant in orange and hydrophilic part in blue) (redrawn from [Biolin-Scientific, 2016] © 2016 Biolin Scientific Holding AB).

The first part of the curve (Figure 1.18 (A)) corresponds to the situation where all the surfactants place themselves at the air/water interface (Figure 1.18 (B)), with the hydrophilic part being in the water and the hydrophobic part pointing out in the air. At low surfactant concentrations, the surface tension has the value of pure water. The sharp transition corresponds to the situation where the interface starts to be saturated by surfactants, reducing the surface tension of the interface. Finally when the saturation is achieved, at a concentration called CMC (Critical Micelle Concentration), the surface tension is minimal and reaches a plateau. If more surfactants are added in the solution, they start forming micelles.

The CMC is characteristic of a given surfactant molecule. Biological surfactants often have the lowest CMC, as low as 10^{-5} and 10^{-4} M, while synthesized surfactants have generally CMC in the range 10^{-3} - 10^{-2} M [Mukerjee, 1971; Desai, 1997]. A few examples of surface tensions and CMCs are given in Table 1.2.

Table 1.2: Examples of biological and synthesized surfactants with their surface tension and CMC values (adapted from [Christofi, 2002] © Copyright 2002 John Wiley & Sons, Inc.).

Nature	Surfactant	Surface tension σ (mN m ⁻¹)	CMC (mg L ⁻¹)
Biological	Rhodococcus ruber glycolipid complex	26.8	54
	Trehalose dicorynomycolate from <i>R. erythropolis</i>	36.0	4.0
	Trehalose tetraester from <i>R. erythropolis</i>	26.0	15 (17 μ M)
	Rhamnolipids from <i>Pseudomonas aeruginosa</i>	29.0	50-200 (80-300 μ M)
	Sophorolipids from <i>Torulopsis bombicola</i>	33.0	82 (126 μ M)
	Surfactin from <i>Bacillus subtilis</i>	27.0	23 (22 μ M)
Synthesized	Sodium dodecyl sulfate	37.0	2120 (7-8 mM)
	Cetyltrimethylammonium bromide	30.0	1300 (3-4 mM)
	Tween 20	30.0	600 (0.5 mM)
	Linear alkylbenzene sulfonate	47.0	590 (1.7 mM)

1.7. Surfactants in aerosols: State of the Science

Because of the lack of interest of the atmospheric community for surfactants, very few studies have been dedicated to these compounds. In the 1990s, a decrease of the surface tension of fog waters and aerosols with increasing water soluble organic fractions evidenced the presence of surfactants (e.g. [Capel, 1990; Facchini, 1999; Facchini, 2000; Hitznerberger, 2002; Latif, 2004; Mircea, 2005]). Humic-like substances (HULIS) extracted from atmospheric aerosols were also reported to decrease the surface tension of water [Kiss, 2005; Salma, 2006; Taraniuk, 2007]. But, beside the HULIS studies, these early works were lacking an appropriate extraction technique, allowing to isolate and characterize specifically surfactants. Such a technique was finally developed in 2010 (double extraction) and was reported to extract the total surfactant fraction from aerosol samples (i.e. the solution left after extraction had the surface tension of pure water) [Ekström, 2010; Baduel, 2012]. This method showed the presence of surfactants in aerosols from many different regions. The surface tension measured were also much lower, $\sigma \sim 30 \text{ mN m}^{-1}$, than reported in the early studies ($\sigma \geq 50 \text{ mN m}^{-1}$ see Figure 1.19). However these surface tension measurements were not combined with concentration measurements, precluding the obtaining of absolute surface tension curves.

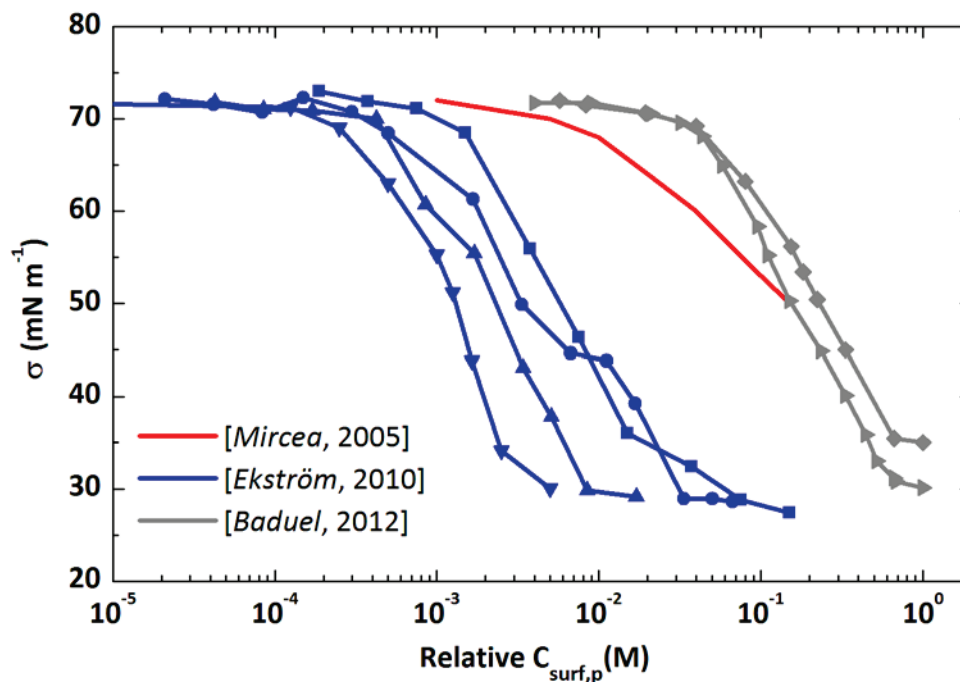


Figure 1.19: Comparison of recent surface tension curves as a function of relative surfactant concentration in aerosol particles $C_{\text{surf,p}}$ (*i.e.* the position of the surface tension curves on the x-axis is estimated) for aerosol extracts obtained with a simple water extraction (red curve) and by a double extraction method (blue and grey curves) (adapted from [Mircea, 2005] © Copyright 2005; [Ekström, 2010] © Copyright 2010; [Baduel, 2012] © Copyright 2012, with permission from Elsevier)

Other groups focused on measuring the concentration of surfactants in atmospheric aerosols and confirmed their presence in aerosols from many different regions. Two types of techniques were used: colorimetric techniques [Latif, 2004; Roslan, 2010; Jaafar, 2014; Mustaffa, 2014] (Section 2.4) providing absolute concentrations and electrochemical ones providing relative concentrations (by comparison with Triton X100 used as reference surfactant) [Orlović-Leko, 2010; Frka, 2012].

In addition to their role in cloud formation, very little was known on the molecular structure and origin of surfactants, which are also important to fully understand their importance in the atmosphere/biosphere system. Some studies suggested an anthropogenic origin, in particular combustion processes, for the surfactants found in aerosols (*e.g.* [Latif, 2004; Asa-Awuku, 2008; Baduel, 2012]). But others, in particular the low surface tension obtained at low concentrations, suggested a biological and probably microbial origin (“biosurfactants”) [Ekström, 2010]. This origin thus needed to be further investigated.

1.8. Objectives of the study

The purpose of this PhD work was to complete the knowledge on the role of surfactants in cloud droplet formation, their mechanism of action, and their sources. The specific objectives of the work were thus to

- ① evidence the role of surfactants in cloud formation and characterize their mechanism of action
 - by characterizing the surfactant properties in aerosols (concentrations, surface tension, CMC, chemical structure...);
 - by finding direct atmospheric evidence (correlations with cloud events);
- ② elucidate the surfactant origin (biogenic or not, and, if possible, specific sources).

1.9. Thesis overview

This work is structured as follows.

Chapter 1 gave an overview of the scientific context underlying the necessity to study the role of surfactants in cloud formation.

Chapter 2 will detail the experimental methods used for the sampling, extraction and analysis of surfactants from aerosols (determination of surfactant concentration by colorimetric methods, surface tension by pendant drop tensiometry, fluorescence spectroscopy, surfactant structure by LC-MS) and the study of micron-sized droplets by “optical trap” and Raman spectrometry. Other atmospheric and geophysical data used to understand the relation between the surfactants and the cloud events or the origin of surfactants will also be described.

Chapters 3 to 6 will present the different studies which investigated the role and origin of surfactants in cloud droplet formation. **Chapter 3** will show the application of the improved extraction and analysis methods on atmospheric aerosols from Askö, Sweden leading to the first absolute surface tension curves of surfactants in atmospheric aerosols. **Chapter 4** will focus, through investigation on aerosols from Northern Finland, on the link between

surfactants properties and cloud events. **Chapter 5** will present an alternative method to study the effects of surfactants on the growth of micron-sized droplets. **Chapter 6** will bring some proofs of the potential biological origin of atmospheric surfactants.

The conclusion and perspective of this study will be given in **Chapter 7**.

A summary of this PhD work can be found in French in **Chapter 9**.

Chapters 8, 10 and 11 contain the appendix, the acknowledgments and the references, respectively.

2. Experimental techniques

2.1. Aerosol sampling

2.1.1. Aerosol sampler

The surfactant samples studied in this work were extracted from atmospheric aerosol particles. These particles were collected with an aerosol sampler on quartz filters (Figure 2.1).

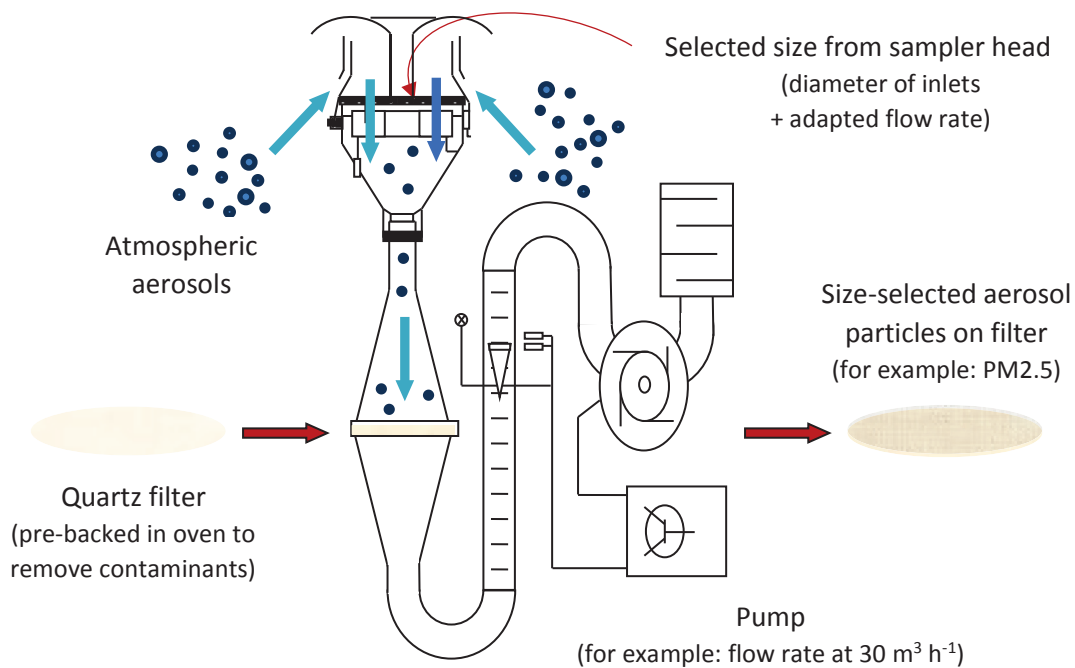


Figure 2.1: Schematic view of aerosol sampling (redrawn and adapted from [Digitel, 2014] © Copyright 2014 DIGITEL Elektronik AG).

The aerosols were pumped through the sampler head and collected on quartz filters. By adapting the head of the sampler (specific diameter of inlets) and the flow rate, only the aerosols with a diameter below a certain size were collected on the filter, the others settled down and were trapped in the layer of grease on the impactor inside the sampler head.

2.1.2. Sampling sites and experimental sampling procedure

For the study, the aerosols were collected at different sampling sites depending of the targeted study:

- Askö station, Sweden, a marine station (Section 2.1.2.1), for the determination of surfactant properties and concentrations in atmospheric aerosols (Chapter 3) and also for their link with biological markers (Chapter 6);
- Lyon 1 Campus, Villeurbanne, France, an urban site (Section 2.1.2.2), for the comparison of surfactant properties with aerosols from cleaner regions (Chapter 6);
- Pallas, Finland, a boreal continental site (Section 2.1.2.3), for the link between surfactant properties and concentrations in aerosols and cloud events (Chapter 4), and for the determination of their potential sources (Chapter 6).

The experimental procedures given in the following parts were published in part in [Gérard, 2016] and have been submitted for publication [Gérard, 2016 under review; Nozière, 2016 under review].

2.1.2.1. Askö, Sweden: coastal station

Askö laboratory belongs to the Stockholm University Baltic Sea Centre and is situated 80 km south of Stockholm in the archipelago of Trosa (58° 49.5' N, 17° 39' E) in Sweden. This island is considered as a coastal and marine region being surrounded by the Baltic Sea. Surfactants in aerosols being suspected to be biological [Ekström, 2010], this site (Figure 2.2) was chosen because it is mostly influenced by marine biogenic emissions that could be potentially sources of biological surfactants.

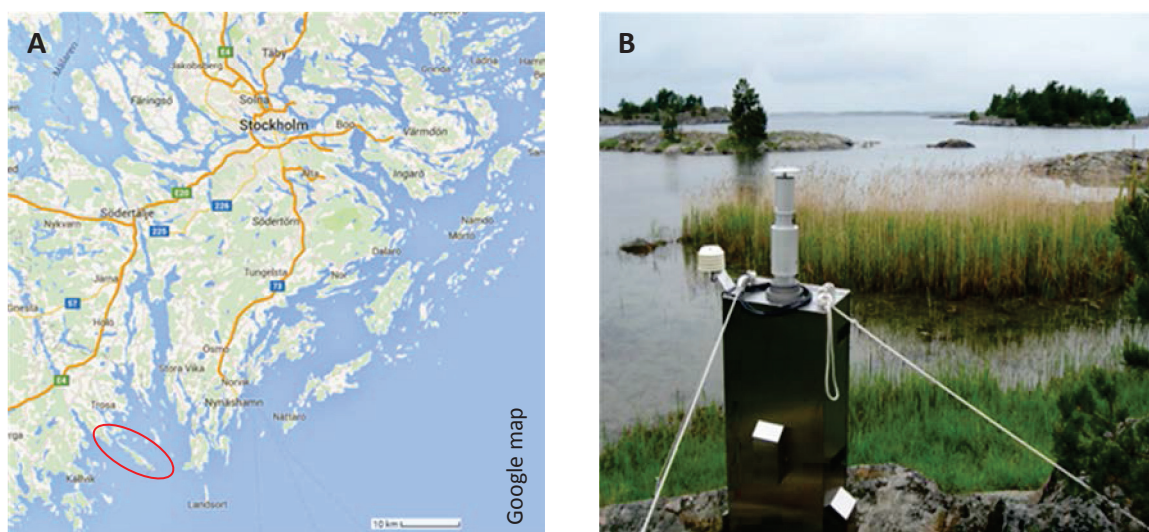


Figure 2.2: (A) Location (red oval) and (B) sampling site at the marine research station of Askö, Sweden.

The aerosols were collected at the marine research station of Askö from July to October 2010 (prior to the work at hand) at ground level on \varnothing 47 mm quartz fiber filters (SKC) with a Leckel SEQ 47/50 sequential filter sampler equipped with PM_{2.5} inlets (for collection of aerosol particles with diameter < 2.5 μ m). Each sample was collected over 72 h at 2.3 m³ h⁻¹, corresponding to about 165 m³ of air. Prior to sampling, the quartz filters were heated at 600°C for 12 h to remove any potential residual contaminants appearing during the filter production. For quality analysis, blank samples (about one for every three filter samples) were also taken by placing clean filters in the sampler for 72 h with the sampling flow off. After sampling, the filters were packed in plastic Petri dishes and stored in a freezer (-18°C) until analysis. The total aerosol particles volume sampled on each filter was determined by weighting the filters before and after sampling under controlled temperature (20°C) and humidity conditions (50 % RH), with an accuracy of 10⁻³ mg and assuming a density of 1 g cm⁻³. For the extractions, the filter samples were grouped together to obtain a sampled aerosol particles mass of about 2 mg, to exceed the detection limit for surface tension measurements, which resulted in a total of 11 samples.

2.1.2.2. Villeurbanne, France: urban station

The city of Villeurbanne in France is urban and situated in a continental polluted region. The aerosols were sampled at the campus of the University of Lyon 1, on the 5th floor of the “Institut de Physique Nucléaire” building (Figure 2.3) near the highway and national roads of Lyon (45°47'00.3"N 4°52'02.9"E). The interest of sampling at this place was especially to compare the properties of the surfactants in polluted and non-polluted aerosols.

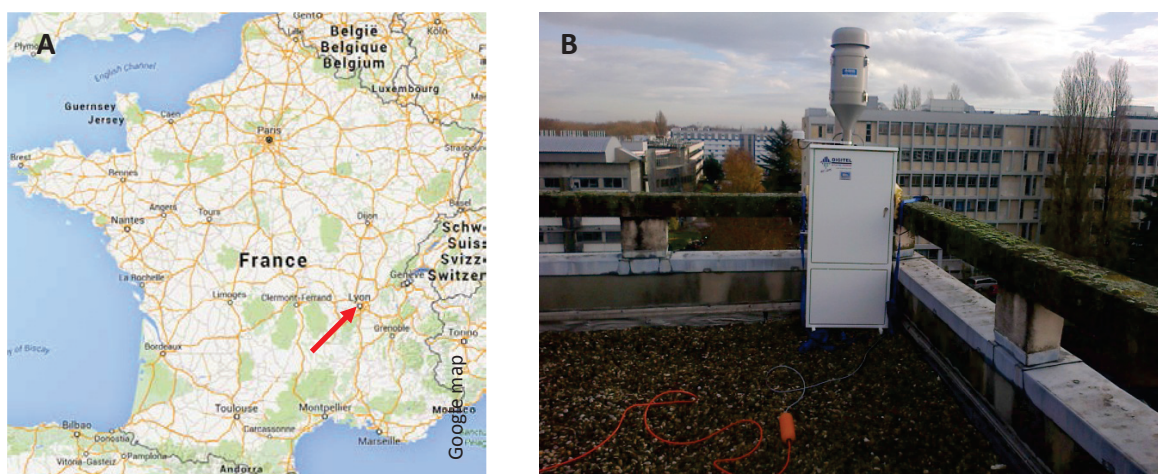


Figure 2.3: (A) Location (red arrow) and (B) sampling site at Villeurbanne, France.

The aerosols were collected from 1st to 17th of December 2014 and from 12th to 19th of January 2015 on \emptyset 150 mm quartz fiber filters (Fioroni) with a DIGITEL DA80 aerosol sampler equipped with PM1 inlets (for collection of aerosol particles with diameter < 1 μ m). PM1 aerosol particles collection was chosen over PM2.5 because this diameter is critical for the formation of cloud droplets, bigger particles being activated more easily. Each sample was collected over 12 h and at a flow rate of 30 m³ h⁻¹ (T = 15°C, P = 1013 hPa), corresponding to a total sampled volume of about 360 m³ of air per sample. Prior to sampling, the quartz filters were backed in oven inside aluminum foils at 500°C for 6 h to remove contaminants and placed in plastic bags before being used. For quality analysis, blank samples (about one for seven filter samples) were also taken. A blank filter corresponded to a clean filter taken on the top of the filter stock in the sampler. This filter was left in the stock during seven days without being sampled. The blanks were subjected to the same analysis as the samples in order to check for potential artefacts or contamination in the sampling or analysis procedure. After sampling, the filters were placed again in the plastic bags in their aluminum foils and stored in a freezer (-18°C) until analysis. The total aerosol particles volume sampled on each filter was

determined by weighting the filters before and after sampling under controlled temperature and humidity conditions, with an accuracy of 10^{-1} mg and assuming a density of 1 g cm^{-3} .

2.1.2.3. Pallas-Sammaltunturi, Finland: boreal station

The Pallas-Sammaltunturi station is situated in northern Finland ($67^{\circ}58.400'N$ $24^{\circ}06.939'E$, 565 meters above sea level, Figure 2.4) inside the Pallas-Yllästunturi National Park and belongs to the Pallas Atmosphere-Ecosystem Supersite in Muonio, Finland, hosted by the Finnish Meteorological Institute (FMI).

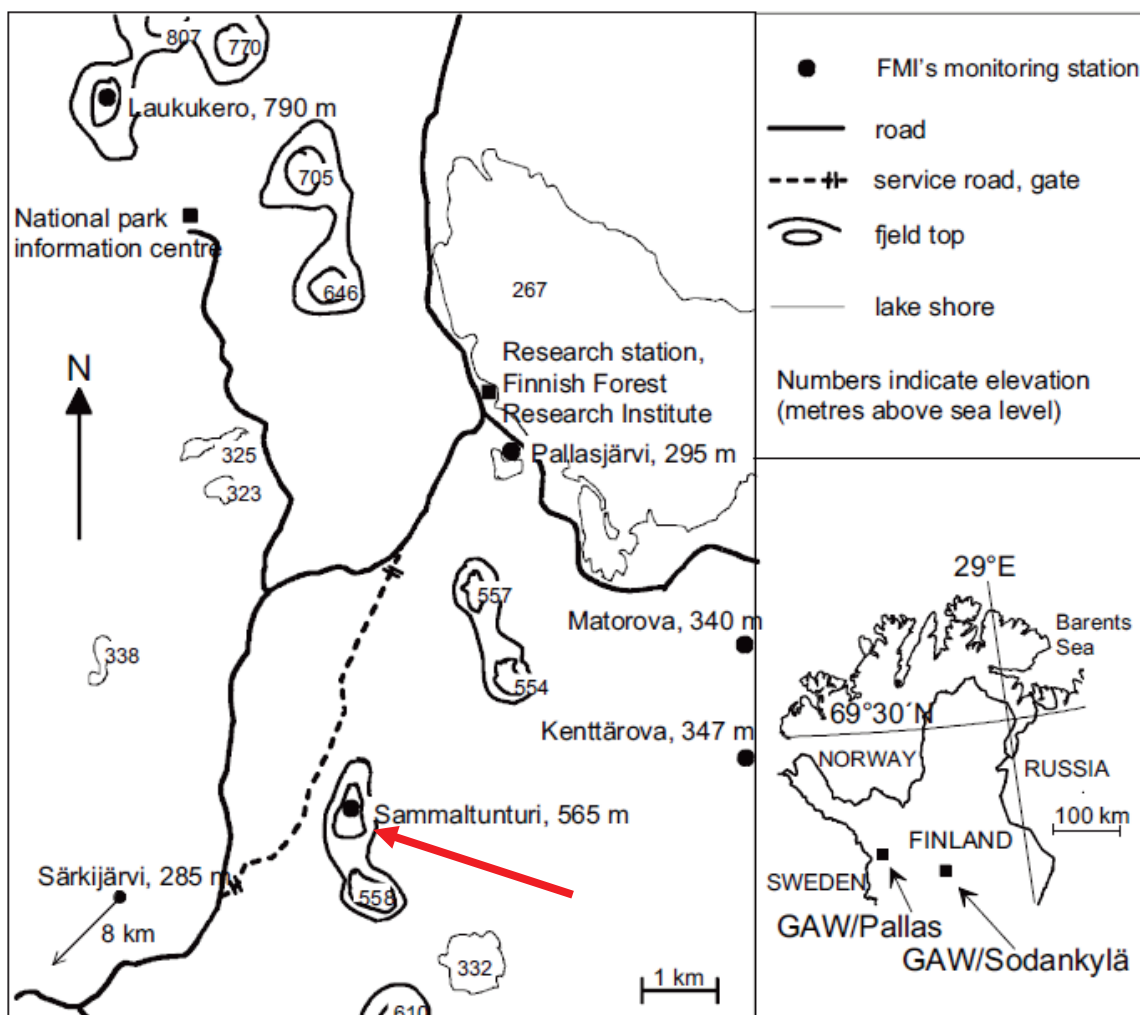


Figure 2.4: Location of Pallas-Sammaltunturi station (red arrow) in Pallas-Yllästunturi National Park (from [Hatakka, 2003] © Copyright 2003 Boreal Environment Research, reproduced with permission from the publisher).

The station is located inside a subarctic region at the northernmost limit of the northern boreal forest zone, on top of a sub-arctic hill about 100 m above the tree line and rises about 300 m above the surrounding area. The vegetation on hill top is sparse, consisting mainly of low vascular plants, moss and lichen (Figure 2.5).

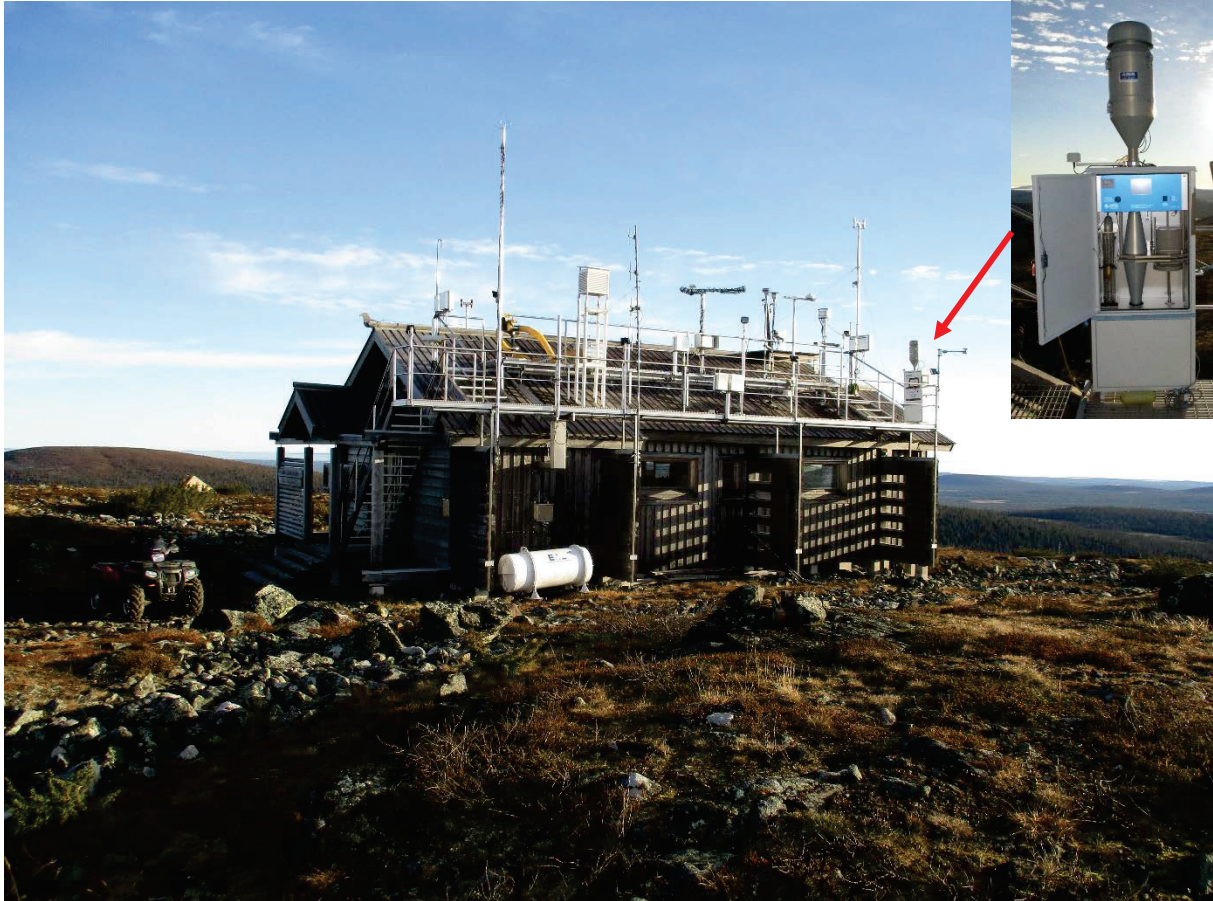


Figure 2.5: Pallas-Sammaltunturi station in October 2015 with the aerosol particles sampler (Digital DA80).

The area to the east and west of the hills is mainly lowland covered with boreal forest and swamps. It can be considered as a remote continental site, since it has an annual average particle concentration below 1000 \# cm^{-3} and because the area has no significant local or regional pollution sources. A more detailed description of the site can be found in [Aalto, 2002; Hatakka, 2003; Lohila, 2015].

The aerosol masses arriving at the station can be marine or continental and can be distinguished into five different sources: Local (North Scandinavia), Arctic, East, South and North Atlantic (Figure 2.6) [Aalto, 2002].

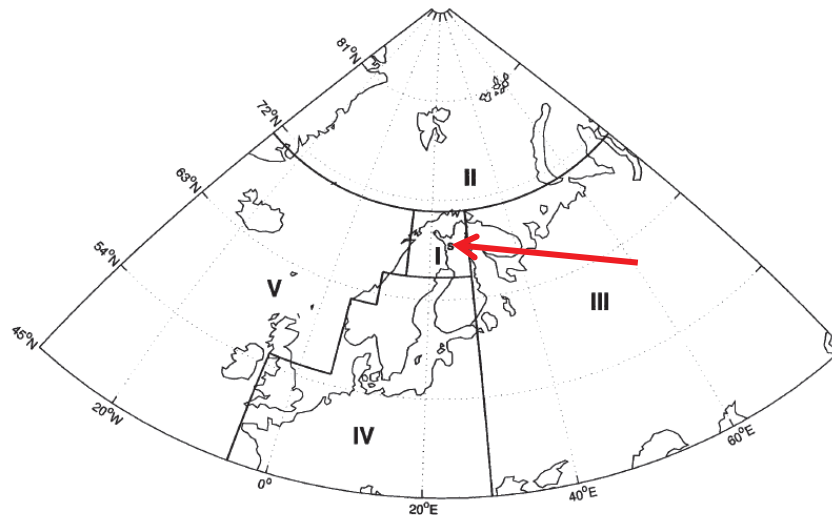


Figure 2.6: Schematic representation of source regions for air parcels arriving to Pallas-Sammaltunturi (red arrow): I Local (North Scandinavia), II Arctic, III East, IV South, V North Atlantic (reproduced from [Aalto, 2002] © Copyright 2002).

This station was chosen for the study of the link between surfactant properties and concentrations and cloud events because it is frequently inside a cloud [Lihavainen, 2008; Anttila, 2012], mostly orographic due to the topography of the surrounding terrain. This type of cloud is produced by orographic lifting of moist air to saturation (example in Figure 2.7).



Figure 2.7: Example of orographic cloud (Pallastunturi-Yllästunturi National Park, Finland, October 2015). Orographic lift occurs when an air mass is forced from a low elevation to a higher elevation in response to the earth topography (mountains for example).

Another advantage of doing the study at this site was the annual presence of several meteorological instruments running in parallel [Hatakka, 2003] (visibility, size distribution of particles,...) essential for the study.

The aerosols were collected at the Pallas-Sammaltunturi station during 7 months from April to November 2015 on \varnothing 150 mm quartz fiber filters (Fioroni) with a DIGITEL DA80 aerosol sampler (Figure 2.5) equipped with PM1 inlets (for collection of aerosols with diameter $< 1 \mu\text{m}$). PM1 aerosol particles collection was chosen because this diameter is critical for the formation of cloud droplets, bigger particles being activated more easily. Each sample was collected over 24 h and at a flow rate of $30 \text{ m}^3 \text{ h}^{-1}$ ($T = 15^\circ\text{C}$, $P = 1013 \text{ hPa}$), corresponding to a total sampled volume of about 720 m^3 of air per sample. Prior to sampling, the quartz filters were baked in oven inside aluminum foils at 500°C for 6 h to remove contaminants and placed in plastic bags before being used. For quality analysis, blank samples (about one for ten filter samples) were also taken. A blank filter corresponded to a clean filter taken on the top of the filter stock in the sampler. This filter was left in the stock during ten days without being sampled. The blanks were subjected to the same analysis as the samples in order to check for potential artefacts or contamination in the sampling or analysis procedure. After sampling, the filters were placed again in the plastic bags in their aluminum foils and stored in a freezer (-18°C) until analysis. The total aerosol particles volume sampled on each filter was obtained from the size distributions of $\text{PM}_{0.5}$ measured with a differential mobility particle sizer (DMPS) connected to an inlet preventing the sampling of cloud droplets, multiplied by a proportional factor obtained from the PM_{10} volume measured in the absence of cloud by another DMPS and an Aerodynamic Particle Sizer (APS) (see Section 2.8.4). The aerosol samples led to a collection of 230 PM_{10} samples during the 7 months (April - November 2015). The station was inside clouds 25 % of the time during the 7-months campaign, which corresponded to 72 cloud events.

2.2. Surfactant extraction from aerosols

After the collection of atmospheric aerosols on filters, the surfactants were extracted from the aerosols on the filters before further analysis.

The development of a method for extracting the surfactants from the aerosols was an important part of the study, but it is presented in the Experimental section for more clarity. This development was carrying out on reference surfactants before applying the method on the genuine environmental samples.

The extraction procedure was published in [*Gérard, 2016*] and more technical details have been submitted for publication [*Nozière, 2016 under review*].

2.2.1. Reference surfactants

To develop the surfactant extraction method, to determine the extraction efficiency (and to perform the surfactant analysis methods), reference surfactants were used (Figure 2.8 and details in Appendix 8.1 and 8.2). The surfactants were chosen with two compounds at least for each type (anionic, cationic and non-ionic) and source (synthesized and biological).

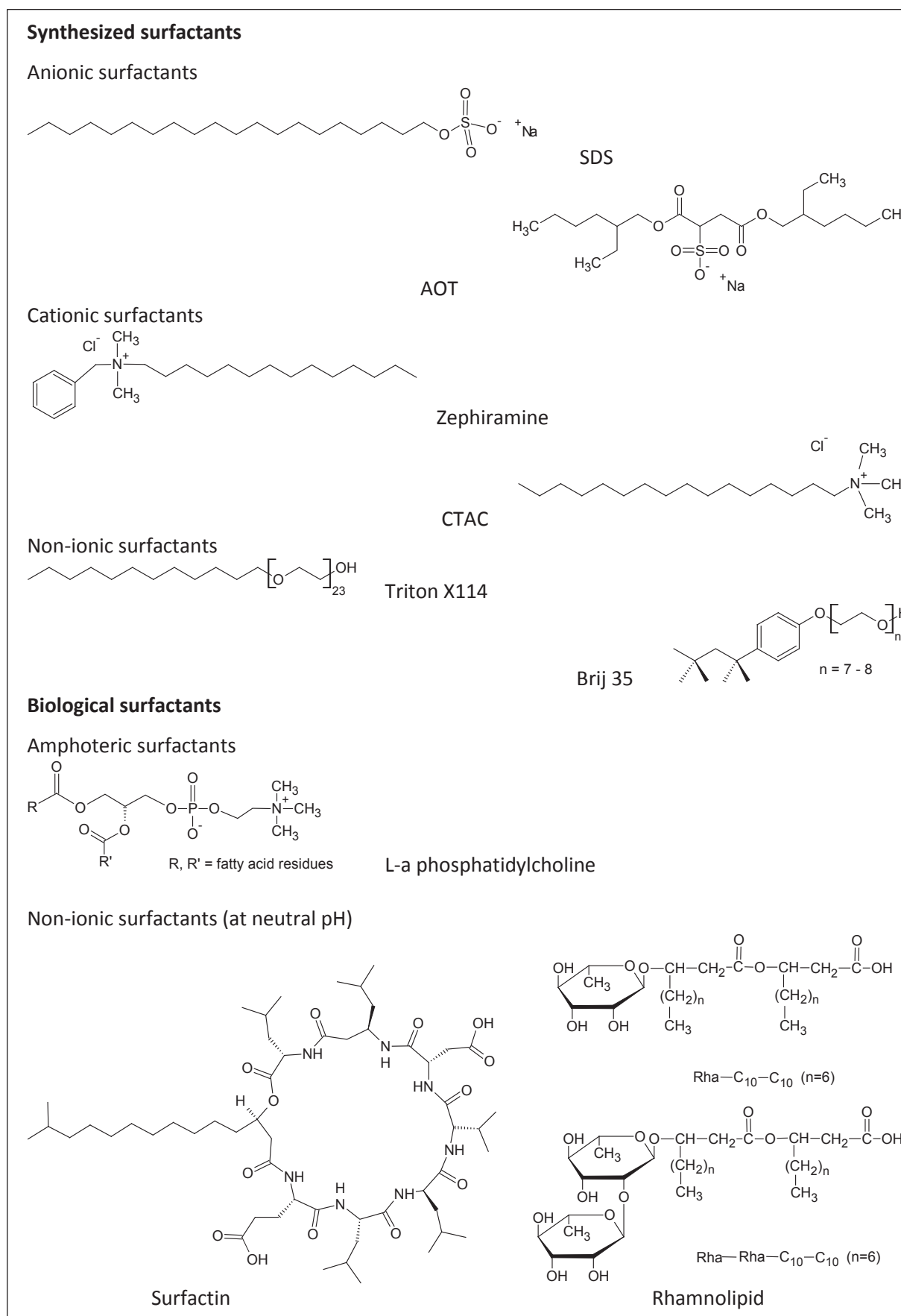


Figure 2.8: Reference surfactants used in this study (details available in Appendix 8.1 and 8.2).

2.2.2. Surfactant extraction

Once the aerosols were collected on the filters, they underwent a double extraction. As explained further, in this work the initial method [Ekström, 2010; Baduel, 2012] was optimized. The first extraction (in water) remained whereas the second extraction was replaced by a Solid-Phase Extraction (SPE).

2.2.2.1. Principle

The first extraction of aerosols was performed by a water extraction. The filters with collected aerosols were soaked in ultrapure water. Because the quartz filter left a few fibers and to remove big particles, the solution needed to be filtered before the second extraction.

In order to concentrate and remove interfering molecules of the aqueous matrix, a second extraction was necessary. The solution underwent a Solid-Phase Extraction (SPE), a sample preparation process used to concentrate and purify liquid samples [Berrueta, 1995; Rouessac, 2004].

The principle of SPE involves a partitioning of compounds between two phases. Extraction is performed by forcing the liquid through the sorbent material (the solid phase, packed into a small cartridge) by means of pressure, vacuum or diffusion. The analytes to be extracted are retained by the solid phase, having a greater affinity for the solid phase than for the sample matrix (retention and absorption step). Compounds retained on the solid phase are then removed by elution with a solvent in which the analytes have a greater affinity than for the solid phase (elution or desorption step). The different mechanisms of retention or elution are due to intermolecular forces between the analytes, the active sites on the surface of the adsorbent and the liquid phase or matrix.

The choice of the cartridge (solid phase) and elution solvent depends on the matrix (interfering compounds, affinity with the analytes,...) and the properties of the analytes to be extracted. For example a normal phase is used for polar molecules (elution with a highly polar solvent or a buffer of the appropriate pH), while a reversed phase is used for molecules with a mid to low polarity due to hydrophobic effects (elution with a weakly polar or non-polar solvent), as in our study.

A simple SPE procedure involves the following steps (Figure 2.9):

1. *Conditioning*: the solid phase of the cartridge is first wetted with the elution solvent (e.g. acetonitrile) for activating the sorbent, then the solid phase is washed with the solvent in which the sample is dissolved (the matrix of the solution, e.g. water);
2. *Sample application*: the liquid sample is loaded in the cartridge. As the sample passes through the stationary solid phase, the analytes which have a better affinity for the phase interact with it and are retained on the sorbent (absorption step), while the solvent and other impurities (molecules which have a better affinity for the solvent than for the solid phase) pass through the cartridge;
3. *Washing*: the interfering compounds retained in step 2 are removed with a solvent which does not remove the analytes;
4. *Elution*: the analytes are eluted from the cartridge with an appropriate solvent (desorption step).

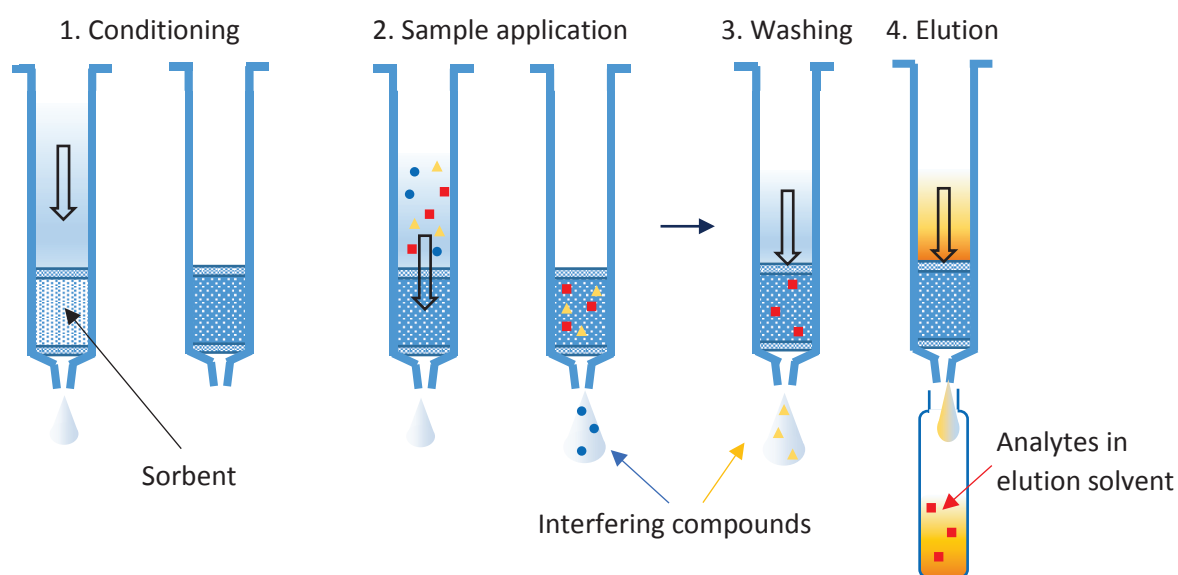


Figure 2.9: Schematic SPE (Solid-Phase Extraction) procedure used for this work (redrawn and adapted from [Macherey-Nagel-GmbH-&Co, 2015] © Copyright 2015 MACHEREY-NAGEL GmbH & Co. KG).

After the elution, the solution of solvent containing the analytes (here, the surfactant fraction) is obtained. The solvent is then evaporated under a nitrogen flux, *i.e.* a constant N_2 flux is applied over the vial containing the solution until complete evaporation of the solvent. A solid or liquid extract is thus obtained (in this study, the surfactant fraction) and redissolved in water (or other solvents) for further experiments.

2.2.2.2. Improvement of the extraction

The extraction method developed prior to this study [Ekström, 2010; Baduel, 2012] involved the following steps:

1. extraction of the filters in ultrapure water followed by filtration;
2. microextraction of the water extracts onto silicon tubes;
3. recovery of the compounds of interest by drying the silicon tubes, eluting with methanol, evaporating, and redissolving in ultrapure water.

This method was improved for the present work. The main improvement was the replacement of the silicon tubes by Solid-Phase Extraction (SPE) cartridges using a derivative of silicon, silica C₁₈, providing a better reproducibility.

Before being applied on the genuine aerosol samples, the method was optimized from the reference surfactants given in Section 2.2.1. To determine the most efficient procedure of each step, the extraction efficiencies were determined from concentration measurements using the colorimetric methods described in Section 2.4.2.

For this study, the water extraction has been tested under different conditions (magnetic stirring, rest, ultrasound bath) and different temperatures (6°C, room temperature of 23°C, 30°C) during 2 h (minimum extraction time defined by [Baduel, 2012]). These different conditions applied on the reference surfactants showed similar extraction efficiencies. However a low temperature is better to avoid potential degradation of molecules. Moreover performing water extraction under stirring or ultrasound bath crumbled the quartz filters making the filtration through the syringe filter more difficult. For these reasons it was decided to perform the water extraction at rest on Petri glass dishes placed in fridge. Concerning the volume of water used for extraction, the minimum volume for a good extraction was 7 mL for Ø 47 mm quartz-filters and 35 mL H₂O for Ø 150 mm quartz filters. Moreover the extraction in water rather than an extraction in an organic solvent was favored because it reduced the number of steps (hence a gain of time and cost and a decrease of contamination probabilities).

For the filtration through syringe filter, a PVDF (PolyVinylidene Fluoride) membrane with pore sizes of 0.40 µm was chosen because of its cost-extraction effectiveness compared to

other materials such as PTFE (PolyTetraFluoroEthylene) or cellulose acetate. The pore size of 0.40 μm was favored over lower pore sizes to reduce the potential surfactant retention on the membrane.

For the SPE procedure, a reversed phase, a silica-based C_{18} cartridge, was chosen because it is widely used for the analysis of surfactants in waters [Olkowska, 2011, 2012]. The type of surfactant in aerosol being not known, the SPE procedure was conducted without adjusting the pH of the solution. For our study, two extraction solvents were tested for the elution: acetonitrile (ACN) and methanol. The methanol gave a better extraction efficiency ($\approx 10 - 20\%$ more than acetonitrile) but the blank method for the surface tension measurements was better if acetonitrile was used. Indeed, impurities due to methanol extraction lowered the surface tension of the blank by $\approx 10 \text{ mN m}^{-1}$ whereas the decrease was $< 5 \text{ mN m}^{-1}$ for ACN. So the acetonitrile was used as solvent for the study. The volumes of water and acetonitrile for conditioning, washing and elution were also optimized by choosing the minimum volume required for an efficient extraction and a satisfactory blank. Note that it was not possible to choose a different procedure for each type of surfactant because of the very low concentrations of surfactant aerosol samples.

2.2.2.3. Experimental procedure

The schematic of the modified and optimized extraction procedure is shown in Figure 2.10. This method was published in [Gérard, 2016] and more technical details have been submitted for publication [Nozière, 2016 under review].

The procedure involved the following steps:

- extraction of quartz filters in ultrapure water (7 mL for $\varnothing 47$ mm quartz-filters and 35 mL for $\varnothing 150$ mm quartz filters) for 2 h at $6 (\pm 1) ^\circ\text{C}$, followed by filtration through precleaned syringe filters (0.40 μm PVDF, Fisherbrand[®]) to remove any particles in suspension;
- a solid-phase extraction on Strata[®] C_{18} -E cartridges (500 mg / 3 mL, Phenomenex). The cartridge was pre-cleaned with 6 mL acetonitrile then 6 mL of water. Then the aerosol solution was loaded onto the cartridge at a flow rate of less than 1 mL/min. Then the

cartridge was cleaned with 1 mL ultrapure water (to remove any traces of the residual interferents from the matrix, such as salts) and dried (for a better elution and to avoid the presence of water in the eluted organic solution). The surfactants absorbed on the SPE cartridge were then eluted with 4 mL of acetonitrile;

- evaporation of the eluted solution under a stream of N₂ and redissolution in 60 µL of ultrapure water (or other solvent).

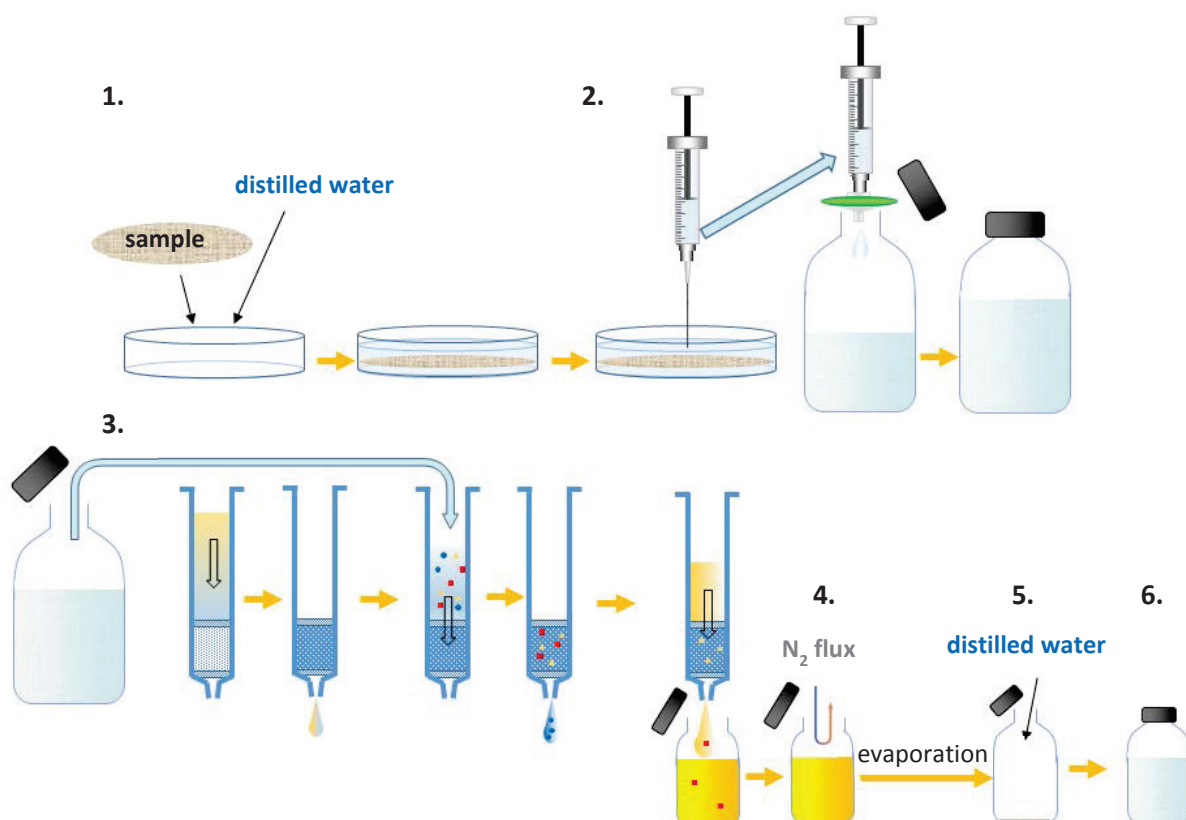


Figure 2.10: Schematic of the developed extraction method: 1. water extraction of aerosols from the sampled filter; 2. filtration of the solution through syringe filter; 3. SPE procedure; 4. Evaporation of SPE extraction solvent under N₂ flux; 5. adding of water on the dry surfactant extract; 6. sample ready for further analysis.

The same procedure was applied to the blank filters.

The extraction efficiency for this extraction procedure, and for each class of surfactant (anionic, cationic, and non-ionic), was determined as the ratio of the concentrations of reference compounds before and after extraction, the concentrations being quantified by the colorimetric techniques described in Section 2.4.2. For this, 10⁻⁹ to 10⁻⁴ moles of reference surfactants (in ~ 0.5 - 1.0 mL ultrapure water) were spiked onto clean quartz filters, which were dried for 24 h and then extracted following the steps described above. The efficiency

was determined for the nine reference surfactants (Section 2.2.1), representing the three classes of surfactants: sodium dodecyl sulfate (SDS) and dioctyl sulfosuccinate sodium (AOT) representing anionic surfactants, benzyltetradecyl dimethylammonium (zephiramine), cetyltrimethyl ammonium chloride (CTAC) representing cationic surfactants, and (1,1,3,3 - tetramethylbutyl) phenyl-polyethylene glycol (Triton X114), polyethylene glycol dodecyl ether (Brij35), surfactin, rhamnolipid, and L- α -phosphatidylcholine representing non-ionic surfactants. For anionic surfactants, the maximum extraction efficiency in the experimental range was 65 (\pm 10) %, for cationic surfactants 20 (\pm 15) % and for non-ionic surfactants 90 (\pm 5) %. The experimental efficiencies were taken into account in the calculations of the concentration values obtained with this method.

For the aerosol samples, the extraction technique was shown to remove the entire surfactant fraction of these samples (*i.e.* all of the aerosol components contributing to the surface tension) by measuring the surface tension of the residual solutions obtained after the first and second extraction steps [Ekström, 2010; Baduel, 2012]. After the first step (water extraction), the surface tension of the residual solutions was around 50 mN m⁻¹, which was consistent with the surface tension of aerosol samples resulting from a simple water extraction [Mircea, 2005]. After the second extraction step, the surface tension of the residual aqueous solutions had increased back to 72.8 (\pm 1) mN m⁻¹ (*i.e.*, the value of pure water), thus demonstrating that all of the surface-active compounds had been transferred to the extracts.

The 60 μ L extracts obtained from each aerosol sample were used as parent solutions for surface tensions, concentration measurements, fluorescence and LC-MS/MS experiments. The surface tension of the extracts was measured first, and then the corresponding surface tension curves were determined by successively diluting the extracts in ultrapure water (see Section 2.3). The diluted solutions obtained at the end of this procedure were then separated into several aliquots and used for the measurement of anionic, cationic, and non-ionic surfactant concentrations (Section 2.4), fluorescence (Section 2.5) and LC-MS/MS measurements (Section 2.6).

2.3. Surface tension by pendant drop tensiometry

For this study, the pendant drop method (also called hanging drop method) was chosen for determining the surface tension of the surfactants in atmospheric aerosols. Indeed, this method requires a small amount of solution, which is an advantage when the available mass of sample is low, and it is currently the only method to determine the surface tension of aerosols. Associated to concentration measurements, surface tension curves could be obtained.

2.3.1. Principle

The principle of the pendant drop method is based on the formation of a small droplet of liquid suspending at the end of a vertical tube (Figure 2.11). The shape of the droplet before it falls is correlated to the surface tension.

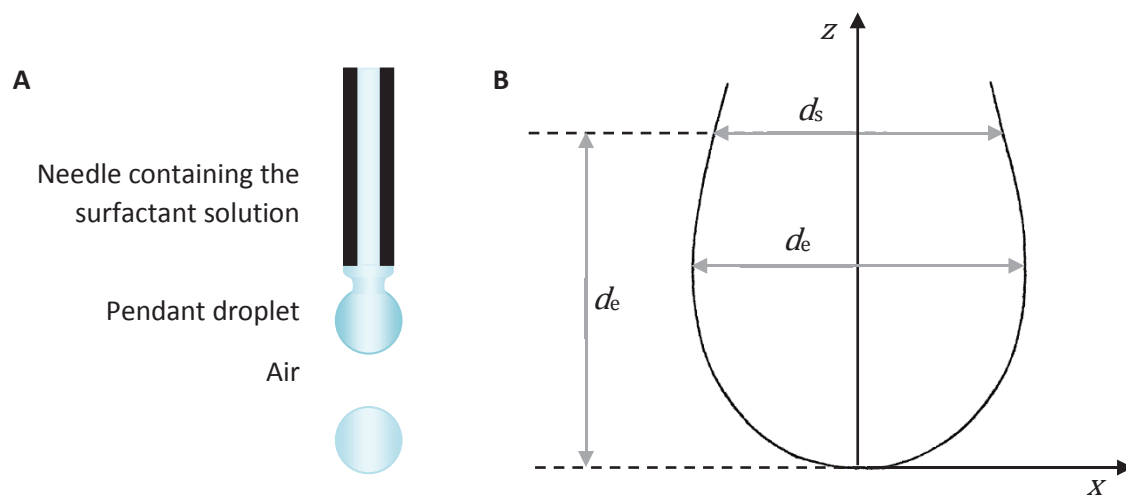


Figure 2.11: Schematic of (A) pendant drop and (B) parameters of droplet shape.

The surface tension, between the droplet and the air surrounding it, can be determined from equation (2.1) resulting from Young-Laplace equation [Bashforth, 1883; Andreas, 1938; Fordham, 1948; Rotenberg, 1983]:

$$\sigma = \frac{g \Delta\rho (d_e)^2}{H} \quad (2.1)$$

where g is the gravitational acceleration, $\Delta\rho$ is the difference of density between the solution and the air, d_e is the main diameter of the pendant droplet and H is function of a shape factor defined by $\frac{d_s}{d_e}$ (Figure 2.11) and is determined from tables (*e.g.* empirical tables such as in [Andreas, 1938; Fordham, 1948]).

The surface tension value for an aqueous solution containing surfactants results only from the total concentration of surfactants in this solution, including those at the surface and those in micelles in the bulk, which are in equilibrium. Thus, sample (or droplet) size should not affect the surface tension value measured. This question has been stirring strong controversies in the atmospheric community. But recent experiments measuring directly the surface tension of micron-sized particles in laboratory have now confirmed that, for a given concentration, the surface tension measured on millimeter droplets is identical to that measured on micron-scale droplets [Morris, 2015; Bzdek, 2016] (Figure 2.12). This remains true even at low concentrations of surfactant (10^{-5} - 10^{-4} M) for strong surfactants (CMC $\sim 10^{-4}$ - 10^{-3} M) [Reid, 2017 in preparation].

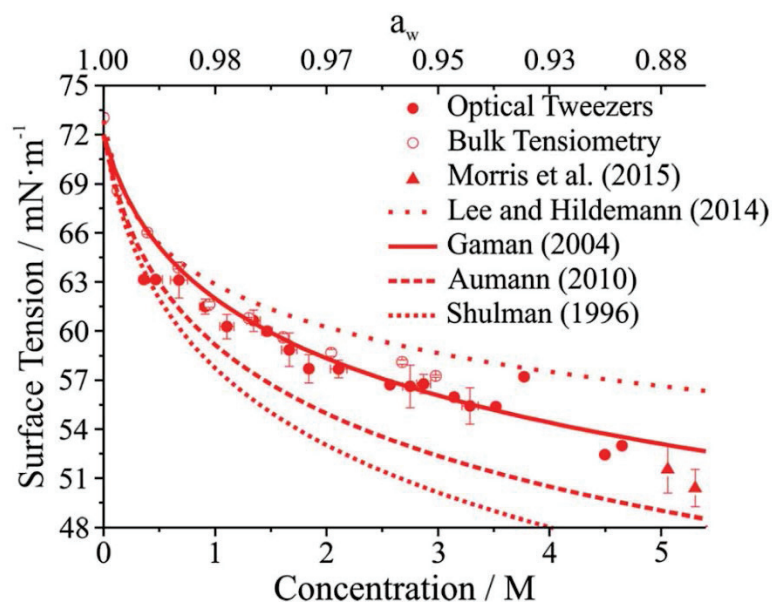


Figure 2.12: Comparison of the surface tension curve (surface tension as a function of surfactant concentration) of the glutaric acid between bulk tensiometry and measurements on micron-sized droplets (atomic force microscopy [Morris, 2015] and optical tweezer). The lines are the surface tension parametrizations performed by [Shulman, 1996; Gaman, 2004; Aumann, 2010; Lee, 2014]. The upper axis gives the water activity a_w (Raoult's term). ([Bzdek, 2016] - Published by The Royal Society of Chemistry)

Thus although the surface tensions measured in this work have been determined from measurements at a macroscopic scale (bulk measurements), they were representative of the surface tension of micron-sized cloud droplets. This validates the principle of measurement applied in this work.

2.3.2. Experimental procedure

This procedure applied to surfactants in aerosols was published in [Gérard, 2016] and more technical details have been submitted for publication [Nozière, 2016 under review].

The surface tension of reference solutions and sample extracts was measured with the pendant drop method using a Dataphysics OCA 15EC tensiometer and Dataphysics SCA software for OCA version 4 - 4.1. The software provided the surface tension of the solution by fitting the Young-Laplace equation to the shape of the drop of solution hanging from the syringe needle before it falls (Figure 2.13).

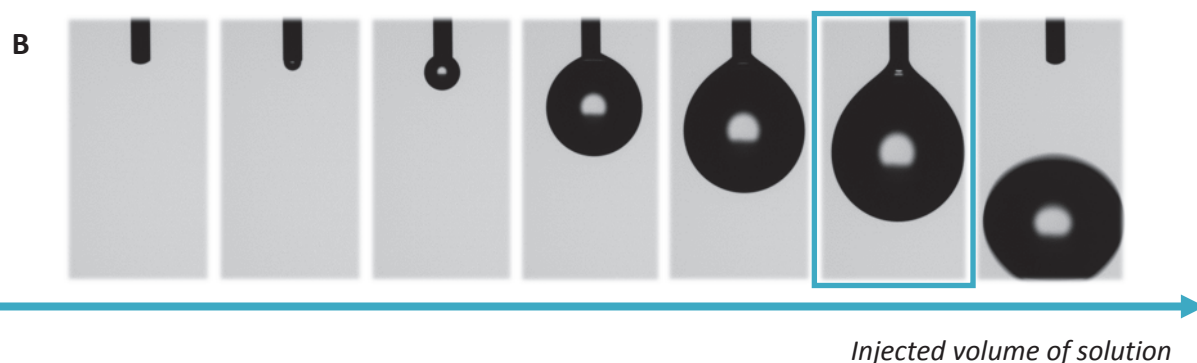
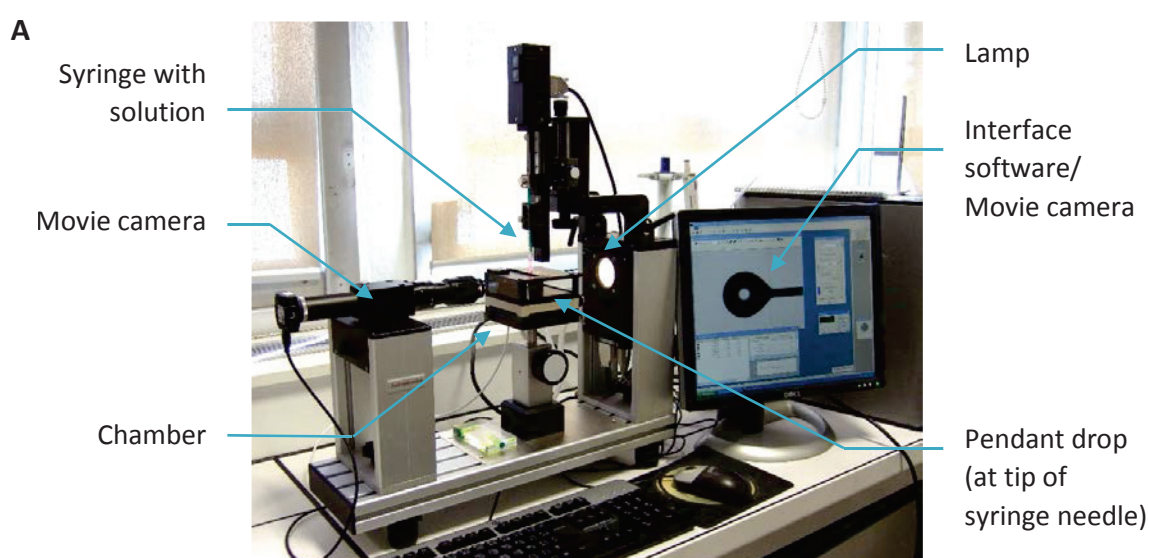


Figure 2.13: (A) Dataphysics OCA 15EC tensiometer and (B) drop formation. The shape of the droplet before it falls is correlated to the surface tension.

Syringes with needle tips thinner than usual were used in order to use a volume of sample as small as possible: \varnothing 0.30 mm tips for solutions with low surface tensions ($< 50 \text{ mN m}^{-1}$) and \varnothing 0.51 mm tips for solutions with larger surface tensions ($> 50 \text{ mN m}^{-1}$). These needle tips produced droplets with diameters between 1.4 and 2.4 mm. The

tensiometer was calibrated with ultrapure water, and the measurements were carried out at $24 (\pm 2) ^\circ\text{C}$. Before each measurement, the droplet was left to equilibrate [Nozière, 2014] until the value of the surface tension did not evolve. Each measurement was repeated five times, and the reproducibility between the results was $\pm (1 - 3) \%$. The instrument also allowed the volume of the droplet to be monitored in real time and ensured that the latter did not significantly evaporate during the measurements. The overall uncertainties on each surface tension measurement were $\pm (0.3 - 1.0) \text{ mN m}^{-1}$.

These surface tension measurements were used not only to determine the surface tension of the sampled aerosols but also to determine the surface tension curves (surface tension σ as a function of surfactant concentration $C_{\text{surf,w}}$) and the Critical Micelle Concentrations (CMC, concentration above which the surface tension has reached its minimum) for the first time for atmospheric surfactants. The CMC was determined graphically on the surface tension curves as the intersection between the sharp slope and the minimum surface tension level (Figure 2.14).

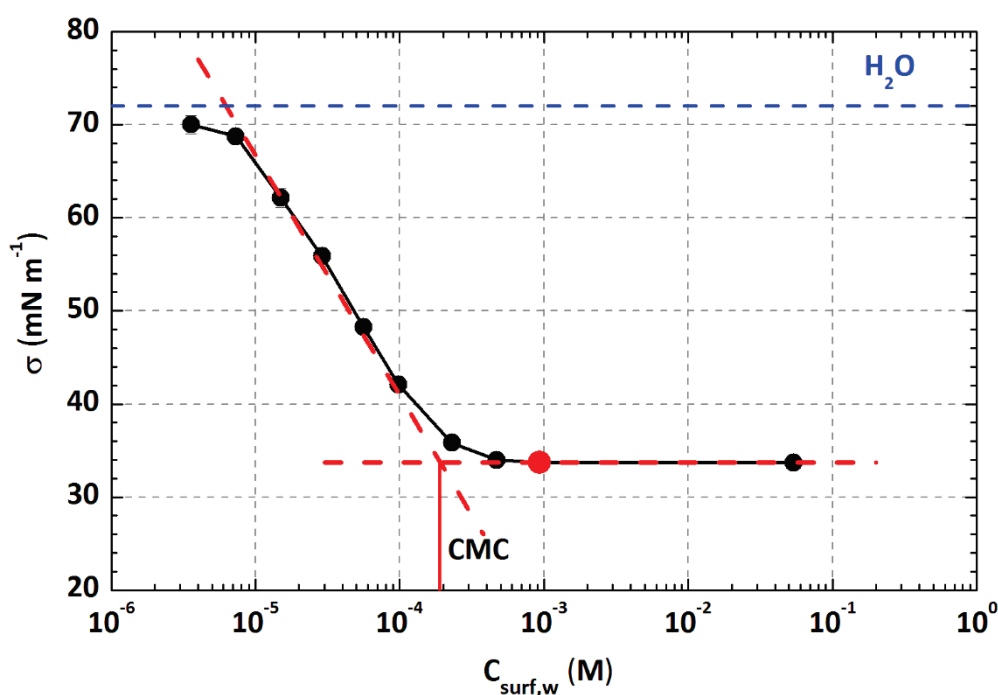


Figure 2.14: Example of determination, from a surface tension curve, of the CMC value for a surfactant extract sample from aerosols. The red dot represents the initial extract, the black dots at lower concentrations are those obtained from successive dilutions, and the black dot at the largest concentration, corresponding to the concentration in the aerosol, is obtained from the volume ratio between the extract and the aerosol. The blue dashed line represents the value for pure water, and red dashed lines illustrate the graphical determination of the CMC. (reproduced with permission from [Gérard, 2016] © Copyright 2016 American Chemical Society)

The surface tension curves, including the minimum surface tensions and CMCs, are characteristic of specific surfactant molecules. Before determining such curves for aerosol surfactants, they were measured for the nine reference surfactants listed in Section 2.2.1: SDS, AOT, zephiramine, CTAC, Triton X114, Brij35, surfactin, rhamnolipid, and L- α -phosphatidylcholine. The surface tension curves, minimum surface tensions, and CMCs obtained were consistent with the literature (see Appendix Section 8.3).

Surface tension curves were then determined for the aerosol samples. First, the surface tension of the 60 μ L extracts obtained from each aerosol sample was measured. The extracts were then successively diluted with ultrapure water, and the surface tension was measured at each dilution step until the surface tension value for pure water was reached (Figure 2.14). For each sample, the absolute position of the curve on the X-axis was given by the surfactant concentrations obtained by the colorimetric techniques described in Section 2.4.2, and the CMC was determined graphically by the same method as described above for the reference surfactants.

For samples from Askö station, in spite of the extraction, a few atmospheric samples had a low surfactant concentration (*i.e.*, close to or slightly larger than the CMC), and their surface tension was slightly larger than their minimum surface tension. Overestimating the minimum surface tension in surface tension curves, in turn, slightly underestimated the CMC value. The uncertainties on these CMCs were thus determined as the combination (the square root of the sum of the squares) of the uncertainties on the concentrations (20 %; see Section 2.4.2.5) and those on the minimum surface tension values. The latter were taken as the relative value of the first derivative of the surface tension curves ($\delta\sigma/\delta C$ as a function of C) at the largest concentration measured, which should be zero if the actual minimum surface tension is reached. In nearly all of the atmospheric samples from Askö station, these uncertainties were less than 3.5 %, corresponding to about 1 mN m⁻¹ and indicating that the surface tension measured for the sample was equal to the minimum surface tension for the surfactant, within uncertainties.

For samples from Pallas-Sammaltunturi station, only the samples attaining the plate were considered so the uncertainties on the measurements of the surface tension were those of the instruments, *i.e.* around 0.3 - 1.0 mN m⁻¹.

2.4. Surfactant concentration by colorimetric methods

Colorimetric techniques were chosen in this work to determine surfactant concentrations in aerosols because they provided absolute concentrations and have been shown to be sensitive enough for aerosol surfactants [Latif, 2004; Roslan, 2010; Jaafar, 2014; Mustaffa, 2014]. However, because there is no dye reacting with all types of surfactants, it was necessary to measure anionic, cationic, and non-ionic surfactants separately to obtain the total surfactant concentration. Although the colorimetric methods were used for the determination of surfactants in aerosols prior to this work, they provided only anionic and cationic surfactant concentrations. In this work we went further by applying in addition a colorimetric method to determine the non-ionic surfactant concentration. **To our knowledge, this is the first time that concentrations for non-ionic surfactants in atmospheric aerosols are reported**, whereas they represent a major fraction of aerosol surfactants, as shown by this work (Section 3.2.2). Moreover, in the previous studies [Latif, 2004; Roslan, 2010; Jaafar, 2014; Mustaffa, 2014] the potential interferences on the method from other species present in aerosols were not checked, whereas a simple water extraction was applied. Thus in addition to surfactants, it was quite certain that other species were extracted such as salts or small non-surfactant organics. Consequently, the possible interferences from other species present in aerosols were also studied in this work.

Thus, in this work, for the first time, a method to determine the total surfactant concentration in atmospheric aerosols including anionic, cationic and non-ionic surfactants **was developed** and the **potential interferences** on the colorimetric methods was **studied**.

The development of the method and the experimental procedure were published in part in [Gérard, 2016] and more technical details about the procedure have been submitted for publication [Nozière, 2016 under review].

2.4.1. Principle

Briefly, the principle of these colorimetric methods is to titrate the surfactants with a dye specific to the surfactant class (anionic, cationic, or non-ionic). The resulting surfactant-dye complex is then extracted in an organic phase and its concentration determined by UV–visible absorption spectroscopy using calibration curves established with reference compounds. The advantage of this technique is to provide a unique calibration curve for each class of surfactants, thus making it possible the determination of the concentration of unknown surfactants belonging to each class.

Thus, the first step of the colorimetric methods is the formation of a surfactant-dye complex (Figure 2.15). For this, a dye is added to the surfactant solution. The surfactants form a complex with the dye. Then a liquid/liquid extraction is performed: a second phase (an organic phase), not miscible with the first one (the aqueous phase), is added and agitated. Because the surfactant-dye complex has a better solubility in the organic phase compared to the aqueous phase, by mixing the solutions the complex goes into the organic phase. To avoid the effect of interfering substances and to increase the extraction efficiency, other compounds such as salting out agents are added to the aqueous solution before introducing the second phase.

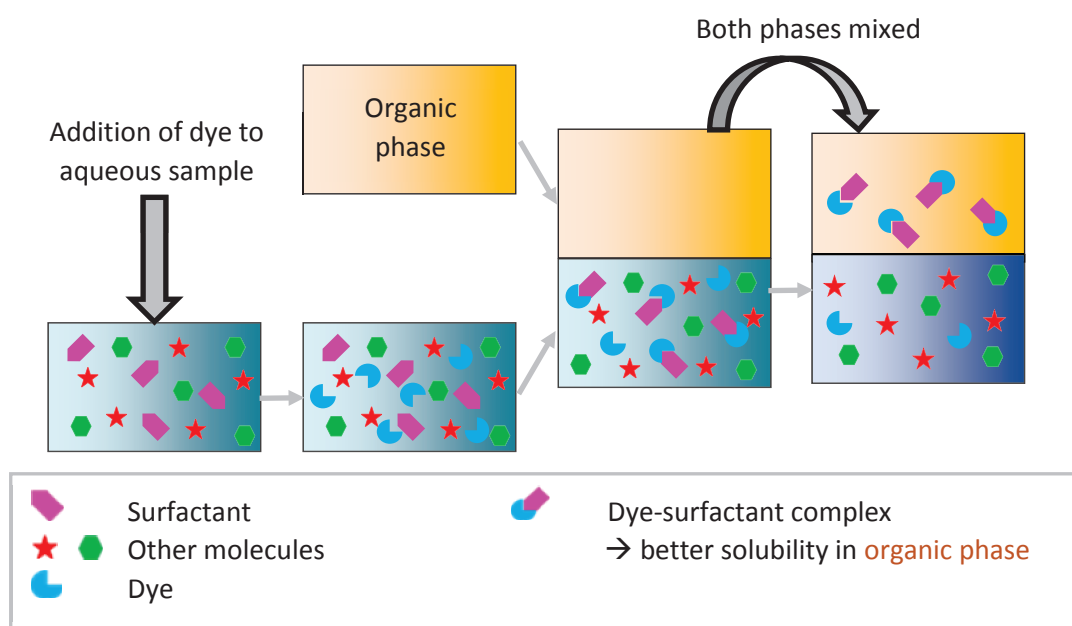


Figure 2.15: Principle of colorimetric method by formation of a surfactant-dye complex followed by a liquid-liquid extraction.

Then the absorbance of the phase containing the dye-surfactant complex is determined from a UV–spectrometer (Figure 2.16). The dye-surfactant complex absorbs in the visible, far from the possible absorbance of interfering molecules from the matrix, which could be extracted at the same time in the organic phase.

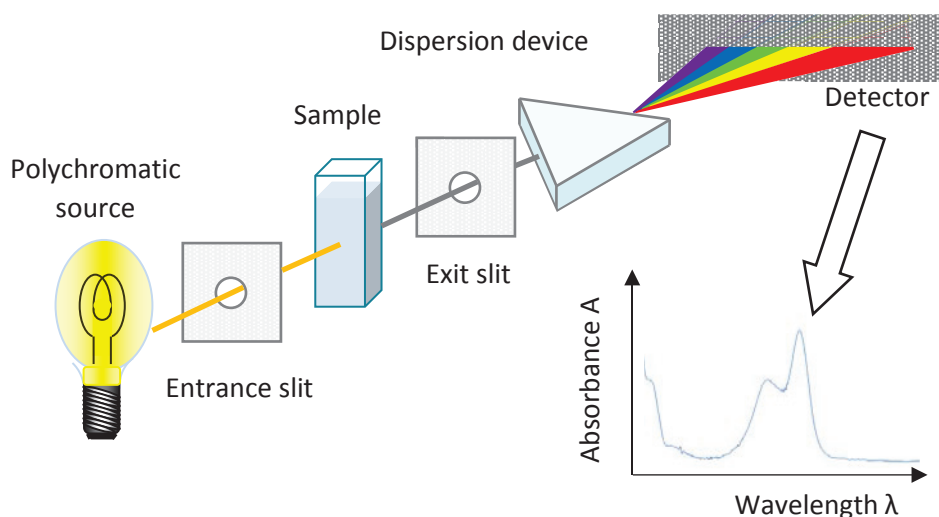


Figure 2.16: Schematic of a UV–visible spectrometer.

At a given wavelength, the absorbance A of a solution is directly proportional to the concentration of the absorbing species in the solution and the path length according to the Beer-Lambert law:

$$A = \log_{10} \left(\frac{I_0}{I} \right) = \epsilon C L \quad (2.2)$$

where I_0 is the intensity of the incident light at a given wavelength, I is the transmitted intensity, L is the path length through the sample, C is the concentration of the absorbing species and ϵ is the absorption coefficient which is specific to each species in a given solvent and at a particular temperature and pressure.

Thus, calibration curves giving the intensity at a maximum of absorption as a function of the concentration can be plotted for a compound. So, measuring the absorbance of the phase containing this compound and using a calibration curve allow the concentration of the compound in the phase to be determined.

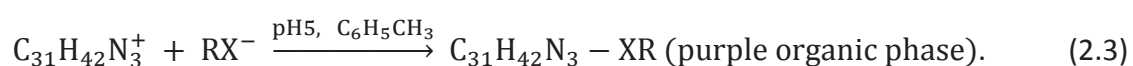
2.4.2. Experimental procedure: adaptation to extracts

As explained at the beginning of Section 2.4, although this section includes some results and graphs which were not present in literature before this work, they will be presented in the experimental section for more clarity. The development of the method and the experimental procedure were published in part in [Gérard, 2016] and more technical details about the procedure have been submitted for publication [Nozière, 2016 under review].

The colorimetric methods used for the determination of surfactant concentrations were specific to each type of surfactants (anionic, cationic and non-ionic) and will be detailed further. This section includes also the determination of the calibration curves for quantification, the uncertainties, the detection limits of the concentrations and the investigation of the potential interferences on the methods from other species found in aerosols.

2.4.2.1. Determination of anionic surfactants concentration

The dye used to quantify anionic surfactants RX^- was ethyl violet ($C_{31}H_{42}N_3Cl$) [Motomizu, 1982; Yamamoto, 1987; Schmitt, 2001; Latif, 2004]:

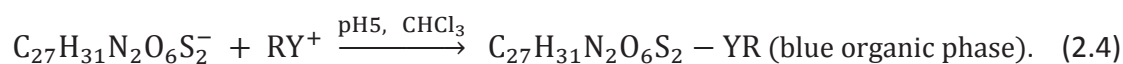


The reaction (2.3) was carried out by adding to 10 mL aqueous samples (surfactant extracts in water): 200 μL of acetate buffer pH = 5 (acetic acid solution 0.2 M / sodium acetate solution 0.2 M, 30 / 70 in volume), 100 μL of EDTA solution 0.1 M, 500 μL of 1 M sodium sulfate solution, and 200 μL of ethyl violet solution (0.49 g L^{-1}). A total of 2.5 mL of toluene was then added, and the solutions were stirred for 1 h. Once the aqueous and organic phases were separated, the toluene phase (upper phase) was removed and analyzed by UV-visible spectroscopy.

Note that the sodium sulfate solution is used to accelerate the phase separation, EDTA is used to reduce interferences of multivalent ions and the reaction is performed at pH = 5 because the extraction has been found to be the most effective at this pH [Motomizu, 1982].

2.4.2.2. Determination of cationic surfactants concentration

The dye chosen to quantify cationic surfactants RY^+ was disulfine blue ($\text{C}_{27}\text{H}_{32}\text{N}_2\text{O}_6\text{S}_2\text{Na}$) [Hummel, 2000; Latif, 2004]:



The reaction (2.4) was carried out by adding to the 10 mL aqueous samples (surfactant extracts in water): 1 mL of acetate buffer (pH = 5), 500 μL of disulfine blue solution (2.58 g L^{-1} in a mixture of 90 / 10 water / ethanol solution), and 2.5 mL of chloroform. The mixture was stirred for 1 h. Once the aqueous and organic phases were separated, the chloroform phase (lower phase) was removed and analyzed by UV-visible spectroscopy.

2.4.2.3. Determination of non-ionic surfactants concentration

The quantification of non-ionic surfactants RZ was more challenging than for anionic and cationic ones because there is no known dye able to react with all types of non-ionic surfactants. In this work, we chose cobalt thiocyanate ($\text{Co}(\text{NCS})_2$) as a reagent because it reacts with compounds containing a wide range of organic groups (in particular, ethoxylated-polyoxyethylene groups (or "EO-PO"), $-(\text{CH}_2)_n\text{-O}-$, that are common in surfactants) [Shin, 1997; Amirov, 2003; Pacheco e Silva, 2013]:



The reaction (2.5) was carried out by adding to the 3 mL aqueous samples (surfactant extracts in water): 1 mL of cobalt thiocyanate solution (6.2 g of ammonium thiocyanate and 2.8 g of cobalt nitrate hexahydrate in 10 mL water) and 2 mL of chloroform. The mixture was stirred for 1 h. Once the aqueous and organic phases were separated, the chloroform phase (lower phase) was removed and analyzed by UV-visible spectroscopy.

The references of chemicals used for these colorimetric methods are given in Appendix 8.2.

2.4.2.4. Quantification, uncertainties and detection limits

The concentrations of the surfactant-dye complexes were quantified by UV–visible absorption spectroscopy by placing small amounts of solutions in a 1 cm quartz cell and measuring the absorption over 190 - 1100 nm with an Agilent 8453 UV–visible spectrophotometer. Calibration curves for each surfactant class were established by measuring the maximum absorbance of known solutions of reference surfactants. For anionic surfactants, the maximum absorbance was at 612 nm, and the reference compounds were SDS and AOT. They resulted in a single calibration curve with a slope of $\epsilon = 0.37 (\pm 0.02) \mu\text{M}^{-1} \text{cm}^{-1}$ (Figure 2.17) at $\lambda_{612\text{nm}}$, and in a detection limit (intercept on the Y-axis + uncertainties) of $0.054 \mu\text{M}$ (or 0.016mg L^{-1} for SDS).

Note that the absorbance at $C_{\text{surf}} = 0$ (corresponding to a water sample in absence of surfactant subjected to the colorimetric method = blank solution) does not correspond to an absorbance $A = 0$ because a small portion of dye alone is extracted in the organic phase.

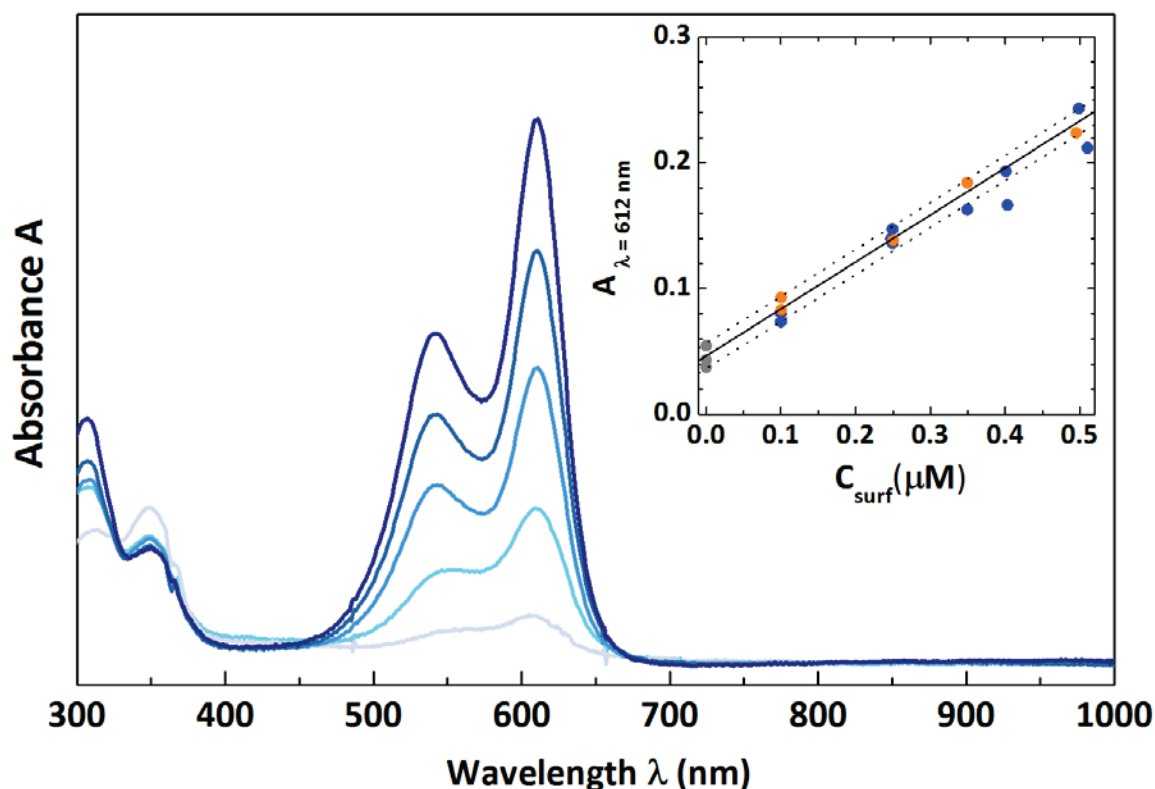


Figure 2.17: UV–visible spectra obtained from the reaction of ethyl violet with various concentrations of SDS. Upper right corner: calibration curve for anionic surfactants obtained from the absorbance at 612 nm for SDS (blue points) and AOT (orange points). Gray points: blanks. (adapted with permission from [Gérard, 2016] © Copyright 2016 American Chemical Society)

For cationic surfactants, the maximum absorbance was at 628 nm, and the reference compounds were zephiramine and CTAC, which resulted in a single calibration curve with a slope of $\epsilon = 0.35 (\pm 0.05) \mu\text{M}^{-1} \text{cm}^{-1}$ (Figure 2.18) at $\lambda_{628\text{nm}}$ and in a detection limit of $0.059 \mu\text{M}$ (thus, 0.011 mg L^{-1} for zephiramine).

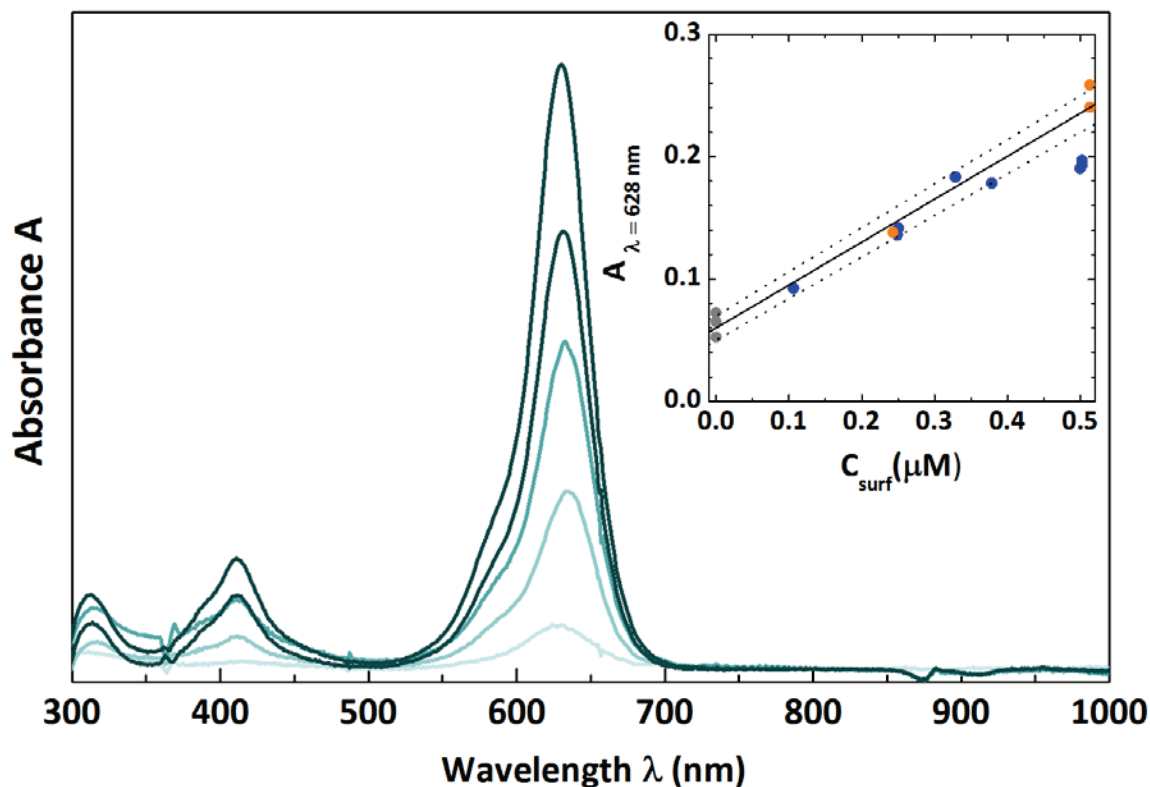


Figure 2.18: UV-visible spectra obtained from the reaction of disulfine blue with various concentrations of zephiramine. Upper right corner: calibration curve for cationic surfactants obtained from the absorbance at 628 nm for zephiramine (blue points) and CTAC (orange points). Gray points: blanks.

Thus, for anionic and cationic surfactants, these colorimetric methods are more sensitive in mass concentration than relative techniques for surfactant concentration measurement (*e.g.* [Orlović-Leko, 2010; Frka, 2012]).

For non-ionic surfactants, two peaks of maximum absorbance could be used (317 and 621 nm), and five reference compounds were used (Triton X114, Brij35, surfactin, rhamnolipid, and L- α -phosphatidylcholine). They resulted in calibration curves containing each $\pm 10\%$ of uncertainties but displaying different slopes, depending on the structure of the surfactant molecule (number of ethoxylated-polyoxyethylene groups EO-PO units) and spanning over nearly a factor of 10 between Triton X114 (7–8 EO-PO units) and Brij35 (23 EO-

PO units). Previous works reported a similar range of variability between seven industrial surfactants measured with cobalt thiocyanate [Amirov, 2003]. Because the objective of this work was to determine the importance of surfactants for cloud formation, we chose to determine lower limits for their concentrations by using the calibration curve with the largest slope (*i.e.*, giving the smallest concentrations), $\epsilon = 0.013 (\pm 0.001) \mu\text{M}^{-1} \text{cm}^{-1}$ at $\lambda_{317\text{nm}}$, which was the one for Brij35 (Figure 2.19).

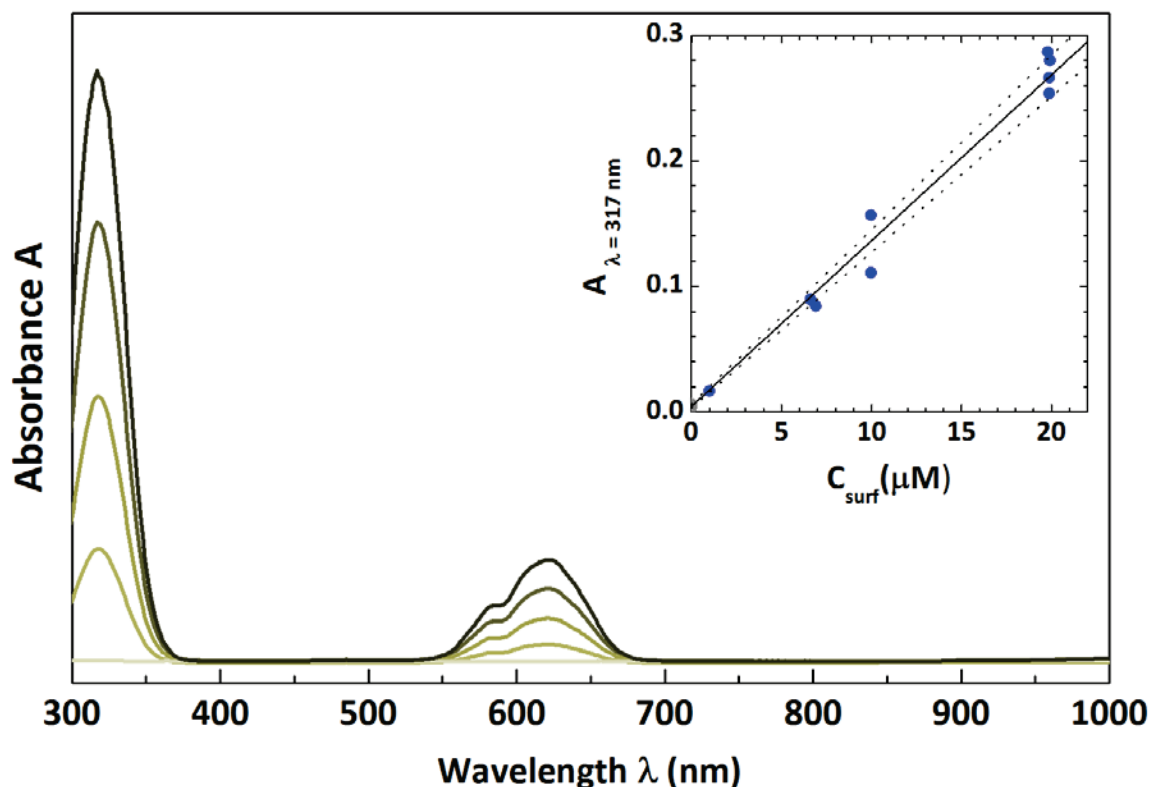


Figure 2.19: UV-visible spectra obtained from the reaction of cobalt thiocyanate with various concentrations of Brij35. Upper right corner: calibration curve for non-ionic surfactants obtained from the absorbance at 317 nm. Gray points: blanks.

With this curve, the detection limit for non-ionic surfactants was estimated to be $0.3 \mu\text{M}$. Because different non-ionic surfactants with different structures are likely to be present in aerosols, using the calibration curve for Brij35 potentially underestimated the overall non-ionic concentrations in aerosols. The extent of this potential underestimation (systematic errors on the measurements) was determined from the calibrations slopes of non-ionic reference compounds with surface tension curves similar to those found for aerosol surfactants in this work ($\text{CMC} \approx 10^{-4} \text{M}$, $\sigma_{\text{min}} \leq 40 \text{mN m}^{-1}$, Chapter 3). Those were surfactin, rhamnolipid, and Triton X114. Their calibration slopes spanned over a factor of 3.5 in total,

thus implying an average underestimation of the concentrations of a mixture of such compounds by a factor of 1.75. However, because the dye could also miss some non-ionic surfactants entirely (those not containing EO-PO units, for instance), the potential underestimation on the non-ionic concentrations in aerosols was estimated to be a factor of 2 on average. The resulting systematic errors in the total surfactant concentrations were, however, lower (see Section 2.4.2.5).

2.4.2.5. Determination of total surfactant concentrations

Before determining the total surfactant concentration in aerosols, it was confirmed, using reference compounds, that the cationic method did not detect any anionic surfactants and vice versa, and that the non-ionic method detected neither anionic nor cationic surfactants. The cationic method was also confirmed not to detect any non-ionic surfactants. Only the anionic method was found to weakly detect some biological non-ionic surfactants (10 - 30 % of the calibration slope). But as these compounds were also weakly detected by the non-ionic method (10 - 50 % of the calibration slope for Brij35), summing up their concentrations obtained with the anionic and the non-ionic methods still accounted for less than 100 % of their concentration. Therefore, the total surfactant concentration in aerosols was determined as the sum of the concentrations of anionic, cationic, and non-ionic surfactants obtained with the different dyes. The uncertainties on these total concentrations were estimated to be $\pm 20\%$ as the square roots of the sums of those on anionic (5 %), cationic (15 %), and non-ionic surfactant concentrations (10 %) and on the extraction efficiencies. In addition to these random errors, the potential underestimation of the non-ionic surfactant concentrations by a factor of 2 was estimated to result in potential underestimation of 33 % on the total surfactant concentrations, as non-ionic surfactants contributed to about 1/3 of the total surfactant concentration in the samples (see Section 3.2).

Once the surfactant concentrations (for each class of surfactant and in total) were determined for each sample volume, they were determined for the corresponding aerosol particles volume by multiplying the concentration in the sample volume by the ratio between the sample volume and the total aerosol particles volume.

For aerosols from Askö station, the total aerosol particles volume was determined by weighting the filters before and after the aerosol sampling. For the aerosols from Pallas-Sammaltunturi station, it was determined from the aerosol particles size distributions measured in parallel to the aerosol particles collection on filters (see Section 2.8.4).

2.4.2.6. Interferences from other species

The possibility of interferences on the measured concentrations due to the reaction of the dyes with other ionic species than surfactants present in the atmospheric samples was studied, what the previous studies [Latif, 2004; Roslan, 2010; Jaafar, 2014; Mustaffa, 2014] did not check. For this, sodium chloride (NaCl), ammonium sulfate ((NH₄)₂SO₄), and oxalic acid, representing some the most abundant species in atmospheric aerosols, were added in concentrations of 1 mM to 1 M to known solutions of reference surfactants, and the surfactant concentrations were measured using the colorimetric methods. All of these compounds were found to interfere positively or negatively (*i.e.*, leading to over - or underestimations) with all classes of surfactants (Figure 2.20).

In the presence of interferents, the absolute differences between the measured concentrations and the calibration curves became larger than the uncertainties for interferent concentrations of the order of 0.01–0.05 M. This showed that using such colorimetric methods directly on water extracts of atmospheric samples might lead to erroneous surfactant concentrations. In our work, however, the surfactant concentrations obtained after the double extraction were unaffected by the presence of these interferents, even in concentrations as high as 1 M. This was because they were not retained (and thus eliminated) by the second (SPE) extraction step. This showed that this second step is essential for the accurate measurement of surfactant concentrations.

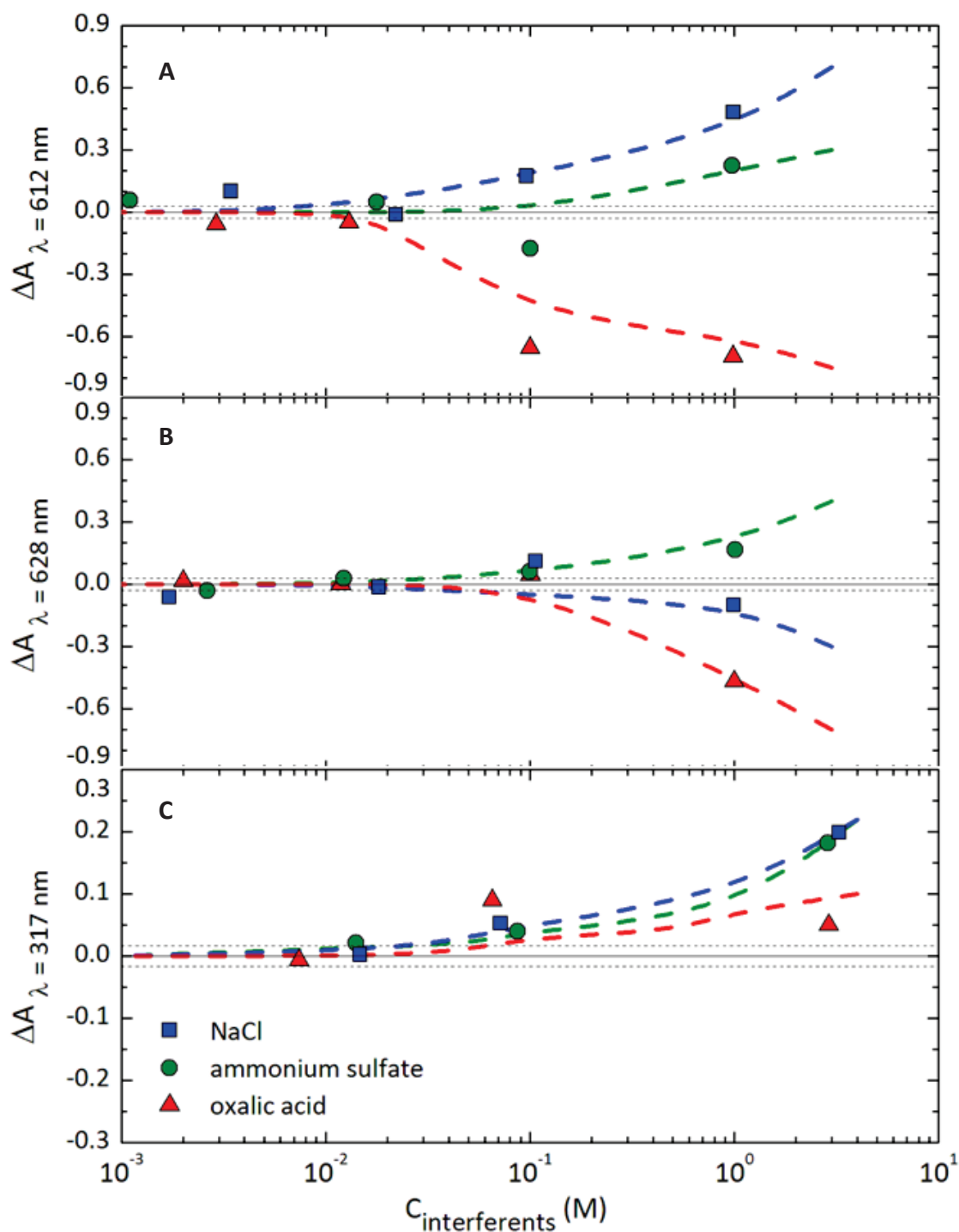


Figure 2.20: Effects of interferents on the measured absorbance for the different types of surfactants relative to the calibration curve (horizontal full lines) and the uncertainty range (horizontal dashed lines): NaCl (blue squares), ammonium sulfate (green circles), and oxalic acid (red triangles). The color dashed curves are the best fits through the experimental points. (A) corresponds to the colorimetric method for anionic surfactants (SDS, 2 μM), (B) for cationic surfactants (zephiramine, 2 μM) and (C) for non-ionic surfactants (Brij35, 20 μM).

2.5. Fluorescence spectroscopy

The investigation of the biological origin of surfactants was done by different approaches. The fluorescence spectroscopy which measures the fluorescence of a sample is one of them.

2.5.1. Principle

The fluorescence spectroscopy measures the emission of light due to the transition from the excited energy state of a compound to its ground energy state following the absorption of a photon by the compound (Figure 2.21).

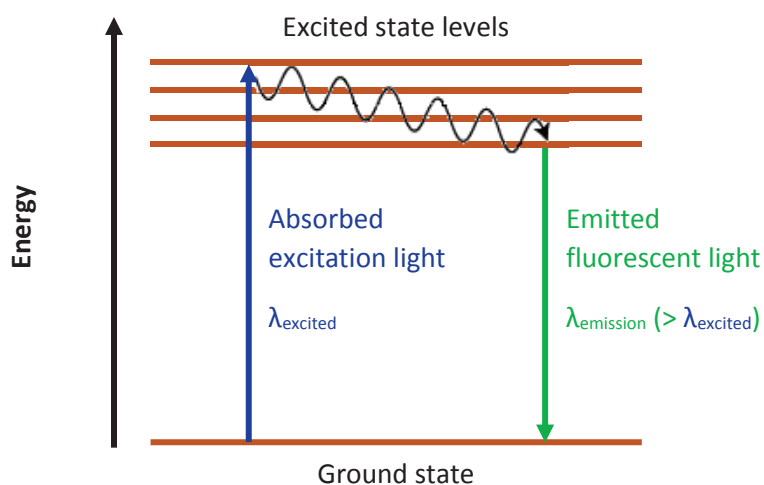


Figure 2.21: Simplified representation of fluorescence principle. After absorption of a photon of high energy by the electrons of the molecule, the system is excited into one of the many higher energy vibrational states. Some energy is transferred into vibrational energy and then the excited electron relaxes into the ground state, releasing a photon of lower energy than the photon initially absorbed. (adapted from Jablonski diagram).

Fluorescent molecules are excited only at specific wavelengths and emit at specific emission wavelengths. For fluorescence emission measurements, the excitation wavelength is kept constant (preferably at a wavelength of high absorption energy) and the detection wavelength varies, while for fluorescence excitation measurements, the detection wavelength (the wavelength passing through the emission filter or monochromator) is fixed and the excitation wavelength is varied across a region of interest (example in Figure 2.22). A three dimensional surface data set can also be measured, *i.e.* emission fluorescence intensity as a function of excitation and emission wavelengths.

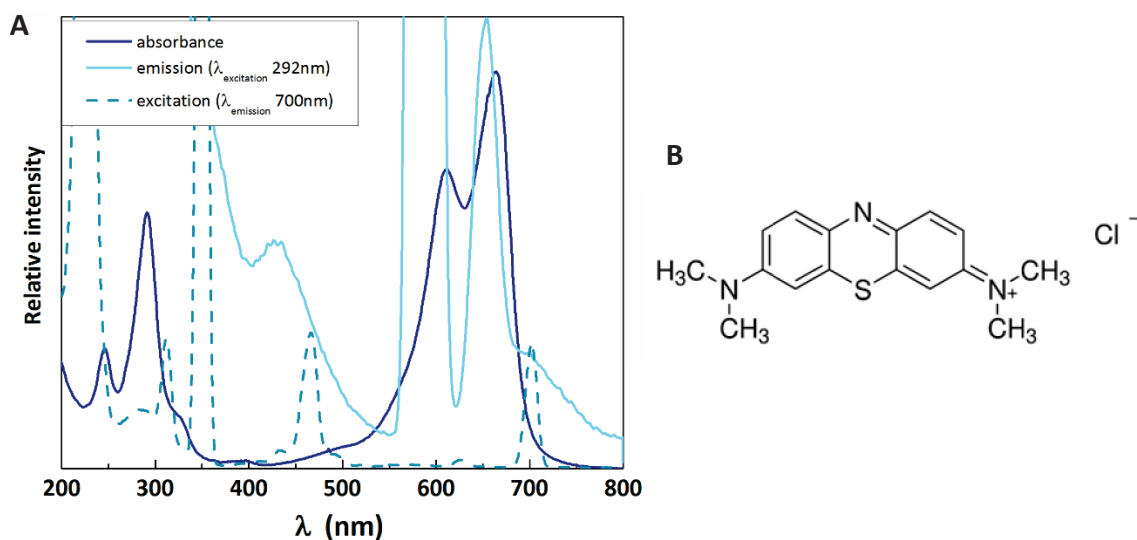


Figure 2.22: (A) Absorbance (dark blue line) and fluorescence spectra of methylene blue solution CAS 61-73-4 (emission spectrum at a fixed excited wavelength of 292 nm in light blue line and excitation spectrum at a fixed emission wavelength of 700 nm in dashed blue-green line) and (B) methylene blue chemical structure (spectra determined in this work, consistent with [Chu, 2009]).

Fluorescence is measured using a fluorescence spectrometer (Figure 2.23).

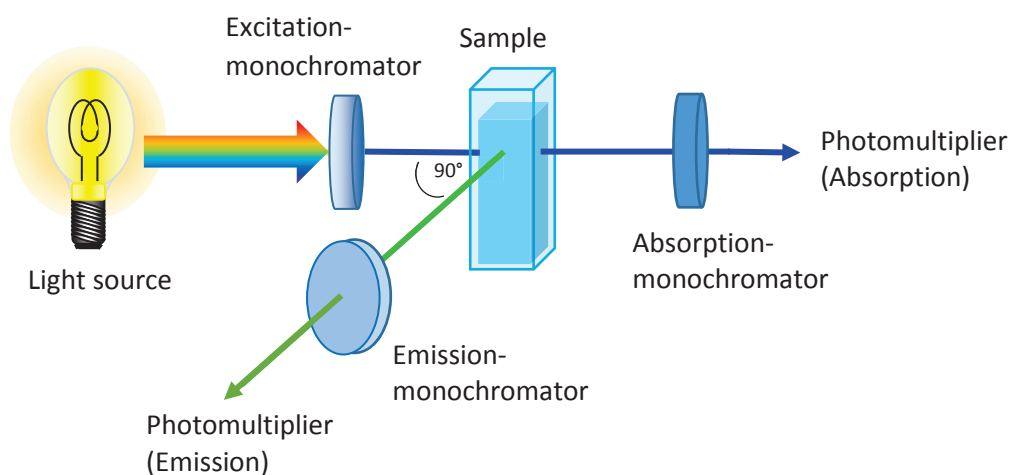


Figure 2.23: Schematic of a fluorescence spectrometer.

The light from an excitation source (for example Pulsed Xenon lamp for a continuous source of radiation) passes through a filter or monochromator (to select a transmitted wavelength) and strikes the sample. A proportion of the incident light is absorbed by the sample, and some of the molecules in the sample fluoresce. The fluorescent light is emitted in all directions. Some of this fluorescent light passes through a second filter or monochromator and reaches

a photodetector that converts any incident fluorescence photons into an electronic signal. The detector is usually placed at 90° to the incident light beam to avoid interference of the transmitted incident light.

Fluorescence can be used qualitatively or quantitatively. Because the composition of surfactant extracts in aerosols is unknown and because fluorescence intensity varies from a species to another, only qualitative fluorescence was used in this work.

2.5.2. Experimental procedure

Three-dimensional fluorescence spectra of the samples were measured using the Perkin Elmer LS 45 fluorescence spectrometer (Figure 2.24) with the software FL WinLab, using quartz cells (1 x 1 cm).

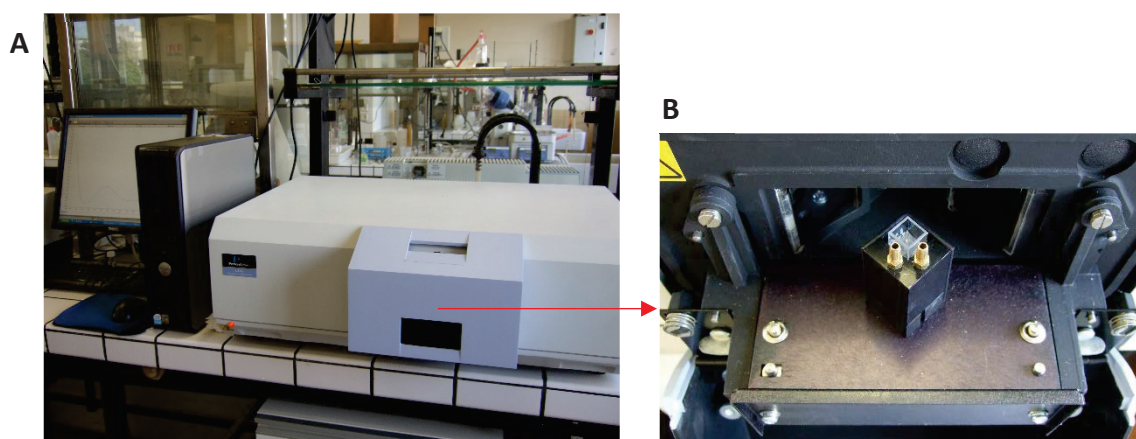


Figure 2.24: (A) Perkin Elmer LS 45 fluorescence spectrometer and (B) quartz cell containing the sample.

For each sample, the aqueous solutions at each step of the surfactant extraction from filters were studied, namely:

- The extract after the first extraction in water (after step 2 Figure 2.10, Section 2.2.2.3);
- The surfactant extract after the whole extraction (step 6 Figure 2.10, Section 2.2.2.3);
- The remaining solution after SPE, *i.e.* the aqueous matrix containing the interferents (step 3 Figure 2.10, Section 2.2.2.3).

The measurements were qualitative. Blanks (extraction method applied to ultrapure water) were analyzed between each measurements.

2.6. Chemical characterization of surfactants by LC-MS/MS

To prove the biological origin of the surfactants, their chemical structure in the aerosol extracts was also investigated. This was done by Liquid Chromatography - Tandem Mass Spectrometry (LC-MS/MS). This study was done at ICCF (Institut de Chimie de Clermont-Ferrand) with the group of Anne-Marie Delort, France, and especially with Pascal Renard.

2.6.1. Principle

The LC-MS/MS method is an analytical chemistry technique used to determine the composition or the structure of molecules in complex mixtures. It combines the molecules separation capabilities of Liquid Chromatography (LC) and the mass analysis capabilities of Mass Spectrometry (MS). The schematic of LC-MS/MS is shown in Figure 2.25.

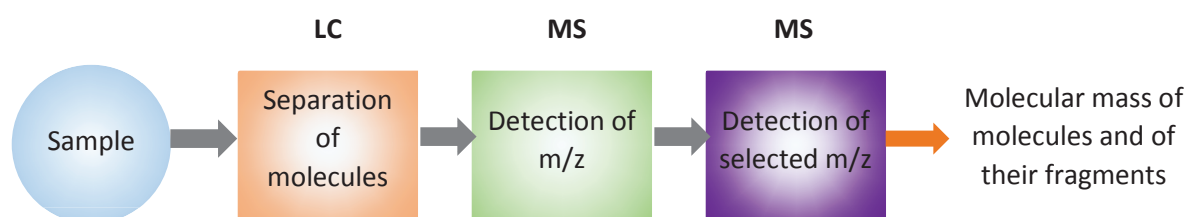


Figure 2.25: Schematic of Liquid Chromatography-Tandem Mass Spectrometry (LC-MS/MS).

Liquid chromatography separates the components of a liquid mixture on the basis of their molecular structure and composition. This involves a stationary phase and a mobile phase. The mobile phase flows through the stationary phase contained in a column and carries the components of the mixture with it. The separation is based on differential partitioning (conducting to a differential retention) between the mobile and stationary phases. Sample components that display stronger interactions with the stationary phase will move more slowly through the column than components with weaker interactions. This difference in speed during the travel into the column causes the separation of various components.

Liquid chromatography can be used for identification and quantification (in simple mixtures) and/or separation. For this study, the LC-step was used to separate as much as possible the components of the complex mixture.

Mass spectrometry is an analytical technique that identifies the chemical composition of a sample based on the mass-to-charge ratio of charged particles [Skoog, 2013]. A mass spectrometer is composed of three essential modules: an ion source, a mass analyzer and a detector (Figure 2.26).

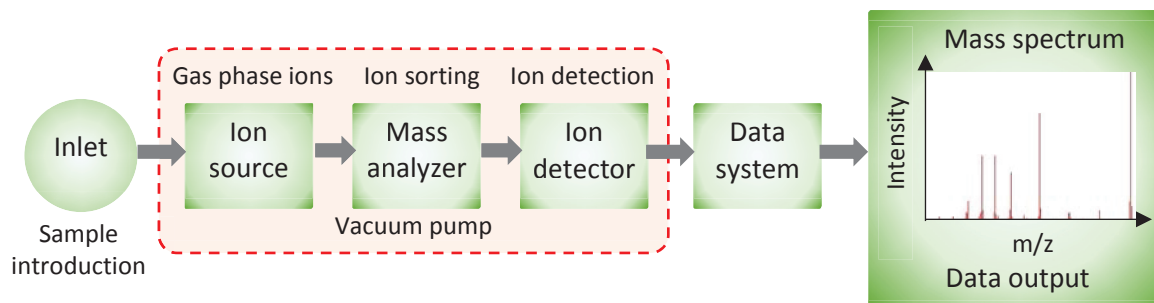


Figure 2.26: Schematic of a Mass Spectrometer (MS) (redrawn from [Premier-Biosoft, 2016] © Copyright 2016 Premier Biosoft).

The sample is loaded onto the instrument and undergoes an ionization of the components in the ion source, which results on the generation of ions (charged molecules or molecule fragments for unstable molecular ions and/or highly energetic sources) involving usually the addition of a proton to the analyte $[M+H]^+$ when the ion source is operated in positive ion mode or the loss of a proton $[M-H]^-$ when operated in negative ion mode. After the ionization, the charged molecules or fragments are then separated and detected according to their mass-to-charge m/z ratio.

However, for structural analysis, that was the interest of Section 6.2.5, LC-MS was not sufficient. Indeed, the mass-to-charge ratios m/z were not enough to determine the structure of the compounds since different molecules can have the same m/z but not the same structure. The only way to determine the structure of a molecule at a given m/z and to distinguish it from another is to break the molecule into fragments and to analyze them, because each molecule produces its own characteristic fragmentation ions. For this, a second MS was required, forming the tandem mass spectrometry (MS/MS) (Figure 2.27).

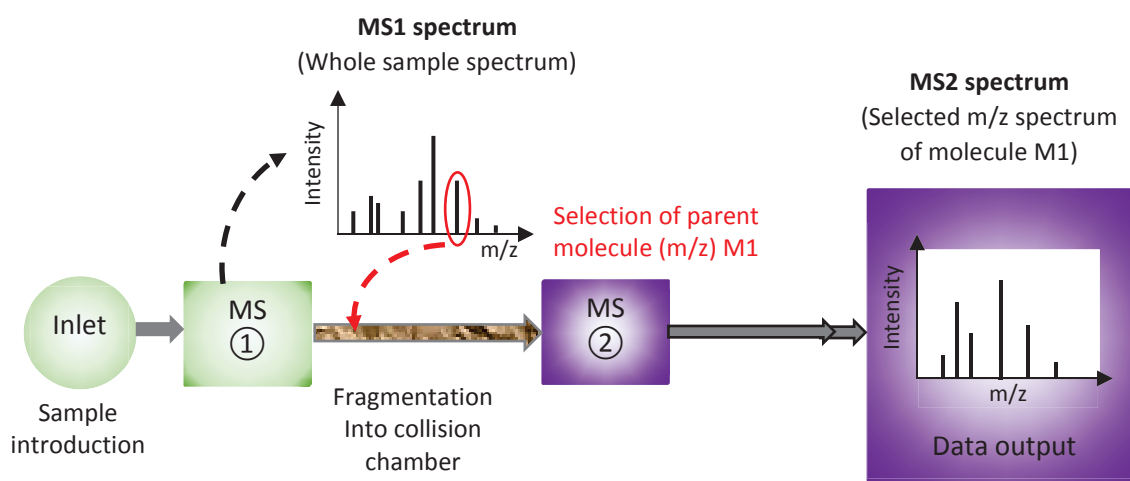


Figure 2.27: Schematic of tandem mass spectrometry (MS/MS) for product or daughter ion scanning (adapted from [ThermoFisher-Scientific, 2015] © 2015 Copyright ThermoFisher Scientific).

The tandem mass spectrometer combines two mass spectrometers: one for selecting the precursor ion from the ions generated in the ion source, and one for analyzing the product ions of the selected precursor produced by the collision chamber. The resulting MS/MS-spectrum consists only of product ions from the selected precursor. The chemical background and other mixture components are absent.

2.6.2. Experimental procedure

The following experimental procedure will be submitted for publication [Renard, 2017 in preparation].

The samples to be analyzed by LC-MS/MS were the surfactant extracts used for the study of Chapter 4, since a part of the surfactant extract in water was kept for LC-MS. To concentrate the aqueous surfactant extracts, a second SPE procedure was performed in the same conditions than the one in Section 2.2.2.3. After the solvent evaporation, the dry surfactant extracts were dissolved in 120 μL ACN/H₂O 1 / 1 for LC-MS/MS analysis.

For this study, the analysis were performed on a UHPLC Dionex Ultimate 3000 Rapid Separation LC (ThermoScientific) with a detector DAD UV/VIS 3000 RS (wavelength 200 - 400 nm) coupled with a Q Exactive Hybrid Quadrupole-Orbitrap mass spectrometer (ThermoScientific) equipped with a Heated Electrospray Ionization source (H-ESI) (Figure 2.28).

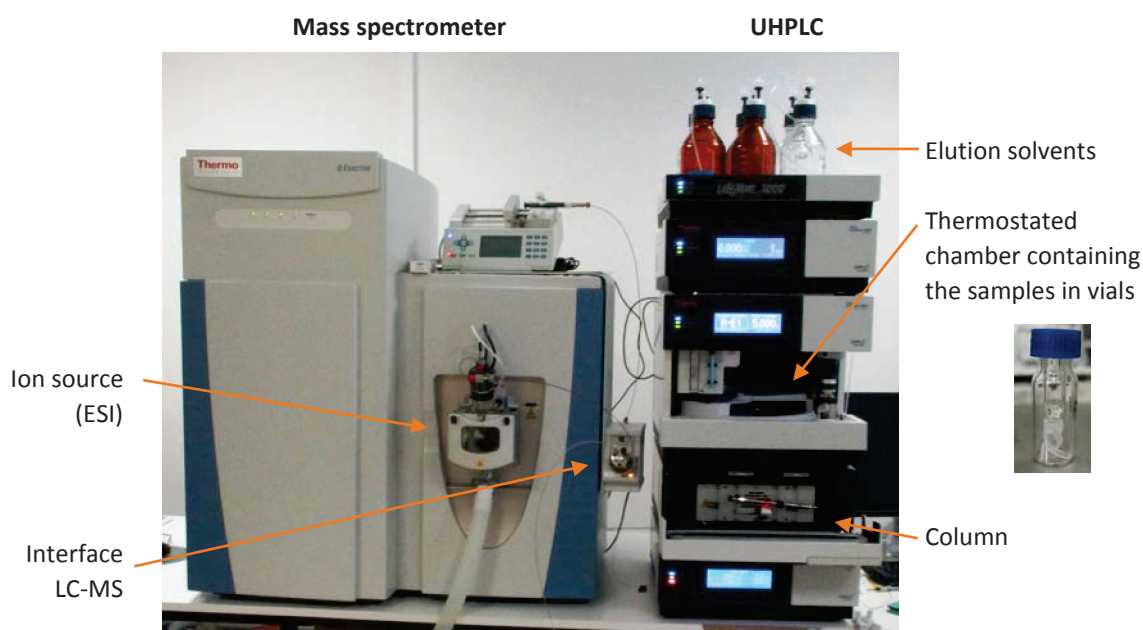


Figure 2.28: LC-MS/MS used for this study: Dionex UltiMate 3000 UHPLC coupled with a Q Exactive Hybrid Quadrupole-Orbitrap mass spectrometer, Thermo Scientific, USA.

The chromatographic separation was performed on a C_{18} column (Kinetex EVO C_{18} ; 100 x 2.1 mm; 1.7 μm , Phenomenex) with a flow rate of 0.45 mL min^{-1} . A volume of 30 μL of sample (on the 120 μL prepared) was injected in the column maintained at 30°C. The mobile phase was composed by (A) water with 0.1 % formic acid and (B) acetonitrile with 0.1 % formic acid. The following elution gradient was used: at initial time (B) was at 5 % and was linearly increased to 99 % within 7.5 min; this ratio was maintained constant for 2 min before returning to initial conditions ((B) at 5 %) in 0.5 min and kept constant for 2 min. Electrospray ionization was performed in positive (ESI+) and negative (ESI-) modes using the following conditions: spray voltage 3.3 kV (ESI+) and -3.0 kV (ESI-), AGC target 10^6 , maximum IT 50 ms, capillary temperature 320°C, sheath gas (N_2) flow rate 50 (arbitrary units), auxiliary gas (N_2) flow rate 10 (arbitrary units), spare gas (N_2) flow rate 2 (arbitrary units), auxiliary temperature 400°C, S-lens RF level 60. Moreover energy collisional dissociation 35 was applied for MS/MS measurements. The data were treated using the software Thermo Xcalibur 4.0.27.10. Before selecting specific masses from the LC-MS/MS measurements, the mass spectrometer was operated in full MS mode with a scanning range from 170 to 2550 m/z (with a mass accuracy < 3 ppm) and a mass resolution of 35 000. Blanks of method and solvent were analyzed every five samples for quality analysis.

Masses with retention time between 5 and 11 min were studied since analyzed reference surfactants appeared in this range of retention time. A particular attention has been paid to surfactant compounds with masses above 800 m/z because masses below 800 could be attributed to HULIS compounds (e.g. [Samburova, 2005; Gao, 2006; Stone, 2009; Chen, 2016]). The masses were compared with surfactants from literature and from the surfactant database created by the group of Anne-Marie Delort, ICCF (Institut de Chimie de Clermont-Ferrand), France.

This study being not finished, only the preliminary results will be presented in Section 6.2.5.

2.7. Study of micron-sized droplets using an optical trap

To study the effect of surfactants on the evaporation and condensation of water on micron-sized cloud droplets, an optical trap, similar to the one described by [Mitchem, 2006] was built by Amanda Frossard from the Ronald C. Cohen research group at the University of California, Berkeley, USA, collaborator of the project. The goal of this technique was to study individual droplets at sizes as close as possible to atmospheric cloud droplets.

We participated, at the University of California, Berkeley, USA, in the preliminary tests that defined the experimental conditions, and we aided in experiments that used different surfactant solutions. We also participated in the discussions about the experiments to be completed and the results. Because we did not participate in building the instrument or in the calculations of droplet radii from Raman spectroscopy, the set-up and the Raman data analysis will be described briefly.

2.7.1. Principle

The aerosol “optical trap” (also called “optical tweezer”) technique holds an individual micron-sized aqueous droplet suspended in air using a focused laser beam [Ashkin, 1986; Omori, 1997]. The change in droplet size with a change in relative humidity is measured using Raman

scattering and bright-field microscopy [Hopkins, 2004; Mitchem, 2006]. The schematic of the set-up is shown in Figure 2.29.

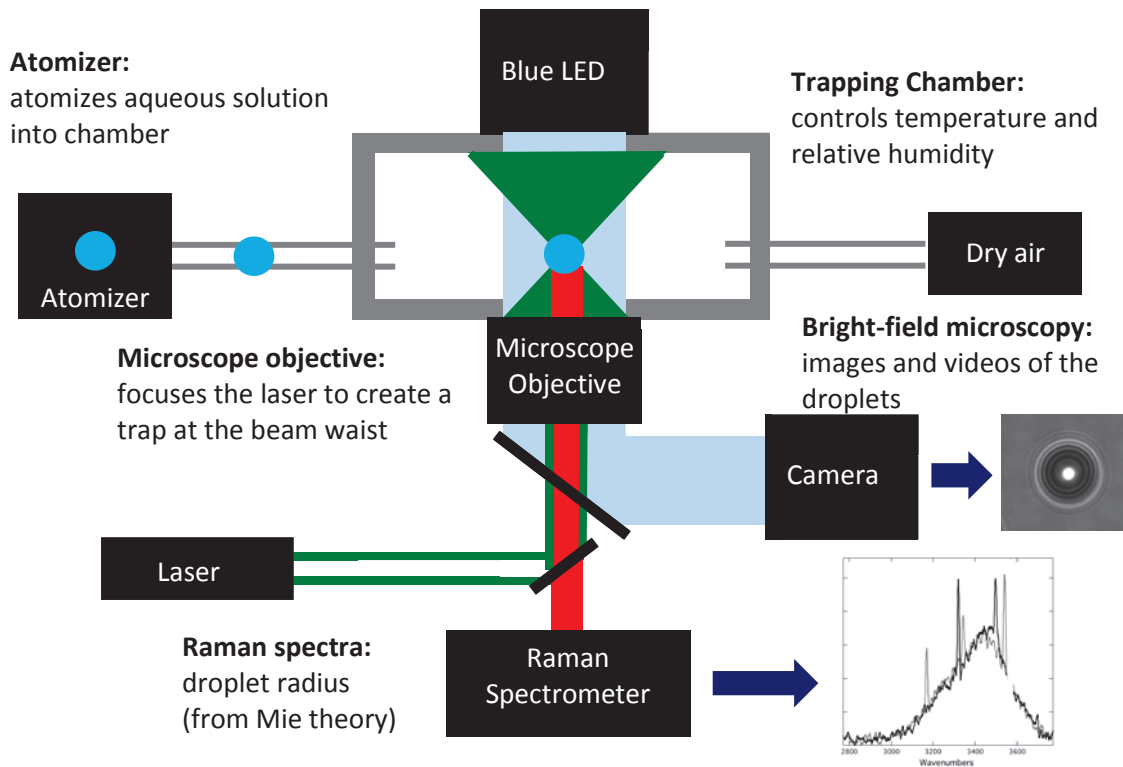


Figure 2.29: Schematic of the optical trap (adapted from [Frossard, 2016 under review]).

Droplets (~ 2 to $4 \mu\text{m}$ in radius) are introduced with an atomizer into the trapping chamber (temperature and relative humidity controlled). A tightly focused laser beam creates a three dimensional trap in the chamber resulting in a suspended individual droplet. The size of the droplet is determined from Raman spectroscopy. When the droplets were too small to size with the Raman method (*i.e.* right before evaporating completely), the normalized radius from the image sizing was used.

Measured Raman scattering spectra, including Whispering Gallery Mode peaks, are matched with predictions from Mie scattering theory (Figure 2.30). Mie theory calculates the pattern of light reflecting in a sphere. The resulting spectral pattern and the peak locations are a function of both droplet size and refractive index [Hopkins, 2004]. Consequently, the optical trap method allows us to measure the radius of a droplet and its evolution with time, given a change in chamber conditions, including relative humidity (*e.g.* [Knox, 2011]).

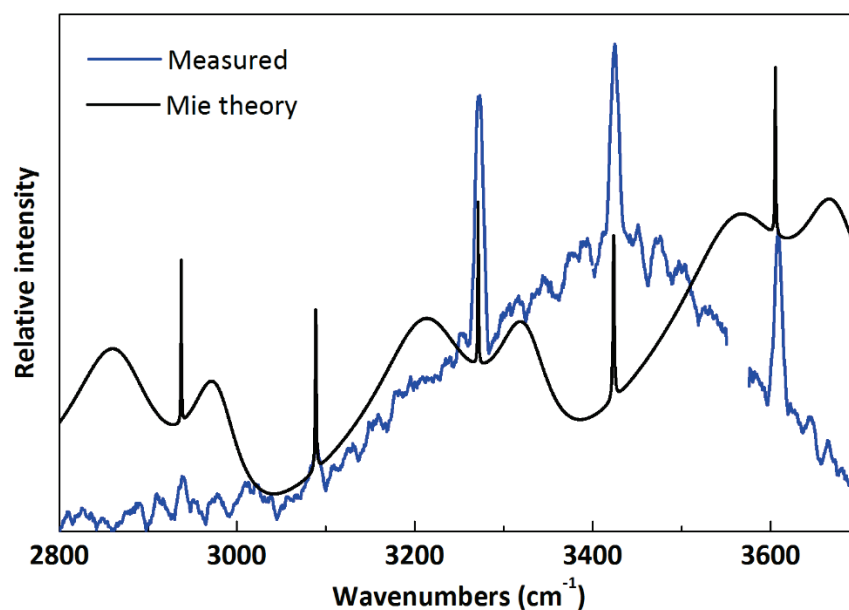


Figure 2.30: Example of measured Raman spectrum from a single droplet (611 mM NaCl in water, droplet diameter 3722 nm) of overlaid on the matching Mie theory spectrum, which is a function of the droplet radius and refractive index.

The optical trap technique has already been used in previous atmospheric studies to measure properties of aerosols, *e.g.* the structure and phase of mixed salt-organic-water aerosols [Buajareern, 2007c, 2007b, 2007a; Dennis-Smith, 2012], the dynamics of water uptake by glassy organic particles [Bones, 2012], the transfer of mass and heat during water evaporation/condensation [Miles, 2010], and the droplet size of salt solutions at equilibrium relative humidity [Mitchem, 2006]. This study is the first use of an optical trap to study the effect of a proxy atmospheric surfactant (Igepal CA-630) on the evaporation of water from droplets 2 - 4 μm in radius.

2.7.2. Experimental procedure

The optical trap set-up (Figure 2.31) and methods used to trap and study the radius of individual droplets for this work are fully detailed in [Frossard, 2016 under review].

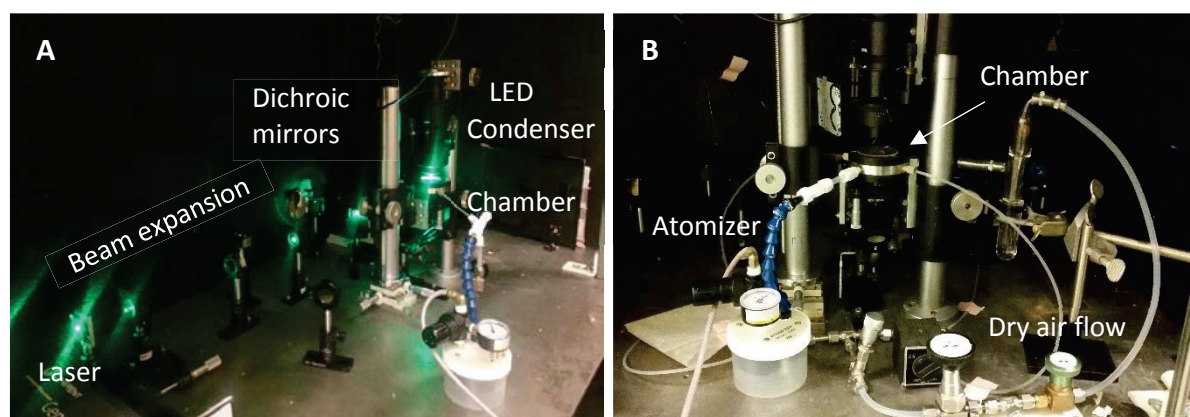


Figure 2.31: (A) Optical trap set-up built by Amanda A. Frossard from Ronald C. Cohen research group, University of California, Berkeley, USA, with (B) zoom on the elements to manipulate for each experiment.

For the study, the radius of individual droplets with different surfactant concentrations of the non-ionic surfactant Igepal was studied. Igepal CA-630 was used as proxy for atmospheric aerosol particles since it has a CMC value (0.08 mM [Mohanty, 2012]) in the range of CMC values of surfactants measured in atmospheric aerosols [Gérard, 2016] (Section 6.2.1). NaCl was also added in each solution to be atomized at a concentration of 0.611 M, similar to the concentration of salt in seawater. This helped to reduce the vapor pressure and allows the droplet to remain trapped in the subsaturated conditions inside the chamber [Hopkins, 2004; Buajarern, 2007a]. To demonstrate the effect of surfactants on the particles growth, individual droplets of solutions with NaCl only were also studied for comparison. The different concentrations and compositions of studied droplets are listed in Table 2.1.

Table 2.1: Concentrations of Igepal and NaCl in the micron-sized droplets studied by the optical trap method (modified from [Frossard, 2016 under review])

Samples	Igepal CA-630 + NaCl				NaCl only
Concentration (relative to CMC)*	0.4x	4x	22x	48x	n/a
Igepal Concentration (mM)**	0.04	0.35	1.76	3.87	0
NaCl Concentration (mM)**	611.2	611.2	611.3	611.1	611.3
Number of droplets	10	10	11	17	10

* Igepal CA-630 CMC value of 0.08 mM [Mohanty, 2012]; Sigma-Aldrich Igepal® CA-630 CAS Number 9002-93-1.

** 50 mL of each solution was prepared for the atomizer container.

The individual droplets from the surfactant solutions described in Table 2.1 were trapped in the chamber. To study the effect of surfactants on the evaporation and condensation of water from and onto cloud droplets, the growth of the droplets by changing the relative humidity in the chamber was recorded. First the droplet was maintained initially at a relative humidity of 80 %, then the relative humidity was reduced to 70 % (evaporation of the droplet) and finally, the relative humidity was brought back up to 80 % (condensation of water onto the droplet) (example in Figure 2.32). For each droplet of a given composition, the procedure lasted ~ 15 minutes and was repeated at least 10 times. In the experiments, the radius of the droplets at 70 - 80 % RH ranged from 2 μm to 4 μm .

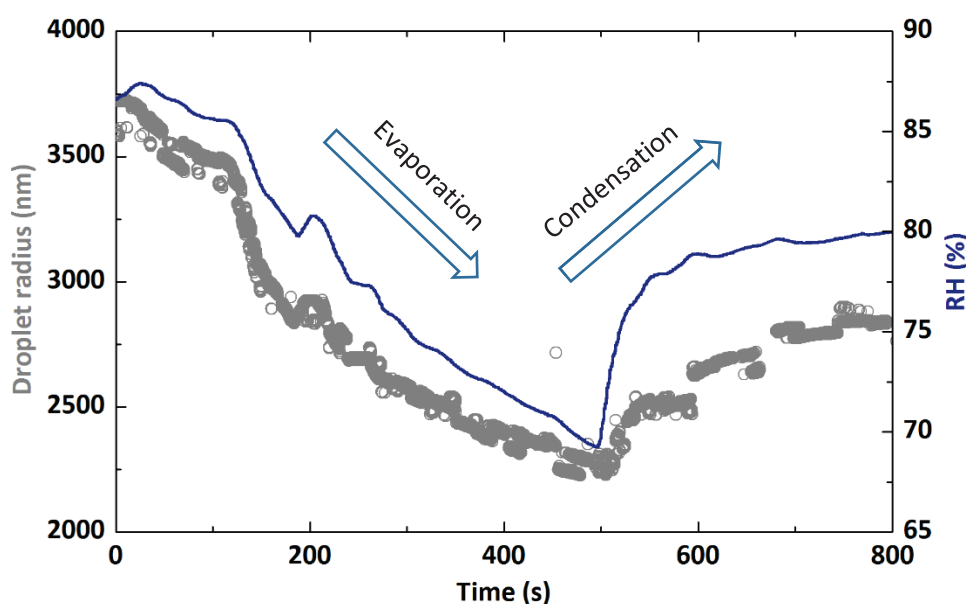


Figure 2.32: Droplet radius as a function of relative humidity and time (with example of a droplet composed of 611 mM NaCl and 0.35 mM Igepal in water). The decrease of the radius corresponds to the evaporation of water at the surface of the droplet and the increase corresponds to the condensation of water onto the droplet.

To attest to the validity of the method for studying the effect of surfactants, the reliability of the set-up measurements was checked. This was done in two ways. First, to test the equilibrium of the chamber, the sizes of the initial and final droplets at 80 % were compared (Figure 2.33 (A)), *i.e.* the radius of the droplet at initial relative humidity of 80 % and after the evaporation and condensation steps. They were found to be unchanged ($R^2 = 0.98$, slope = 1.01). This held true for both the NaCl only and the NaCl with Igepal droplets. Secondly, the consistency between the experimental and theoretical diameters of droplets for which the behavior was known, namely droplets containing NaCl only, was confirmed by

comparison with Köhler theory [Köhler, 1936] and a previous study of sea salt particles [Tang, 1997; Lewis, 2004] (Figure 2.33 (B)). These measurements also showed that the concentration of the solution in the container of the atomizer was representative of the concentration in the individual droplets sent to the optical trap by the atomizer.

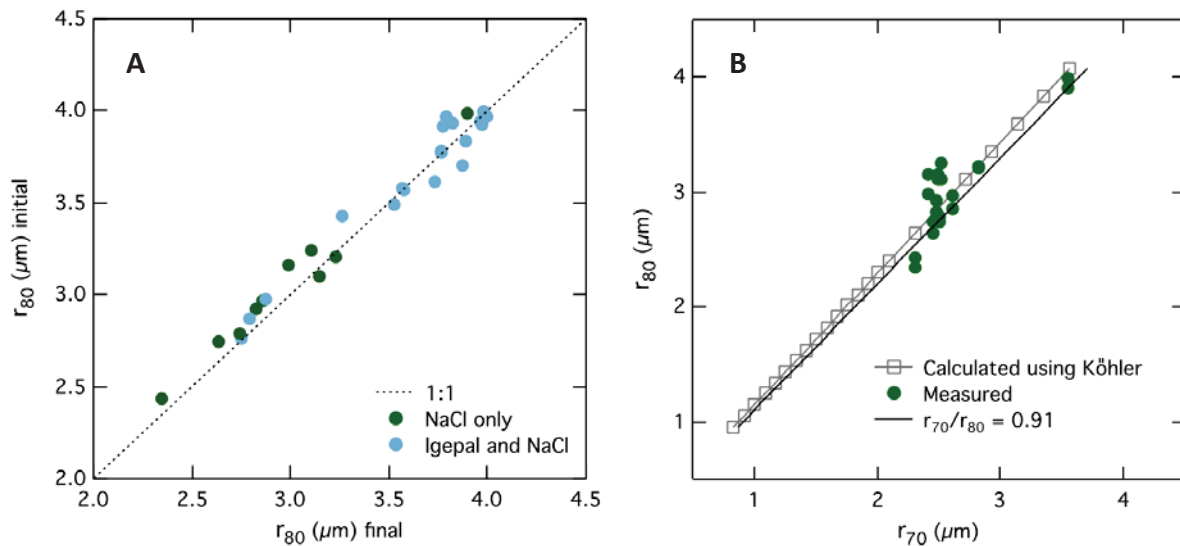


Figure 2.33: (A) Comparison of droplet radii initially and finally at 80 % RH for all of the droplets in the evaporation and condensation experiment. (B) Comparison of droplet radii of aqueous NaCl at 80 % and 70 % RH calculated using Köhler theory (grey squares) and measured in the experiment (circles). The black line represents the r_{70}/r_{80} ratio (0.91 [Tang, 1997; Lewis, 2004]) for similar droplets (reproduced from [Frossard, 2016 under review]).

Both verifications attested to the validity of the method (for more details, see [Frossard, 2016 under review]).

2.8. Other atmospheric and geophysical data

Parallel to sampling, extraction and characterization of surfactants in atmospheric aerosols, other devices and techniques were used to characterize the aerosols masses: chlorophyll-*a* data and back trajectories provided by the NOAA (National Oceanic and Atmospheric Administration) for Askö campaign and data provided by the instruments in the station (cloud events, volume of aerosol particles) for Pallas-Sammaltunturi campaign.

2.8.1. Chlorophyll data from MODIS aqua satellite

Because the surfactants in aerosols were expected to be mostly biological [Ekström, 2010], for the study of Askö campaign, a correlation with biological parameters around the station was investigated (Section 6.2.3).

Seawater concentrations of chlorophyll-*a* and other biological seawater markers near Askö station and at other locations in the Baltic Sea were available in the SHARK database (Svenskt HavsARKiv, Swedish Meteorological and Hydrological Institute, SMHI). However, because these data were missing for too many days over the sampling period, concentrations of chlorophyll-*a*, from the aqua MODIS satellite instrument (Level L3, 1 day composite) (Figure 2.34), provided by the National Oceanic and Atmospheric Administration (NOAA) ERDDAP data server, were preferred. Whenever they were available, they agreed within 10 % with those given by the SHARK database.

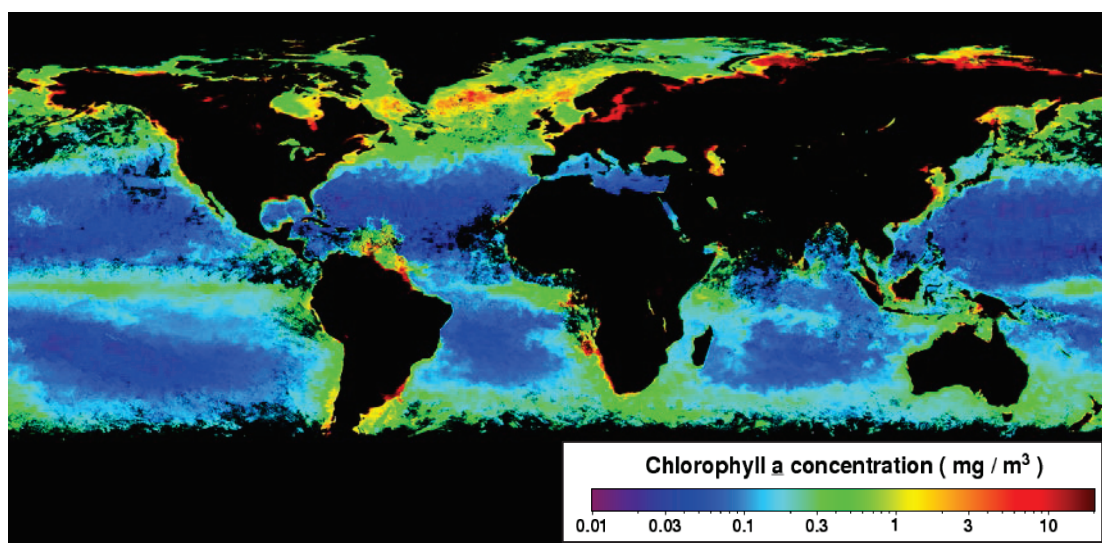


Figure 2.34: Example of data given by the MODIS Aqua satellite (Level 3 Global Monthly): Chlorophyll-*a* in July 2010 [OceanColor-NASA, 2015].

The daily chlorophyll-*a* MODIS concentrations were averaged over the time periods corresponding to each aerosol sample and over areas between 50 and 300 km² around Askö. A total of 10 % of uncertainties was attributed to the chlorophyll concentrations thus obtained to account for the fact that these data were available only for about 70 % of the days over the sampling period.

2.8.2. Air mass sources by HYSPLIT model trajectories

Another indirect way to learn more about the surfactants in atmospheric aerosols was to study their origin, namely the air masses history. For this, HYSPLIT (Hybrid Single Particle Lagrangian Integrated Trajectory) Model vertical velocity provided by the National Oceanic and Atmospheric Administration NOAA (<https://ready.arl.noaa.gov/HYSPLIT.php>) was used [Draxler, 2015; Rolph, 2015]. This model can calculate air parcel backward trajectories (example in Figure 2.35).

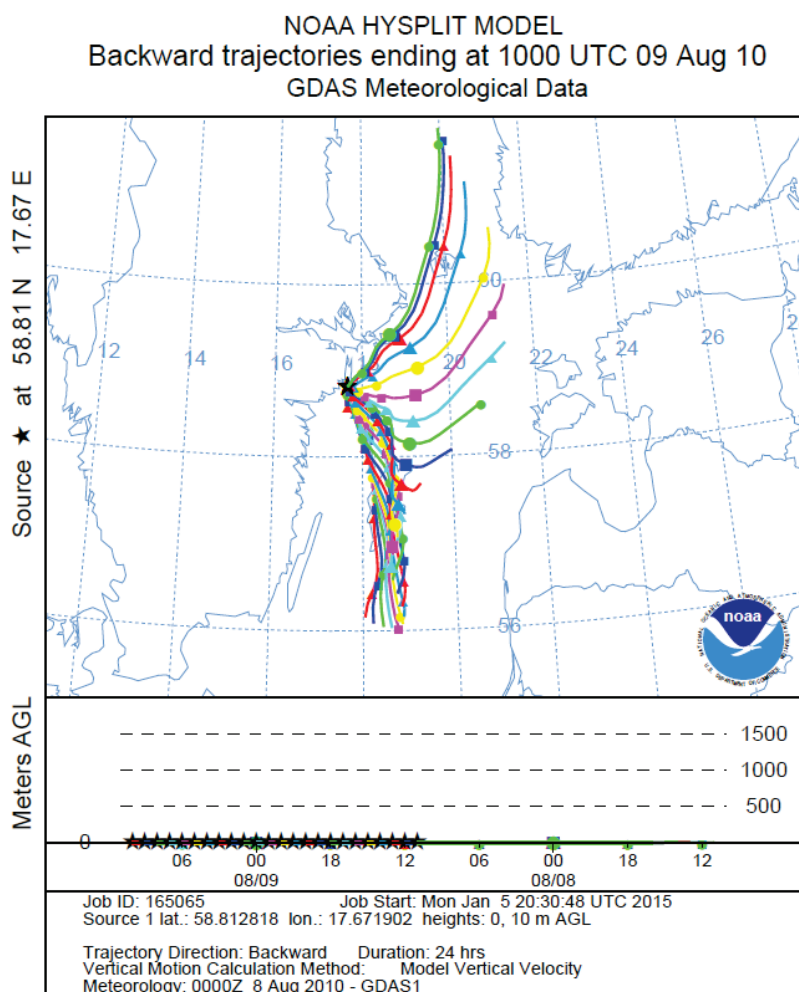


Figure 2.35: Example of 24 h - back trajectories (with a new trajectories starting every hour) at Askö station, Sweden, obtained from HYSPLIT model [Draxler, 2015; Rolph, 2015].

For Askö campaign, back trajectories were used to check if the air masses came majority from the Sea. For Pallas-Sammaltunturi campaign, they were used to classify the samples according to their sources.

2.8.3. Presence of clouds by visibility data

The visibility was used to determine the presence of clouds at Pallas-Sammaltunturi station using a Vaisala FD12P weather sensor (Figure 2.36).

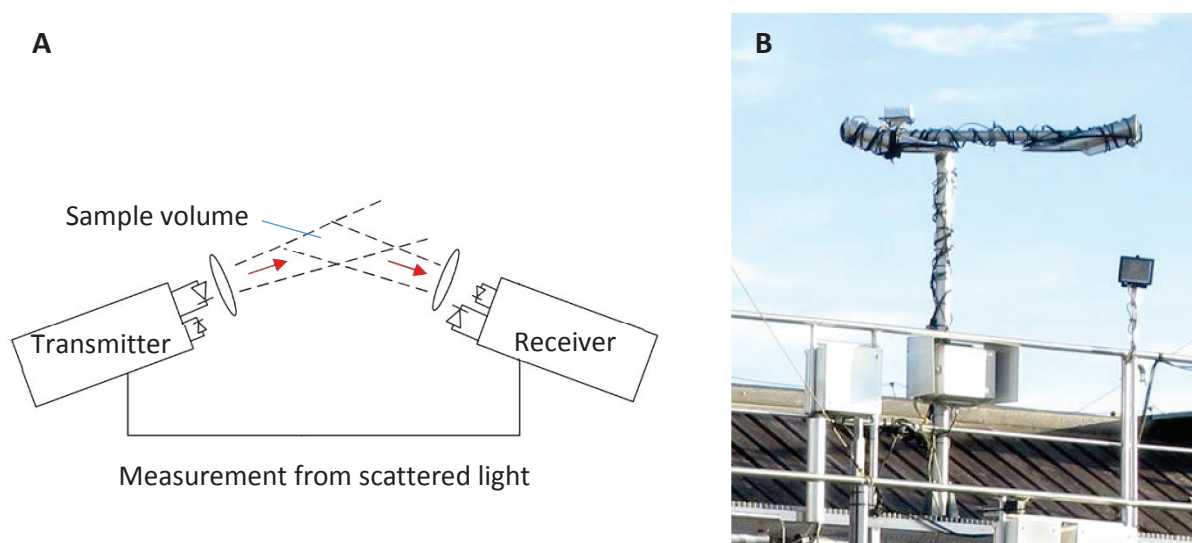


Figure 2.36: (A) Simplified schematic of visibility measurement ([Vaisala, 2002] © Copyright 2002 Vaisala) operated by (B) the Vaisala FD12P weather sensor.

The sensor combines forward scatter visibility meter, a weather sensor (temperature, humidity, wind speed) and can measure the amount of liquid precipitation. The part measuring the visibility is composed by a transmitter that pulses near-infrared light and a receiver that measures the scattered part of the light from the transmitter. The visibility was measured every minute on a scale of 10 - 50 000 m with the Vaisala FD12P weather sensor installed on the roof of the Pallas-Sammaltunturi station.

The presence of clouds was defined by a visibility ≤ 1000 m [Anttila, 2012] (example in Figure 2.37).

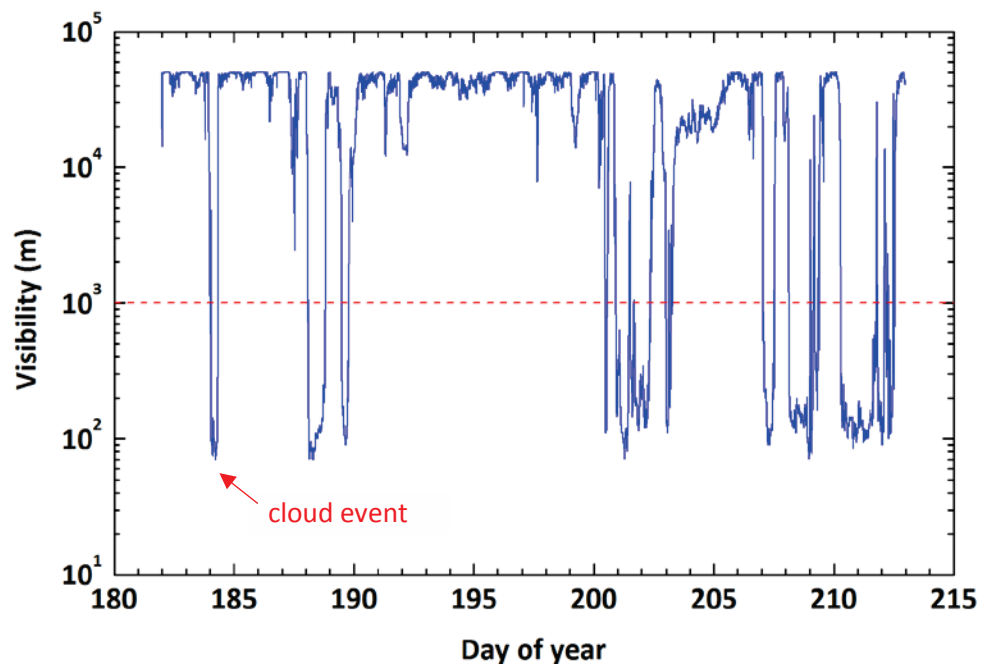


Figure 2.37: Example of visibility data (blue line) at Pallas-Sammaltunturi in July 2015. Cloud events were considered when a sudden drop in the visibility below 1000 m (red dashed line) appeared.

2.8.4. Volume of PM1 aerosol particles by DMPS and APS

For Pallas-Sammaltunturi campaign, the volume of aerosol particles collected on the filters was determined from aerosol size distributions from on-line instruments: Differential Mobility Particle Sizers (size range 7 - 500 nm) and Aerodynamic Particle Sizer (size range 500 - 20 000 nm) combined. Indeed, the determination of the volume by weighting the filters was not convenient since it required specific conditions (micro-balance with large chamber for the \varnothing 150 mm filters, long conditioning and storage of filters at controlled relative humidity and temperature,...). Moreover, to calculate the volume of aerosol particles from masses, the density of the aerosol would have been approximated from aerosol composition measurement running in parallel to the aerosols sampler.

2.8.4.1. Principle

- **DMPS**

A Differential Mobility Particle Sizer (DMPS) is a standard tool in atmospheric science to measure the particle size distribution of a size range 7 - 500 nm. The DMPS consists of a Differential Mobility Analyzer (DMA) and a Condensation Particle Counter (CPC) (Figure 2.38).

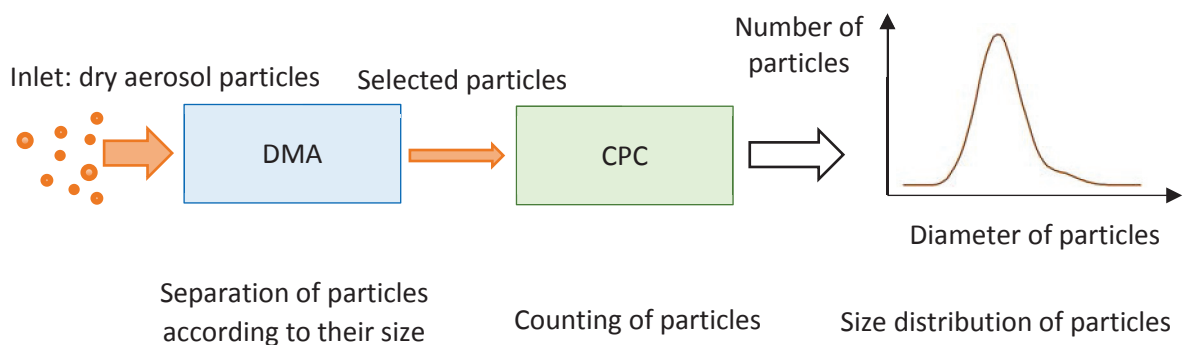


Figure 2.38: Simplified principle of the operating of the Differential Mobility Particle Sizer (DMPS) constituted of a Differential Mobility Analyzer (DMA) and a Condensation Particle Counter (CPC).

The particles are first size selected with the DMA, by separating the generated charged particles according to their electrical mobility in an electric field. Then the CPC counts the particles of a specific mobility [Morawska, 2006; Kulkarni, 2011]. The schematic of the DMA and CPC is shown in Figure 2.39.

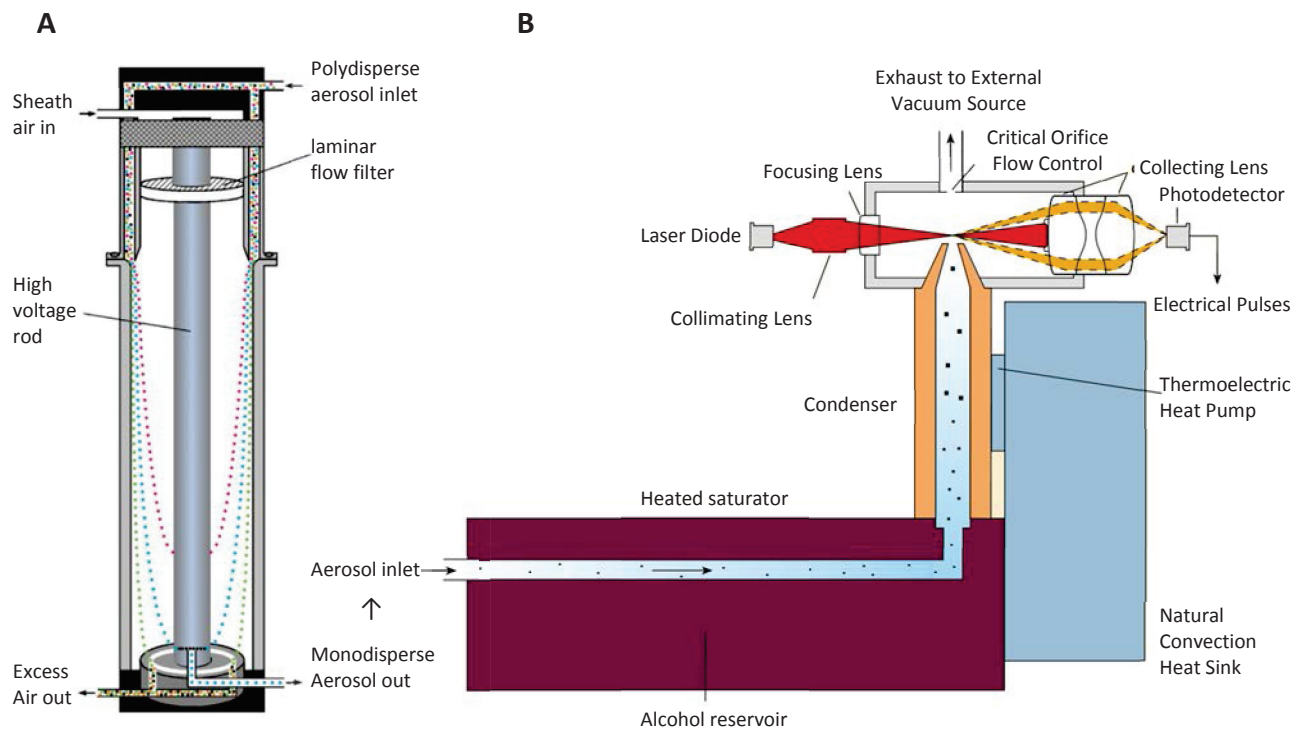


Figure 2.39: Schematic of the two main parts composing the DMPS: (A) Differential Mobility Analyzer (DMA) and (B) Condensation Particle Counter (CPC) ([TSI, 2002, 2014] © Copyright 2002, 2014, TSI Incorporated).

The principle of the DMA is the following. The aerosols enter a cylindrical chamber through an annular slit and are carried downward in a laminar flow parallel to the axis of the cylinder. A high voltage is applied between the walls of the cylinder and a central rod. The difference of voltage generates an electric field, which deflects the charged particles toward the center rod by a radial electric field. At a particular applied voltage, particles of a specific mobility exit through the slit in the lower part of the center rod. The CPC counts the aerosol particles that pass through the DMA and outputs a particulate concentration. It involves three processes: supersaturation of a fluid, growth of particles by condensation of vapors and detection of particles. Particles are grown by creating vapor from a working fluid (usually butanol) which condenses onto the particles so they grow in size and can be optically detected with a laser beam. The scattered light from the aerosol is detected in the photodetector. The signal from individual particles (pulses of scattered light) can be identified and counted, or the intensity of the scattered light is used as an indication of the particle concentration.

Figure 2.40 shows an example of data provided by the DMPS.

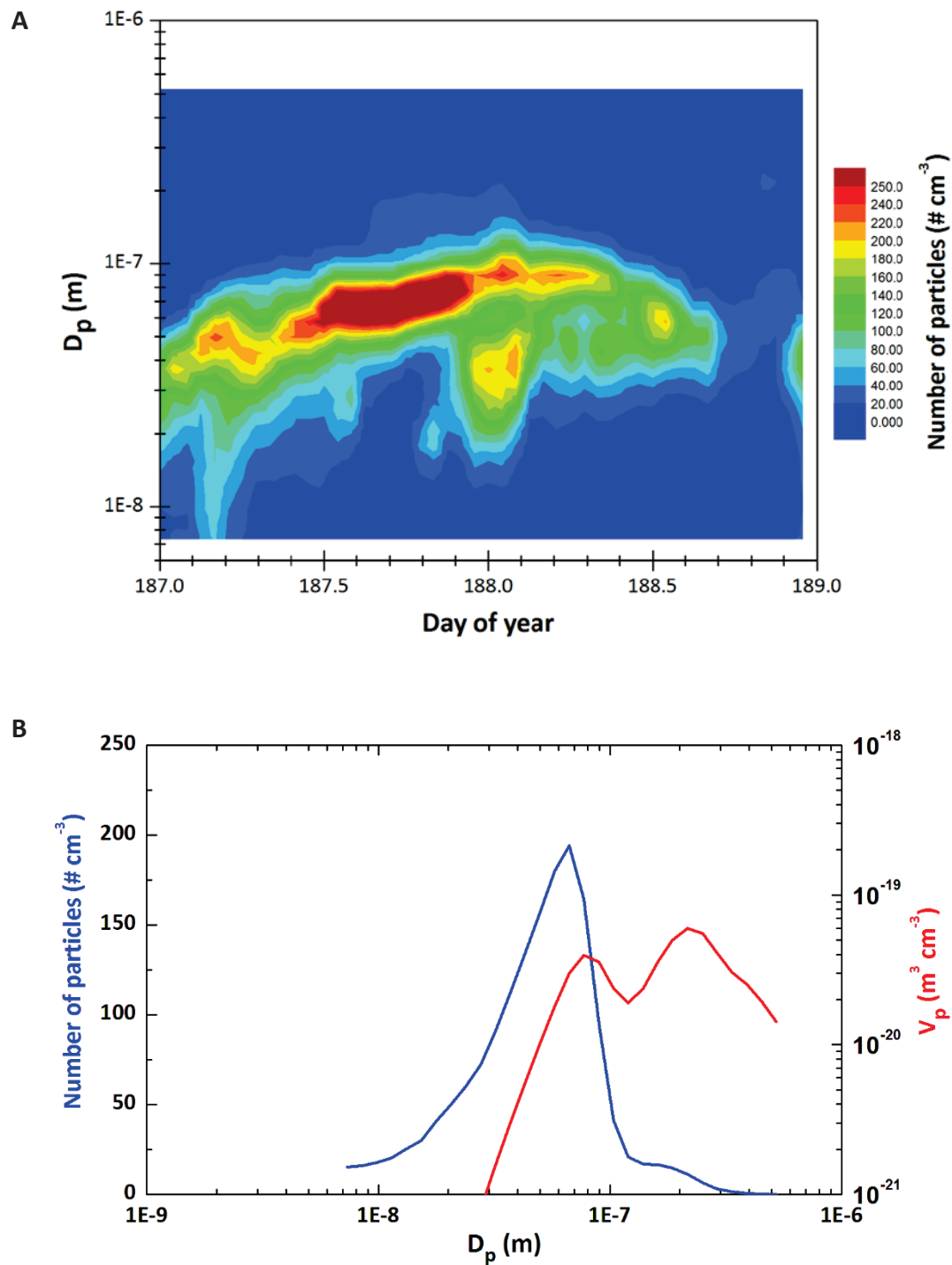


Figure 2.40: Example of size distribution graphs obtained from the DMPS instruments, at Pallas-Sammaltunturi in 2015: (A) time resolved PM_{0.5} size distribution for days 187-189 (year 2015) and (B) average number of particles (blue line) and calculated particles volume (red line) as a function of particle diameter for day 187.

- **APS**

For the size distribution of larger particles, an Aerodynamic Particle Sizer (APS) was used. As for the DMPS, the APS provides real-time aerodynamic measurements of particles but covers size range of larger particles with diameters from 0.5 to 20 μm [Peters, 2003]. The particles are separated according to their size using a time-of-flight method and their size and distribution are determined using light scattering measurements. A schematic of the APS is given in Figure 2.41.

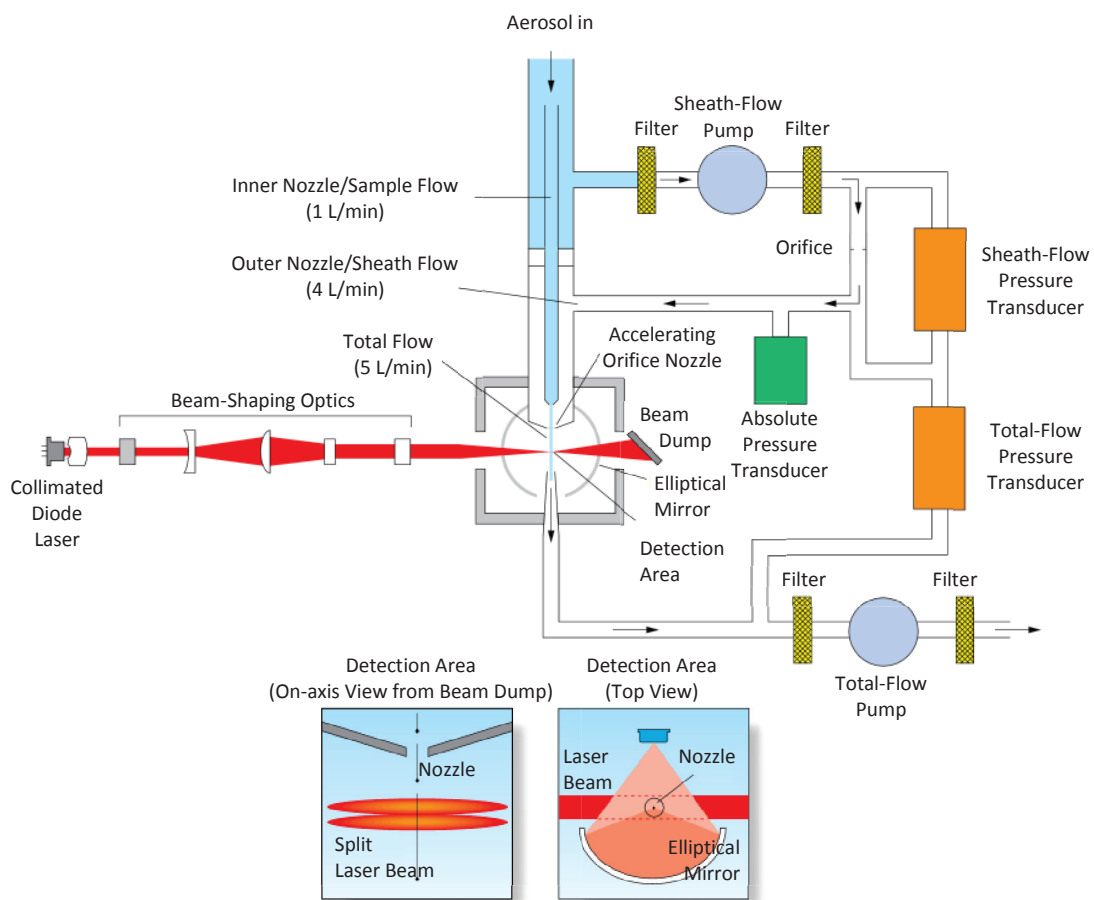


Figure 2.41: Schematic of an aerosol flow through an Aerodynamic Particle Sizer Spectrometer (APS) ([TSI, 2012] © Copyright 2012 TSI Incorporated).

The particles are accelerating in a flow field and are constricted through a nozzle. The particles pass through two laser beams separated by about 200 μm . An elliptical mirror collects scattered light onto a photodetector. A particle passing through both beams produces two pulses of scattered light. The time delay between the pulses is related to the velocity of the particle and hence to the aerodynamic diameter of the particle, which is defined as a particle that has the same settling speed than a solid spherical particle with the density of

1 g cm^{-3} and thus depends on the particle mass (the larger particles exhibit greater inertia and thus accelerate more slowly, thereby attaining lower velocities).

2.8.4.2. Experimental procedure

In order to obtain the volume of PM₁ (diameter < 1 μm) aerosol particles, the data of the following devices were combined (Figure 2.42): two differential mobility particle sizers (DMPSs) for size range of 7 - 500 nm (total inlet and inlet preventing cloud droplets to enter) and an Aerodynamic Particle Sizer (APS) for size range 500 - 20 000 nm (total inlet). At the Pallas-Sammaltunturi station, the two DMPSs had the structure described by [Komppula, 2005]. The APS was an Aerodynamic Particle Sizer® 3321 built by TSI. The DMPSs and APS measured the size distribution of the aerosols entering in the inlet after evaporating the water in the particles by heating them to 70°C. The whole size distributions were scanned every 5 minutes.

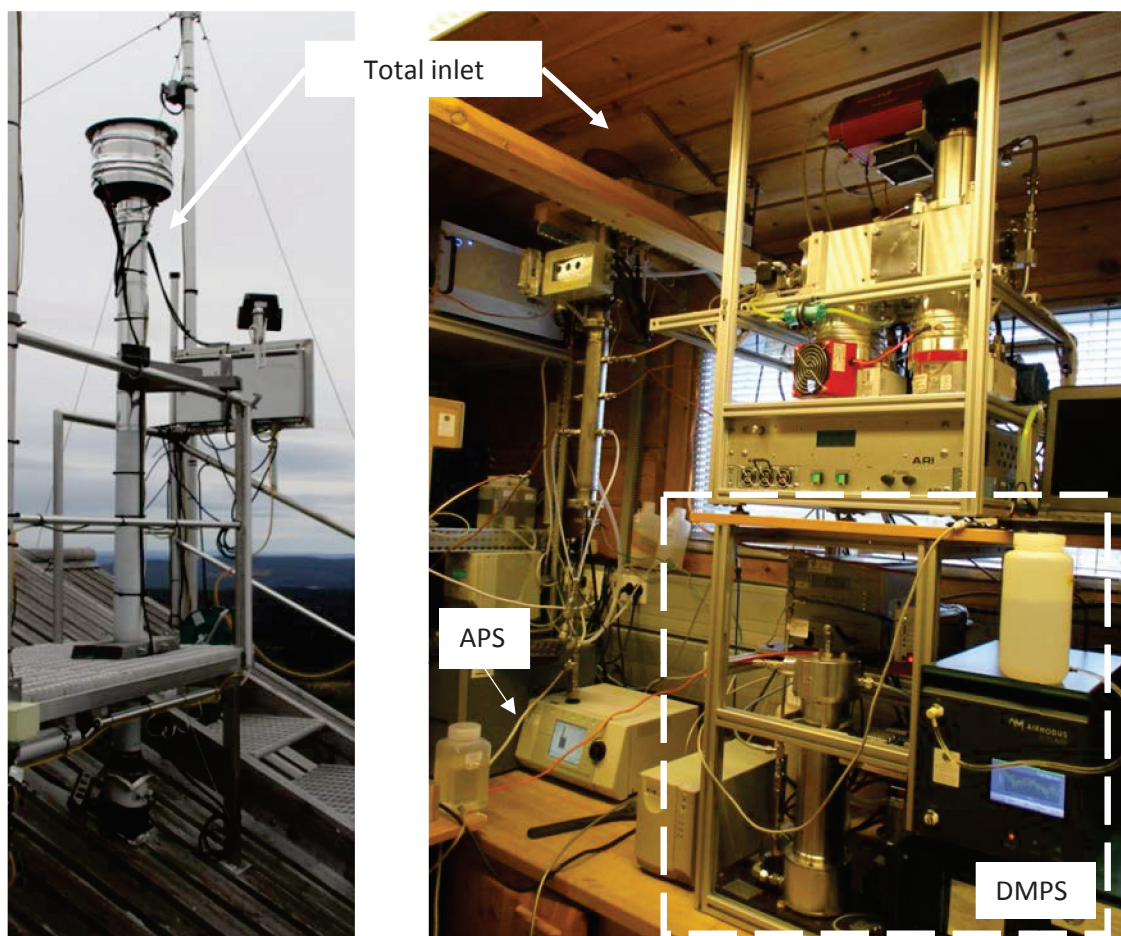


Figure 2.42: DMPS and APS instruments with the total inlet at Pallas-Sammaltunturi station.

The volume of PM1 aerosol particles per m³ air per day V_{day} was calculated by summing the volume V_{PM1} of all particles with a diameter below 1 μm , assuming spherical particles over 24 h, corresponding to the time of aerosol sampling:

$$V_{\text{day}} = \sum_{t_{0:00}}^{t_{24:00}} V_{\text{PM1},t_i} \quad (2.6)$$

$$\text{with } V_{\text{PM1},t_i} = \sum_{D_{\text{p,dry},7 \text{ nm}}}^{D_{\text{p,dry},1 \mu\text{m}}} V_{D_{\text{p,dry},i,t_i}} = \sum_{D_{\text{p,dry},7 \text{ nm}}}^{D_{\text{p,dry},1 \mu\text{m}}} \left(\frac{4}{3} \pi \left(\frac{D_{\text{p,dry},i}}{2} \right)^3 * N_{D_{\text{p,dry},i,t_i}} \right) \quad (2.7)$$

where $V_{D_{\text{p,dry},i,t_i}}$ is the total volume of all dry particles having a diameter i (i ranging from 7 nm to 1 μm), $N_{D_{\text{p,dry},i,t_i}}$ is the number of particles at diameter $D_{\text{p,dry},i}$ at the time t_i obtained from the DMPS and APS data.

The PM1 volume of aerosol particles collected on the filters was obtained from the size distributions of PM0.5 measured with the differential mobility particle sizers (DMPS) connected to the inlet preventing the sampling of cloud droplets, multiplied by a proportional factor obtained from the PM1 aerosol particles volume measured in the absence of cloud by the other DMPS and the Aerodynamic Particle Sizer (APS) combined, connected to the total inlet. The correlation coefficient between the volume $V_{\text{PM0.5}}$ given by the first DMPS and the volume V_{PM1} obtained from the second DMPS and the APS with the total inlet was $R^2 = 0.97$ (for data during no-cloud periods over the 7 months of aerosol sampling) making this extrapolation reliable. This method ensured that the PM1 volume, V_{PM1} , did not include any activated particles.

2.8.5. Calculation of theoretical number of activated particles

To illustrate the importance of surfactants evidenced in this work for the Pallas-Sammaltunturi campaign (Chapter 4), the theoretical number of activated particles, CCN numbers, was calculated for various ratios $C_{\text{surf},p}/\text{CMC}$ and average conditions at the Pallas-Sammaltunturi site during the campaign. Three scenarios were considered: $\sigma = \sigma_w$, as currently assumed in all cloud models, and σ corresponding to surface tension curves with $C_{\text{surf},p}/\text{CMC} = 100$ and 3000, covering the variability found in this work for aerosol surfactants (Chapter 4, Figure 4.5).

CCN number concentrations in the PM1 population at the site were obtained for different values of the saturation, S (%), by summing the number of particles exceeding the critical size in this population. For this, the critical saturation and critical diameter were first calculated for each size bin in the population, using the original Köhler equation:

$$S(\%) = 100 * \left(a_w \times \exp^{\frac{4 \sigma_{sol} M_w}{D_p \rho_w R T}} \right) \quad (2.8)$$

$$\text{where } a_w = \frac{\frac{1000}{M_w}}{\frac{1000}{M_w} + C_{osm}} \quad [Kiss, 2004] \quad . \quad (2.9)$$

In this equation, D_p (m) is the diameter of the particle, thus the main variable, σ_{sol} (N m^{-1}) is the surface tension of the droplet evolving with D_p , while T the temperature (277 K, corresponding to the average temperature at the Pallas-Sammaltunturi site over the 7-months campaign), R the gas constant, M_w the molecular mass of water ($0.018 \text{ kg mol}^{-1}$), and ρ_w the density of water (1000 kg m^{-3}), are constant.

The two ratios $C_{surf,p}/CMC$ studied in these calculations corresponded to two different surface tension curves for the surfactants in the particles. For each value of D_p and corresponding value of $C_{surf,w}$, the surface tension of the particle, σ_{sol} , was obtained from these surface tension curves and used in the Köhler equation.

For the Raoult's term, a_w , depending on the bulk composition of the particles, an average composition of 50 % $(\text{NH}_4)_2\text{SO}_4$ and 50 % organics, the latter represented by succinic acid, was assumed, according to a recent Aerosol Mass Spectrometer analysis of the PM1 aerosol particles at the site [Jaatinen, 2014]. For each value of D_p (m), corresponding to a different concentration of the mixture $(\text{NH}_4)_2\text{SO}_4$ /organics, the Raoult's term was calculated from the osmotic pressure, C_{osm} (kg^{-1}), the latter being calculated as the combination of the osmotic pressures of both components, the variations of each of them with concentration being taken from [Ekström, 2009]:

$$C_{\text{osm}} = \frac{C_{\text{osm,succinic acid}} + C_{\text{osm,(NH}_4)_2\text{SO}_4}}{2} \quad (2.10)$$

$$\text{where, } \begin{cases} C_{\text{osm,succinic acid}} = (1018.1 C + 9.8) * 10^{-3} \text{ kg}^{-1} \\ C_{\text{osm,(NH}_4)_2\text{SO}_4} = (1946 C + 15.3) * 10^{-3} \text{ kg}^{-1} \end{cases} \quad (2.11)$$

$$\text{with } C = \frac{\rho_{\text{p,dry}} * V_{\text{p,dry}}}{M_{\text{p,dry}} * V_{\text{sol}}} \text{ and } \begin{cases} V_{\text{p,dry}} = \frac{4}{3} \pi \left(\frac{D_{\text{p,dry}}}{2} \right)^3 \\ V_{\text{sol}} = \frac{4}{3} \pi \left(\frac{D_{\text{p}}}{2} \right)^3 \end{cases} \quad (2.12)$$

where $M_{\text{p,dry}} = 0.118 \text{ kg mol}^{-1}$ and $\rho_{\text{p,dry}} = 1572 \text{ kg m}^{-3}$ for the succinic acid and $M_{\text{p,dry}} = 0.132 \text{ kg mol}^{-1}$ and $\rho_{\text{p,dry}} = 1770 \text{ kg m}^{-3}$ for $(\text{NH}_4)_2\text{SO}_4$.

The determination of the critical saturation S_c was graphical (Figure 2.43). The critical saturation at a given particle size corresponds to the maximum of its Köhler curve. If the ambient saturation S_c exceeds the critical saturation for this size of particles, for a same composition, every particle at this size and above activates and grows into a cloud droplet.

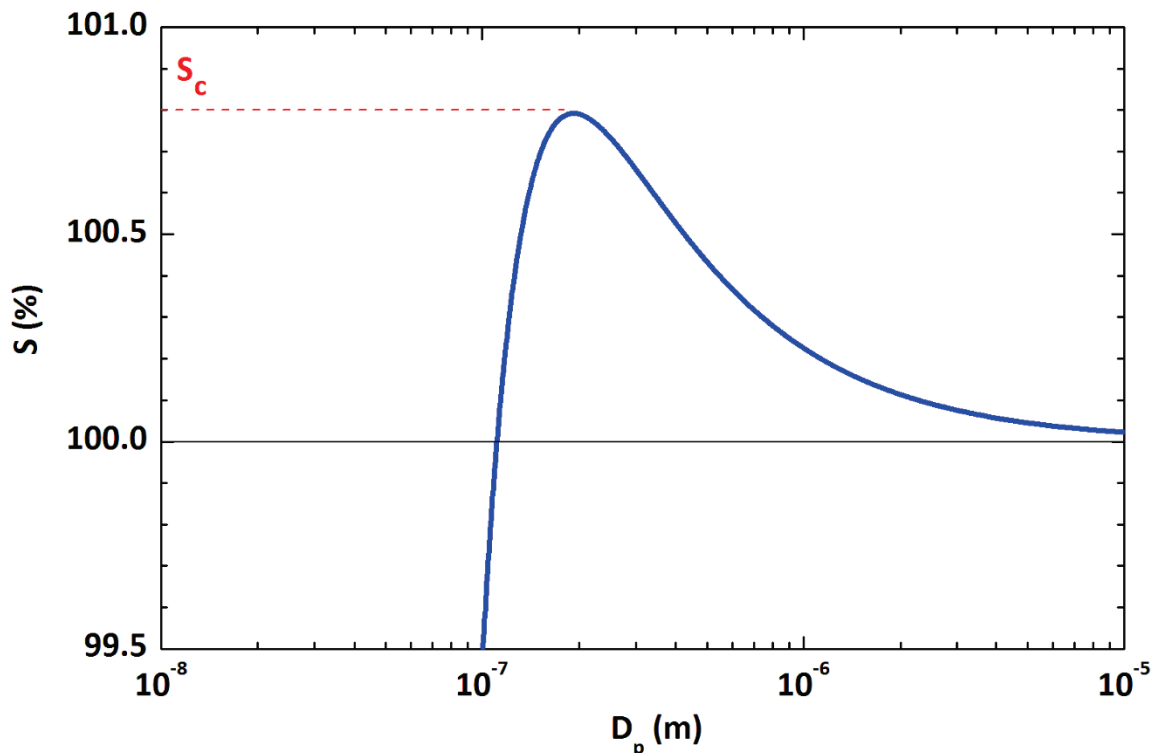


Figure 2.43: Example of determination of critical saturation S_c from Köhler curve calculated as explained in Section 2.8.5, for a dry particle with a diameter $D_{\text{p,dry}} = 43 \text{ nm}$ and with $\sigma = \sigma_w = 72.8 \text{ mN m}^{-1}$. The critical saturation S_c corresponds to the maximum of the Köhler curve. For this example, at $S = S_c = 100.8 \%$ and for a same composition, all particles with a diameter $D_{\text{p,dry}} \geq 43 \text{ nm}$ are activated.

The ratio of activated particles CCN over the number of initial particles CN was determined for each value of S (%). The number of particles was determined from the average size distribution over the 7-months campaign at Pallas-Sammaltunturi (Figure 2.44).

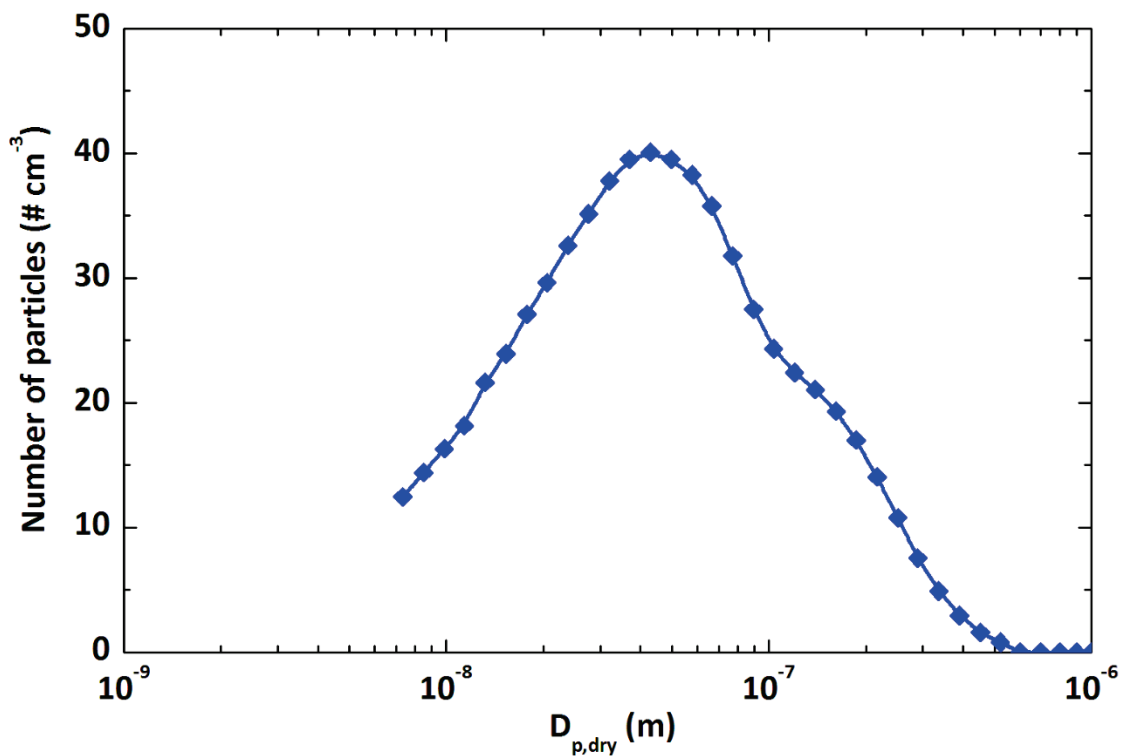


Figure 2.44: Average size distribution of PM1 determined from DMPS and APS data at Pallas-Sammaltunturi station (Section 2.8.4.2) over the 7-months campaign (Avril-November 2015).

All the experimental methods detailed in the Chapter 2 were applied to the samples of the studies developed in the next Chapters (3, 4, 5 and 6).

3. First study: Absolute concentrations and surface tension curves of surfactants in aerosols at a coastal site in Sweden

This chapter focuses on the application of the developed methods for the extraction and analysis of surfactants from environmental aerosols collected on filters. This study allowed us to investigate the potential implication of surfactants for cloud droplet formation, by determining the absolute concentrations of surfactants in aerosols and their absolute surface tension curves.

The results presented in this chapter constituted the first part of this PhD work and were published in part in [Gérard, 2016].

3.1. Objectives and method

Prior to the study on the surfactant properties in atmospheric aerosols, an important part of this work was the development of a method to extract and to analyze the surfactants from atmospheric aerosols for a better characterization of surfactants. For more clarity, this development is detailed in the Experimental Section (Chapter 2) but the main points will be reminded.

In order to determine the surfactant properties in atmospheric aerosols, which could influence the cloud droplet formation, the developed method was applied to PM_{2.5} aerosol collected at the coastal marine research station of Askö, Sweden (Section 2.1.2.1). This site was chosen in particular because it is influenced by biogenic emissions from the sea. Indeed the interest of collecting the aerosols at this site was also to investigate the potential origin of surfactants by comparing their concentrations found in aerosols to biological markers at the site (this part of the study will be described in Section 6.2.3). The PM_{2.5} aerosols were collected from July to October 2010 (Section 2.1.2.1) resulting in 11 samples, listed in Table 3.1.

3.2. Results and discussion

3.2.1. Development of a method for the extraction and analysis of surfactants in aerosols

The development of a method for the extraction and analysis of surfactants in aerosols was an important part of this work. This included the improvement of the extraction of surfactants from atmospheric aerosols and the determination of their absolute surfactant concentrations in order to determine absolute surface tension curves.

These methods have been fully detailed in the Experimental Section (Chapter 2). Briefly, the aerosols were collected on quartz filters (Section 2.1). Then, the total surfactant fraction was extracted with a double extraction method: a water extraction followed by a Solid-Phase Extraction (SPE) removing interferences and concentrating the surfactants (Section 2.2). The surface tension curves of the aerosol surfactants were determined with the pendant drop technique (Section 2.3) and the absolute surfactant concentrations were measured by colorimetric methods (Section 2.4).

The main points of the development were the following:

- the **double extraction** method recently developed [Ekström, 2010; Baduel, 2012] was improved by **replacing the second extraction by SPE** (Solid-Phase Extraction). This provided a better reproducibility and extraction efficiency;
- the **colorimetric methods** to determine the surfactant concentration in aerosols were **improved** by introducing a method to determine the concentration of non-ionic surfactants in addition to the ionic surfactants and by studying the potential effect of interferences. This allowed us to obtain the **absolute total concentration of surfactants in aerosols** including anionic, cationic and non-ionic surfactants. Indeed, to our knowledge, it was the first time that the absolute concentration of non-ionic surfactants in aerosol was determined. This measurement was challenging because the calibration curves used to determine their absolute concentrations had a different

slope according to the structure of the non-ionic surfactant. So it was decided to consider the largest slope to avoid the overestimation of the surfactant concentration;

- the **study of potential interferences** on the colorimetric methods showed that a simple extraction in water could bias the measurements, whereas **the double extraction** developed in this work **allowed the interferences to be removed** providing more reliable results than previous studies (*e.g.* [Latif, 2004; Roslan, 2010; Jaafar, 2014; Mustaffa, 2014]) which used a simple extraction of surfactants in water;
- combining the improved extraction and colorimetric methods allowed us to obtain **for the first time absolute surface tension curves** for surfactants in atmospheric aerosols.

3.2.2. Atmospheric surfactant concentrations

The first application of the method was the determination of the absolute surfactant concentrations in the aerosol extracts. The surfactant concentrations in aerosol particles volume, $C_{\text{surf,p}}$, and in air, $C_{\text{surf,a}}$, obtained for the 11 atmospheric samples, are shown in Figure 3.1.

The surfactant concentrations, $C_{\text{surf,p}}$ and $C_{\text{surf,a}}$, varied between 27 (± 6) and 143 (± 29) mM and 104 (± 21) and 785 (± 157) pmol m⁻³, respectively, and, as discussed in the Experimental Section 2.4.2.5, were potentially underestimated by 33 %. The concentrations in volume of air $C_{\text{surf,a}}$ reported in this work are consistent with those reported for PM2.5 aerosols from the Middle Adriatic using a relative method (224 - 496 pmol m⁻³) [Frka, 2012] and with the anionic and cationic surfactant concentrations measured in aerosols from rural and semi urban locations with similar colorimetric methods (1 - 1000 pmol m⁻³) [Latif, 2004; Roslan, 2010; Jaafar, 2014; Mustaffa, 2014].

As shown in Figure 3.1, in the Askö aerosols, the total surfactant fraction was dominated by anionic and non-ionic compounds, while cationic surfactants were in very small concentration and below the detection limit (0.06 μM) in a number of samples. However, as explained in the Experimental Section 2.4.2.4, the concentrations for non-ionic surfactants could be underestimated by up to a factor of 2, and these compounds could thus have been even more abundant in the samples than suggested by Figure 3.1.

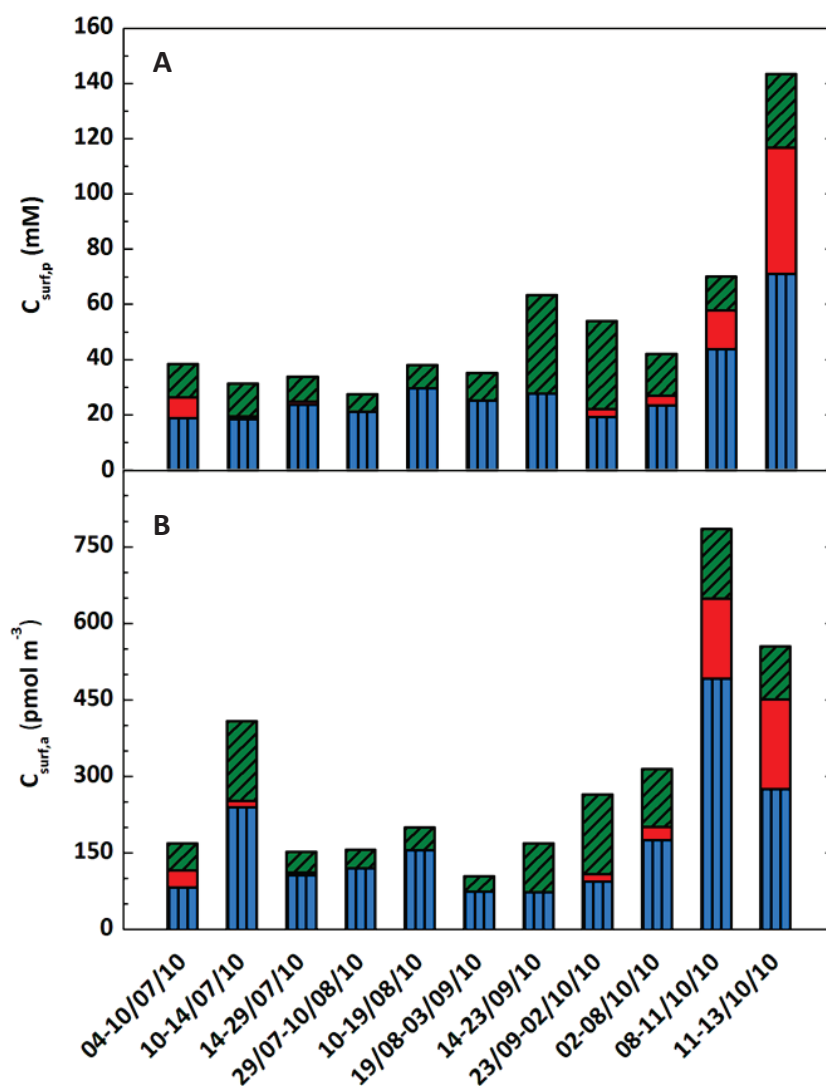


Figure 3.1: Concentration of anionic (blue and vertical lines), cationic (red), and non-ionic (green and diagonal lines) surfactants in the aerosols sampled at Askö, Sweden, from July to October 2010: (A) in the aerosol particles volume and (B) in sampled air. Concentrations not shown (in particular for cationic surfactants) are under the detection limit. (reproduced with permission from [Gérard, 2016] © Copyright 2016 American Chemical Society)

Figure 3.1 also shows that the relative abundance of anionic, cationic, and non-ionic surfactants in the aerosols remained relatively constant from July to October (60, 8, and 32 %, on average, respectively, with only 10 - 15 % of variability). This suggested that the sources for these surfactants remained the same throughout the sampling period. However, no significant correlations were found between the different classes of surfactants, suggesting that anionic, cationic, and non-ionic surfactants had distinct sources. The main variability observed between the samples from July to October was in the total surfactant

concentrations. This suggested that the surfactant sources varied mostly in intensity, rather than in composition, over the sampling period.

3.2.3. Absolute surface tension curves and CMC values

Combining the measurement of surfactant concentrations and surface tension curves, we obtained for the first time absolute surface tension curves (Figure 3.2).

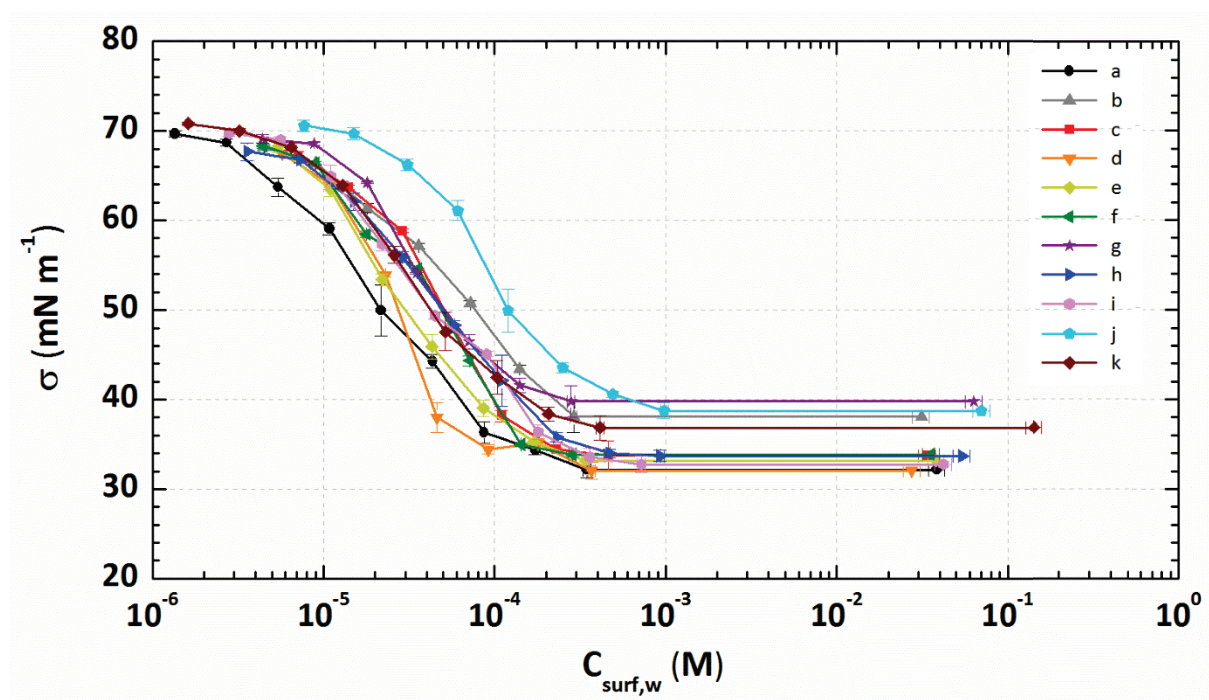


Figure 3.2: Absolute surface tension curves for the surfactant fractions of the 11 aerosol samples collected in Askö, Sweden. See the sample list in Table 3.1. (reproduced with permission from [Gérard, 2016] © Copyright 2016 American Chemical Society)

These absolute surface tension curves showed the presence of strong surfactants in all the aerosols sampled, with surface tension values of $\sigma_{min} = 32 - 40 \text{ mN m}^{-1}$. These values were consistent with the surface tensions reported for aerosols from other regions, using a similar method [Ekström, 2010; Baduel, 2012]. The surface tension values for aerosol and fog water samples reported previously by other groups were, however, significantly larger (usually $\geq 50 \text{ mN m}^{-1}$) [Capel, 1990; Facchini, 1999; Mircea, 2005; Salma, 2006; Taraniuk, 2007] and did not display any lower plateau, indicating that the minimum surface tension was not reached. This indicated that the surfactants were not concentrated enough in the samples and underlines the importance of using a targeted extraction for this type of investigation.

For each sample, the CMC values and $C_{\text{surf,p}}/\text{CMC}$ ratio (Table 3.1) were also determined from the absolute surface tension curves, which, to our knowledge, is the first time for aerosol surfactants. In previous works, surface tension was only related to the total organic fraction in aerosols or fog water because the compounds responsible for the surface tension effect were not isolated [Capel, 1990; Facchini, 1999; Mircea, 2005].

Table 3.1: List of aerosol samples, CMC (μM) values determined in this work from Askö field campaign and ratios to the aerosol surfactant concentration ($C_{\text{surf,p}}$ in μM) (adapted with permission from [Gérard, 2016] © Copyright 2016 American Chemical Society).

Sample label	Sample dates	CMC (μM)	$C_{\text{surf,p}}/\text{CMC}$
a	04–10/07/10	96 ± 19	417
b	10–14/07/10	245 ± 69	139
c	14–29/07/10	129 ± 26	279
d	29/07–10/08/10	49 ± 10	580
e	10–19/08/10	118 ± 24	338
f	19/08–03/09/10	139 ± 28	268
g	14–23/09/10	95 ± 20	694
h	23/09–02/10/10	210 ± 42	268
i	02–08/10/10	212 ± 42	207
j	08–11/10/10	232 ± 46	315
k	11–13/10/10	134 ± 27	1117

Figure 3.2 and Table 3.1 provided also valuable information on a possible biological origin of surfactant. This aspect will be discussed in Chapter 6 (Section 6.2.1).

3.2.4. Implications for particle activation

The quantitative results obtained for aerosol surfactants in this work bring some unique information for the prediction of cloud droplet activation, which cannot be obtained by other techniques. During activation, an aerosol particle typically undergoes a radius increase between 3 and 10 (ratios of critical radius over dry radius), which is true both for inorganic salt particles [McFiggans, 2006] and for mixed organic-inorganic particles such as secondary organic aerosols [McFiggans, 2006]. This corresponds to a volume increase by a factor of 27 to 1000. The surface tension curves determined in this work show that lowering the surfactant concentrations by these factors still leads to low surface tension values, typically below 50 mN m^{-1} (Figure 3.3).

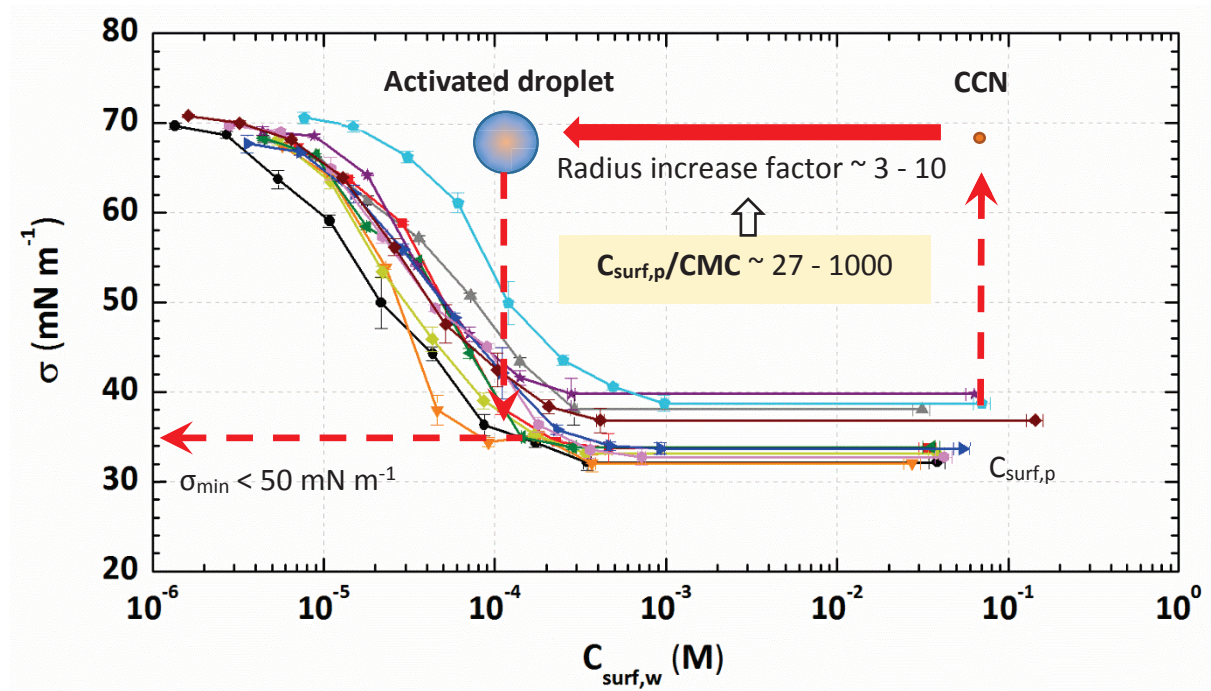


Figure 3.3: Schematic representation of the importance of $C_{surf,p}/CMC$ in particle activation, based on the absolute surface tension curves determined at Askö station. The average $C_{surf,p}/CMC$ being at 27 - 1000 means that the CCN particle can take water and grow by about a factor of 3 - 10 in radius, while keeping a low surface tension ($< 50 \text{ mN m}^{-1}$).

These results thus show that surfactant concentrations in atmospheric aerosols are large enough to maintain the surface tension of growing droplets very low ($\leq 50 \text{ mN m}^{-1}$) until activation and that the $C_{surf,p}/CMC$ ratio is a critical parameter. This conclusion is reinforced by the fact that the concentrations determined in this work are likely to be underestimated and that the surfactants might not have been present in all the aerosol particles collected but only in some of them, where they would have been at even larger concentrations. Lowering the surface tension of growing droplets to 50 mN m^{-1} or less until activation is, in turn, expected to have substantial effects on the activation efficiency of aerosol particles. For instance, using surface tension values of about 50 mN m^{-1} was shown previously to predict 30 - 50 % larger CCN numbers in various regions of the atmosphere [Irwin, 2010].

Another implication of these results is that the surface tension of forming droplets would vary little or not at all with surfactant concentration during activation. This is because, as shown by the ratios $C_{surf,p}/CMC$ in Table 3.1, a particle volume increase by a factor of 27 to 1000 at activation, corresponds to a surfactant concentration of the order of, or slightly larger than, the CMC. In nearly all of the samples studied, the particles can undergo a volume

increase by at least a factor of 200 until activation (*i.e.*, a radius increase by at least a factor of 6) without any significant change on their surface tension. Such a nearly constant and minimal surface tension in growing droplets is in contradiction with the Szyszkowski equation, [Sorjamaa, 2004; Prisle, 2008; Farmer, 2015] which is used in nearly all models for cloud droplet activation and assumes a decrease of σ with the log of surfactant concentration. Using this equation is thus likely to significantly underestimate the effects of aerosol surfactants on cloud droplet formation.

3.3. Conclusion

In conclusion, **for the first time, absolute surface tension curves were determined using an improved method** providing absolute concentrations thanks to an extraction method which removes the interferent and the use of colorimetric methods providing absolute total surfactant concentrations. They showed that **surfactants are concentrated enough in atmospheric aerosols to keep the surface tension of growing droplets very low until activation, which should enhance the cloud-forming efficiency**. This ability is reflected by the $C_{\text{surf,p}}/\text{CMC}$ ratio, which is a critical parameter (this statement is reinforced by the study in Chapter 4). The results also show that the surface tension of growing droplets remains nearly constant and close to its minimum during activation, and thus does not follow the Szyszkowski equation. Models using this equation are thus expected to significantly underestimate the role of surfactants on cloud droplet formation. All of these conclusions are reinforced by the fact that the concentrations reported in this work might be underestimated by about 30 % and that the surfactants might have been present in only a fraction of the collected particles, in which their concentration would have been much larger than reported here.

This study was also used to investigate the origin of surfactants in Chapter 6 (Section 6.2.1 and 6.2.3).

This work was pursued (Chapter 4) by the application of the developed method on smaller aerosol size fractions (PM₁), which are more critical for CCN numbers, to investigate the role of surfactants in cloud formation directly from atmospheric observations.

4. Second study: Atmospheric evidence for the role of aerosol surfactants in cloud formation at a boreal site in northern Finland

This chapter follows the study of Chapter 3 but goes further: it focuses on the investigation of direct proofs in atmosphere of the role of surfactants in cloud formation.

The results presented in this chapter have been submitted for publication [G erard, 2016 under review].

4.1. Objectives and method

In the previous study (Chapter 3), we showed that the properties and concentrations of surfactants found in atmospheric aerosols should enhance cloud formation but no real link with cloud events was shown.

The purpose of this study was to **obtain direct proofs in atmosphere of the role of surfactants in cloud formation**. For this, we investigated the relationship between surfactants and clouds by a statistical analysis based on the surfactant properties and concentrations over several months' field campaign in a site frequently impacted by cloud events.

The boreal Pallas-Sammaltunturi station (Section 2.1.2.3) was chosen for this study because this station is frequently inside clouds [Komppula, 2005] and because CCN numbers at this site have been previously underestimated by models [Jaatinen, 2014] suggesting the contribution of other effects than those commonly taken into account in modeling of cloud formation, such as those of surfactants. The measurements were performed continuously over a 7-months campaign (April - November 2015) to have enough data and cloud events for statistical analysis (Figure 4.1, with the example of the surfactant concentration in air $C_{\text{surf,a}}$). A collection of 230 PM1 aerosol samples (24 h-sampling) corresponding to 72 cloud events were obtained. PM1 aerosols were collected instead of PM2.5 (as the previous study in Section 3) since the aerosol composition (so their potential effect on the surface tension σ) is

4. Second study: Atmospheric evidence for the role of aerosol surfactants in cloud formation at a boreal site in northern Finland

more critical for submicron particles. As explained further, the **collected aerosols** were interstitial but **representative of CCNs**. The analysis were not performed for all samples, being very time- and sample-consuming. Thus the surfactant concentrations were analyzed for about 150 of them covering the entire campaign and the surfactant properties were determined on a sub-set of 35 samples but included 5 - 6 samples per month of the campaign on average and covered the entire range of % cloud time. Clouds events were monitored by recording visibility (Section 2.8.3), a quantity shown previously to be a reliable proxy for the CCN efficiency of the PM1 population at the site [Kivekäs, 2009].

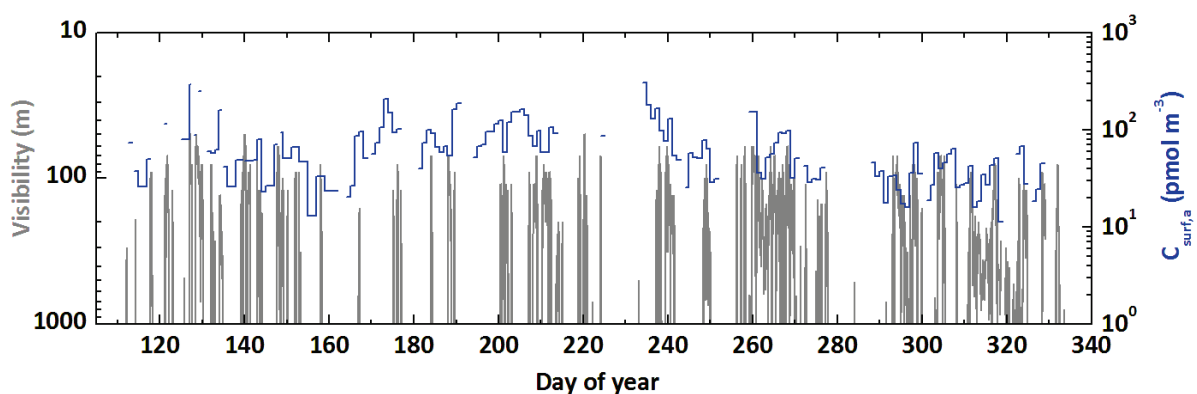


Figure 4.1: Overview of the period of sampling at Pallas-Sammaltunturi (April - November 2015): cloud events determined from visibility < 1000 m (grey lines) and measured concentration of surfactants in air $C_{surf,a}$ (blue line) over 24-h sampling in the 150 analyzed samples.

The experimental details concerning the extraction and analysis of surfactants are detailed in the Experimental Section (Chapter 2): the aerosol sampling in Section 2.1.2.3, the extraction of surfactants in Section 2.2.2, the surface tension measurements in Section 2.3.2, the determination of surfactant concentration in Section 2.4.2, the volume of aerosol particles in Section 2.8.4.2, and the CCN efficiency calculations in Section 2.8.5.

For the study, we compared the concentrations and properties of surfactants in aerosols, representative from CCNs, with cloud events by introducing a new variable: “% cloud time”. This variable was determined over the same timescale than the aerosol samples and calculated by summing up the total cloud duration (determined from visibility data, Section 2.8.3) over the 24 h-sampling and dividing it by 24 h. Thus the “% cloud time” took into account both the frequency and duration of the clouds. Moreover from the results we calculated the impact of CCN efficiency in this site, *i.e.* the fraction of particles that activate into cloud droplets at a given supersaturation.

4.2. Results and discussion

4.2.1. Correlation between cloud occurrence and surfactant concentrations

The first result obtained in this work was that cloud occurrence at the site, quantified as “% cloud time”, increased proportionally with surfactant concentration in the aerosol particles volume $C_{\text{surf,p}}$ (mM) (Figure 4.2 (A)).

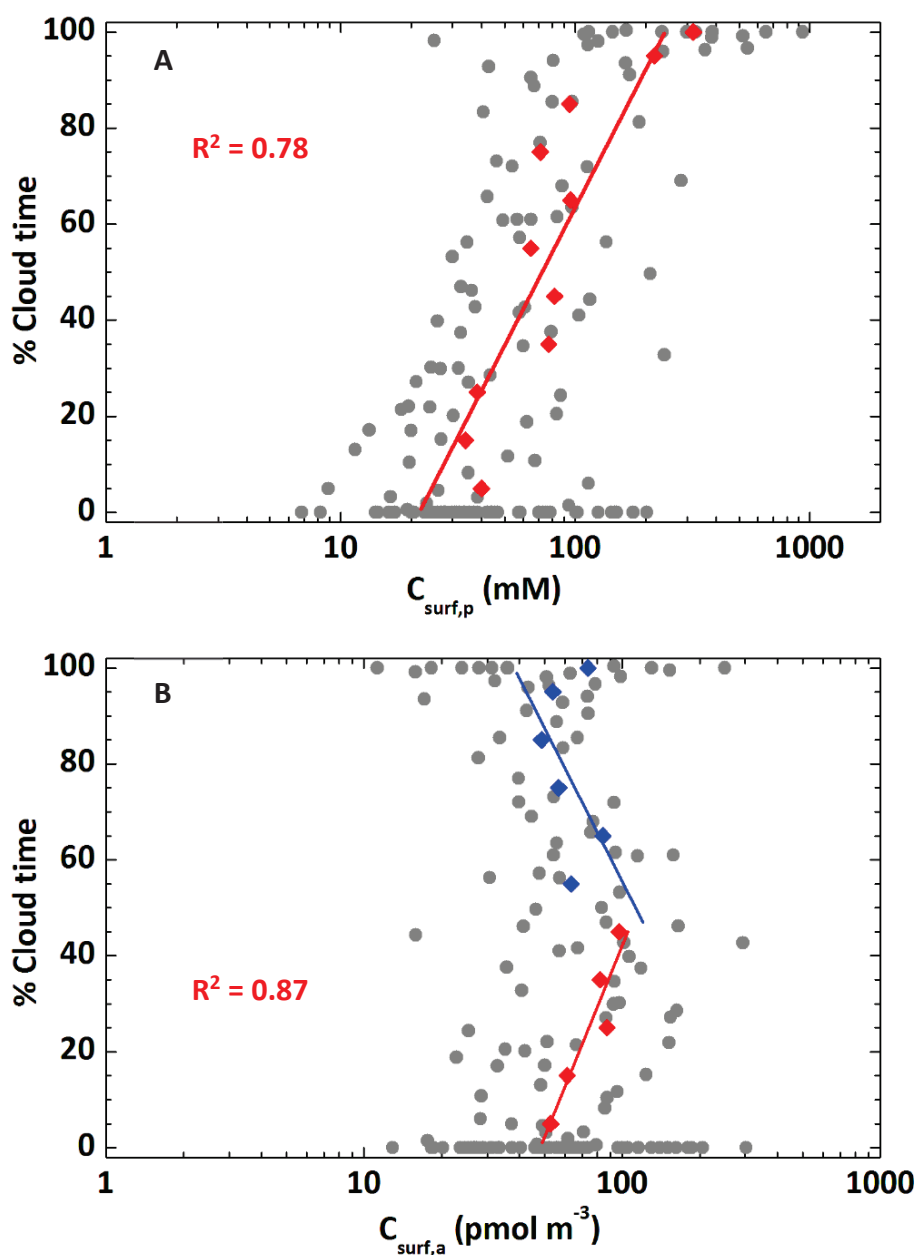


Figure 4.2: Correlations between surfactant concentrations in PM1 aerosols with % cloud time for all the aerosol samples analyzed in this work over the 7-months campaign: (A) $C_{\text{surf,p}}$ in aerosol particles volume (mM) and (B) $C_{\text{surf,a}}$ in air (pmol m^{-3}). The grey points are the original data, and the red and blue ones are the averaged data over 10% - increments in % cloud time [Gérard, 2016 under review].

The trend is clear in Figure 4.2 (A) in spite of the scatter in the data, and the average $C_{\text{surf,p}}$ values over 10 % increments in % cloud time resulted in a large correlation coefficient ($R^2 \sim 0.8$). This provided the first indication that surfactants might play a role in cloud formation at the site. The scatter in the data was attributed to the contribution of additional parameters beside surfactant effects to the observed cloud events, such as meteorological parameters (*i.e.* temperature, relative humidity, etc.) or other CCN properties (hygroscopicity). The samples for which % cloud time was equal to 0 or 100 % were more widely scattered around the regression line, which was attributed to cloud events where these other parameters were probably the main controlling factors. But, despite these larger scatters, the average values were in reasonable agreement with the regression line.

Figure 4.2 also shows that, even for the samples with % cloud time = 0, $C_{\text{surf,p}}$ was above the detection limit in surfactant concentrations, indicating the presence of surfactants in the PM1 aerosols even in the absence of cloud event (“background surfactants”).

The next result obtained in this work was that the surfactants concentrations and their variations were identical in the interstitial and activated particles during the cloud events. This was shown by correlating the surfactant concentrations in air volume, $C_{\text{surf,a}}$ (pmol m^{-3}), with % cloud time (Figure 4.2 (B)), instead of $C_{\text{surf,p}}$. $C_{\text{surf,a}}$ (pmol m^{-3}) also increased with % cloud time for low values of this variable, but decreased beyond about 50 % cloud time. This decrease resulted from the activation, thus apparent removal, of the surfactant-containing particles from the interstitial PM1 aerosol during the cloud events. This was demonstrated by the decrease of PM1 volume, V_{PM1} on filters, observed in real-time during nearly all cloud events (Figure 4.3 and Figure 8.2 in Appendix Section 8.5 and discussion in next paragraph). The fact that dividing $C_{\text{surf,a}}$ by V_{PM1} to obtain $C_{\text{surf,p}}$ compensated for the removal of surfactants at large % cloud time and resulted in the continuous increase shown in Figure 4.2 (A). This implied that the amount of surfactants removed by activation was proportional to the volume of the particles, thus that these compounds were homogeneously distributed between the interstitial and activated particles. This, in turn, implied that their particulate-phase concentrations were equal in the interstitial and activated particles.

4.2.2. Real-time evolution of surfactant concentration and visibility

The variations of $C_{\text{surf},a}$ (pmol m^{-3}) and $C_{\text{surf},p}$ (mM) were further investigated in the time-dependent profiles (Figure 4.3 and Figure 8.2 in Appendix Section 8.5).

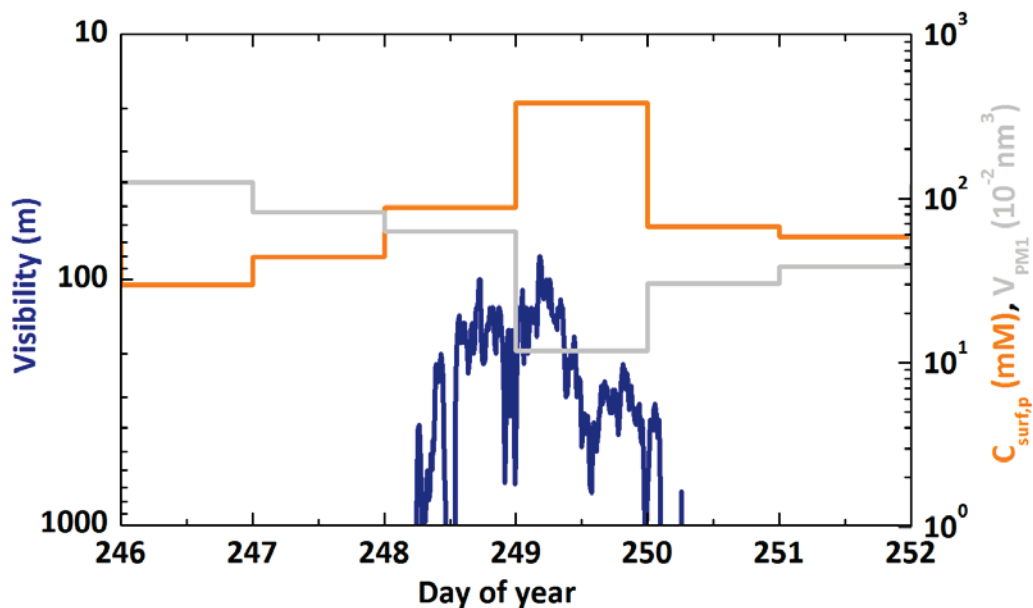


Figure 4.3: Example of real-time evolution of the visibility (m) (blue line), the surfactant concentration in aerosol particles volume $C_{\text{surf},p}$ (mM) (orange line) and the PM1 volume on filters V_{PM1} (10^{-2} nm^3) (grey line) during the cloud event of days 246 - 252 [Gérard, 2016 under review].

In nearly all the observed cloud events (67 out of 72), these concentrations increased around the time of cloud formation. In most of these events, 39 out of 72, the time-profiles clearly showed that both concentrations had increased before cloud formation itself, and independently of the variations of V_{PM1} . For 28 other events, $C_{\text{surf},a}$ (pmol m^{-3}) and $C_{\text{surf},p}$ (mM) also increased at the beginning of the event, but the sampling resolution prevented to determine if this had happened before or during the cloud event. Only in 5 out of 72 events no increase of surfactant concentration was observed connected to the cloud event, suggesting that cloud formation was controlled by other parameters than surfactants. Thus, in most of the observed events, the increase in surfactant concentration with % cloud time displayed in Figure 4.2 (A) had occurred before cloud formation itself, suggesting a cause-effect relationship.

4.2.3. Correlation between cloud occurrence and surfactant properties

It was shown in Section 4.2.1 and 4.2.2 that surfactant concentrations correlated strongly with cloud events and a cause-effect relationship was suggested. However, although these conditions are necessary if surfactants play a role in cloud formation, there were not sufficient to prove their role.

To determine if cloud occurrence increased specifically because of surfactants and not because of other parameters or compounds that correlated with them, the surfactants present in the PM1 samples were further analyzed. The average surface tension of the PM1 samples, σ_{dry} (mN m^{-1}), and the surface tension curves for the corresponding surfactants were investigated. The resulting surface tension curves are shown in Figure 4.4.

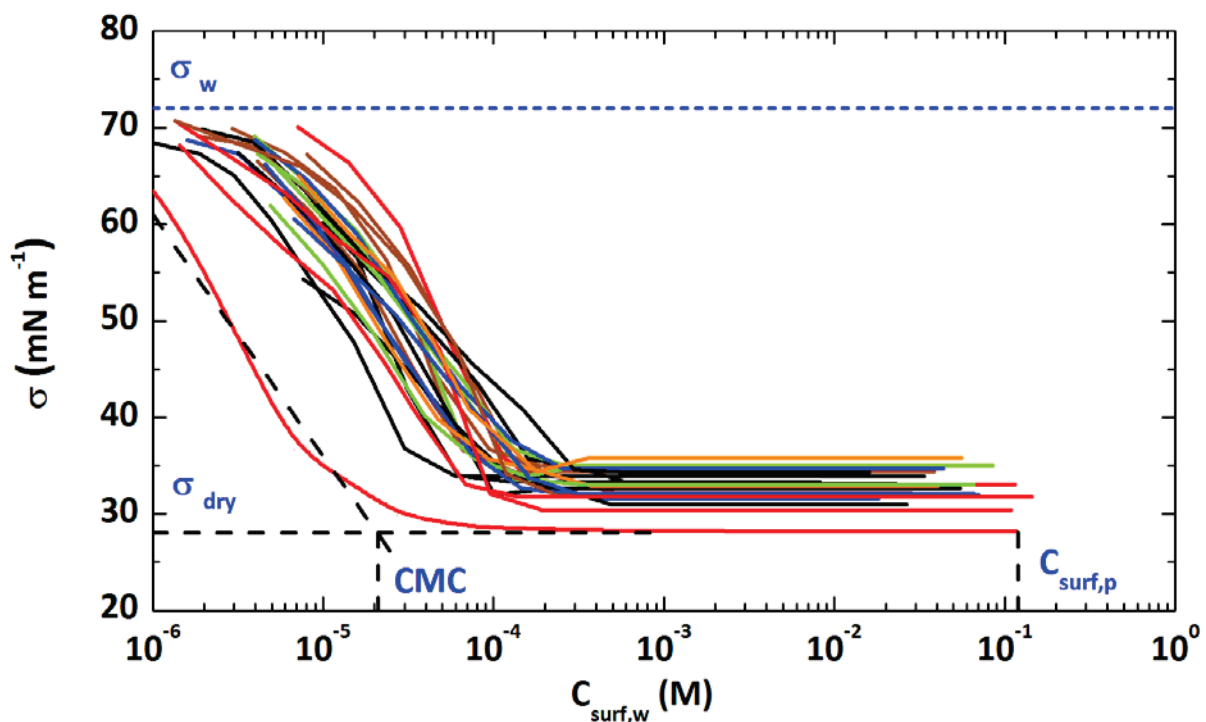


Figure 4.4: Absolute surface tension curves for the surfactants extracted from the 35 PM1 samples (including on average 5 to 6 samples per month of campaign and covering the entire range of % cloud time). Each color represents a range of % cloud time: black = 0 %; brown = 0 - 20 %; blue = 20 - 40 %; green = 40 - 60 %; orange = 60 - 90 %; red = 100 %. The blue dashed line represents the surface tension of pure water, and black dashed lines illustrate the graphical determination of the CMC. [Gérard, 2016 under review].

The end point of these curves represent the surfactant concentrations $C_{\text{surf,p}}$ (M) and surface tension of the dry aerosol samples σ_{dry} (mN m^{-1}), while the curves represent the evolution of the surface tension of the growing droplet, σ (mN m^{-1}), upon water uptake.

Figure 4.4 shows that σ (mN m^{-1}) did not vary much between samples, with an average value of $\sigma_{\text{dry}} = 33 (\pm 5) \text{ mN m}^{-1}$. Such a low surface tension was consistent with those measured for aerosols from other regions in previous works ([*Ekström, 2010; Baduel, 2012; Gérard, 2016*], Section 3.2.3) and confirmed that the surface tension of atmospheric CCNs is much lower than that of pure water ($\sigma_{\text{w}} = 72.8 \text{ mN m}^{-1}$), unlike what is systematically assumed in cloud models. However, the lack of variability of σ_{dry} between samples, thus with % cloud time, indicated that this parameter alone was not controlling cloud formation.

In contrast with σ_{dry} , $C_{\text{surf,p}}$ (M) and the CMC, the value of the surfactant concentrations at the beginning of the lowest plateau, varied each by about one order of magnitude between samples (Figure 4.2 (A) and Figure 4.5). The CMC is a characteristic of the air-water interface represented by the surface tension curves. It is thus as compound-specific as vapor pressure in phase diagrams, for instance, but much less affected by temperature and chemical composition [*Kang, 2001; Helvacı, 2004; Mohajeri, 2012*]. The CMC of a surfactant is important for cloud droplet formation as it determines the amount of water that a droplet can take up before its surface tension increases compared to σ_{dry} (the lower the CMC, the more water can be taken up while maintaining a low surface tension). Maintaining a low surface tension during droplet growth, in turn, controls whether this droplet can reach its critical size and be activated ([*Gérard, 2016*], Section 3.2.4). In this work, comparing the CMC of the surfactants in the PM1 samples with % cloud time (Figure 4.5 (A)) resulted in a very strong anti-correlation ($R^2 = 0.94$).

4. Second study: Atmospheric evidence for the role of aerosol surfactants in cloud formation at a boreal site in northern Finland

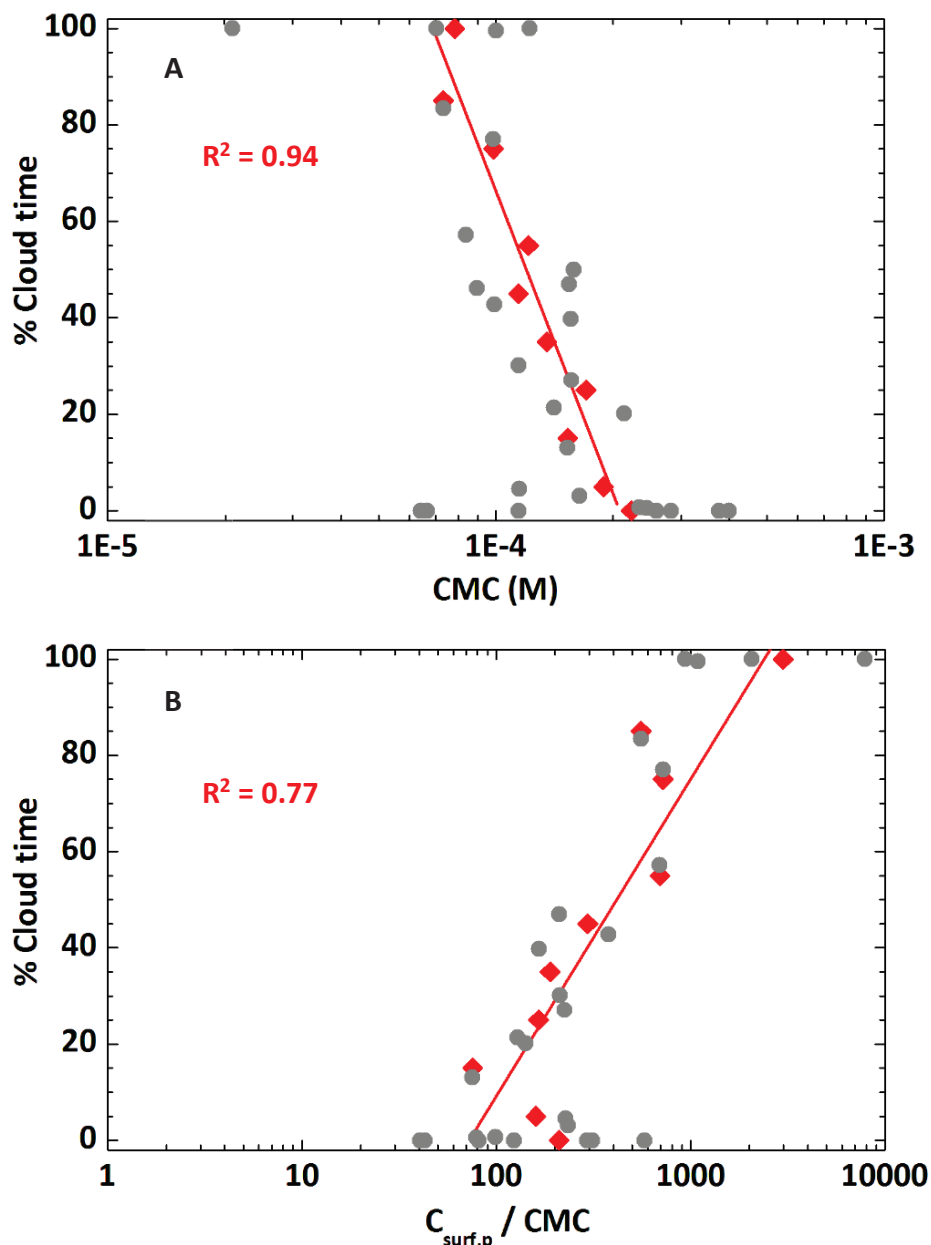


Figure 4.5: Correlations between (A) CMC values and (B) ratios $C_{surf,p}/CMC$ with % cloud time. Grey points are the original data and red ones are the averaged data over 10 % - increments in % cloud time [Gérard, 2016 under review].

As the CMC is an intrinsic property of surfactants, the correlation in Figure 4.5 (A) cannot be biased by parameters such as particle size, shape, chemical composition, or meteorological variables (water vapor, temperature, etc.) that might correlate with cloud events. Experimental biases can also be excluded as the CMC values have been obtained by absolute concentration measurements in the sample extracts, thus were not impacted by any field parameter that could be correlated with the cloud events (PM1 volume or number,

temperature, relative humidity, etc.). The strong correlation displayed in Figure 4.5 (A) is thus a solid evidence that cloud occurrence at the site increased specifically because of surfactants, and not because of other parameters or compounds correlated to them.

The order of magnitude of variability in the CMC values displayed in Figure 4.5 (A) reflected the presence of very different surfactants in the different samples. Thus, cloud occurrence at the site resulted not simply from an increase in concentration of the background surfactants, but rather from the influx of a new population of surfactants with low CMC values. The real-time PM₁ measurements did not display any significant increase in particle number concentration or volume before the cloud events, indicating that these new surfactants were internally mixed with the background ones. This was also consistent with the increase in total surfactant concentration, $C_{\text{surf,p}}$ (mM), in Figure 4.2 (A). Thus, both types of surfactants would be equally removed by activation during cloud events, resulting in the same average CMC values in the activated and interstitial particles. The CMC values reported in Figure 4.5 (A) were thus also those in activated particles, even though they were determined in interstitial ones.

As explained in Sections 3.2.3 and 3.2.4, the combined effect of $C_{\text{surf,p}}$ and CMC, *i.e.* the $C_{\text{surf,p}}/\text{CMC}$ ratio, gives the full range of water volume that a droplet can take up before its surface tension increases, thus directly affects CCN numbers. This ratio was plotted against % cloud time in Figure 4.5 (B), where, as with $C_{\text{surf,p}}$ and CMC, it represented both the activated and the interstitial particles. It can be seen in this figure that combining the factor 10 of variability in $C_{\text{surf,p}}$ and CMC resulted in about a factor 30 of variability in their ratio, which also displayed a strong correlation with % cloud time, confirming its importance for CCN numbers.

4.2.4. CCN efficiency calculation

The factor 30 of variability in the $C_{surf,p}/CMC$ ratio (Figure 4.5 (B)) meant that the presence of the new surfactants in the PM1 aerosol particles increased by a factor up to 30 the volume of water that these particles could take up before their surface tension increased. As this was expected to directly affect the CCN numbers at the site, the extreme values of the ratio obtained in Figure 4.5 (B) (~ 100 to 3000), together with typical conditions and PM1 distribution at the site [Jaatinen, 2014] were used to calculate CCN numbers using a simple Köhler model (see Experimental Section 2.8.5 for details). The results are presented in Figure 4.6.

Over the supersaturation range $S = 0 - 0.5\%$, the CCN numbers, corresponding to aerosol particles where the surfactants had a $C_{surf,p}/CMC$ ratio of 3000, were on average three times larger than those where this ratio was equal to 100, and nearly four times larger than when assuming $\sigma = \sigma_w$. These results clearly show that effects of surfactants on CCN numbers can be very significant, and underline the importance of taking them into account in CCN calculations and cloud models.

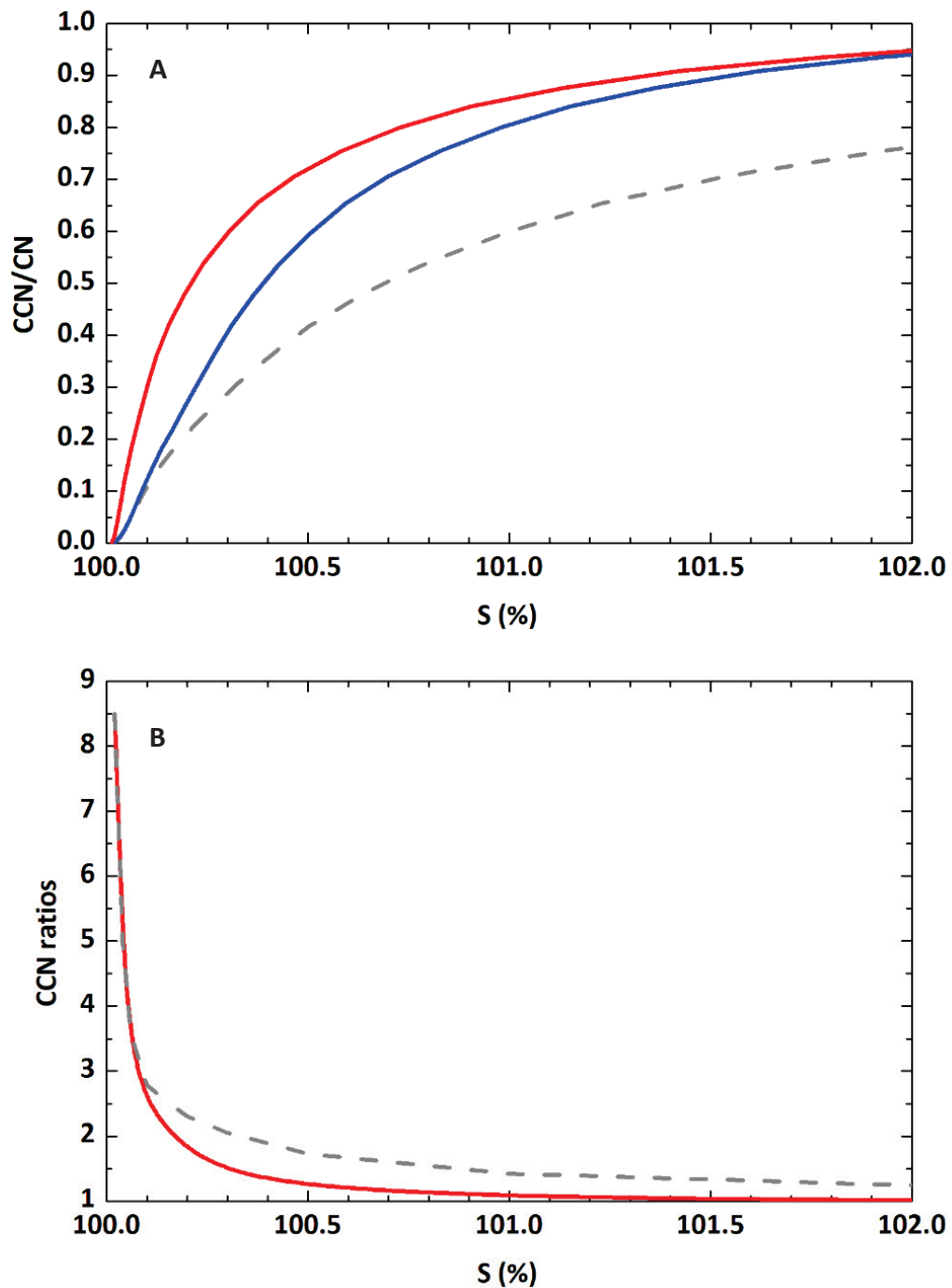


Figure 4.6: Results of the CCN calculations as a function of saturation S (%): (A) CCN efficiency (“ CCN/CN ”) for the PM1 population for $\sigma = \sigma_w$ (grey dashed line), $C_{surf}/CMC = 100$ (blue line) and 3000 (red line) and (B) corresponding ratios $CCN_{3000}/CCN_{\sigma_w}$ (grey dashed curve) and CCN_{3000}/CCN_{100} (red line) between the different scenarios [Gérard, 2016 under review].

4.3. Conclusion

To conclude, we reported for the first time evidence of the role of surfactants in cloud droplet formation from direct observations of cloud events and aerosol surfactants in the atmosphere.

Indeed, the investigation of surfactants in the PM₁ aerosols from Pallas-Sammaltunturi site during 72 cloud events and 7 months showed that, at this site:

- 1) Surfactants were homogeneously distributed between the interstitial and activated particles, therefore **the analysis performed on the interstitial PM₁ aerosols were representative of the CCNs.**
- 2) **Cloud occurrence correlated strongly with surfactant concentrations and average CMC in PM₁ aerosols.** In particular, the correlation with CMC provided the first clear atmospheric evidence for a specific role of surfactants in cloud formation.
- 3) In most cases, **cloud formation was clearly consecutive to, thus resulted from, an increase in surfactant concentration and a decrease in their CMC**, indicating the influx of new, internally mixed, surfactants with low CMCs.
- 4) The combined increase in concentration and decrease in CMC enhanced the volume of water that the PM₁ particles could take up, while maintaining a low surface tension, by about a factor of 30. This ability was represented by **the $C_{\text{surf,p}}/\text{CMC}$ ratio**, which is therefore a **critical parameter in the activation** of cloud droplets.
- 5) Simple Köhler calculations showed that **these conditions corresponded to CCN numbers about four times larger than when assuming the surface tension of water.**

These results underline the quantitative effect of surfactants on CCN activation and numbers and the importance of taking them into account in the prediction of clouds in atmospheric and climate models.

5. Third study: Effect of surfactants on the growth of individual micron-sized droplets using an optical trap

This chapter focuses on the investigation of the effect of surfactants on the condensation of water onto micron-sized droplets using an aerosol optical trap.

The results presented in this chapter have been submitted for publication [Frossard, 2016 under review]. As mentioned earlier, this work was done in collaboration with the Ronald C. Cohen research group, and especially with Amanda A. Frossard, at the University of California, Berkeley, USA, where the experiments were carried out.

5.1. Objectives and method

It was shown in the previous chapters, by direct proofs in atmosphere, that the presence of surfactants should enhance cloud droplet formation. However the measurements were done at a macroscopic scale (bulk measurements) and were not studied on droplets at the scale of cloud droplets. Thus the purpose of the study presented in this chapter was to demonstrate, in laboratory, that the effect of surfactants on cloud droplet formation remained true at a microscopic scale on individual droplets.

A few studies have been carried out on micron-sized droplets. For example, recent work has demonstrated that the surface tension depression within a micron-sized droplet is the same as that within a bulk system [Bzdek, 2016]. This attests that the measurements done at a macroscopic scale (Chapters 3 and 4) should be valid. Moreover, the effect of surfactants on micron-sized droplets using an optical trap has been studied [Buajarern, 2007c; Davies, 2012] and recently laboratory experiments have demonstrated that surface-active compounds enhance the formation of cloud droplets [Ruehl, 2016]. However no experiments at a microscopic scale have been reported using real surfactants with the properties and concentrations found in atmospheric aerosols.

To our knowledge, this study is the first use of an optical trap to study the effect of surfactants on the growth of individual micron-sized droplets, using a proxy atmospheric surfactant (Igepal CA-630) having a similar concentration and CMC value to the surfactants extracted from atmospheric aerosol particles determined in this study (Chapters 3 and 4).

In this work, the effect of the proxy surfactant, Igepal CA-630, on the growth of individual micron-sized droplets was investigated using an aerosol optical trap set-up, coupled with bright-field microscopy and Raman spectroscopy (see Experimental Section 2.7). The change in radius of individual droplets containing NaCl and the surfactant Igepal CA-630 was studied at different surfactant concentrations (Table 2.1 Section 2.7.2) evolving with the relative humidity from 80 % to 70 % (evaporation step) and 70 % to 80 % (condensation step).

5.2. Results and discussion

5.2.1. Effect of surfactants on the change of droplet size

For this study, the ratio of the droplet radii at 70 % RH compared to that at 80 % RH (r_{70}/r_{80}) was used to quantify the change in droplet size. The advantage of this method, in addition to being able to study individual micron-sized droplets, was the possibility to maintain the droplet trapped long enough to give to the surfactants time in the droplet and the surface tension of the droplet to come to equilibrium (more than 10 seconds for some surfactants and on the order of minutes for others [Nozière, 2014]), contrary to traditional on-line instruments.

The radius changes of the droplets containing the different concentrations of the surfactant Igepal compared to the droplets without any surfactant, obtained in this work, are given in Figure 5.1.

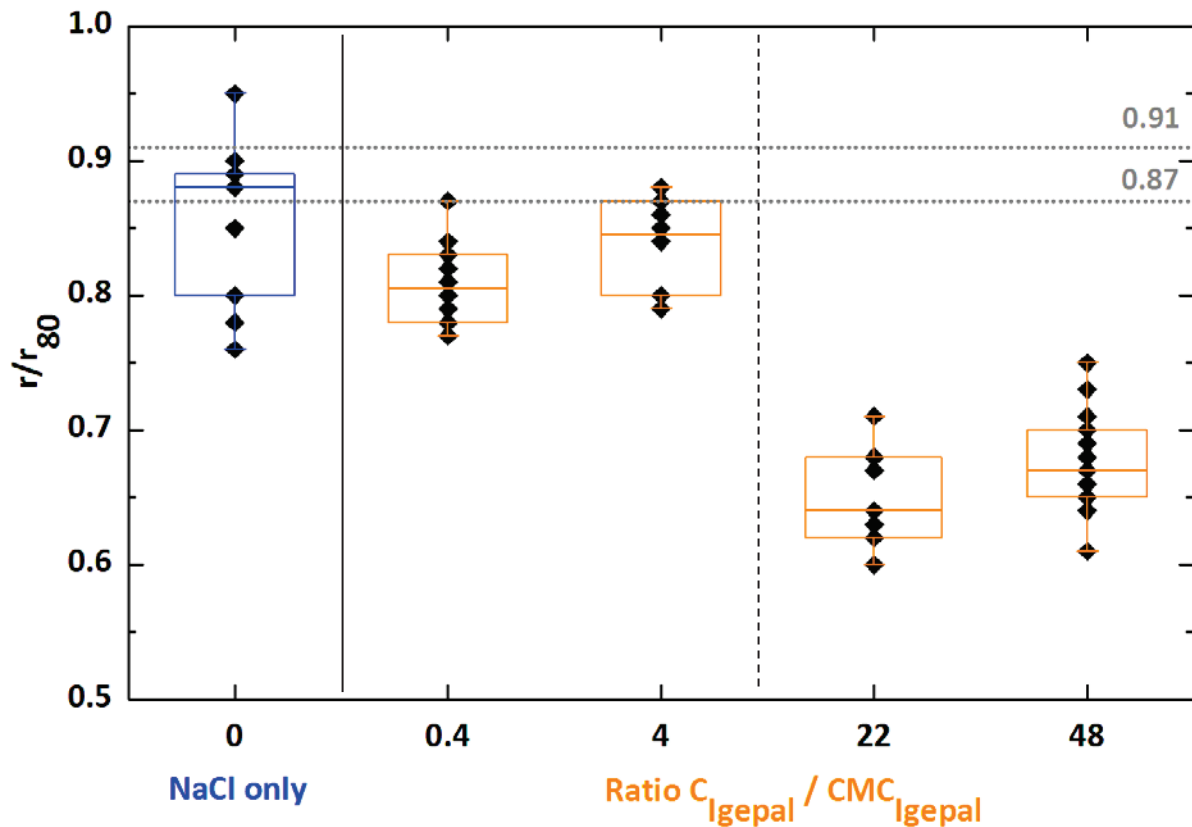


Figure 5.1: Ratio of the equilibrium radius at 70 % RH ($r = r_{70}$) to the equilibrium radius at 80 % RH (r_{80}) for droplets containing NaCl only and NaCl with 0.4 and 4 times the CMC concentration of Igepal ($r = r_{70}$). For droplets with NaCl and 22 and 48 times the CMC concentration of Igepal, the equilibrium radius at the point the droplet was lost (higher than 70 % RH) is used in the ratio ($r = r_{lost}$). The black markers represent individual values. The solid line is the median, boxes represent the 25 to 75 percentiles, and the whiskers are the 10 and 90 percentiles. The dashed horizontal lines are at $r_{70}/r_{80} = 0.87$ (Köhler theory) and 0.91 [Tang, 1997] for droplets containing NaCl only (adapted from [Frossard, 2016 under review])

Figure 5.1 shows that droplets containing the surfactants at a concentration of about half the CMC value (0.04 mM) have a smaller r_{70}/r_{80} ratio (0.81 ± 0.03) compared to the NaCl only droplets (0.86 ± 0.06). This means that, for a given % RH change (here from 70 to 80 % RH), the presence of the surfactants allows the formation of larger droplets (as illustrated in Figure 5.2), which may be the consequence of a reduction in surface tension caused by the presence of surfactants in the droplets. For surfactant concentrations about 4 times greater than the CMC (0.35mM), the same trend was observed with an average r_{70}/r_{80} ratio of 0.84 ± 0.04 . These results indicated that low concentrations of surfactant Igepal could influence the surface tension and affect the water evaporation from and condensation onto the droplet.

Figure 5.1 shows also that increasing the Igepal concentration to more than 20 times the CMC value (22 times the CMC (1.76 mM) and 48 times the CMC (3.87 mM)) corresponds to a higher size change (0.67 ± 0.04 on average) compared to droplets without surfactants but results in a different behavior than droplets with a lower surfactant concentration (0.4 and 4 times the CMC). Indeed, when the RH was decreased in the chamber, the water from these droplets started rapidly to evaporate at 75 ± 2 % RH and the droplets were too small to remain trapped. As a result, the condensation step could not be completed. So for these cases, the ratios of the radius were calculated when the droplet was lost (r_{lost}) to r_{80} .

The larger change in the size of droplets containing surfactants compared to droplets without surfactant is consistent with a surface tension depression that enables water to evaporate from droplets more easily during a decrease in RH or to condense onto the droplets more easily during an increase in RH. Lowering the surface tension should decrease the energy barrier (as illustrated in Figure 5.2) and allow water to move across the interface more easily. However the difference in $r_{70 \text{ or lost}}/r_{80}$ ratios and apparent stronger effect for more than 20 times the CMC (0.67 ± 0.04 together) compared to 0.4 and 4 times the CMC (0.82 ± 0.04 together) is not explained yet. This effect certainly resulted from effects other than the surface tension depression, such as the formation of a monolayer, a phase separation, or other effects, due to the higher concentration of surfactants.

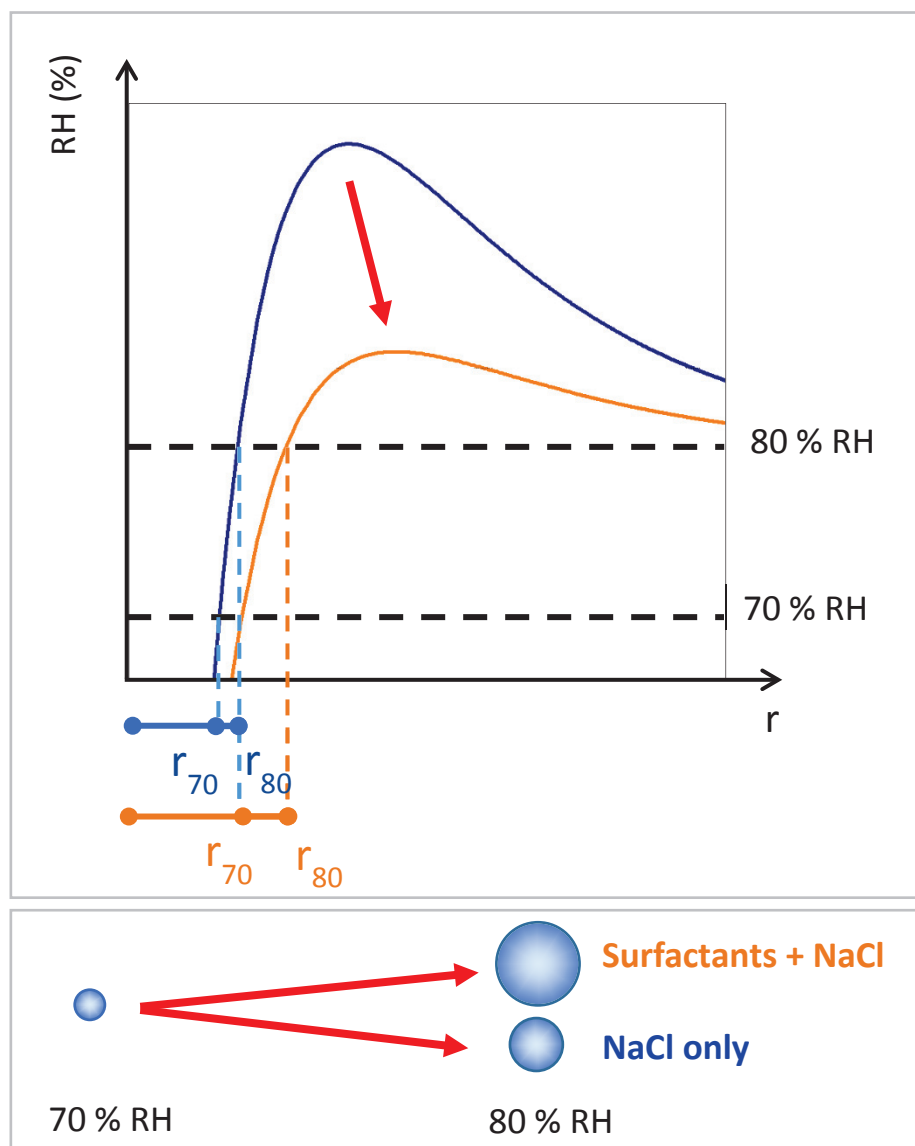


Figure 5.2: Illustration of comparison between different r_{70}/r_{80} ratios (blue: higher ratio; orange: lower ratio) with (A) schematic Köhler curves representing RH (%) as a function of the droplet radius r (blue line: droplet with NaCl only; orange line: droplet with surfactant Igepal + NaCl) and (B) corresponding droplet growth for RH varying from 70 to 80 % RH. (Note: schematics not at scale).

In studies adhering to the partitioning theory (*e.g.* [Sorjamaa, 2004]), the surfactant effect on the hygroscopicity of the droplet is neglected: the decreasing of the surface tension by the surfactant would be canceled out by their effect on the Raoult's term. But this claim is controversial and it was shown that this theory was inaccurate [Nozière, 2014]. Moreover, in this study, the Igepal concentrations relative to the concentrations of NaCl (see Table 2.1 in Section 2.7.2) were low enough to not significantly affect the hygroscopicity (Raoult's term)

of the droplet (while being kept in the concentration range of measured atmospheric aerosol particles of Chapter 3). Consequently, it was guaranteed that the changes in the droplet behavior with the addition of Igepal were attributed to the change in surface tension.

The r_{70}/r_{80} ratio for the droplets containing Igepal was less than the value predicted by Köhler theory for the large droplets used in this experiments. This observation is consistent with [Petters, 2016] where they found that the CCN activity of non-ionic surfactants was greater than predicted by Köhler theory including surface tension reduction and surface partitioning. The difference between the predicted values and the ones determined in this work shows that the role of surfactants in atmospheric particles may be to enhance droplet growth with changing meteorological conditions by even more than predicted by Köhler theory.

5.2.2. Implication for droplet size distribution

It was shown in the previous part that an increase of 10 % in RH (from 70 % to 80 % RH) for droplets containing Igepal (from 0.4 times to 4 times the CMC) can increase their growth compared to droplets without surfactants. This effect was illustrated with an example of size distribution of aerosol particles. The resulting size distribution at 70 % RH and 80 % RH was estimated from Köhler theory (Figure 5.3), assuming properties of NaCl particles, since Igepal contributed only for 0.06 % - 0.6 % of the dry particle mass in the proxy aerosol studied in this work.

5. Third study: Effect of surfactants on the growth of individual micron-sized droplets using an optical trap

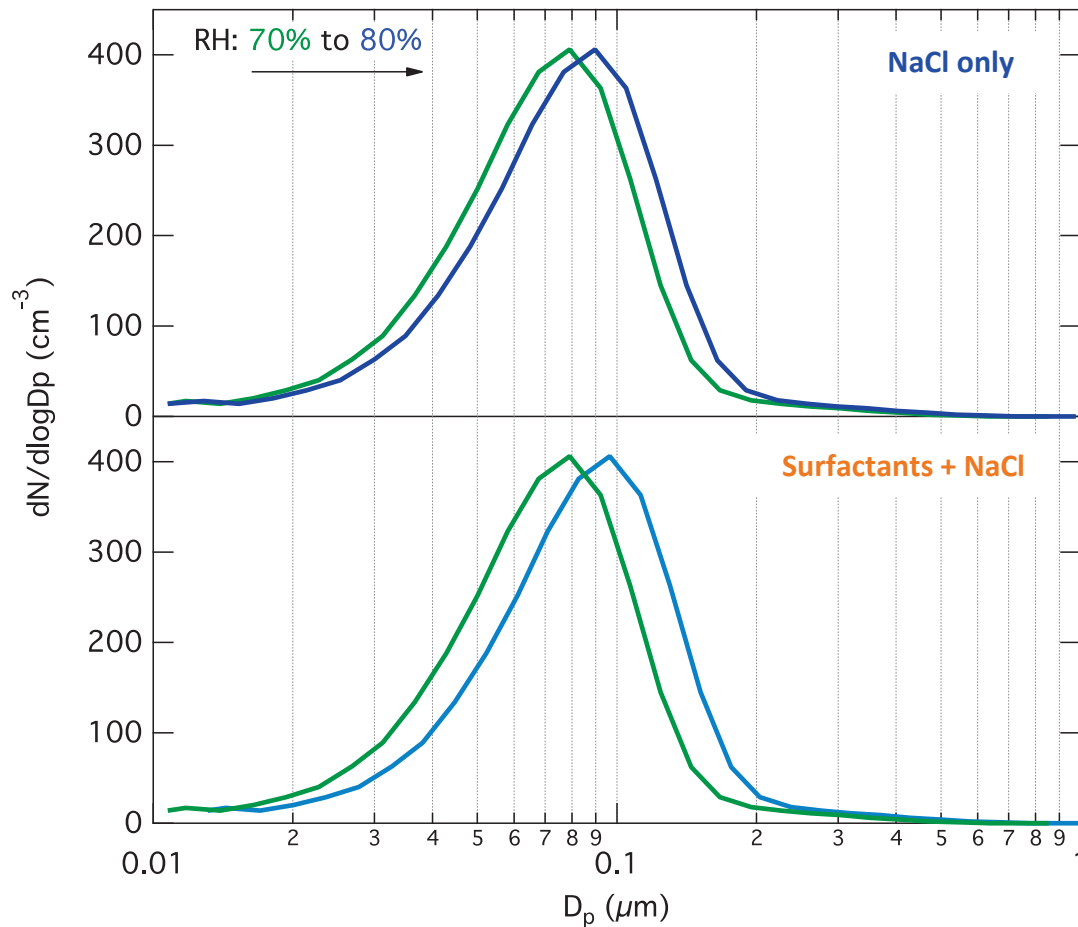


Figure 5.3: Number size distributions at an initial RH of 70 % (green) and final RH of 80 %. For NaCl at 80 % RH (dark blue), the number size distribution was calculated using Köhler theory growth from 70 % to 80 % RH. For the NaCl and Igepal mixtures, the number size distribution at 80 % RH (light blue) was calculated using the average ratio of r_{70}/r_{80} (0.82) measured in the experiment for low Igepal concentrations of 0.4 or 4 times the CMC value (reproduced from [Frossard, 2016 under review]).

Figure 5.3 shows that for particles containing surfactants with similar properties to Igepal, the size distribution from 70 % RH to 80 % RH would shift to higher diameters than those without surfactants. Thus for a same change in relative humidity, this increase of droplet diameters should favor the growth into cloud droplets for the particles containing surfactants which may activate before those without. Therefore, the fraction of particles activated as CCN should be larger for particles containing surfactants.

5.3. Conclusion

In this work, we observed that **the evaporation and growth of individual micron-sized droplets containing surfactants was greater than those that did not contain any surfactants, even for a small change in RH.** If extended to higher RH values, this would imply that droplets containing surfactants would grow larger, given the same increase in RH. This larger growth in droplet size could lead to increased formation of cloud droplets or activation of particles at lower critical supersaturations. This is consistent with Köhler theory calculations, which predict lower required critical supersaturations for droplets with lower surface tensions. The broader scale or cloud-level scale of this effect, however, should be investigated.

Thus this study allowed us to show that surfactants have an effect on the growth of micron-sized droplet and reinforces our claims from macroscopic experiments that surfactants should enhance cloud formation (Chapter 3 and 4). Moreover, the possibility to study the growth of droplets without time limitation using an optical trap with Raman spectroscopy is a real advantage for studying the effect of surfactants on cloud droplets. Next steps could be to compare the effects of different types of surfactants (especially the ones found in genuine atmospheric aerosol extracts) and to study mixtures of surfactants with other organics and salts found in atmospheric aerosols.

6. Fourth study: Investigation of the origin of surfactants in aerosols

This chapter focuses on the investigation of the origin of surfactants present in atmospheric aerosols. Indeed, since the importance of surfactants in cloud droplet formation has been shown (Chapters 3, 4 and 5), it is important to know their origin to understand the mechanisms and efficiency due to their structure and the relationship between the biosphere and the clouds.

6.1. Objectives and method

Surfactants found in atmospheric aerosols are suspected to be from biological origin (*e.g.* [Delort, 2010; Ekström, 2010]). Thus in this work we tried to find evidence of this biological origin using different approaches, all of them based on the study on the environmental samples. This included:

- the comparison of the surfactant properties found in aerosols with references,
- fluorescence measurements,
- the comparison of surfactant concentrations with a marine biological marker, the chlorophyll-*a*,
- the comparison of surfactant concentrations and properties with sources (vegetation and seas),
- the investigation of the surfactants chemical structure.

The different studies presented in this chapter gather results from [Gérard, 2016], [Gérard, 2016 under review], [Renard, 2017 in preparation] and preliminary results.

6.2. Results and discussion

6.2.1. Surfactant properties (CMC)

This biological origin of surfactants from atmospheric aerosols was first investigated based on their surfactant properties.

The average surface tension curves of the aerosols collected from the different regions in this work (Section 2.1.2) were compared with references (Figure 6.1 and Table 8.3 in Appendix Section 8.4).

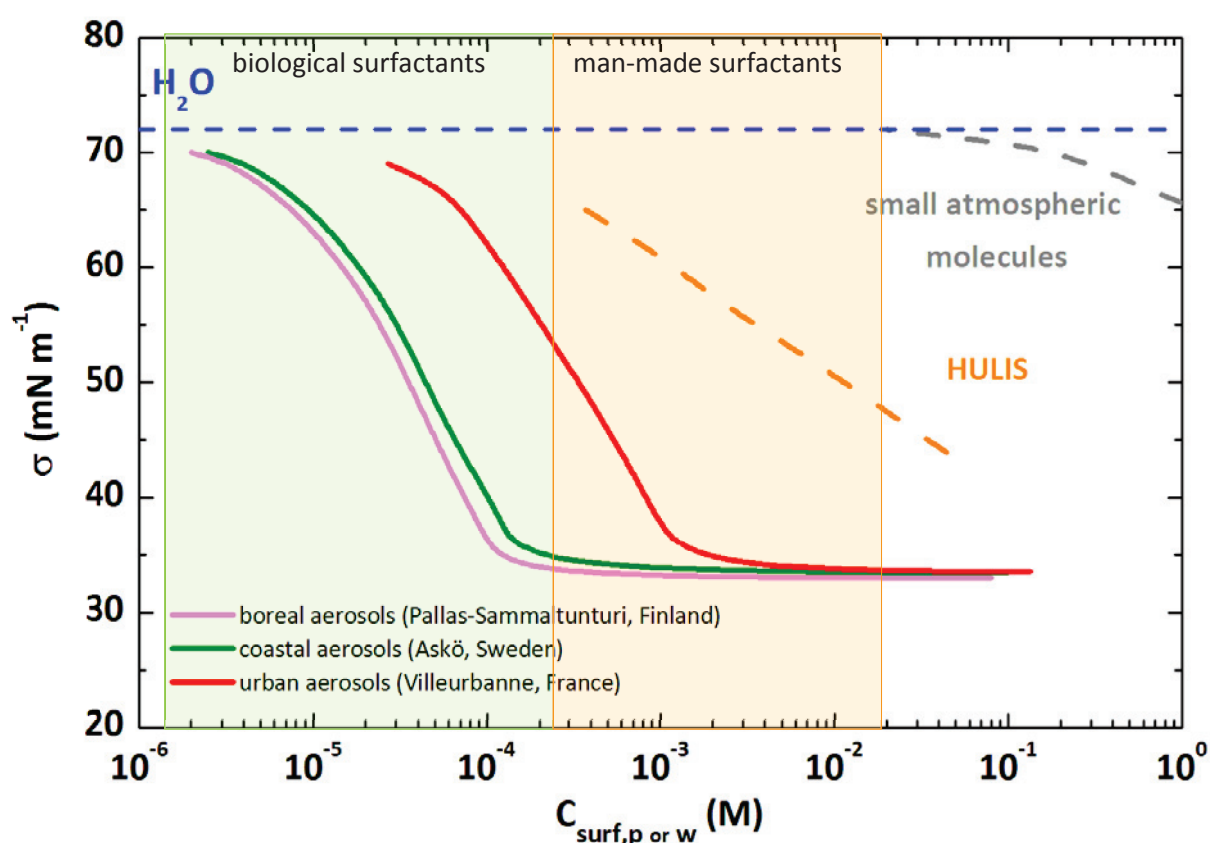


Figure 6.1: Comparison of average surface tension curves of aerosols extracts with reference surfactants: coastal aerosols PM_{2.5} from Askö, Sweden (green line); boreal aerosols PM₁ from Pallas-Sammaltunturi, Finland (pink line); urban aerosols PM₁ from Villeurbanne, France (red line); HULIS (Humic-like substances) (dashed orange line) [Salma, 2006]; salt and small organic molecules found in atmospheric aerosols (dashed grey line) [Ekström, 2010]; typical ranges of CMC of man-made surfactants (orange area) [Mukerjee, 1971] and biological surfactants (green area) [Desai, 1997].

The surface tension curves determined in this work show the presence of strong surfactants in the atmospheric aerosols, which are unlikely small molecules according to their properties. Note that one must be careful using the term “surfactants”. Some small organic molecules found in atmospheric aerosols (*e.g.* carboxylic acids) and HULIS (Humic-like substances) are considered as surface-active agents in the atmospheric literature [McNeill, 2014], but this is untrue, compared to strong surfactants. Indeed for this species, as shown in Figure 6.1, the surface tension decrease is not significant, especially for the small molecules ($\sigma \sim 65 \text{ mN m}^{-1}$), and/or is effective only for high concentrations ($> 10^{-2} \text{ M}$).

For the investigation of the origin of surfactants (biological or not), although Figure 6.1 shows that the minimum surface tension of the different aerosols is very low (30 - 35 mN m^{-1}), this did not constitute a proof of the biological origin of surfactant, since these values are comparable to those of strong surfactants whether biological or not, such as the reference compounds used in this work (SDS, AOT, zephiramine, CTAC, Triton X114, Brij35, surfactin, rhamnolipid, and L- α -phosphatidylcholine, see Section 8.3).

The CMC, intersection between the sharp slope and the minimum surface tension level of the surface tension curves, is much more characteristic of specific surfactants and is used for comparison with reference surfactants. As shown in Figure 6.1, the CMC of the aerosols from the clean stations (coastal and boreal) is situated in the typical range of biological surfactants, suggesting a biological origin, whereas the one from the polluted urban site is situated in the typical range of man-made surfactants, suggesting an anthropogenic origin or a mixture between biological surfactants and Humic-like substances (HULIS) that could have been extracted with the surfactants.

This could imply that efficient surfactants are mostly biological but their effect is reduced by the presence of anthropogenic surfactants in polluted regions.

However although these results constituted a first proof of the biological origin of surfactants, they were not enough, since artificial surfactants can also have a low CMC and at the contrary biological surfactants can have a high CMC (see examples in Table 8.2 in Appendix Section 8.3). Thus other evidences to prove the biological origin of surfactants have been investigated (see next sections of this chapter).

6.2.2. Fluorescence

The fluorescence spectroscopy was used in this work to investigate if the surfactants in aerosols had a specific biological signature (*e.g.* [Hoekstra, 2007; Pan, 2015]).

The fluorescence spectra of samples for two different regions (boreal aerosols from Pallas-Sammaltunturi and urban aerosols from Villeurbanne) and at the different steps of the extraction (details of the method in Section 2.5.2) were measured and compared (Figure 6.2 and Figure 6.3).

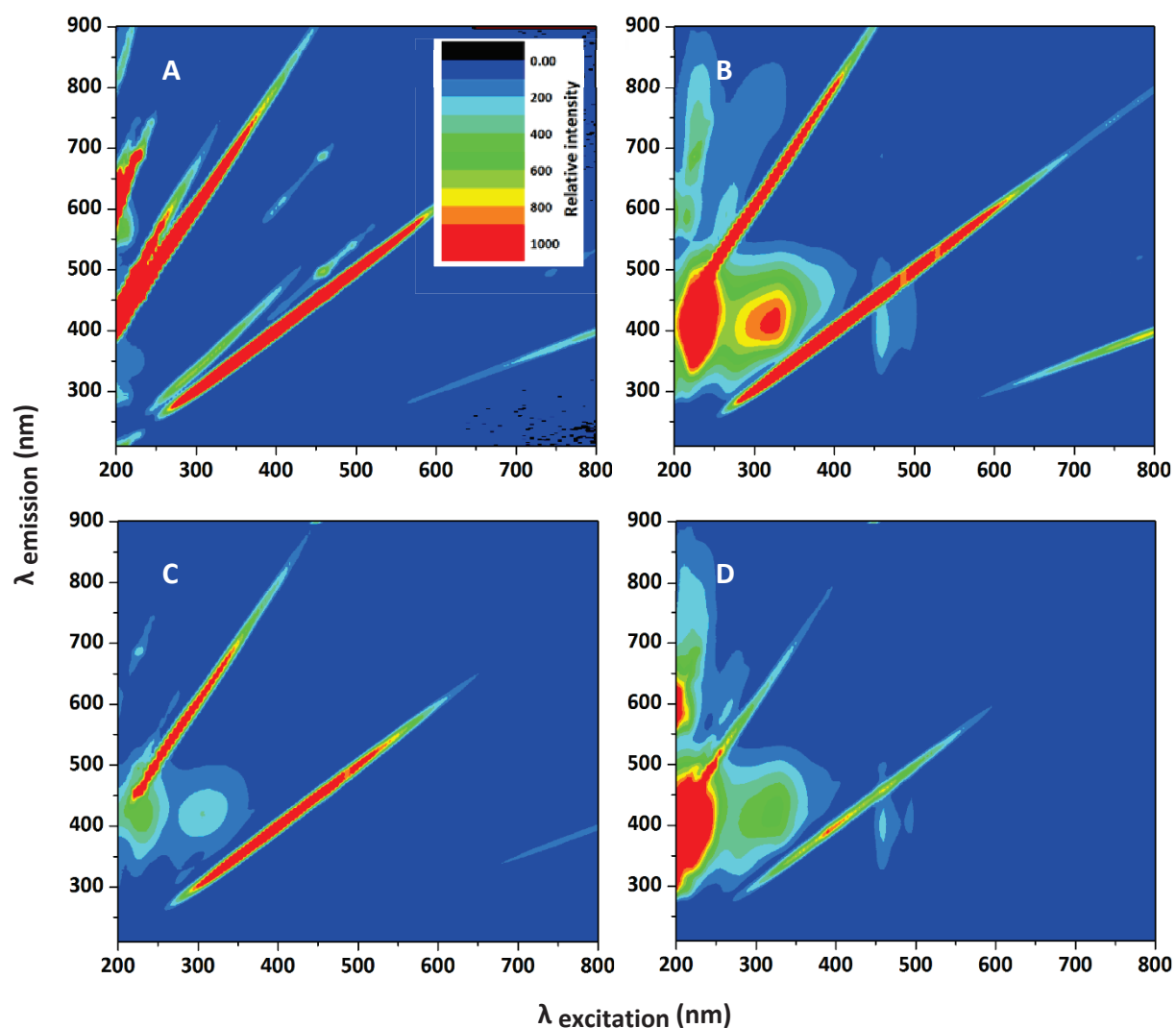


Figure 6.2: Fluorescence spectra at the different steps of extraction of PM₁ collected on quartz filters at Villeurbanne, France: (A) blank method, (B) after water extraction, (C) remaining solution after SPE (matrix containing the interferents) and (D) surfactant fraction extracted after SPE. The diagonal lines appearing in the blank are interferences (Rayleigh scattering and Raman scattering) but do not prevent (here) the observation of the fluorescence spectra of the samples.

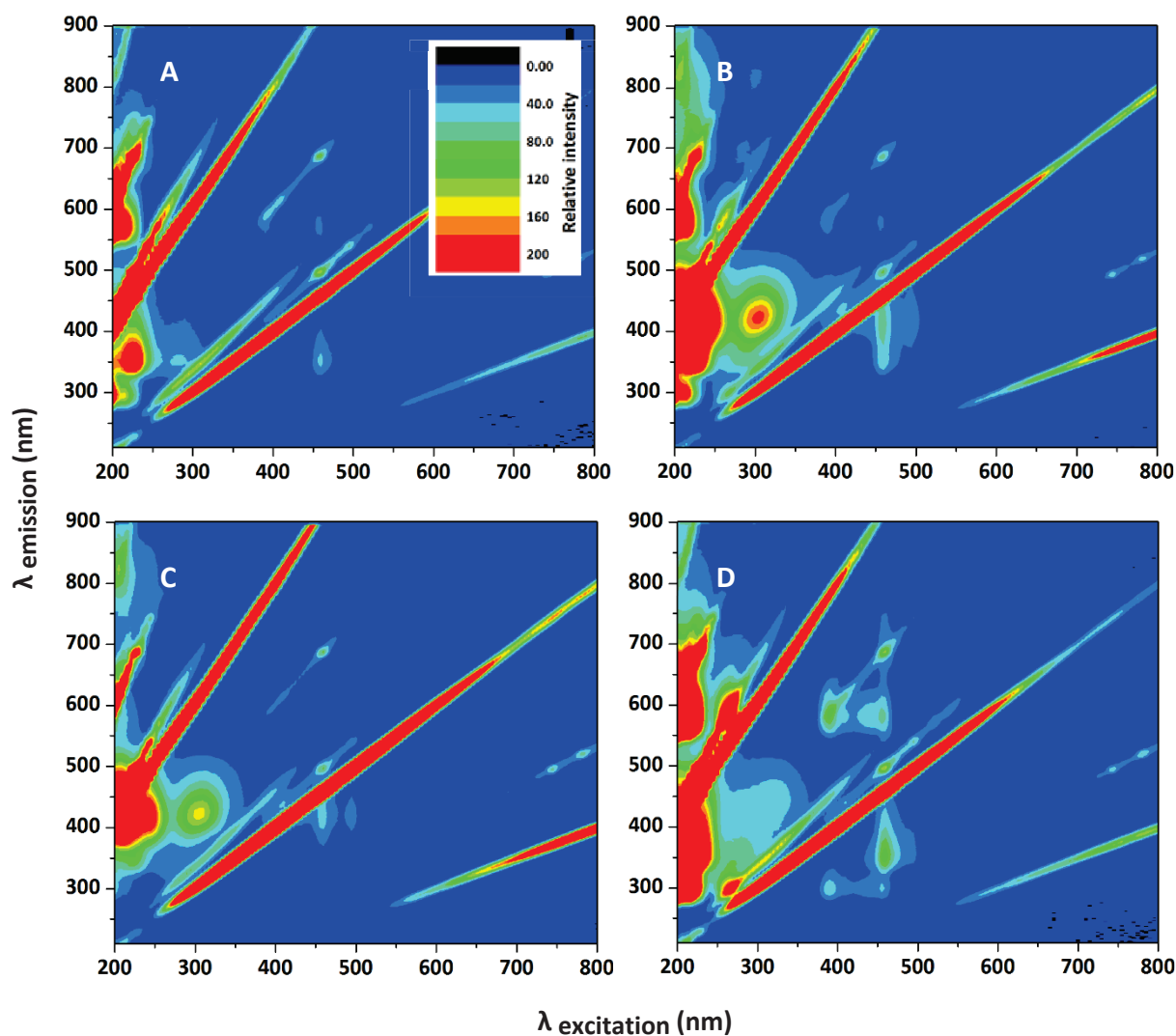


Figure 6.3: Fluorescence spectra at the different extraction steps of PM1 collected on quartz filters at Pallas-Sammaltunturi, Finland: (A) blank method, (B) after water extraction, (C) remaining solution after SPE (matrix containing the interferences) and (D) surfactant fraction extracted after SPE. The diagonal lines appearing in the blank are interferences (Rayleigh scattering and Raman scattering) but do not prevent (here) the observation of the fluorescence spectra of the samples.

The fluorescence spectra (Figure 6.2 and Figure 6.3) are quite similar between each step of extraction (regardless the intensities of fluorescence). The spectra show a broad emission band between 300 and 500 nm for an excitation band between 250 and 400 nm, with a maximum at $\lambda_{\text{emission}} = 400 (\pm 15)$ nm for $\lambda_{\text{excitation}} = 325 (\pm 15)$ nm for Villeurbanne aerosols, and $\lambda_{\text{emission}} = 425 (\pm 10)$ nm for $\lambda_{\text{excitation}} = 300 (\pm 10)$ nm for Pallas-Sammaltunturi aerosols. The fluorescent molecules seem to be shared between the matrix and the surfactant extract, which were separated by the second extraction of the double extraction method, regarding the decrease of intensity compared to the first extraction. The fluorescence spectra result from the average of the different fluorescent properties of the components mixed in the

samples, but the solutions at the different steps having similar spectra does not mean necessarily that the same species were present in each solution. Besides, because other compounds could have been potentially extracted by our method (such as HULIS), it was not possible to know if the fluorescence in the extracts (Figure 6.2 (D) and Figure 6.3 (D)) resulted from these other compounds and/or the surfactants. Moreover the comparison of the spectra did not reveal any specific signature or an obvious differences between the surfactant extracts from the different regions (Figure 6.2 (D) and Figure 6.3 (D)), except a slightly broader range of emission for the aerosols from Villeurbanne. This could be explained by the presence of a higher number and variety of molecules present in the aerosols of Villeurbanne, being more impacted by pollution than the boreal aerosols from Pallas-Sammaltunturi.

Thus, it was not possible to deduce the nature of the extracted surfactants using this method. To be able to distinguish different species, another method should have been developed. For example the components of the extracts should have been separated (for example using chromatography techniques) and concentrated before fluorescence measurements. However this study was not continued and other methods more adapted to the study were favored to investigate the biological origin of the surfactants in atmospheric aerosols.

6.2.3. Comparison with a marine biological marker: chlorophyll-*a*

To further examine the origin of the aerosol surfactants studied in this work, we compared the surfactant concentrations in air, $C_{\text{surf},a}$, of the aerosols from Askö campaign with the concentrations of a tracer for biological activity in seawater: seawater chlorophyll-*a* concentrations, $C_{\text{chlorophyll-}a}$ (Figure 6.4), from MODIS aqua satellite data (Experimental Section 2.8.1). Indeed, the aerosols at this station were expected to contain a major part of aerosols produced from seawater since at this site the aerosol air mass sources (HYSPLIT back trajectories, Section 2.8.2) were dominated by the sea.

When averaged over an area of 50 km × 50 km around the Askö station, the surfactant and chlorophyll-*a* concentrations displayed some correlations with anionic ($R^2 = 0.65$), cationic ($R^2 = 0.75$), and total ($R^2 = 0.67$) surfactant concentrations, the correlation with total surfactants not resulting directly from those with anionic and cationic surfactants. These correlations suggested a biological and marine origin for these compounds.

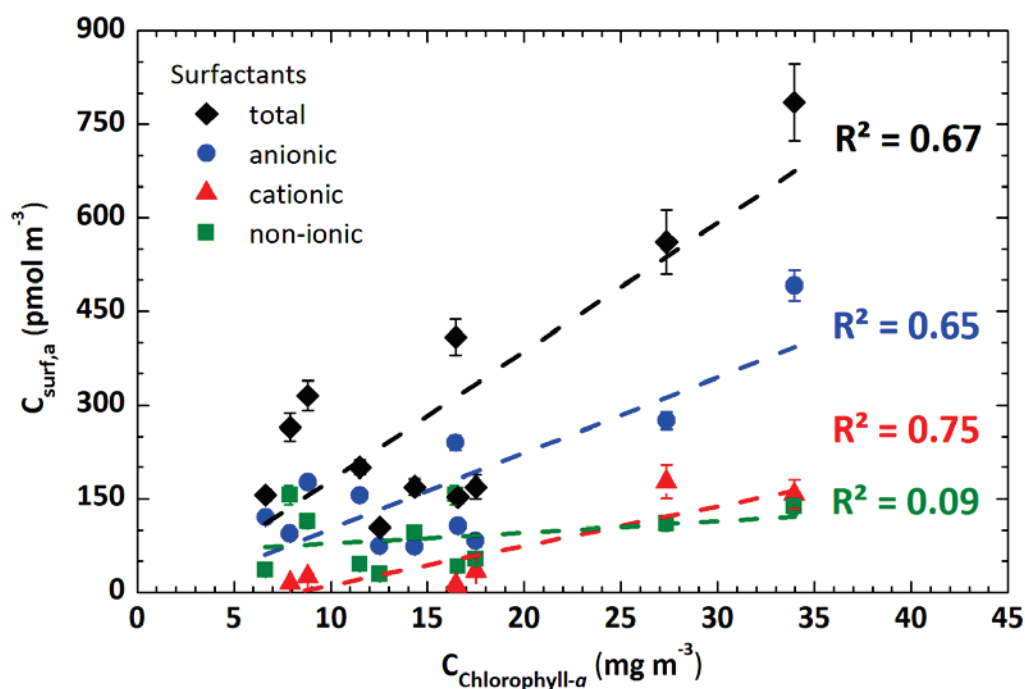


Figure 6.4: Correlations between anionic (blue circles), cationic (red triangles), non-ionic (green squares), and total surfactant (black diamonds) concentrations in the atmospheric samples and seawater chlorophyll-*a* concentrations, provided by aqua MODIS satellite (adapted with permission from [Gérard, 2016] © Copyright 2016 American Chemical Society).

Note that chlorophyll-*a* concentrations $C_{\text{chlorophyll-}a}$ averaged over larger areas ($100 \text{ km} \times 100 \text{ km}$) did not correlate with the surfactant concentrations $C_{\text{surf},a}$ ($R^2 < 0.35$), indicating that, if the surfactants were indeed produced by biological sources in seawater, these sources were local.

A marine and biological origin for the surfactants might seem contradictory with the lack of correlation between non-ionic surfactants and chlorophyll concentrations because most biological surfactants are non-ionic. This lack of correlation could be attributed either to large uncertainties (mostly underestimations) in the non-ionic concentrations or to the choice of the wrong marker for their sources. Chlorophyll-*a* was chosen in this work mostly because the available data had a frequency similar to those of our samples but has been reported not to be the best surrogate for the organic matter transferred from the sea surface to atmospheric aerosols [Rinaldi, 2013] or for the biological processes controlling the sea-surface organic composition [Vaida, 2015; Wang, 2015]. In future studies, correlations between aerosol surfactants and other seawater markers should thus be sought and with more statistics to be more compelling.

6.2.4. Comparison with vegetation and seas

To have a first idea of the sources of air masses bringing the most efficient surfactants, we tried to find links between the surfactant properties or concentrations and the different air mass sources determined from air masses back trajectories (Section 2.8.2). Different approaches were possible. The sources defined by the vegetation (and seas) rather than directions were chosen first, since [Renard, 2016] suggested a link between the vegetation and phyllosphere (bacteria living on plants) and because the purpose of this study was to prove the biological origin of surfactants. This study being not finished, only preliminary results will be presented and briefly discussed.

The study was done on the aerosol samples from the boreal Pallas-Sammaltunturi station (Section 2.1.2.3). The surfactant concentrations and properties (Section 4.2.1 and 4.2.3) were compared to the different air mass sources. Six sources have been distinguished: boreal vegetation, temperate vegetation, tundra vegetation and Arctic sea, North Atlantic sea and Baltic sea as marine sources (Figure 6.5 (A)). For each sample, the sources were determined from the HYSPLIT 72 h - back trajectories (Section 2.8.2) (see examples in Figure 6.5 (B) and Figure 8.3 in Appendix Section 8.6).

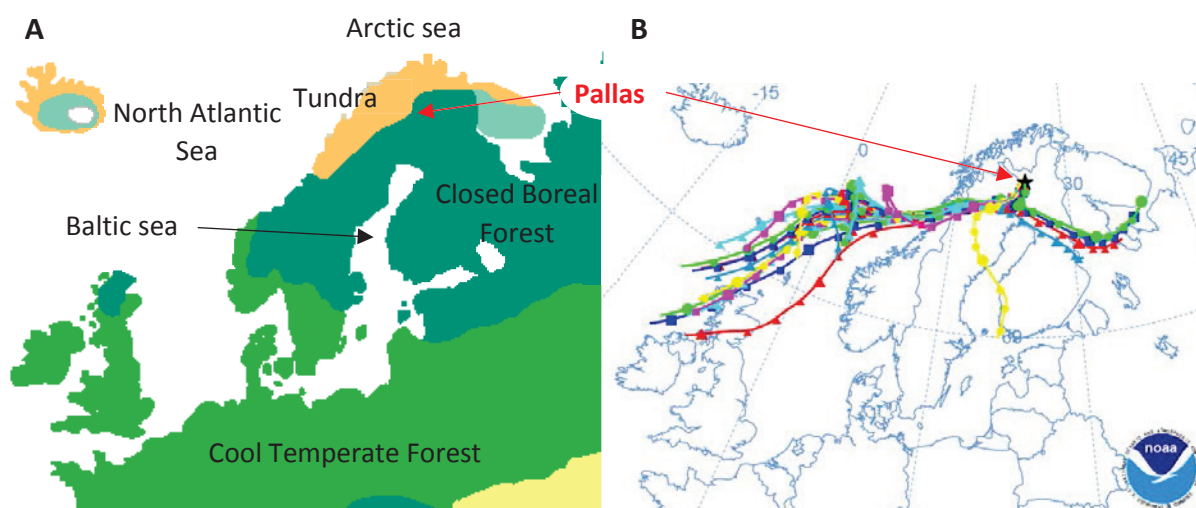


Figure 6.5: (A) Vegetation map of Europe (adapted from [Adams, 1997]) and (B) Example of back trajectories (30/08/15 22:00 UTC) arriving at the station Pallas-Sammaltunturi (red arrows). The trajectories were obtained from HYSPLIT back trajectories ([Draxler, 2015; Rolph, 2015]): source at 67.97N 24.12E, 72 h - back trajectories (with a new trajectories starting every three hours during the 72 h), model vertical velocity, height 10 m AGL (above ground level).

72 h-backward trajectories were chosen because this duration is about the life time of aerosol particles in air masses. A sample was considered from a certain source if more than the half part or the totality of the back trajectories were coming from this source.

The comparison between the surfactant concentrations and properties with the different sources are given in Figure 6.6.

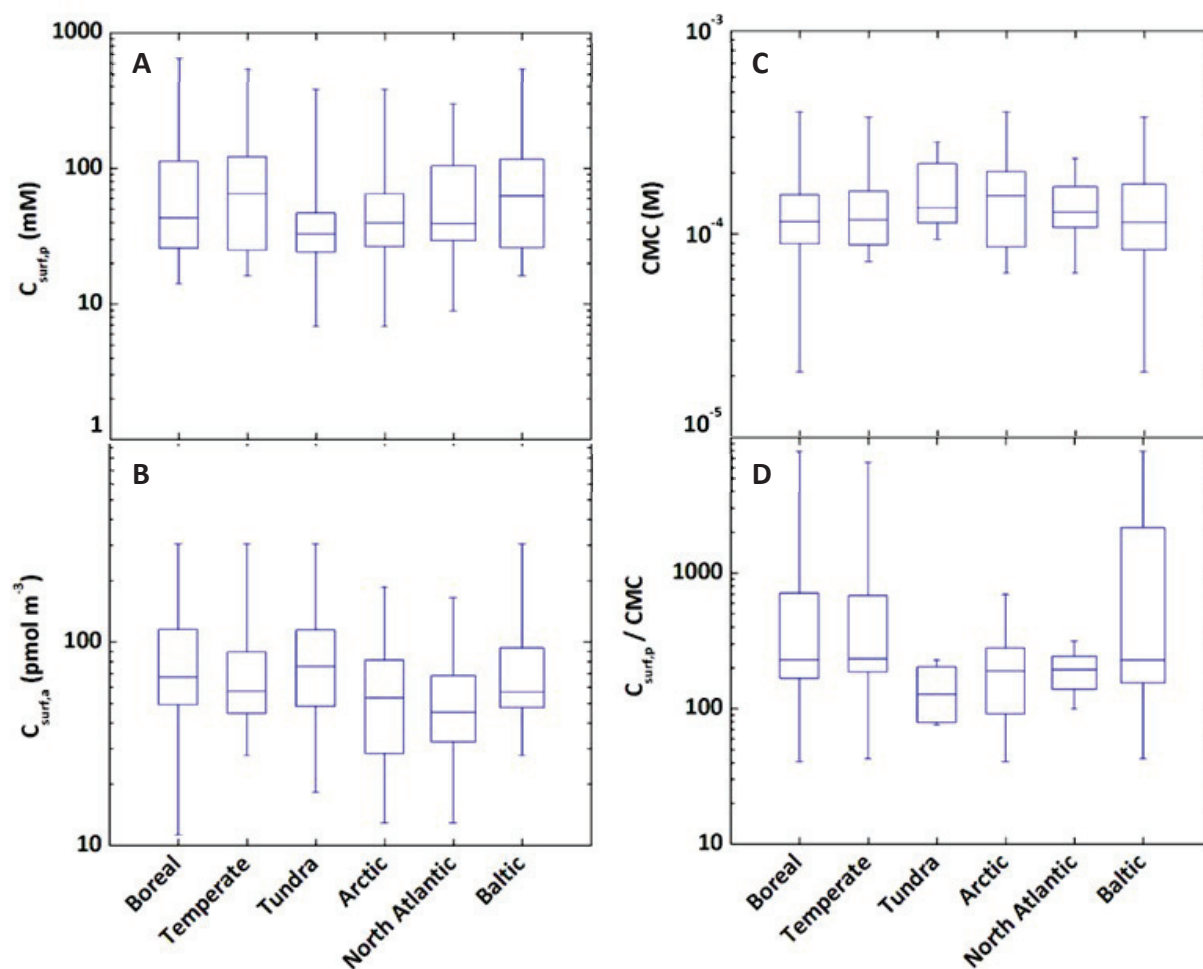


Figure 6.6: Comparison of the surfactant concentrations ((A) concentration in aerosol particle $C_{surf,p}$ and (B) concentration in air volume $C_{surf,a}$) and properties ((C) CMC and (D) $C_{surf,p}/\text{CMC}$) in aerosols from Pallas-Sammaltunturi with the air mass sources. The solid line is the median, boxes represent the 25 to 75 percentiles, and the whiskers are the minimum and maximum values (note: preliminary results).

From Figure 6.6, it seems that the aerosols with the highest surfactant concentrations in aerosol particles volume $C_{\text{surf},p}$, the most powerful surfactants (lowest CMC) and consequently the highest $C_{\text{surf},p}/\text{CMC}$ ratio come from:

- regions with trees (boreal and temperate vegetation) rather than lichen (tundra) that could confirm the “phyllosphere hypothesis” from [Renard, 2016];
- the Baltic sea, where the biology such as the presence of algae is active, rather than colder seas (Arctic and North Atlantic).

Besides, the surfactant concentration in air masses $C_{\text{surf},a}$ seems higher for aerosols from tundra and boreal vegetation, which are sources situated close to the site. This could imply that the sources bringing the higher number of surfactants (but not necessarily the strongest) would be rather local and/or that a part of the surfactants brought by sources from further would be lost during the travel of the air masses.

Thus, this study suggests a link between the biology (from vegetation and sea) and the surfactant efficiency, strengthening the hypothesis of the biological origin of surfactants.

These results are preliminary and would be worth to be investigated deeper. For example, other sources area (continental or marine, directional, specific area...) could be considered to define more precise sources of surfactants. Moreover the results could be refined by considering only the samples from a unique source. Indeed the values considered in Figure 6.6 corresponded to samples from mixed air masses, for most of them, due the high aerosol collection time (24 h) during which air masses from different sources could pass at the sampling site. This could bias the comparison between the different sources. These results could also be compared by seasons or with cloud events.

6.2.5. Chemical structure

Finally, to prove the biological origin of surfactants, their chemical structure has been investigated by liquid chromatography coupled to tandem mass spectrometry (LC-MS/MS). The analysis were made in collaboration with the group of Anne-Marie Delort, especially with

Pascal Renard, at ICCF (Institut de Chimie de Clermont-Ferrand), France. The study being not finished, only preliminary results will be presented. The results of this study will be submitted for publication [Renard, 2017 in preparation].

LC-MS/MS experiments were performed on the surfactant extracts from aerosols from Pallas-Sammaltunturi (Chapter 4) with the LC-MS/MS method described in Section 2.6.2.

The LC-MS spectra of these extracts are complex but revealed the presence of compounds with high m/z ratio (example in Figure 6.7).

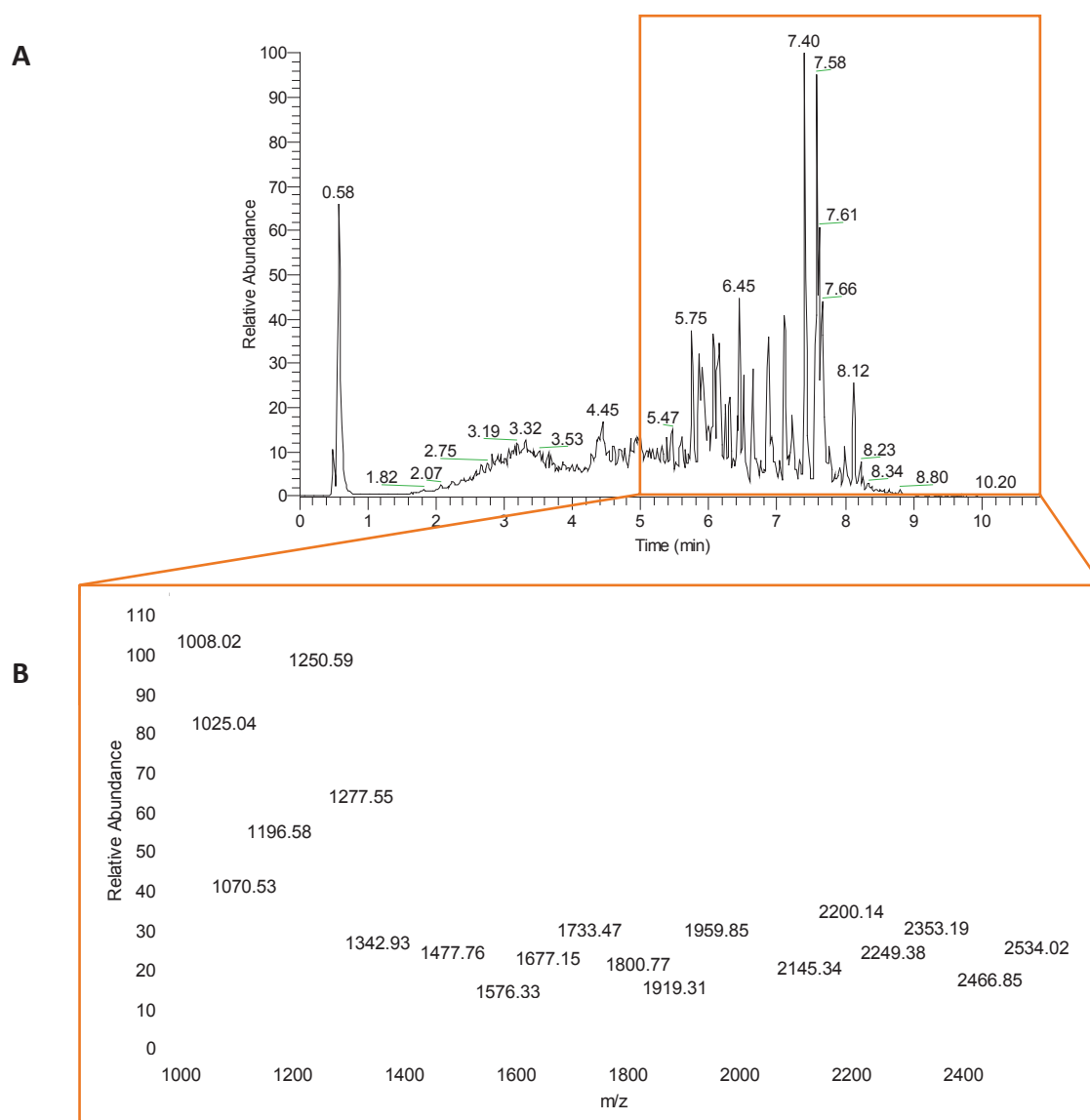


Figure 6.7: Example of LC-MS (ESI+, full MS) spectra of a surfactant aerosol extract from Pallas-Sammaltunturi: (A) LC-chromatogram and corresponding (B) MS-spectra for the retention time range 5 - 11 min and $m/z > 1000$.

Since surfactants in aerosols are expected to be biological as shown previously (Section 6.2.1 and 6.2.3), these high m/z ratio are certainly the signature of biological surfactants, generally macromolecules. These masses need now to be compared with reference surfactant molecular masses and the structure of the corresponding surfactants needs to be checked from MS/MS measurements to confirm their nature and structure.

6.3. Conclusion

This study brought some **evidence of the biological origin** of surfactants in atmospheric **aerosols from different approaches**. The biological origin was suspected from the **low CMC values similar to the ones of biological surfactants** and the slight **correlation of surfactant concentrations with chlorophyll- a from seawater**. Moreover comparisons between surfactant concentrations and properties with the **air mass sources suggested a link between surfactants and vegetation**. In addition, **structural analysis** from LC-MS/MS started to show the **presence of macromolecules** in the samples suspected to be from a biological origin.

Thus all these studies **support the biological origin of surfactants** but need to be further investigated. This should help to understand the biosphere-atmosphere exchanges and the climate system.

7. Summary and outlook

Although the role of surface tension and surfactants in cloud droplet formation from fine aerosol particles ($< 1 \mu\text{m}$) was predicted 80 years ago by Köhler theory, it has been largely neglected in the studies of cloud formation until now. The reasons for this were, on one hand, the lack of observation of surfactant effects on cloud droplet formation with the classical (“on-line”) investigation techniques and, on the other hand, the absence of technique to determine the concentration of surfactants in atmospheric aerosols and their effects on the surface tension.

This PhD work has resulted **in the development of the first method**, to our knowledge, **to determine the absolute concentration of surfactants in atmospheric aerosols**, which, **combined with extraction and surface tension measurements**, has led to the **first determinations of the surface tension of atmospheric aerosols and of the absolute surface tension curves for atmospheric surfactants**. These measurements were applied to aerosol samples from different regions and brought some important progress in the understanding of atmospheric surfactants and their role in cloud formation such as

- **evidencing the role of surfactants on clouds, for the first time from atmospheric observations**, by correlating surfactant properties and cloud formation events,
- showing the mode of action of surfactants, that the **C/CMC ratio controls cloud droplet formation**, and **not the surface tension** of the particles itself or the total concentration of surfactants only,
- bringing evidence that the surfactants found in aerosols from various regions **have a biological origin**, which is important for the understanding of the biosphere-atmosphere exchanges and the climate system.

In addition, the importance of surfactants in cloud droplet formation was investigated in laboratory on micron-sized particles using an optical tweezer set-up. **The results confirmed that the presence of surfactants should enhance droplet radius changes, in particular droplet growth.**

None of these results were expected before these studies, and they are generally contradicting many conventions in the disciplines. In addition, **they lead to calculations of Cloud Condensation Nuclei numbers, thus eventually cloud droplets, that are much larger (factor four) than when neglecting surfactants,** as it is currently done in all models. Thus, unlike what is currently believed in the community, taking into account surfactant effects should be important when predicting cloud formation and precipitation, and in the climate budget.

Several steps could be taken to further improve and validate the methods and applications presented in this work:

- identifying a better (more “universal”) dye to detect non-ionic surfactants and improving the extraction of cationic surfactants (which are often at the detection limit). This would lower the main source of uncertainties in the concentration measurements,
- intercomparing the surfactant concentrations obtained with the colorimetric method with those obtained with the electrochemical method (*e.g.* [Frka, 2012]),
- adding a separation step to eliminate UV- or fluorescent-active compounds from the extracts, to remove any potential contribution of HULIS.

Moreover, the investigations presented, in particular the correlations clouds / surfactants, would need to be performed at other locations and seasons to confirm our results.

As the role of surfactants on clouds is currently denied by most of the community, all these studies will probably be necessary to change the opinions.

However, while the topic of surfactants had been neglected for decades, it has been undergoing some fast changes in the last years, which might have been inspired by the work performed in this PhD work and the SONATA project. In particular, the role of surfactants in droplet growth was evidenced for the first time in laboratory and acknowledged by a journal with large impact factor [Ruehl, 2016]. And while, until recently, no technique was able to measure directly the surface tension of micron- or submicron-sized particles, several groups have now developed such techniques, either by atomic force microscopy [Morris *et al.* 2015] or optical tweezer [Bzdek, 2016; Reid, 2017 in preparation]. In particular, these works have now confirmed that, for a given concentration of surfactant, the surface tension measured on macroscopic samples is identical to that measured on micron-sized particles, thereby validating the methods in this PhD work. The optical tweezer studies have also confirmed the minute-long delay to equilibration of surfactants in micron-particles [Reid, 2017 in preparation] recently predicted from dynamic surface tension measurements of aerosol surfactants [Nozière, 2014]. These delays imply that classical instruments cannot measure surfactant effects and that, for decades, the absence of observation of surfactant effects in cloud formation was in fact due to instrumental artifacts. Even more recently, another group previously known for their study of the Raoult's term, has now started to study surfactants [Petters, 2016]. All this new interests for this topic might be indicating the beginning of a change in the community.

An important evolution that will be necessary to further investigate this topic is to modify the “on-line” instruments to allow them to detect surfactant effects (extend their measurement times). It will be also necessary to develop techniques to measure more directly the Raoult's term and the surface tension of atmospheric particles, as current techniques are too indirect and involve too many assumptions.

Finally, in parallel to demonstrating the effects of surfactants on clouds, the investigation of their origins will need to be pursued, by investigating chemical structures or correlations with biogenic tracers. Determining the exact size fraction in which surfactants are presents, by analyzing different particles sizes, for instance, could also help identifying their sources.

We hope that the present work and resulting interactions with the atmospheric community will be a decisive factor in the recognition of the role of chemistry, and in particular of surfactants, in cloud formation and properties.

8. Appendix

8.1. Reference surfactants

The list of reference surfactants used in this study is given in Table 8.1.

Table 8.1: Name, formula, CAS and molecular mass of reference surfactants used for the development of the extraction and analysis methods of surfactants in aerosols.

Name and formula	CAS	Molecular mass M (g mol ⁻¹)
SDS Sodium dodecyl sulfate C ₁₂ H ₂₅ NaO ₄ S	151-21-3	288.4
AOT Diocetyl sulfosuccinate sodium salt CH ₃ (CH ₂) ₃ CH(C ₂ H ₅)CH ₂ O ₂ CCH ₂ CH(SO ₃ Na)CO ₂ CH ₂ CH(C ₂ H ₅)(CH ₂) ₃ CH ₃	577-11-7	444.56
Zephiramine Benzyltetradecyldimethylammonium chloride CH ₃ (CH ₂) ₁₃ N(Cl)(CH ₃) ₂ CH ₂ C ₆ H ₅	139-08-2	368.04
CTAC Cetyltrimethylammonium chloride CH ₃ (CH ₂) ₁₅ N(Cl)(CH ₃) ₃	112-02-7	320.00
Triton X114 (1,1,3,3-Tetramethylbutyl)phenyl-polyethylene glycol (C ₂ H ₄ O) _n C ₁₄ H ₂₂ O, n = 7 or 8	9036-19-5	~537
Brij® 35 Polyethylene glycol dodecyl ether C ₁₂ H ₂₅ (OCH ₂ CH ₂) _n OH, n~23	9002-92-0	1199.54
L-α-Phosphatidylcholine from egg yolk 1,2-Diacyl-sn-glycero-3-phosphocholine	8002-43-5	~768
Surfactin from <i>Bacillus subtilis</i> C ₅₃ H ₉₃ N ₇ O ₁₃	24730-31-2	1036.34
Rhamnolipid Dirhamnolipid : Decanoic acid,3-((6-deoxy-2-O-(6-deoxy-alpha-L-mannopyranosyl)-alpha-L-mannopyranosyl)oxy)-,1-(carboxymethyl)octyl ester C ₃₂ H ₅₈ O ₁₃	4348.76-9	650.80
R-95Dd rhamnolipid (95 % dirhamnolipid, 5 % monorhamnolipid)	1492023-69-4	~ 643
Igepal CA-630* Nonylphenyl-polyethylenglycol, Octylphenoxy poly (ethyleneoxy) ethanol, branched (C ₂ H ₄ O) _n C ₁₄ H ₂₂ O	9002-93-1	~603

* used only for the study in Chapter 5

8.2. Chemicals used in the study

All of the chemicals used in the study were purchased directly from the manufacturers and used without further purification.

They included: Sodium dodecyl sulfate, ≥ 98.5 % Bioreagent, Sigma-Aldrich; Dioctyl sulfosuccinate sodium salt, 98 %, Aldrich; Benzyltetradecyldimethylammonium, ≥ 99.0 % anhydrous, Fluka; Cetyltrimethylammonium chloride solution, 25 wt % in H₂O, Aldrich; Triton X114, laboratory grade, Sigma-Aldrich; Brij35, Fluka Bio Chemika; L- α -phosphatidylcholine from egg yolk, type XVI-E, lyophilized powder, ≥ 99 %, Sigma-Aldrich; Surfactin from *Bacillus subtilis*, ≥ 98 %, Sigma-Aldrich; R-95Dd Rhamnolipid (95 % dirhamnolipid, 5 % monorhamnolipid) Aldrich; Igepal® CA-630 CMC 0.083 mM, Sigma-Aldrich; Ethyl violet, cationic triarylmethane dye, Sigma-Aldrich; Patent Blue VF, dye content 50 %, Sigma-Aldrich; Ammonium thiocyanate, ≥ 99 % puriss. p.a., ACS reagent; Sigma-Aldrich; Cobalt(II) nitrate hexahydrate, ≥ 98 % ACS reagent, Sigma-Aldrich; Sodium acetate, ≥ 99.0 % anhydrous Reagent Plus, Sigma-Aldrich; Ethylenediaminetetraacetic acid, 99.4 - 100.6 % ACS reagent powder, Sigma-Aldrich; Sodium sulfate anhydrous, ≥ 99.0 % granulated puriss. p.a. ACS reagent, Fluka; Ammonium thiocyanate, ≥ 99.5 % puriss. ACS reagent, Fluka Chemika Sigma-Aldrich; Ethanol puriss. p.a. ACS Reagent reagent Ph. Eur. 96 % (v/v), Sigma-Aldrich; Oxalic acid, ≥ 99 %, Aldrich; Ammonium sulfate, ≥ 99.0 % BioXtra; Sigma-Aldrich; Sodium chloride, ≥ 99.5 %, puriss. P.a., ACS reagent; Methanol, ≥ 99.9 % Chromasolv for HPLC, Sigma-Aldrich; acetonitrile, ≥ 99.9 % HiPerSolv Chromanorm Reagent Ph. Eur. (European Pharmacopoeia Reagent) grade gradient for HPLC, VWR BDH Prolabo; Chloroform (99 % stable) with 0.8–1 % ethanol, Alfa Aesar; Toluene, > 99 %, Chimie Plus.

8.3. Surface tension curves and surfactant properties (σ_{\min} , CMC) of reference surfactants

The surface tension curves and the comparison between reference surfactant properties (CMC and σ_{\min}) determined from the procedure detailed in Section 2.3.2 using thin needles are given in Figure 8.1 and Table 8.2. The surface tension curves, minimum surface tensions σ_{\min} , and CMCs obtained from the procedure used in this study were consistent with the literature.

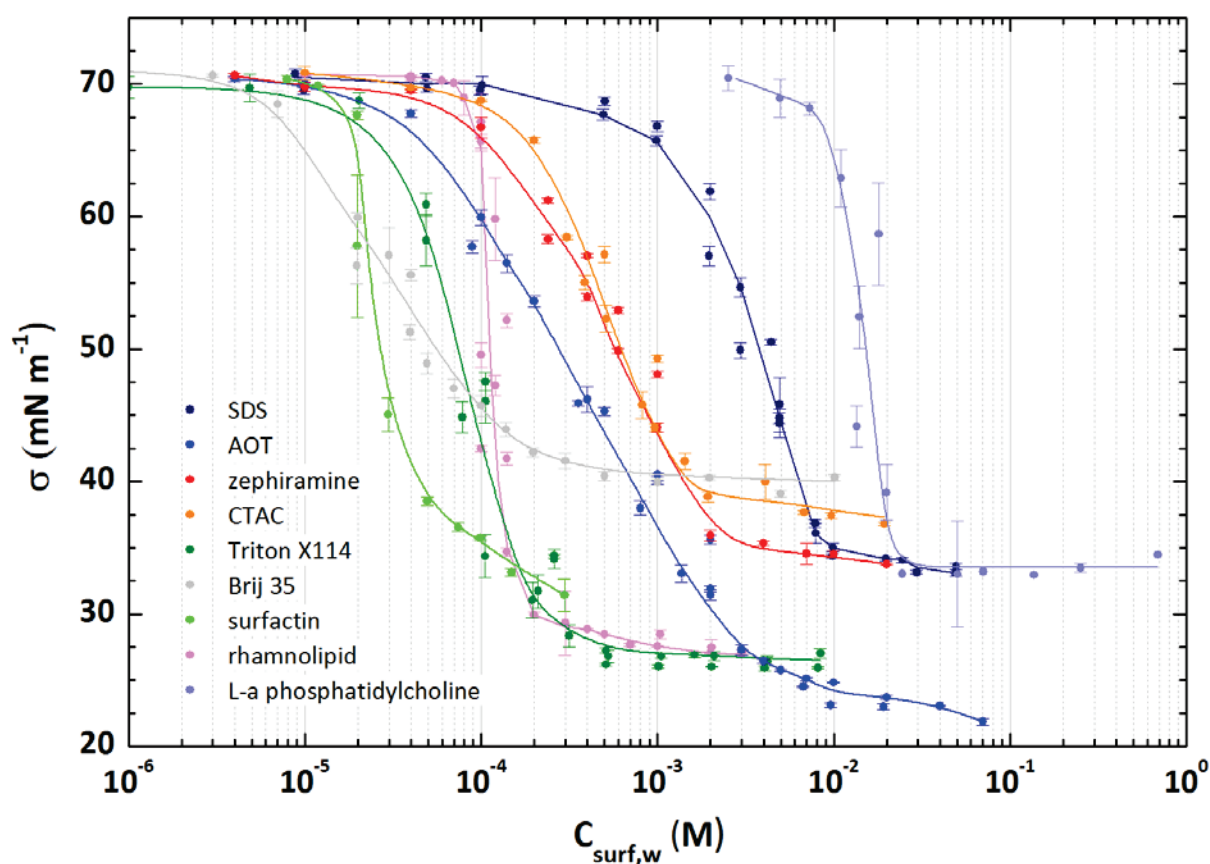


Figure 8.1: Surface tension curves of reference surfactants (listed in Sections 8.1 and 8.2) plotted as explained in Experimental Section 2.3.2.

Table 8.2: Comparison between experimental values of σ_{\min} and CMC of reference surfactants (listed in Sections 8.1 and 8.2) determined from experimental procedure described in Section 2.3.2 and values from literature, at room temperature. The differences can be attributed to differences of purity.

Surfactants	Experimental		In literature		Ref.*
	CMC (μM)	σ_{\min} (mN m^{-1})	CMC (μM)	σ_{\min} (mN m^{-1})	
SDS	8 000	33-34	5 000-10 000	30-37	a
AOT	3 200	22-26	600-10 000	32-33	b
Zephiramine	2 000	34-36	2 000		c
CTAC	1 400	37-39	1 300-3 000		d
Triton X114	200	26-28	200-300	31-33	e
Brij 35	150	40-42	30-100		f
L-a phosphatidylcholine	20 000	33-35	2 000-20 000	26-31	g
Surfactin	34	31-38	20-40 (until 500)	27-49	h
rhamnolipid	130	27-30	0.4-200	25-33	i

*

- a. [Mysels, 1986; Rana, 2002; Cheikh, 2005; Mitsionis, 2012]
- b. [Mohammad, 2004; Sansanwal, 2006; Mahajan, 2011; Mitsionis, 2012]
- c. [Asakawa, 2001; González-Pérez, 2003]
- d. [Asakawa, 2001; Asakawa, 2005; Cepeda, 2013]
- e. [Schulze, 1985]
- f. [Patist, 2000; Sansanwal, 2006]
- g. [Tausk, 1974; Eastoe, 1998]
- h. [Arima, 1968; Cooper, 1981; Bodour, 2003; Razafindralambo, 2004; Abdel-Mawgoud, 2008; Ekström, 2010]
- i. [Parra, 1989; Bodour, 2003; Helvacı, 2004; Costa, 2010; Ekström, 2010; Mańko, 2014]

8.4. Average and range of CMC values of surfactants in atmospheric aerosols and of reference surfactants

Table 8.3: Comparison of CMC between aerosol samples determined in this work and known microbial and artificial surfactants.

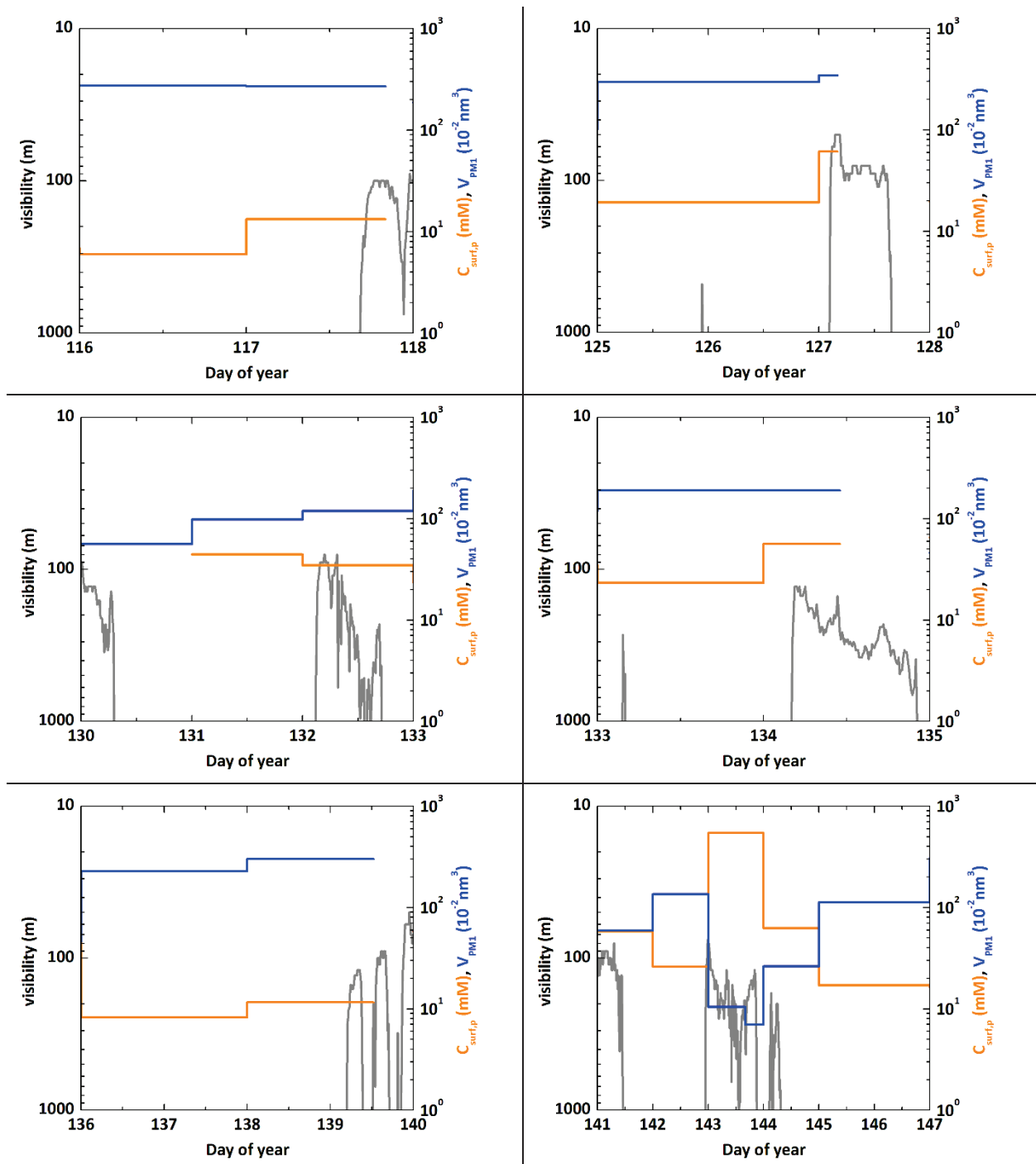
	Samples	Average CMC (μM)	Range of CMC (μM)	Number of samples
Aerosol samples	PM2.5, Askö, Sweden Coastal site July-October 2010	151 \pm 30	49 - 245	11 samples
	PM1, Villeurbanne, France Urban site December 2014-January 2015	1011 \pm 202	34 - 2171	14 samples
	PM1, Pallas-Sammaltunturi, Finland Boreal site April-November 2015	140 \pm 28	21 - 398	35 samples
Bacterial surfactants	Trehalose dicorynomycolate, surfactin, sophorolipids, viscosin, rhamnolipids		3 - 200 ^a	
Artificial surfactants	Triton X114, Tween 20, CTAC, zephiramine, AOT, SDS		200 - 10 000 ^b	

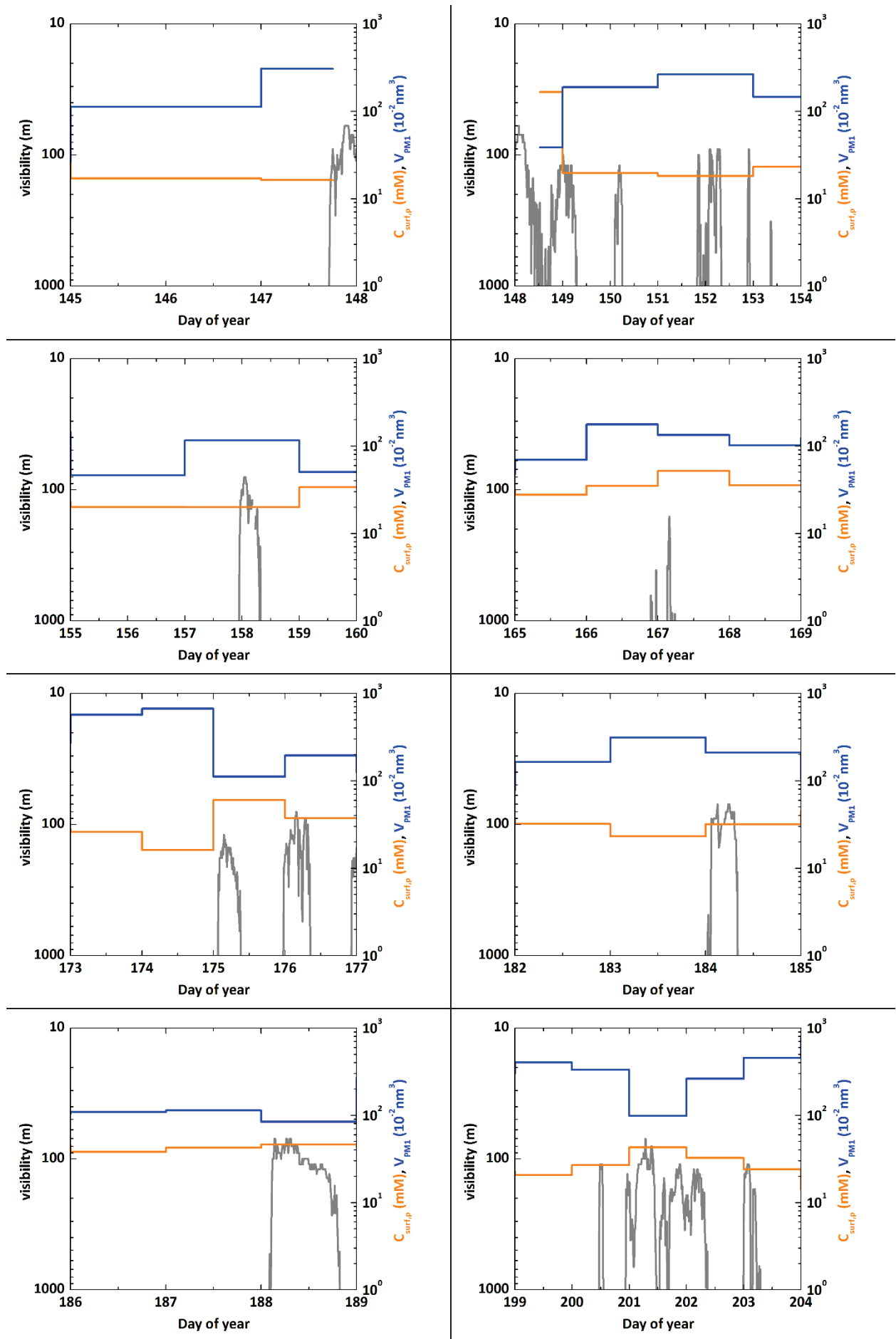
^a [Desai, 1997] and this work (Table 8.2 in Appendix Section 8.3)

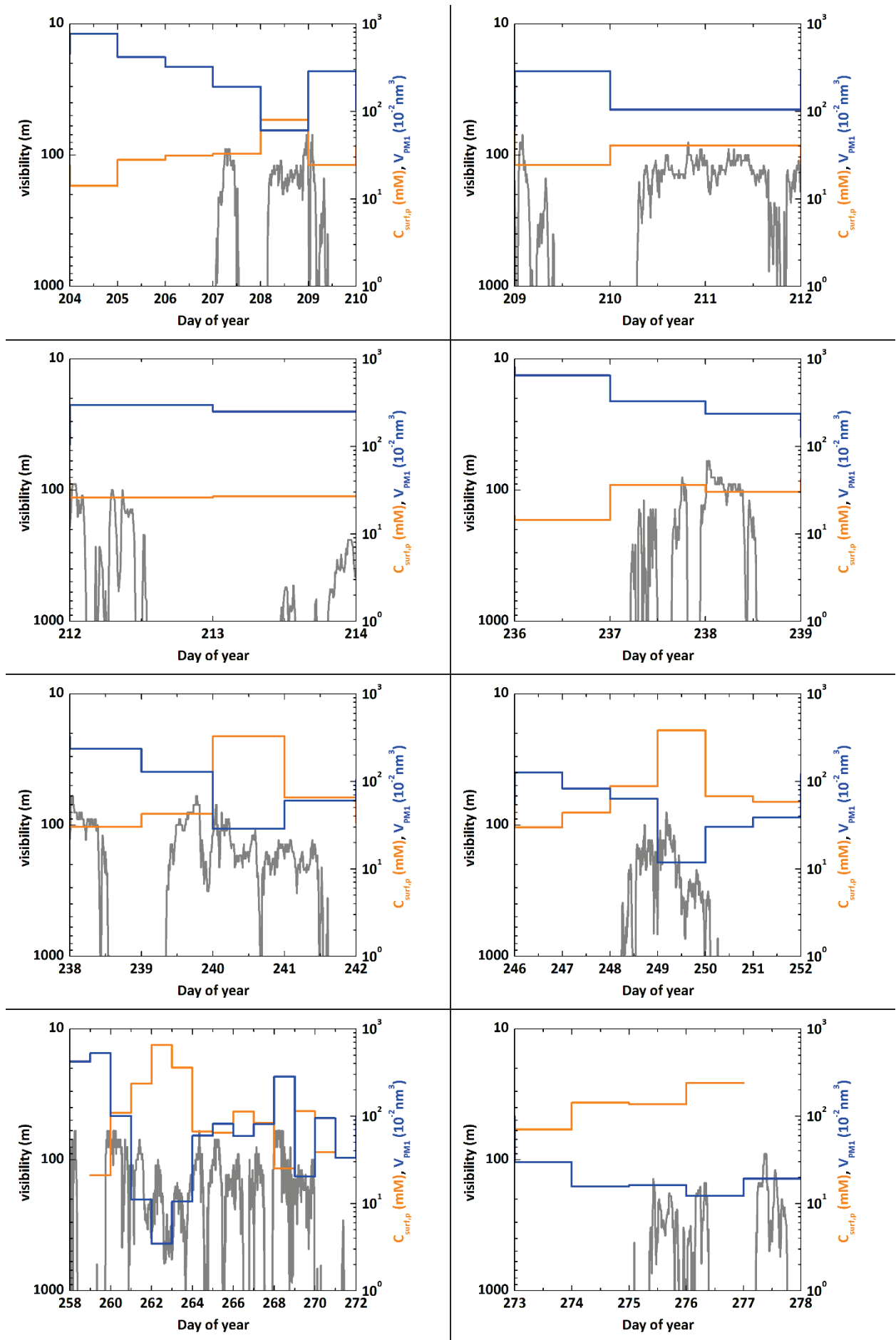
^b [Christofi, 2002] and this work (Table 8.2 in Appendix Section 8.3)

8.5. Real-time evolution of visibility and surfactant concentration in aerosols at Pallas-Sammaltunturi

Figure 8.2 gives the real time evolution of the visibility data and corresponding surfactant concentrations in aerosol particles volume and aerosol particles volume on filters for the different cloud events for the campaign at Pallas-Sammaltunturi.







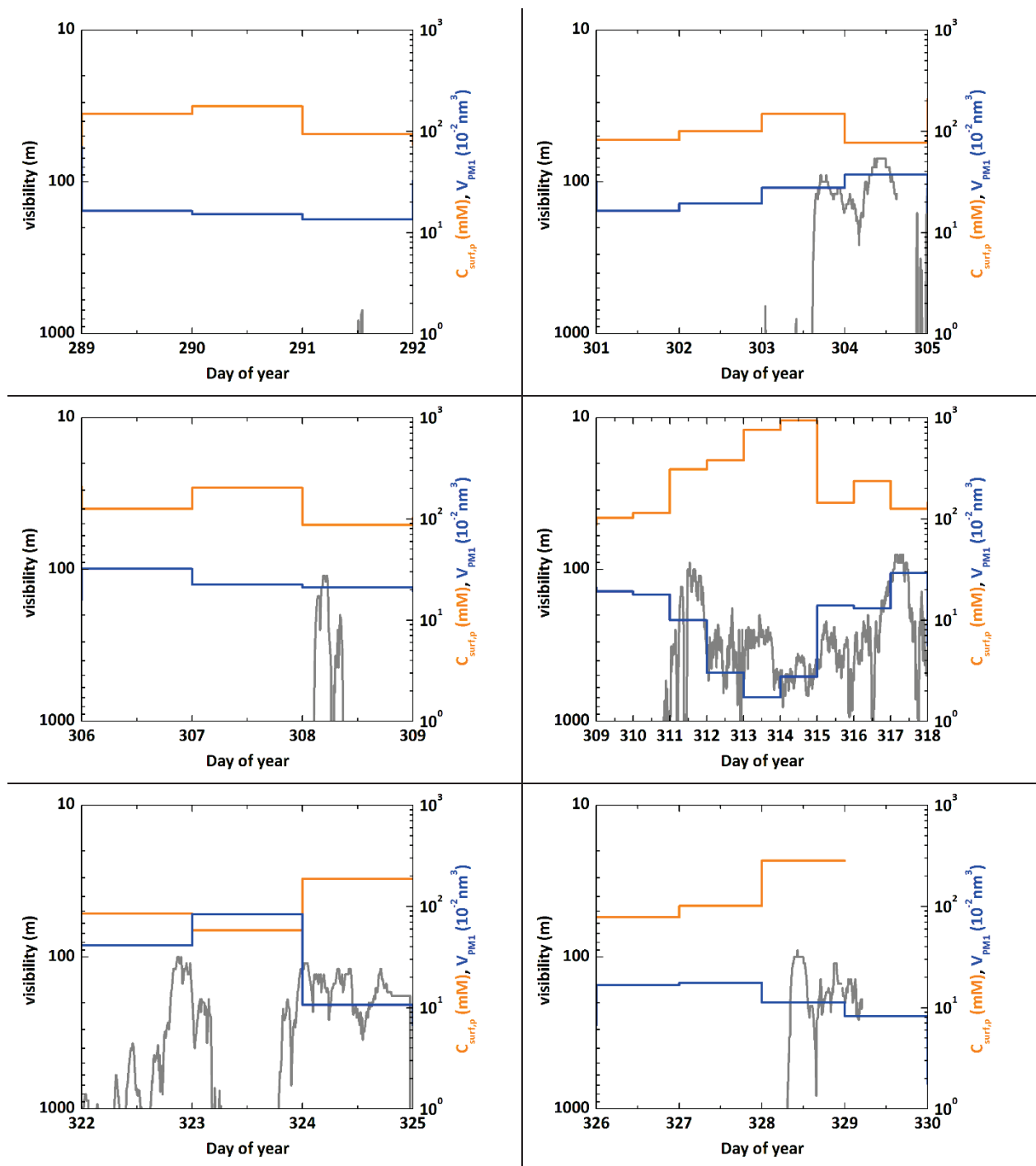


Figure 8.2: Real-time evolution of the visibility (m) (grey lines), the 24 h - averaged surfactant concentrations in aerosol particles volume, $C_{surf,p}$ (mM) (orange lines) and the PM1 volumes on filters, V_{PM1} (10^{-2} nm^3) (blue lines), for the 72 cloud events observed during the campaign at Pallas-Sammaltunturi [G erard, 2016 under review]

8.6. Back trajectories at Pallas-Sammaltunturi

Examples of back trajectories for each air mass type, classified by vegetation and seas, coming at Pallas-Sammaltunturi, are shown in Figure 8.3.

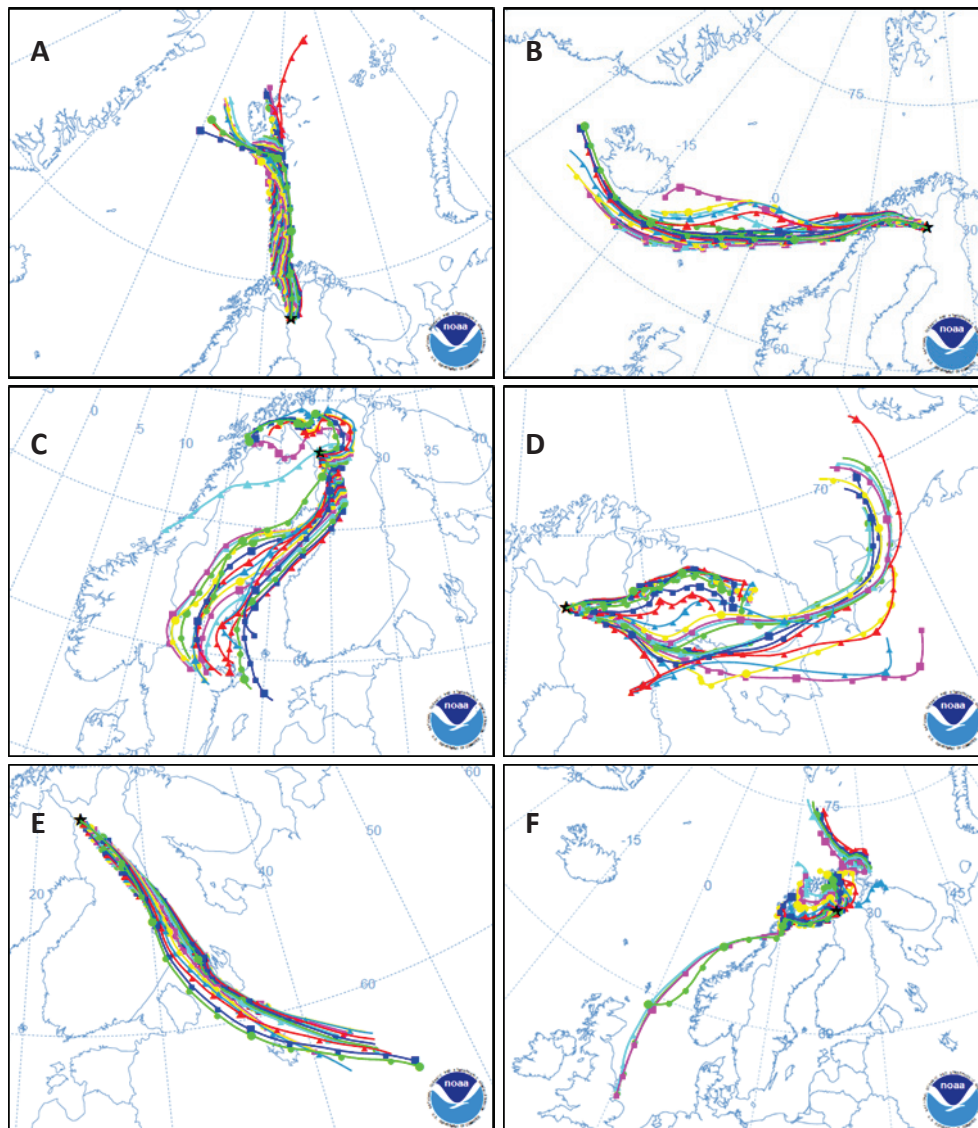


Figure 8.3: Example of 72 h - back trajectories arriving at the station Pallas-Sammaltunturi classified by vegetation and seas: (A) Arctic sea (05/07/15 22:00 UTC), (B) North Atlantic sea (13/08/15 22:00 UTC), (C) Baltic sea (22/08/15 22:00 UTC), (D) boreal vegetation (26/07/15 22:00 UTC), (E) temperate vegetation (18/11/16 UTC+2) and (F) Tundra (03/07/15 22:00 UTC). The trajectories were obtained from HYSPLIT back trajectories [Draxler, 2015; Rolph, 2015]: source at 67.97N 24.12E, 72 h -back trajectories (with a new trajectories starting every three hours during the 72h), model vertical velocity, height 10 m AGL (above ground level).

9. Résumé étendu de la thèse en français

La formation des nuages est essentielle dans le cycle de l'eau et demeure le principal facteur refroidissant du budget climatique, mais elle est également la plus grande source d'incertitude. Les processus de formation ne sont pas encore totalement compris, notamment le rôle des composés chimiques et en particulier celui des surfactants. La formation des gouttes de nuage à partir des particules d'aérosols est dictée par la théorie de Köhler qui ne repose que sur deux facteurs: le terme de Raoult, reliant la pression de vapeur d'eau à la composition volumique des particules, et la tension de surface des gouttelettes qui peut être affectée par la présence de molécules surfactantes. Cependant le rôle des surfactants n'est actuellement pas pris en compte dans les modèles prédisant la formation des gouttes de nuage; la tension de surface est alors considérée comme celle de l'eau pure. Au moment de ce travail de thèse, quelques études avaient commencé à apporter des preuves du contraire par des expériences en laboratoire et sur des aérosols atmosphériques. En effet, des études ont démontré l'importance des surfactants dans le grossissement des gouttes de nuage en laboratoire et la présence de surfactants forts a été mise en évidence dans des aérosols atmosphériques. Mais jusqu'à ce jour aucune étude n'avait apporté de preuves directes, dans l'atmosphère, du rôle des surfactants dans la formation des gouttes de nuage.

Ainsi le but de cette étude, présentée dans cette thèse, était notamment de prouver le rôle des surfactants dans la formation des nuages par l'étude de leurs propriétés et concentrations dans les aérosols atmosphériques et de leurs liens avec les nuages. De plus l'origine des surfactants dans les aérosols, suspectés d'être d'origine biologique, a été étudiée.

Le premier chapitre présente le contexte scientifique. L'atmosphère terrestre, où les nuages se forment, y est brièvement décrite, ainsi que leur importance. Ensuite la formation des gouttes de nuage est expliquée : les gouttes ne se forment que sur des petites particules d'aérosols atmosphériques appelées « noyaux de condensation » et leur grossissement est contrôlé par l'équation de Köhler [Köhler, 1936] qui dépend, en dehors de la taille des particules initiales, du terme de Raoult et de la tension de surface, dont les valeurs dépendent de la composition chimique de l'aérosol. Dans cette partie, les mesures actuellement

effectuées sur le terrain et en laboratoire, pour l'étude de l'activation et le grossissement des aérosols en gouttes de nuage, sont également discutées ainsi que leurs limites et les développements récents. Ensuite ce chapitre introduit les surfactants et leurs propriétés étudiées dans cette étude. Puis l'état actuel des connaissances des surfactants dans les aérosols atmosphériques est présenté. Enfin les objectifs de cette étude sont définis. Il s'agit 1) de mettre en évidence le rôle des surfactants dans la formation des nuages et de caractériser leur mécanisme d'action (caractérisation de leurs propriétés dans les aérosols et preuves directes dans l'atmosphère de leur lien avec l'apparition de nuages) et 2) de déterminer leur origine.

Le deuxième chapitre détaille le principe et la procédure expérimentale de chaque méthode utilisée dans cette étude. Ces méthodes incluent en particulier : l'échantillonnage des aérosols atmosphériques et les différents sites de mesure, l'extraction des surfactants de ces aérosols, les mesures de tension de surface par méthode de la goutte pendante et la détermination de la concentration en surfactants dans les extraits par méthodes colorimétriques amenant à des courbes de tension de surface absolues. Il est à noter qu'une partie importante de cette étude était le développement de ces méthodes. Pour l'étude, les techniques suivantes ont également été employées : la fluorescence, la caractérisation chimique des surfactants par chromatographie liquide couplée à la spectrométrie de masse en tandem et l'étude de gouttes microscopiques par pince optique associée à la spectrométrie Raman. De plus, des données atmosphériques et géophysiques ont été utilisées : la concentration en chlorophylle-*a* dans la mer obtenue par des données satellites, les sources des masses d'air par modèle HYSPLIT, la présence de nuages par mesures de visibilité, la mesure de la distribution en taille des particules pour le volume d'aérosols et les calculs du nombre de particules activées en gouttes de nuage.

Les chapitres 3 à 6 présentent les différentes études répondant à la problématique de cette thèse.

Le troisième chapitre présente le développement et l'application de la méthode pour l'extraction et l'analyse des propriétés et concentrations des surfactants dans les aérosols atmosphériques. Cette première étude a été effectuée sur des aérosols atmosphériques de

zone côtière PM_{2.5} (particules de diamètre < 2.5 µm) provenant de la station d'Askö en Suède. Elle a permis notamment de mettre en évidence des surfactants forts dans les aérosols atmosphériques avec des concentrations suffisantes pour que la tension de surface des gouttes de nuage reste basse même au moment de l'activation, ce qui devrait favoriser la formation des gouttes.

Le quatrième chapitre poursuit l'étude du troisième chapitre, c'est-à-dire l'extraction et l'analyse des propriétés et concentrations des surfactants dans les aérosols atmosphériques, mais va plus loin puisqu'elle amène pour la première fois des preuves directes dans l'atmosphère, de l'effet des surfactants dans la formation des nuages. En effet, cette étude appliquée sur des aérosols PM₁ (particules de diamètre < 1 µm) provenant de la station boréale Pallas-Sammaltunturi en Finlande, un site fréquemment impacté par la présence de nuages, a montré qu'à ce site l'apparition de nuages était fortement corrélée à la concentration et aux propriétés des surfactants. Cette corrélation est notamment importante au niveau du ratio de la concentration en surfactants dans les particules sur la CMC (Concentration Micellaire Critique), paramètre intrinsèque des surfactants obtenu par la détermination de courbes de tensions de surface absolues, qui semble être un facteur critique déclencheur de la formation des gouttes. Des calculs ont également mis en évidence l'importance de prendre en compte la tension de surface réelle des aérosols et non celle de l'eau pure comme considérée actuellement dans les modèles. En effet, négliger les surfactants sous-estime quantitativement le nombre de gouttes de nuage prédit.

Le cinquième chapitre se concentre sur l'effet des surfactants en laboratoire sur des gouttes individuelles microniques produites par une pince optique par faisceau laser couplée à la spectrométrie Raman dans une cellule à température et humidité contrôlées. En effet les études du troisième et du quatrième chapitre ont été réalisées à une échelle macroscopique alors que les gouttes de nuages se forment à une échelle microscopique ou sous-microscopique. Il était donc nécessaire de vérifier que les effets des surfactants restaient vrais à cette échelle. Cette étude a permis alors de montrer que la présence de surfactants, aux propriétés similaires à celles trouvées dans les aérosols atmosphériques, conduisait à un changement du rayon des gouttes supérieur à celui des gouttes n'en contenant pas, quand elles étaient soumises à des changements d'humidité dans la cellule de mesure. Ce résultat a

permis de confirmer la fiabilité des résultats des chapitres précédents qui avaient été déterminés à une échelle macroscopique.

Le sixième chapitre s'intéresse à l'origine des surfactants dans les aérosols atmosphériques. En effet, puisque l'importance des surfactants pour la formation des nuages a été démontrée dans les chapitres précédents, il est nécessaire de connaître leur origine pour mieux comprendre les mécanismes mis en jeu entre atmosphère et biologie. Puisque les surfactants étaient suspectés être d'origine biologique, différentes approches ont été utilisées pour démontrer cette origine. Les propriétés des surfactants ont été comparées à des surfactants de référence, à des marqueurs biologiques (chlorophylle-*a*) ou encore aux sources des masses d'air apportant les aérosols; la structure chimique des surfactants extraits des aérosols a également été étudiée. Les résultats ont montré que ces surfactants étaient des macromolécules et ont commencé à démontrer leur origine biologique.

Enfin le septième chapitre vient résumer les travaux décrits et leurs perspectives. Les études présentées dans cette thèse ont permis une grande avancée dans le domaine de la formation des nuages. En effet, par le développement d'une méthode d'extraction et d'analyse des surfactants dans les aérosols atmosphériques, pour la première fois, des preuves de l'importance des surfactants dans la formation des gouttes de nuage à partir de mesures directes dans l'atmosphère ont été apportées. De plus les travaux récents effectués par d'autres groupes viennent confirmer nos conclusions. Cela souligne l'importance de prendre en compte l'effet des surfactants dans les modèles prédisant la formation des nuages. Pour aller plus loin, ces études devraient être réalisées sur d'autres sites afin d'obtenir une vision plus globale du rôle des surfactants dans l'atmosphère. Une meilleure compréhension de la formation des nuages devrait être bénéfique pour les prédictions météorologiques, hydrologiques et climatiques.

10. Acknowledgments

10.1. Funding

This project was mostly funded by the French Agence Nationale de la Recherche (ANR) and U.S. National Science Foundation (NSF) on a joint ANR-NSF project (SONATA project 2013-2016, ANR-13-IS08-0001 and NSF-International Collaboration in Chemistry (1303763)).



This PhD work was mainly carried out at IRCELYON (Institut de recherches sur la catalyse et l'environnement de Lyon, UMR 5256), CNRS, Université Claude Bernard Lyon 1, France, and a part was carried out at the Department of Chemistry, University of California, Berkeley, USA, and at the ICCF (Institut de Chimie de Clermont-Ferrand, UMR 6296), CNRS, University of Clermont-Ferrand, France.



Institut de recherches sur la catalyse et l'environnement de Lyon **IRCELYON**



College of Chemistry
UNIVERSITY OF CALIFORNIA, BERKELEY



**Institut de Chimie de
Clermont-Ferrand**

10.2. People

I would like to thank my supervisor at IRCELYON, Dr. Barbara Nozière, for having given me the opportunity to complete my PhD thesis on a hot topic in the atmospheric field that made this work really exciting. Moreover I would like to thank her for her scientific expertise in the field of atmospheric chemistry, her continuous enthusiasm for the research, for the autonomy she has given to me, and particularly for letting me carrying out experiments and conducting field campaigns in collaboration with people from different research groups and countries; this was a very enriching experience!

I also would like to thank warmly our partners for this project.

Thanks to Ronald C. Cohen, Professor at the Department of Chemistry and of Earth and Planetary Science at the University of California, Berkeley, USA, and Amanda A. Frossard, postdoctoral researcher from his research group, for their warm welcome in their laboratory during a few weeks, their collaboration on the project and their fruitful scientific discussions. I thank also Amanda for her help with the optical trap in Berkeley, the experiments in Lyon, for her advices and friendly support.

Thanks to Anne-Marie Delort, Director of the ICCF (Institut de Chimie de Clermont-Ferrand, UMR 6296), CNRS, France, and Pascal Renard, postdoctoral researcher from her research group, for their collaboration and fruitful discussions on the investigation of surfactant structures.

Moreover I would like to thank the other people who contribute to this project during my PhD.

For their help during the field campaign at Pallas-Sammaltunturi in Finland and their contribution to the data treatment of this campaign, thanks to Eija Asmi, Niku Kivekäs, David Brus, Kimmo Neitola, Konstantinos Doulgeris, Minna Aurela, Juha Hatakka, Matti Monto, Heikki Lihavainen, Priit Tisler from FMI (Finnish Meteorological Institute), Helsinki, Finland; Ahti Ovaskainen, Sami Lapinniemi and Päivi Pietikäinen from Metsä/Metla, Muonio, Finland;

Keri Nicoll and Giles Harrison from Reading University, UK; Petr Vodicka from Institute of Chemical Process Fundamentals, Prague, Czech Republic.

For preliminary tests done on the aerosol sampler on the roof of their building, thanks to the IPNL (Institut de Physique Nucléaire de Lyon), University Claude Bernard Lyon 1, France.

For their help during a field campaign at Marina Frapa, Rogoznica, Croatia, whose preliminary analysis and equipment challenges contributed to prepare at best the field campaign in Finland, thanks to Marija Marguš, Ana Cvitešić, Sanja Frka Milosavljević and Irena Ciglenceki, from “Division for marine and environmental research” at the Rudjer Boskovic Institute of Zagreb, Croatia.

For the fluorescence experiments, thanks to Didier Fournier and Julie Bertrand from “Plateforme travaux-pratiques du Master Analyse et Contrôle”, Bâtiment Berthollet, University Claude Bernard Lyon 1, France.

For the LC-MS/MS measurements at ICCF (Institut de Chimie de Clermont-Ferrand), France, thanks to Martin Lereboure from “Service de spectrométrie de masse”.

I thank also the members of the PhD defense committee who honored me by accepting to examine my work. Thanks to Anne-Marie Delort, Director of the ICCF (Institut de Chimie de Clermont-Ferrand, UMR 6296), CNRS, France and to Ronald C. Cohen, Professor at the Department of Chemistry and of Earth and Planetary Science at the University of California, Berkeley, USA (reviewers of this PhD thesis). Thanks also to Corinne Ferronato, “Maitre de Conférence” at IRCELYON (Institut de recherches sur la catalyse et l'environnement de Lyon), CNRS, UMR 5256, France, and to Didier Léonard, Professor at ISA (Institute of Analytical Sciences), UMR 5280, University Claude Bernard Lyon 1, France.

Furthermore, I would like to express my deep gratitude to my colleagues at IRCELYON who created a pleasant work atmosphere by their kindness, help and support. Thanks to the non-permanent staff Aurelia Maxut, Liselotte Tinel, Maxime Français, Diego Lopez Gonzalez, Adrien Serve, Stéphanie Rossignol, Beatriz Delgado, Alexandre Westermann, Badr R’Mili, José “Nico” Diaz, Didier Grondin, Monica Passananti, Jesus Garcia-Vargas, Géraldine Ferré, Alvaro

10. Acknowledgments

Martinez-Valiente, Paola Anguita, Hayfa Jannadi, Milena Ponczek, Nathalie Hayeck, Martin Brüggerman, Andreas Ganzler, Ioanna Kalaitzidou, Guillaume Pétaud, Peter Alpert, Vincent Frizzon, Loic Gonzalez, Aurélie Même, Liliane Ismail, Lina Laama, Lei Zhou, Chunhua Zhao, Kifle Aregahegn, Marc Mallet, Roeland Jansen, Chao Wang, Raluca Ciuraru, Nayeli Pineda, Quentin Andries, Mariana Simoes-Botto-Dos-Santos-Oliveira, Foteini Sapountzi, Mihalis Tsampas, the permanent scientific staff Sonia Gil-Villarino, Nicolas Charbonnel, Ludovic “Michel” Fine, Corinne Ferronato, Christian George, Antoinette Boréave, Laurence Retailleau-Mevel, Sébastien Perrier, Philippe Vernoux, Barbara D’Anna, Jean-Marc Chovelon, Anne Giroir-Fendler, and the other members of the Institute Sébastien Albert, Christine Delbecque, Evelyne Bonhomme, Anne-Marie Grézaud, Narayman El-Jerrari, Marie-Laure Venditti, Christine Babolat, Géraldine Chapuis and because this list is not exhaustive, all the members of the Institute.

I am also extremely grateful to my family for their constant support throughout the years, and to Joffrey Huve, who supported me every day during these three years!

Finally, I thank all people who directly or indirectly contributed to the completion of this PhD work.



11. References

- Aalto, T., Hatakka, J., Paatero, J., Tuovinen, J.-P., Aurela, M., Laurila, T., Holmén, K., Trivett, N., and Viisanen, Y., **2002**: Tropospheric carbon dioxide concentrations at a northern boreal site in Finland: basic variations and source areas. *Tellus*, 54(B), 110-126.
- Abdel-Mawgoud, A. M., Aboulwafa, M. M., and Hassouna, N. A.-H., **2008**: Characterization of Surfactin Produced by *Bacillus subtilis* Isolate BS5. *Applied Biochemistry and Biotechnology*, 150(3), 289-303.
- Adams, J. M., and Faure, H., **1997**, cited 2016: "Vegetation map of Europe, Quaternary Environments Network (QEN)", Review and Atlas of Palaeovegetation: Preliminary land ecosystem maps of the world since the Last Glacial Maximum. Oak Ridge National Laboratory, TN, USA. [Available online at <http://www.esd.ornl.gov/projects/qen/eur%28pre.gif>].
- Ahern, H. E., Walsh, K. A., Hill, T. C. J., and Moffett, B. F., **2007**: Fluorescent pseudomonads isolated from Hebridean cloud and rain water produce biosurfactants but do not cause ice nucleation. *Biogeosciences*, 4(1), 115-124.
- Aitken, J., **1880**: On Dust, Fogs, and Clouds. *Nature*, 23, 195-197.
- Amato, P., Parazols, M., Sancelme, M., Laj, P., Mailhot, G., and Delort, A.-M., **2007a**: Microorganisms isolated from the water phase of tropospheric clouds at the Puy de Dôme: major groups and growth abilities at low temperatures. *FEMS Microbiology Ecology*, 59(2), 242-254.
- Amato, P., Demeer, F., Melaouhi, A., Fontanella, S., Martin-Biesse, A. S., Sancelme, M., Laj, P., and Delort, A. M., **2007b**: A fate for organic acids, formaldehyde and methanol in cloud water: their biotransformation by micro-organisms. *Atmospheric Chemistry and Physics*, 7(15), 4159-4169.
- Amirov, R. R., Skvortsova, E. A., and Saprykova, Z. A., **2003**: Complexation of Cobalt(II) with Thiocyanate Ions in Aqueous Solutions of Nonionogenic Surfactants. *Russian Journal of Coordination Chemistry*, 29(8), 554-558.
- AMS, **2016**, cited 2016: Climatology. Glossary of Meteorology (American Meteorological Society). [Available online at http://glossary.ametsoc.org/wiki/Cloud_classification].
- Andreae, M. O., and Rosenfeld, D., **2008**: Aerosol-cloud-precipitation interactions. Part 1. The nature and sources of cloud-active aerosols. *Earth-Science Reviews*, 89(1-2), 13-41.
- Andreas, J. M., Hauser, E. A., and Tucker, W. B., **1938**: Boundary tension by pendant drops. *The Journal of Physical Chemistry*, 42(8), 1001-1019.

- Anttila, T., Brus, D., Jaatinen, A., Hyvärinen, A. P., Kivekäs, N., Romakkaniemi, S., Komppula, M., and Lihavainen, H., **2012**: Relationships between particles, cloud condensation nuclei and cloud droplet activation during the third Pallas Cloud Experiment. *Atmospheric Chemistry and Physics*, 12(23), 11435-11450.
- Arima, K., Kakinuma, A., and Tamura, G., **1968**: Surfactin, a crystalline peptidelipid surfactant produced by *Bacillus subtilis*: Isolation, characterization and its inhibition of fibrin clot formation. *Biochemical and Biophysical Research Communications*, 31(3), 488-494.
- Asa-Awuku, A., Sullivan, A. P., Hennigan, C. J., Weber, R. J., and Nenes, A., **2008**: Investigation of molar volume and surfactant characteristics of water-soluble organic compounds in biomass burning aerosol. *Atmospheric Chemistry and Physics*, 8(4), 799-812.
- Asakawa, T., Kitano, H., Ohta, A., and Miyagishi, S., **2001**: Convenient Estimation for Counterion Dissociation of Cationic Micelles Using Chloride-Sensitive Fluorescence Probe. *Journal of Colloid and Interface Science*, 242(2), 284-287.
- Asakawa, T., Kubode, H., Ozawa, T., Ohta, A., and Miyagishi, S., **2005**: Micellar Counterion Binding Probed by Fluorescence Quenching of 6-methoxy-N-(3-sulfopropyl)quinolinium. *Journal of Oleo Science*, 54(10), 545-552.
- Ashkin, A., Dziedzic, J. M., Bjorkholm, J. E., and Chu, S., **1986**: Observation of a single-beam gradient force optical trap for dielectric particles. *Optics Letters*, 11(5), 288-290.
- Aumann, E., Hildemann, L. M., and Tabazadeh, A., **2010**: Measuring and modeling the composition and temperature-dependence of surface tension for organic solutions. *Atmospheric environment*, 44(3), 329-337.
- Baduel, C., Nozière, B., and Jaffrezo, J.-L., **2012**: Summer/winter variability of the surfactants in aerosols from Grenoble, France. *Atmospheric environment*, 47, 413-420.
- Bashforth, F., and Adams, J. C., **1883**: *An Attempt to test the theories of capillary action by comparing the theoretical and measured forms of drops of fluid*. University Press, Cambridge, England.
- Berrueta, L. A., Gallo, B., and Vicente, F., **1995**: A review of solid phase extraction: Basic principles and new developments. *Chromatographia*, 40(7), 474-483.
- Biolin-Scientific, **2016**, cited 2016: Precision Tensiometers, Measurements. [Available online at <http://www.biolinscientific.com/application/critical-micelle-concentration-measurement>].
- Bodour, A. A., Drees, K. P., and Maier, R. M., **2003**: Distribution of Biosurfactant-Producing Bacteria in Undisturbed and Contaminated Arid Southwestern Soils. *Applied and Environmental Microbiology*, 69(6), 3280-3287.

- Bones, D. L., Reid, J. P., Lienhard, D. M., and Krieger, U. K., **2012**: Comparing the mechanism of water condensation and evaporation in glassy aerosol. *Proceedings of the National Academy of Sciences*, 109(29), 11613-11618.
- Boucher, O., **2012**: *Aérosols atmosphériques Propriétés et impacts climatiques*. Springer Paris.
- Boucher, O., Randall, D., Artaxo, P., Bretherton, C., Feingold, G., Forster, P., Kerminen, V.-M., Kondo, Y., Liao, H., Lohmann, U., Rasch, P., Satheesh, S. K., Sherwood, S., Stevens, B., and Zhang, X. Y., **2013**: Clouds and Aerosols. *Climate Change 2013: The Physical Science Basis. Contribution of Working Group I to the Fifth Assessment Report of the Intergovernmental Panel on Climate Change*, T. F. Stocker, D. Qin, G.-K. Plattner, M. Tignor, S. K. Allen, J. Boschung, A. Nauels, Y. Xia, V. Bex, and P. M. Midgley, Eds., Cambridge University Press, Cambridge, United Kingdom and New York, NY, USA.
- Buajarnern, J., Mitchem, L., and Reid, J. P., **2007a**: Characterizing Multiphase Organic/Inorganic/Aqueous Aerosol Droplets. *The Journal of Physical Chemistry A*, 111(37), 9054-9061.
- Buajarnern, J., Mitchem, L., and Reid, J. P., **2007b**: Characterizing the Formation of Organic Layers on the Surface of Inorganic/Aqueous Aerosols by Raman Spectroscopy. *The Journal of Physical Chemistry A*, 111(46), 11852-11859.
- Buajarnern, J., Mitchem, L., and Reid, J. P., **2007c**: Manipulation and Characterization of Aqueous Sodium Dodecyl Sulfate/Sodium Chloride Aerosol Particles. *The Journal of Physical Chemistry A*, 111(50), 13038-13045.
- Bzdek, B. R., Power, R. M., Simpson, S. H., Reid, J. P., and Royall, C. P., **2016**: Precise, contactless measurements of the surface tension of picolitre aerosol droplets. *Chemical Science*, 7(1), 274-285.
- Capel, P. D., Gunde, R., Zuercher, F., and Giger, W., **1990**: Carbon speciation and surface tension of fog. *Environmental Science & Technology*, 24(5), 722-727.
- Cepeda, M., Davina, R., Garcia-Rio, L., Parajo, M., Rodriguez-Dafonte, P., and Pessego, M., **2013**: Competition between surfactant micellization and complexation by cyclodextrin. *Organic & Biomolecular Chemistry*, 11(7), 1093-1102.
- Cheikh, C., and Koper, G., **2005**: Friction in surfactant layers at solid-liquid interfaces. *Colloids and Surfaces A: Physicochemical and Engineering Aspects*, 270-271(0), 252-256.
- Chen, Q., Ikemori, F., Higo, H., Asakawa, D., and Mochida, M., **2016**: Chemical Structural Characteristics of HULIS and Other Fractionated Organic Matter in Urban Aerosols: Results from Mass Spectral and FT-IR Analysis. *Environmental Science & Technology*, 50(4), 1721-1730.
- Christofi, N., and Ivshina, I. B., **2002**: Microbial surfactants and their use in field studies of soil remediation. *Journal of Applied Microbiology*, 93(6), 915-929.

- Chu, M., and Wan, Y., **2009**: Sentinel lymph node mapping using near-infrared fluorescent methylene blue. *Journal of Bioscience and Bioengineering*, 107(4), 455-459.
- Colbeck, I., **1998**: *Physical and chemical properties of aerosols*. Blackie Academic & Professional.
- Cooper, D. G., Macdonald, C. R., Duff, S. J. B., and Kosaric, N., **1981**: Enhanced Production of Surfactin from *Bacillus subtilis* by Continuous Product Removal and Metal Cation Additions. *Applied and Environmental Microbiology*, 42(3), 408-412.
- Costa, S. G. V. A. O., Nitschke, M., Lépine, F., Déziel, E., and Contiero, J., **2010**: Structure, properties and applications of rhamnolipids produced by *Pseudomonas aeruginosa* L2-1 from cassava wastewater. *Process Biochemistry*, 45(9), 1511-1516.
- Davies, J. F., Haddrell, A. E., Miles, R. E. H., Bull, C. R., and Reid, J. P., **2012**: Bulk, Surface, and Gas-Phase Limited Water Transport in Aerosol. *The Journal of Physical Chemistry A*, 116(45), 10987-10998.
- Delort, A.-M., Vaïtilingom, M., Amato, P., Sancelme, M., Parazols, M., Mailhot, G., Laj, P., and Deguillaume, L., **2010**: A short overview of the microbial population in clouds: Potential roles in atmospheric chemistry and nucleation processes. *Atmospheric Research*, 98(2-4), 249-260.
- Dennis-Smith, B. J., Miles, R. E. H., and Reid, J. P., **2012**: Oxidative aging of mixed oleic acid/sodium chloride aerosol particles. *Journal of Geophysical Research: Atmospheres*, 117(D20), D20204.
- Desai, J. D., and Banat, I. M., **1997**: Microbial production of surfactants and their commercial potential. *Microbiology and Molecular Biology Reviews*, 61(1), 47-64.
- Digitel, **2014**: DIGITEL High Volume Aerosol Sampler Manual Version Hxx.50 March 2014.
- Draxler, R. R., and Rolph, G. D., **2015**: HYSPLIT (HYbrid Single-Particle Lagrangian Integrated Trajectory) Model access via NOAA ARL READY Website [Available online at <http://ready.arl.noaa.gov/HYSPLIT.php>] NOAA Air Resources Laboratory, Silver Spring, MD.
- Duplissy, J., Gysel, M., Sjogren, S., Meyer, N., Good, N., Kammermann, L., Michaud, V., Weigel, R., Martins dos Santos, S., Gruening, C., Villani, P., Laj, P., Sellegri, K., Metzger, A., McFiggans, G. B., Wehrle, G., Richter, R., Dommen, J., Ristovski, Z., Baltensperger, U., and Weingartner, E., **2009**: Intercomparison study of six HTDMAs: results and recommendations. *Atmospheric Measurement Techniques*, 2(2), 363-378.
- Eastoe, J., Dalton, J. S., and Heenan, R. K., **1998**: Dynamic Surface Tensions and Micelle Structures of Dichained Phosphatidylcholine Surfactant Solutions. *Langmuir*, 14(20), 5719-5724.

- Ekström, S., Nozière, B., and Hansson, H. C., **2009**: The Cloud Condensation Nuclei (CCN) properties of 2-methyltetrols and C3-C6 polyols from osmolality and surface tension measurements. *Atmospheric Chemistry and Physics*, 9(3), 973-980.
- Ekström, S., Nozière, B., Hultberg, M., Alsberg, T., Magnér, J., Nilsson, E. D., and Artaxo, P., **2010**: A possible role of ground-based microorganisms on cloud formation in the atmosphere. *Biogeosciences*, 7(1), 387-394.
- Encyclopædia-Britannica, **2016**, cited 2016: Types of clouds and heights of formation. Art. Britannica Online for Kids. [Available online at <http://kids.britannica.com/elementary/art-87616>.]
- Facchini, M. C., Mircea, M., Fuzzi, S., and Charlson, R. J., **1999**: Cloud albedo enhancement by surface-active organic solutes in growing droplets. *Nature*, 401, 257-259.
- Facchini, M. C., Decesari, S., Mircea, M., Fuzzi, S., and Loglio, G., **2000**: Surface tension of atmospheric wet aerosol and cloud/fog droplets in relation to their organic carbon content and chemical composition. *Atmospheric environment*, 34(28), 4853-4857.
- Farmer, D. K., Cappa, C. D., and Kreidenweis, S. M., **2015**: Atmospheric Processes and Their Controlling Influence on Cloud Condensation Nuclei Activity. *Chemical Reviews*, 115(10), 4199-4217.
- Fordham, S., **1948**: On the Calculation of Surface Tension from Measurements of Pendant Drops. *Proceedings of the Royal Society of London. Series A. Mathematical and Physical Sciences*, 194(1036), 1-16.
- Frka, S., Dautović, J., Kozarac, Z., Čosović, B., Hoffer, A., and Kiss, G., **2012**: Surface-active substances in atmospheric aerosol: an electrochemical approach. *Tellus B*, 64, 18490.
- Frossard, A. A., Li, W., Gérard, V., Nozière, B., and Cohen, R. C., **2016 under review**: Surfactants Enhance Growth of Individual Water Droplets. *Geophysical Research Letters*.
- Gaman, A. I., Kulmala, M., Vehkamäki, H., Napari, I., Mircea, M., Facchini, M. C., and Laaksonen, A., **2004**: Binary homogeneous nucleation in water–succinic acid and water–glutaric acid systems. *The Journal of Chemical Physics*, 120(1), 282-291.
- Gao, S., Surratt, J. D., Knipping, E. M., Edgerton, E. S., Shahgholi, M., and Seinfeld, J. H., **2006**: Characterization of polar organic components in fine aerosols in the southeastern United States: Identity, origin, and evolution. *Journal of Geophysical Research: Atmospheres*, 111(D14314).
- Gérard, V., Nozière, B., Baduel, C., Fine, L., Frossard, A. A., and Cohen, R. C., **2016**: Anionic, Cationic, and Nonionic Surfactants in Atmospheric Aerosols from the Baltic Coast at Askö, Sweden: Implications for Cloud Droplet Activation. *Environmental Science & Technology*, 50(6), 2974-2982.

- Gérard, V., Nozière, B., Fine, L., Ferronato, C., Frossard, A. A., Cohen, R. C., Asmi, E., Lihavainen, H., Kivekäs, N., Aurela, M., and Brus, D., **2016 under review**: Atmospheric evidence for the role of aerosol surfactants in cloud formation. *Nature Geoscience*.
- Giordano, M. R., Short, D. Z., Hosseini, S., Lichtenberg, W., and Asa-Awuku, A. A., **2013**: Changes in Droplet Surface Tension Affect the Observed Hygroscopicity of Photochemically Aged Biomass Burning Aerosol. *Environmental Science & Technology*, 47(19), 10980-10986.
- González-Pérez, A., Czapkiewicz, J., Del Castillo, J. L., and Rodríguez, J. R., **2003**: Micellar behavior of tetradecyldimethylbenzylammonium chloride in water-alcohol mixtures. *Journal of Colloid and Interface Science*, 262(2), 525-530.
- Good, N., Coe, H., and McFiggans, G., **2010a**: Instrumentational operation and analytical methodology for the reconciliation of aerosol water uptake under sub- and supersaturated conditions. *Atmospheric Measurement Techniques*, 3(5), 1241-1254.
- Good, N., Topping, D. O., Allan, J. D., Flynn, M., Fuentes, E., Irwin, M., Williams, P. I., Coe, H., and McFiggans, G., **2010b**: Consistency between parameterisations of aerosol hygroscopicity and CCN activity during the RHaMBLe discovery cruise. *Atmospheric Chemistry and Physics*, 10(7), 3189-3203.
- Hatakka, J., Aalto, T., Aaltonen, V., Aurela, M., Hakola, H., Komppula, M., Laurila, T., Lihavainen, H., Paatero, J., Salminen, K., and Viisanen, Y., **2003**: Overview of the atmospheric research activities and results at Pallas GAW Station. *Boreal Environmental Research*, 8, 365-383.
- Helvacı, S. S., Peker, S., and Özdemir, G., **2004**: Effect of electrolytes on the surface behavior of rhamnolipids R1 and R2. *Colloids and Surfaces B: Biointerfaces*, 35, 225-233.
- Hitzenberger, R., Berner, A., Kasper-Giebl, A., Löflund, M., and Puxbaum, H., **2002**: Surface tension of Rax cloud water and its relation to the concentration of organic material. *Journal of Geophysical Research: Atmospheres*, 107(D24), AAC 5-1-AAC 5-6.
- Hoekstra, A., Maltsev, V., and Videen, G., **2007**: *Optics of Biological Particles, II. Mathematics, Physics and Chemistry – Vol. 238, NATO Science Series*. Springer Netherlands.
- Hopkins, R. J., Mitchem, L., Ward, A. D., and Reid, J. P., **2004**: Control and characterisation of a single aerosol droplet in a single-beam gradient-force optical trap. *Physical Chemistry Chemical Physics*, 6(21), 4924-4927.
- Houze, R. A., **2014**: *Cloud Dynamics, International Geophysics*. Vol. 104, Academic Press, Elsevier Science.
- Hummel, D. O., **2000**: *Handbook of Surfactant Analysis: Chemical, Physico-chemical and Physical Methods*. Wiley, 412 pp.

- Irwin, M., Good, N., Crosier, J., Choularton, T. W., and McFiggans, G., **2010**: Reconciliation of measurements of hygroscopic growth and critical supersaturation of aerosol particles in central Germany. *Atmospheric Chemistry and Physics*, 10(23), 11737-11752.
- Jaafar, S. A., Latif, M. T., Chian, C. W., Han, W. S., Wahid, N. B. A., Razak, I. S., Khan, M. F., and Tahir, N. M., **2014**: Surfactants in the sea-surface microlayer and atmospheric aerosol around the southern region of Peninsular Malaysia. *Marine Pollution Bulletin*, 84(1-2), 35-43.
- Jaatinen, A., Romakkaniemi, S., Anttila, T., Hyvärinen, A. P., L-Q., H., Kortelainen, A., Miettinen, P., Mikkonen, S., Smith, J. N., Virtanen, A., and Laaksonen, A., **2014**: The third Pallas Cloud Experiment: Consistency between the aerosol hygroscopic growth and CCN activity. *Boreal Environmental Research*, 19(suppl. B), 368-382.
- Kang, K.-H., Kim, H.-U., and Lim, K.-H., **2001**: Effect of temperature on critical micelle concentration and thermodynamic potentials of micellization of anionic ammonium dodecyl sulfate and cationic octadecyl trimethyl ammonium chloride. *Colloids and Surfaces A: Physicochemical and Engineering Aspects*, 189(1-3), 113-121.
- Kiss, G., and Hansson, H. C., **2004**: Application of osmolality for the determination of water activity and the modelling of cloud formation. *Atmospheric Chemistry and Physics Discussion*, 4(6), 7667-7689.
- Kiss, G., Tombácz, E., and Hansson, H.-C., **2005**: Surface Tension Effects of Humic-Like Substances in the Aqueous Extract of Tropospheric Fine Aerosol. *Journal of Atmospheric Chemistry*, 50(3), 279-294.
- Kivekäs, N., Kerminen, V. M., Raatikainen, T., Vaattovaara, P., Laaksonen, A., and Lihavainen, H., **2009**: Physical and chemical characteristics of aerosol particles and cloud-droplet activation during the Second Pallas Cloud Experiment (Second PaCE). *Boreal Environmental Research*, 14, 515-526.
- Knox, K. J., **2011**: *Light-Induced Processes in Optically-Tweezed Aerosol Droplets*. Springer Berlin Heidelberg.
- Köhler, H., **1936**: The nucleus in and the growth of hygroscopic droplets. *Transactions of the Faraday Society*, 32, 1152-1161.
- Komppula, M., Lihavainen, H., Kerminen, V.-M., Kulmala, M., and Viisanen, Y., **2005**: Measurements of cloud droplet activation of aerosol particles at a clean subarctic background site. *Journal of Geophysical Research: Atmospheres*, 110(D6).
- Kosaric, N., and Sukan, F. V., **1993**: *Biosurfactants: Production: Properties: Applications*. Vol. 48, Marcel Dekker, New York.
- Kulkarni, P., Baron, P. A., and Willeke, K., **2011**: *Aerosol Measurement: Principles, Techniques, and Applications*. Wiley.

- Latif, M. T., and Brimblecombe, P., **2004**: Surfactants in Atmospheric Aerosols. *Environmental Science & Technology*, 38(24), 6501-6506.
- Lee, J. Y., and Hildemann, L. M., **2014**: Surface tensions of solutions containing dicarboxylic acid mixtures. *Atmospheric environment*, 89, 260-267.
- Lewis, E. R., and Schwartz, S. E., **2004**: *Sea Salt Aerosol Production: Mechanisms, Methods, Measurements, and Models - A Critical Review, Geophysical Monograph Series*. Vol. 152, American Geophysical Union, Wiley.
- Lihavainen, H., Kerminen, V. M., Komppula, M., Hyvärinen, A. P., Laakia, J., Saarikoski, S., Makkonen, U., Kivekäs, N., Hillamo, R., Kulmala, M., and Viisanen, Y., **2008**: Measurements of the relation between aerosol properties and microphysics and chemistry of low level liquid water clouds in Northern Finland. *Atmospheric Chemistry and Physics*, 8(23), 6925-6938.
- Lohila, A., Penttilä, T., Jortikka, S., Aalto, T., Anttila, P., Asmi, E., Aurela, M., Hatakka, J., Hellén, H., Henttonen, H., Hänninen, P., Kilkki, J., Kyllönen, K., Laurila, T., Lepistö, A., Lihavainen, H., Makkonen, U., Paatero, J., Rask, M., Sutinen, R., Tuovinen, J.-P., Vuorenmaa, J., and Viisanen, Y., **2015**: Preface to the special issue on integrated research of atmosphere, ecosystems and environment at Pallas. *Boreal Environmental Research*, 20, 431-454.
- Macherey-Nagel-GmbH-&Co, **2015**, cited 2016: Basic principle of SPE procedure. [Available online at <http://www.mn-net.com/tabid/11444/default.aspx>].
- Mahajan, R. K., and Sharma, R., **2011**: Analysis of interfacial and micellar behavior of sodium dioctyl sulphosuccinate salt (AOT) with zwitterionic surfactants in aqueous media. *Journal of Colloid and Interface Science*, 363(1), 275-283.
- Mańko, D., Zdziennicka, A., and Jańczuk, B., **2014**: Thermodynamic properties of rhamnolipid micellization and adsorption. *Colloids and Surfaces B: Biointerfaces*, 119(0), 22-29.
- McFiggans, G., Artaxo, P., Baltensperger, U., Coe, H., Facchini, M. C., Feingold, G., Fuzzi, S., Gysel, M., Laaksonen, A., Lohmann, U., Mentel, T. F., Murphy, D. M., O'Dowd, C. D., Snider, J. R., and Weingartner, E., **2006**: The effect of physical and chemical aerosol properties on warm cloud droplet activation. *Atmospheric Chemistry and Physics*, 6(9), 2593-2649.
- McNeill, V. F., Sareen, N., and Schwier, A. N., **2014**: Surface-Active Organics in Atmospheric Aerosols. *Atmospheric and Aerosol Chemistry*, F. V. McNeill, and A. P. Ariya, Eds., Springer Berlin Heidelberg, 201-259.
- Miles, R. E. H., Knox, K. J., Reid, J. P., Laurain, A. M. C., and Mitchem, L., **2010**: Measurements of Mass and Heat Transfer at a Liquid Water Surface during Condensation or Evaporation of a Subnanometer Thickness Layer of Water. *Physical Review Letters*, 105(11), 116101.
- Mircea, M., Facchini, M. C., Decesari, S., Cavalli, F., Emblico, L., Fuzzi, S., Vestin, A., Rissler, J., Swietlicki, E., Frank, G., Andreae, M. O., Maenhaut, W., Rudich, Y., and Artaxo, P.,

- 2005:** Importance of the organic aerosol fraction for modeling aerosol hygroscopic growth and activation: a case study in the Amazon Basin. *Atmospheric Chemistry and Physics*, 5(11), 3111-3126.
- Mitchem, L., Buajarern, J., Hopkins, R. J., Ward, A. D., Gilham, R. J. J., Johnston, R. L., and Reid, J. P., **2006:** Spectroscopy of Growing and Evaporating Water Droplets: Exploring the Variation in Equilibrium Droplet Size with Relative Humidity. *The Journal of Physical Chemistry A*, 110(26), 8116-8125.
- Mitsionis, A. I., and Vaimakis, T. C., **2012:** Estimation of AOT and SDS CMC in a methanol using conductometry, viscometry and pyrene fluorescence spectroscopy methods. *Chem. Phys. Lett.*, 547(0), 110-113.
- Mohajeri, E., and Noudeh, G. D., **2012:** Effect of Temperature on the Critical Micelle Concentration and Micellization Thermodynamic of Nonionic Surfactants: Polyoxyethylene Sorbitan Fatty Acid Esters. *E-Journal of Chemistry*, 9(4).
- Mohammad, A., and Hena, S., **2004:** Use of sodium bis (2-ethyl hexyl) sulfosuccinate (AOT) anionic surfactant mobile phase systems in thin-layer chromatography of amino acids : simultaneous separation of thioamino acids. *Chromatography*, 25(3), 111-118.
- Mohanty, S., and Mukherji, S., **2012:** Alteration in cell surface properties of Burkholderia spp. during surfactant-aided biodegradation of petroleum hydrocarbons. *Applied Microbiology and Biotechnology*, 94(1), 193-204.
- Morawska, L., and Salthammer, T., **2006:** *Indoor Environment: Airborne Particles and Settled Dust*. Wiley.
- Morris, H. S., Grassian, V. H., and Tivanski, A. V., **2015:** Humidity-dependent surface tension measurements of individual inorganic and organic submicrometre liquid particles. *Chemical Science*, 6(5), 3242-3247.
- Motomizu, S., Fujiwara, S., Fujiwara, A., and Toei, K., **1982:** Solvent extraction-spectrophotometric determination of anionic surfactants with ethyl violet. *Analytical Chemistry*, 54(3), 392-397.
- Mukerjee, P., and Mysels, K. J., **1971:** *Critical micelle concentrations of aqueous surfactant systems*. U.S. National Bureau of Standards; for sale by the Supt. of Docs., U.S. Govt. Print. Off.
- Mustaffa, N., Latif, M., Ali, M., and Khan, M., **2014:** Source apportionment of surfactants in marine aerosols at different locations along the Malacca Straits. *Environmental Science and Pollution Research*, 21(10), 6590-6602.
- Myers, D., **2005:** *Surfactant Science and Technology*. Wiley.
- Mysels, K. J., **1986:** Surface tension of solutions of pure sodium dodecyl sulfate. *Langmuir*, 2(4), 423-428.

- Nozière, B., Baduel, C., and Jaffrezo, J.-L., **2014**: The dynamic surface tension of atmospheric aerosol surfactants reveals new aspects of cloud activation. *Nature Communications*, 5, 3335.
- Nozière, B., Gérard, V., Baduel, C., and Ferronato, C., **2016 under review**: Extraction and characterization of surfactants from atmospheric aerosols. *Journal of Visualized Experiments*.
- OceanColor-NASA, **2015**, cited 2015: OceanColor Web (<http://oceancolor.gsfc.nasa.gov/cgi/l3>). Aqua MODIS Chlorophyll Concentration, OCI Algorithm [Available online at https://oceancolor.gsfc.nasa.gov/cgi/l3/A20101822010212.L3m_MO_CHL_chl_ocx_9km.nc.png?sub=img]. Maintained by NASA Ocean Biology Distributed Active Archive Center (OB.DAAC), Goddard Space Flight Center, Greenbelt MD.
- Olkowska, E., Polkowska, Ż., and Namieśnik, J., **2011**: Analytics of Surfactants in the Environment: Problems and Challenges. *Chemical Reviews*, 111(9), 5667-5700.
- Olkowska, E., Polkowska, Ż., and Namieśnik, J., **2012**: Analytical procedures for the determination of surfactants in environmental samples. *Talanta*, 88(0), 1-13.
- Omori, R., Kobayashi, T., and Suzuki, A., **1997**: Observation of a single-beam gradient-force optical trap for dielectric particles in air. *Optics Letters*, 22(11), 816-818.
- Orlović-Leko, P., Kozarac, Z., Čosović, B., Strmečki, S., and Plavšić, M., **2010**: Characterization of atmospheric surfactants in the bulk precipitation by electrochemical tools. *Journal of Atmospheric Chemistry*, 66(1-2), 11-26.
- Pacheco e Silva, V., Wanderley Bratfisch Pace, L., and Carone JR., E., **2013**: Method to measure surfactant in fluid, US 2013/0337568 A1.
- Pan, Y.-L., **2015**: Detection and characterization of biological and other organic-carbon aerosol particles in atmosphere using fluorescence. *Journal of Quantitative Spectroscopy and Radiative Transfer*, 150, 12-35.
- Parra, J. L., Guinea, J., Manresa, M. A., Robert, M., Mercadé, M. E., Comelles, F., and Bosch, M. P., **1989**: Chemical characterization and physicochemical behavior of biosurfactants. *Journal of the American Oil Chemists Society*, 66(1), 141-145.
- Patist, A., Bhagwat, S. S., Penfield, K. W., Aikens, P., and Shah, D. O., **2000**: On the measurement of critical micelle concentrations of pure and technical-grade nonionic surfactants. *Journal of Surfactants and Detergents*, 3(1), 53-58.
- Peters, T. M., and Leith, D., **2003**: Concentration measurement and counting efficiency of the aerodynamic particle sizer 3321. *Journal of Aerosol Science*, 34(5), 627-634.
- Petters, M. D., and Kreidenweis, S. M., **2007**: A single parameter representation of hygroscopic growth and cloud condensation nucleus activity. *Atmospheric Chemistry and Physics*, 7(8), 1961-1971.

- Petters, S. S., and Petters, M. D., **2016**: Surfactant effect on cloud condensation nuclei for two-component internally mixed aerosols. *Journal of Geophysical Research: Atmospheres*, 121(4), 1878-1895.
- Premier-Biosoft, **2016**, cited 2016: Mass Spectrometry. [Available online at http://www.premierbiosoft.com/tech_notes/mass-spectrometry.html].
- Prisle, N. L., Raatikainen, T., Sorjamaa, R., Svenningsson, B., Laaksonen, B., and Bilde, M., **2008**: Surfactant partitioning in cloud droplet activation: a study of C8, C10, C12 and C14 normal fatty acid sodium salts. *Tellus*, 60B(3), 416-431.
- Rana, D., Neale, G., and Hornof, V., **2002**: Surface tension of mixed surfactant systems: lignosulfonate and sodium dodecyl sulfate. *Colloid and Polymer Science*, 280(8), 775-778.
- Razafindralambo, H., Thonart, P., and Paquox, M., **2004**: Dynamic and equilibrium surface tensions of surfactin aqueous solutions. *Journal of Surfactants and Detergents*, 7(1), 41-46.
- Reid, J. P., Bzdek, B. R., Miles, R. E. H., Haddrell, A. E., and Hall, A. D., **2017 in preparation**: Direct Surface Tension and Viscosity Measurements of Aqueous-Organic Aerosol Droplets from Particle Coalescence Measurements. *Study presented (oral presentation) at the 22nd European Aerosol Conference EAC 2016, Tours, France, September, 8, 2016 (O29-AMT-INST-19)*.
- Renard, P., Canet, I., Sancelme, M., Wirgot, N., Deguillaume, L., and Delort, A. M., **2016**: Screening of cloud microorganisms isolated at the Puy de Dôme (France) station for the production of biosurfactants. *Atmospheric Chemistry and Physics*, 16(18), 12347-12358.
- Renard, P., Delort, A.-M., Canet, I., Sancelme, M., Gérard, V., and Nozière, B., **2017 in preparation**: Biosurfactants from fine atmospheric aerosols.
- Rinaldi, M., Fuzzi, S., Decesari, S., Marullo, S., Santoleri, R., Provenzale, A., von Hardenberg, J., Ceburnis, D., Vaishya, A., O'Dowd, C. D., and Facchini, M. C., **2013**: Is chlorophyll-a the best surrogate for organic matter enrichment in submicron primary marine aerosol? *Journal of Geophysical Research: Atmosphere*, 118(10), 4964-4973.
- Rolph, G. D., **2015**: Real-time Environmental Applications and Display sYstem (READY) Website [Available online at <http://ready.arl.noaa.gov>] NOAA Air Resources Laboratory, Silver Spring, MD.
- Roslan, R. N., Hanif, N. M., Othman, M. R., Azmi, W. N. F. W., Yan, X. X., Ali, M. M., Mohamed, C. A. R., and Latif, M. T., **2010**: Surfactants in the sea-surface microlayer and their contribution to atmospheric aerosols around coastal areas of the Malaysian peninsula. *Marine Pollution Bulletin*, 60(9), 1584-1590.
- Rotenberg, Y., Boruvka, L., and Neumann, A. W., **1983**: Determination of surface tension and contact angle from the shapes of axisymmetric fluid interfaces. *Journal of Colloid and Interface Science*, 93(1), 169-183.

- Rouessac, F., Rouessac, A., and Cruché, D., **2004**: *Analyse chimique - 6e éd.: Méthodes et techniques instrumentales modernes*. Dunod.
- Ruehl, C. R., and Wilson, K. R., **2014**: Surface Organic Monolayers Control the Hygroscopic Growth of Submicrometer Particles at High Relative Humidity. *The Journal of Physical Chemistry A*, 118(22), 3952-3966.
- Ruehl, C. R., Davies, J. F., and Wilson, K. R., **2016**: An interfacial mechanism for cloud droplet formation on organic aerosols. *Science*, 351(6280), 1447-1450.
- Ruehl, C. R., Chuang, P. Y., Nenes, A., Cappa, C. D., Kolesar, K. R., and Goldstein, A. H., **2012**: Strong evidence of surface tension reduction in microscopic aqueous droplets. *Geophysical Research Letters*, 39(23), L23801.
- Russell, R., **2015**, cited 2016: Layers of Earth's Atmosphere, UCAR (University Corporation for Atmospheric Research) Center for Science education [Available online at <http://scied.ucar.edu/atmosphere-layers>].
- Salma, I., Ocskay, R., Varga, I., and Maenhaut, W., **2006**: Surface tension of atmospheric humic-like substances in connection with relaxation, dilution, and solution pH. *Journal of Geophysical Research: Atmospheres*, 111(D23), D23205.
- Samburova, V., Zenobi, R., and Kalberer, M., **2005**: Characterization of high molecular weight compounds in urban atmospheric particles. *Atmospheric Chemistry and Physics*, 5(8), 2163-2170.
- Sansanwal, P. K., **2006**: Effect of co-solutes on the physico-chemical properties of surfactant solutions. *Journal of Scientific and Industrial Research*, 65(1), 57-64.
- Schmitt, T. M., **2001**: *Analysis of Surfactants, Second Edition (Surfactant Science)*. Vol. 96, Marcel Decker, Inc., 637 pp.
- Schulze, H.-U., Kannler, R., and Junker, B., **1985**: Latency studies on rat liver microsomal glucose-6-phosphatase. Correlation of membrane modification and solubilization by Triton X-114 with the enzymatic activity. *BBA - Biomembranes*, 814(1), 85-95.
- Seinfeld, J. H., and Pandis, S. N., **2006**: *Atmospheric Chemistry and Physics: From Air Pollution to Climate Change, 2nd Edition*. John Wiley & Sons, Inc.
- Shin, M., Umebayashi, Y., and Ishiguro, S.-i., **1997**: Distribution Thermodynamics of Metal Complexes in Micelles of Nonionic Surfactants. *Analytical Sciences*, 13(Supplement), 115-118.
- Shulman, M. L., Jacobson, M. C., Carlson, R. J., Synovec, R. E., and Young, T. E., **1996**: Dissolution behavior and surface tension effects of organic compounds in nucleating cloud droplets. *Geophysical Research Letters*, 23(3), 277-280.
- Skoog, D. A., West, D. M., Holler, F. J., and Crouch, S. R., **2013**: *Fundamentals of Analytical Chemistry*. Brooks/Cole, Cengage Learning.

- Sorjamaa, R., Svenningsson, B., Raatikainen, T., Henning, S., Bilde, M., and Laaksonen, A., **2004**: The role of surfactants in Köhler theory reconsidered. *Atmospheric Chemistry and Physics*, 4(8), 2107-2117.
- Stocker, T. F., Qin, D., Plattner, G.-K., Alexander, L. V., Allen, S. K., Bindoff, N. L., Bréon, F.-M., Church, J. A., Cubasch, U., Emori, S., Forster, P., Friedlingstein, P., Gillett, N., Gregory, J. M., Hartmann, D. L., Jansen, E., Kirtman, B., Knutti, R., Krishna Kumar, K., Lemke, P., Marotzke, J., Masson-Delmotte, V., Meehl, G. A., Mokhov, I. I., Piao, S., Ramaswamy, V., Randall, D., Rhein, M., Rojas, M., Sabine, C., Shindell, D., Talley, L. D., Vaughan, D. G., and Xie, S.-P., **2013**: Technical Summary. *Climate Change 2013: The Physical Science Basis. Contribution of Working Group I to the Fifth Assessment Report of the Intergovernmental Panel on Climate Change*, T. F. Stocker, D. Qin, G.-K. Plattner, M. Tignor, S. K. Allen, J. Boschung, A. Nauels, Y. Xia, V. Bex, and P. M. Midgley, Eds., Cambridge University Press, Cambridge, United Kingdom and New York, NY, USA.
- Stone, E. A., Hedman, C. J., Sheesley, R. J., Shafer, M. M., and Schauer, J. J., **2009**: Investigating the chemical nature of humic-like substances (HULIS) in North American atmospheric aerosols by liquid chromatography tandem mass spectrometry. *Atmospheric environment*, 43(27), 4205-4213.
- Tadros, T. F., **2006**: *Applied Surfactants: Principles and Applications*. Wiley.
- Tang, I. N., **1997**: Thermodynamic and optical properties of mixed-salt aerosols of atmospheric importance. *Journal of Geophysical Research: Atmospheres*, 102(D2), 1883-1893.
- Taraniuk, I., Graber, E. R., Kostinski, A., and Rudich, Y., **2007**: Surfactant properties of atmospheric and model humic-like substances (HULIS). *Geophysical Research Letters*, 34(16), L16807.
- Tausk, R. J. M., Karmiggelt, J., Oudshoorn, C., and Overbeek, J. T. G., **1974**: Physical chemical studies of short-chain lecithin homologues. I.: Influence of the chain length of the fatty acid ester and of electrolytes on the critical micelle concentration. *Biophysical Chemistry*, 1(3), 175-183.
- ThermoFisher-Scientific, **2015**, cited 2016: Overview of Mass Spectrometry for Protein Analysis. [Available online at <https://www.thermofisher.com/fr/fr/home/life-science/protein-biology/protein-biology-learning-center/protein-biology-resource-library/pierce-protein-methods/overview-mass-spectrometry.html.html>].
- Trenberth, K. E., Fasullo, J. T., and Kiehl, J., **2009**: Earth's Global Energy Budget. *Bulletin of the American Meteorological Society*, 90(3), 311-323.
- TSI, **2002**: Model 3010 Condensation Particle Counter, Instruction Manual P/N 1933010, Revision F, August 2002, TSI.
- TSI, **2012**: *Model 3321 Aerodynamic Particle Sizer® Spectrometer, TSI, Operation and Service Manual, P/N 1930092, Revision G, February 2012.*

- TSI, **2014**: *Fundamentals of Condensation Particle counters (CPC) and scanning Mobility Particle sizerTM (SMPSTM) spectrometers-application note CPC-003-US (10/30/2014)*, TSI.
- Vaida, V., **2015**: Ocean Sea Spray, Clouds, and Climate. *ACS Central Science*, 1(3), 112-114.
- Vaisala, **2002**: *Weather Sensor FD12P User's guide M210296en-A May 2002 Vaisala*.
- Väitilingom, M., Deguillaume, L., Vinatier, V., Sancelme, M., Amato, P., Chaumerliac, N., and Delort, A.-M., **2013**: Potential impact of microbial activity on the oxidant capacity and organic carbon budget in clouds. *Proceedings of the National Academy of Sciences*, 110(2), 559-564.
- Väitilingom, M., Attard, E., Gaiani, N., Sancelme, M., Deguillaume, L., Flossmann, A. I., Amato, P., and Delort, A.-M., **2012**: Long-term features of cloud microbiology at the puy de Dôme (France). *Atmospheric environment*, 56(0), 88-100.
- Wang, X., Sultana, C. M., Trueblood, J., Hill, T. C. J., Malfatti, F., Lee, C., Laskina, O., Moore, K. A., Beall, C. M., McCluskey, C. S., Cornwell, G. C., Zhou, Y., Cox, J. L., Pendergraft, M. A., Santander, M. V., Bertram, T. H., Cappa, C. D., Azam, F., DeMott, P. J., Grassian, V. H., and Prather, K. A., **2015**: Microbial Control of Sea Spray Aerosol Composition: A Tale of Two Blooms. *ACS Central Science*, 1(3), 124-131.
- Web-of-Science, **2016**, cited 2016: Published items in each year relative to the article "A single parameter representation of hygroscopic growth and cloud condensation nucleus activity" [Petters 2007], Citation Report from Web of Science Core Collection.
- WMO, **1975**: *International Cloud Atlas - Volume 1: Manual on the Observation of Clouds and Other Meteors (annex 1 to WMO Technical Regulations)*. Vol. 407.
- Yamamoto, K., and Motomizu, S., **1987**: Solvent extraction-spectrophotometric determination of anionic surfactants in sea water. *Analyst*, 112(10), 1405-1408.

Title

Surfactants in atmospheric aerosols and their role on cloud formation

Author of the PhD thesis

Violaine Myriam Francine GÉRARD (PhD student 2013/2016)

Supervisor of the PhD thesis

Dr. Barbara Nozière, *Chargée de Recherche* (CR1), CNRS

Abstract

Clouds are essential components of the Earth's hydrological system and climate but some aspects of their formation are still not completely understood. In particular, although Köhler theory predicts that surfactants should enhance cloud droplet activation, current models consider this role negligible. At the time of this PhD work, a few studies had started to demonstrate the contrary but atmospheric evidence for the role of these compounds was still missing and very little was known about their atmospheric concentrations, sources, and mechanism of action.

The objective of this PhD work was to investigate these aspects to improve the understanding of atmospheric surfactants and their role in cloud formation. Several milestones were achieved. First, a method was developed to quantify surfactant concentrations in aerosols, which was applied to samples from different regions. This method led to the first absolute surface tension curves for atmospheric surfactants, in PM_{2.5} aerosols from a coastal region in Sweden, and to the identification of the key parameter controlling the cloud-forming efficiency of aerosols, the C/CMC ratio. A second study revealed strong correlations between cloud occurrence and intrinsic surfactant properties in PM₁ aerosols in a boreal region in Finland, thus demonstrating for the first time the role of surfactants in cloud formation from direct atmospheric observations. The results predicted Cloud Condensation Nuclei numbers four times larger on average than when neglecting surfactant effects, showing the quantitative importance of including surfactant effects in cloud predictions. The importance of surfactants inferred from macroscopic measurements was confirmed by laboratory experiments on individual micron-sized droplets showing an increase of droplet growth in the presence of surfactants. Finally, observations from the different field studies (correlations with biological markers, chemical structure ...) concurred to indicate a biological origin for the surfactants present in atmospheric aerosols.

This work thus accomplished some important steps in the understanding of atmospheric surfactants and their role in cloud formation.

Key words

Surfactants – atmospheric aerosols – cloud droplet – surface tension – CMC – micron-sized droplet – optical trap – origin of surfactants in atmosphere

Laboratory

IRCELYON (Institut de Recherches sur la Catalyse et l'Environnement de Lyon), CNRS (Centre National de la Recherche Scientifique) - UMR 5256, Université Claude-Bernard Lyon 1
2 avenue Albert Einstein – 69626 Villeurbanne – FRANCE